Modelling the Temporal Variation of the Ionosphere in a Network-RTK Environment

Scott John Wyllie
Bachelor of Applied Science (RMIT)

Thesis submitted for the fulfilment of the degree of Doctor of Philosophy

School of Mathematical and Geospatial Sciences
RMIT University
GPO Box 2476V
Melbourne, Victoria 3001
Australia

June 2007

Declaration by the Candidate

This thesis contains no material that has been accepted for the award of any other higher degree or graduate diploma in any tertiary institution. This thesis contains work of mine alone and the best of my knowledge and belief contains no material previously published or written by another person, except where due reference is made in the text. Furthermore, the work presented has been carried out after the official starting date of the program.

Scott John Wyllie
June 2007

Acknowledgements

I would firstly like to thank my supervisors Professor Kefei Zhang and Dr. Nick Talbot for providing many useful suggestions regarding the content and direction of my research program. I would like to acknowledge the partial support of the Australian Research Council project (LP0455170) endorsed to Professor Kefei Zhang. I would also like to thank all of the staff in Geospatial Science for their help and support throughout my education, you are a credit to the University.

To all of my fellow postgraduate students who have helped make my time in the department so enjoyable, thanks for the fantastic memories.

I would like to acknowledge Lucas Holden for his constructive input with regard to the technical side of this thesis and his greatly valued friendship. Thanks Lucas.

The staff at Land Victoria are thanked for providing all of the GPS data necessary to undertake this research.

I would like to thank my family and friends for their never ending support and encouragement throughout my intellectual endeavours. I would like to offer my sincere thanks to my parents for providing their encouragement and financial support throughout my education, and instilling in me the self belief that anything is possible with a little hard work. To my son Liam and daughter Caitlin, thanks for putting up with my frequent absence during this research program. Finally, I would like to thank my wonderful wife Tonia, for her continued patience, support and encouragement throughout the course of this research program. Your understanding has made this possible.

Abstract

The Global Positioning System (GPS) has been widely used for precise positioning applications throughout the world. However, there are still some limiting factors that affect the performance of satellite-based positioning techniques. One of the most significant sources of error experienced over the receiver-satellite path is due to the ionosphere. The ionosphere is a dispersive medium for GPS signals. Many factors influence the degree of the ionosphere's effect on positional accuracy. These include: user location, time of day and solar activity. The level of solar activity is the major influence on the Earth's ionosphere. The Sun has an eleven year cycle, with the next solar maximum expected around 2011. The scientific community has developed a number of different global empirical ionospheric models to estimate the effect of the ionosphere for a given time and location. The GPS Network-RTK concept has been developed in an attempt to remove the ionospheric bias from user observations within the network. The Network-RTK technique involves the establishment of a series of GNSS reference stations, spread over a wide geographical region. Data from each reference station is collected in real-time and transferred to a computing facility where the various spatial and temporal errors affecting the GNSS satellite observations are estimated. These Network-RTK corrections are then transmitted to users in the field as a means of correcting their observations. As part of a Victorian state government initiative to implement a cm-level real time positioning service across the state, Victoria's GPSnet is currently undergoing extensive infrastructure upgrades to meet high user demand for precise positioning state-wide. Due to the sparse (+100km) configuration of GPSnet's reference stations, the precise modelling of Victoria's ionosphere will play a key role in providing a state-wide cm-level service.

The aim of this thesis is to develop a temporal model for the ionospheric bias within a Victorian Network-RTK scenario. As a first step towards achieving this aim, this research has comprehensively analysed the temporal variability of the ionosphere over Victoria. It is important to quantify the variability of the ionosphere as it is essential that Network-RTK corrections are delivered sufficiently often with a small enough latency so that they adequately model variations in the ionospheric bias. This will promote the efficient transmission of correctional data to the rover whilst still achieving cm-level accuracy. The temporal analysis of the ionosphere revealed that,

during stable ionospheric conditions, Victoria's double differenced ionospheric bias remains correlated to within ±5cm out to approximately two minutes over baselines of approximately 100km. However, the data revealed that during more disturbed ionospheric conditions this may decrease to a low of one minute.

As a preliminary investigation, four global empirical ionospheric models (Broadcast, Bent, IRI2001, CODE) were tested in order to assess their ability to estimate the double differenced ionospheric bias. Three temporal predictive modelling schemes were tested to assess their suitability for providing ionospheric corrections in a Network-RTK environment. The analysis took place over four different seasonal periods during the previous solar maximum in 2001 and 2002. It was found that due to the global nature of their coefficients, the four global empirical models were unable to provide ionospheric corrections to a level sufficient for precise ambiguity resolution within a Network-RTK environment.

Three temporal ionospheric predictive schemes were developed and tested. These included a moving average model, a linear model and an ARIMA (Auto-Regressive Integrated Moving Average) time series analysis. The moving average and ARIMA approaches gave similar performance and both out-performed the linear modelling scheme. It is shown that both of these approaches were able to predict the double differenced ionosphere to ±5cm within a 99% confidence interval, out to an average of approximately two minutes, on average 90% of the time when compared to the actual decorrelation rates of the ionosphere. These results suggest that a simple modelling technique, such as the moving average scheme, could enhance the implementation of next generation Network-RTK systems by predicting the double differenced ionospheric bias to latencies that would enable cm-level positioning.

Table of Contents

List of Figures

List of Tables

Acronyms

ACM	Area Correction Model
ARIMA	AutoRegressive Integrated Moving Average
BABE	BAllarat to BEndigo baseline
CODE	Center for Orbit Determination in Europe
CORS	Continuosly Operating Reference Stations
DDI	Double Difference Ionosphere
GIM	Global Ionospheric Map
GLONASS	GLobal Orbiting NAvigation Satellite System
GNSS	Global Navigation Satellite Systems
GPS	Global Positioning System
IAF	Ionospheric Amplification Factor
IPP	Ionospheric Pierce Point
IRI	International Reference Ionosphere
LT	Local Time
MCS	Master Control Station
MEBA	MElbourne to BAllarat baseline
MEBE	MElbourne to BEndigo baseline
RTCM	Radio Technical Commission for Maritime Services
RTK	Real Time Kinematic
TEC	Total Electron Content
UT	Universal Time
VRS	Virtual Reference Station

Chapter 1 Introduction

1.1 Background

The introduction of the Global Positioning System (GPS) into the field of land surveying has revolutionised the art of positioning. GPS provides a powerful and versatile system that can be adapted and exploited to allow for the development of new technologies within the surveying industry. A wide range of precise positioning applications have emerged in such fields as: machine guidance and control, precision farming, land surveying and geodesy.

Traditional terrestrial surveying techniques rely upon the inter-visibility of points, whereas GPS satellite technology allows for the positioning of points that are able to view common satellites. In some instances, where impractical to use traditional surveying methods, GPS provides the surveyor in the field with a quick, accurate and reliable means of positioning. The use of GPS does however, have limitations. For example, its need for an unobstructed view of the sky is one constraint. Therefore, GPS should be seen as another tool in the surveyor's repertoire, to be used in conjunction with traditional methods, so as both method's strengths and weaknesses can be drawn upon (Hill, 1999).

Positioning techniques developed with the United States GPS are being enhanced with advent of the Russian GLONASS and European planned GALILEO system. The

term GNSS (Global Navigation Satellite Systems) was coined some years ago as a means of describing current and future satellite navigational systems.

Although GPS techniques have been significantly advanced over the past two decades, there are still several error sources that limit the accuracy, practical operation and performance of precise positioning. For example, the atmosphere, primarily the ionosphere and to a lesser degree the troposphere, provide a significant source of range degradation for GPS users. The ionosphere is the largest error source for GPS positioning, since Selective Availability was decommissioned in May, 2000 (White House, 2000). The ionospheric range error at zenith can vary from a few metres, to many tens of metres, whereas the tropospheric range error at zenith is usually between two to three metres.

The ionosphere is located between approximately 50km and 1000km above the Earth's surface. In this region, ionising radiation from the Sun causes electrons to exist in such quantities that they affect the propagation of radio waves (Kleusberg & Teunissen, 1996). The ionosphere is a dispersive medium for radio waves which causes GPS code pseudoranges to be measured too long, and the carrier phase pseudoranges measured too short, from the actual geometric range between the orbiting satellites and Earth bound receivers (Hofmann-Wellenhof *et al.*, 1997). The number of electrons encountered by an electromagnetic wave travelling through the ionosphere is commonly known as the Total Electron Content (TEC). The integrated electron density along the signal path between the satellite and GPS receiver is expressed in units of electrons per cubic metre.

The ionosphere is a very complex and unpredictable body (Gorney, 1990). Its behaviour can vary quite significantly from day to day and from one location to the next. The level of solar activity is the major influence on the Earth's ionosphere. The Sun has an eleven year cycle, with the next solar maximum expected around 2011. The day to day variability of the TEC values from the monthly average is in the region of 20-25% (Wu *et al.*, 2006; Wyllie *et al.*, 2006). Current predictive ionospheric models are considered exceptional if the difference between the predicted and actual monthly mean TEC value is within $\pm$10% (Klobuchar, 1996). Satellite-ionosphere-

user geometry changes rapidly because of satellite motion. This can lead to rapid variation of ionospheric delay.

The ionospheric effect on radio waves is frequency-dependent. GPS satellites currently broadcast on two frequencies so that the ionospheric effect can be accounted for. Dual frequency receivers are able to form linear combinations of the L1/L2 phase observables to remove the first order effects of the ionosphere (Wells *et al.*, 1987; Wang *et al.*, 2004). Georgiadou & Kleusberg (1988a) and Schaer (1999) suggest the use of the L4 Geometry-Free linear combination as a means of measuring the change in the ionosphere to a high degree of accuracy.

In order to reduce the impact of the ionosphere, cm-level applications use a technique known as differential positioning. The Differential GPS (DGPS) technique involves the differencing of code and phase data collected simultaneously from the same satellites, at two different receivers. This allows an accurate difference in position to be calculated between the two receiving stations, as many errors affecting one receiver are common to the other. This technique forms the basis for all precise geodetic positioning using the GPS/GNSS.

Real Time Kinematic (RTK) positioning refers to high-precision GPS positioning in the field (Talbot, 1991a). The RTK technique involves at least two receivers tracking a common set of satellites simultaneously. The reference receiver broadcasts its carrier phase and code measurements to a roving receiver, where the rover combines the reference data with its observations to produce cm-level position estimates. High precision GPS positioning requires the use of carrier phase observables, however, carrier measurements contain an initial cycle ambiguity (integer) term that needs to be resolved. Centimeter level accuracies can be achieved at the rover, only once integer ambiguities are resolved.

In order to accurately and reliably resolve carrier phase ambiguities at the rover, the ionospheric bias needs to be known to better than a quarter of a wavelength or $\pm$5cm (Teunissen *et al.*, 2000). Therefore, the accurate modelling of the ionosphere over the rover's position is critical. Furthermore, accurate ionospheric bias corrections can aid positioning estimates. This $\pm$5cm criteria is not however a definitive number, as

correct ambiguity resolution can be achieved with greater errors using modern ambiguity resolution strategies. It will however be used throughout this thesis as the bench mark for assessing ionospheric estimation performance. The accuracy achievable using the RTK system is usually dependent on the baseline length between the rover and base receivers. The fast and accurate resolution of ambiguities is heavily reliant on the correlation of atmospheric refraction biases (Featherstone & Stewart, 2001). These biases can be categorised as dispersive (ionosphere) and non-dispersive (troposphere and satellite orbital errors). The ionospheric error has a greater influence on ambiguity resolution as both the ionospheric delay and ambiguities are frequency dependent (Kashani *et al.*, 2004a). As the baseline lengths increase beyond 10km, the positional solutions tend to degrade as the ionospheric refraction effect becomes decorrelated, and will no longer cancel out through differencing (Rizos, 2002). In the past ionospheric decorrelation restricted RTK operations to 10km baselines under normal ionospheric conditions.

In order to mitigate distance dependent biases that limit the application of RTK surveying, a concept known as Network-RTK (Vollath *et al.*, 2000a) has been recently developed, which aims to provide cm-level positional accuracy over baseline lengths of many tens of kilometres (Zhang & Roberts, 2003; Roberts *et al.*, 2004). This is achieved by the use of multiple reference stations spread over a wide geographical area, which allows for the empirical modelling of these spatially dependent measurement biases, thus producing corrections that can be transmitted to users in the field.

In recent years a number of first generation Network-RTK services have been established in many countries world wide. These include: USA, Germany, UK, Sweden, Switzerland and Japan (Trimble, 2005). In 1994 a state-wide continuously operating reference station (CORS) network (GPSnet) was established by the Victorian Government in support of geodesy, surveying, mapping and high-end navigation users (Hale, 2000). At present GPSnet consists of 23 reference stations (February, 2007) providing online GPS data access. Users are able to combine these files with GPS data collected across Victoria, for both post processing and real time positioning applications, at selected sites. These real-time services have only recently become operational with the introduction of the VICpos and MELBpos

services (Zhang *et al.*, 2006). VICpos offers a state-wide networked DGPS correctional service, providing sub-metre level positioning, based upon 17 base stations distributed around the state. The MELBpos service is able to provide real time cm-level accuracies in Melbourne and its immediate surrounding areas via a number of selected GPSnet sites that stream correctional data to a network server. The server then generates a network correction for the MELBpos region (DSE, 2006). Initial testing of the MELBpos system has produced cm-level accuracies on baselines out to 70km (Gordini *et al.*, 2006). It is envisaged that this service will be extended state-wide in the future (Zhang *et al.*, 2007). Planning is also underway to enhance Australia's geodetic framework to such an extent that cm-level positioning will be available nation wide (NCRIS, 2007). One of the main limitations relating to GPSnet's configuration is the long baseline separations across the state (between 50 – 200km), and the ionospheric errors experienced over these lines. In order to overcome this potential barrier to performance and implementation, the key to achieving real-time state-wide centimeter level performance is the precise modelling of Victoria's ionosphere (Han, 1997; Zhang & Roberts, 2003).

In addition to the problem of sparse (+100km) network station configuration, a number of other challenges confront the efficient implementation of Network-RTK resources. One such challenge is the reduction of data transmission volume and message complexity to the rover (Euler *et al.*, 2001). This will reduce the computational burden at the rover, or at the Master Control Station (MCS) providing the corrections. The issue of bandwidth efficiency is also another concern at the forefront of current research (Kalafus & Van Dierendonck, 2003; Brown *et al.*, 2005).

In a Network-RTK environment the ionosphere needs to be predicted forward, as real time positioning requires corrections to the rover's observations to provide instantaneous positioning. The delivery of Network-RTK corrections involves the following latencies:

- Collection of observations at each reference station;
- Transmission of reference station data to a central server, via the internet, phone line or satellite etc;

- Processing of the data by the network server and generation of corrections for users;
- Transmission of corrections to users;
- Decoding of corrections by user equipment; and
- Application of corrections to rover observations.

The total of these latencies can be in the order of a few seconds to tens of seconds. It is important that the corrections are delivered sufficiently often and with a small enough latency so that they are still applicable, given that the ionospheric bias is rapidly changing. In support of promoting efficient data transmission to the rover within a Network-RTK environment, it is important to quantify the necessary update rate for ionospheric corrections in order to maintain the required cm-level accuracy, thus allowing accurate rover position estimation within a network. In addition, telecommunication companies often charge the users of correction data according to the amount of data traffic. It is important therefore, that network correction services consider the minimum frequency required to deliver the required level of accuracy.

A subset of GPS stations operating within the GPSnet configuration, have been chosen to provide the raw data needed to analyse the temporal variation of the ionosphere over Victoria and provide a suitable means of modelling its effect. Data for this study was intentionally captured during the solar maximum period between 2001-2002, in an attempt to study the mid-latitude ionospheric effect during active ionospheric conditions.

1.2 Aims and hypotheses

The aim of this research is to develop a high precision temporal model for the ionospheric bias for Network RTK applications. The model is developed and analysed for the state of Victoria under solar maximum conditions. Given advanced knowledge of the temporal nature of the differential ionospheric bias, it should be possible to design Network RTK ionospheric correction messages that meet high precision GNSS user requirements.

Based on this aim, the following hypothesis has been formulated:

A temporal ionospheric model unique to Victorian conditions can be developed to improve the efficiency of Network-RTK corrections.

In order to test this hypothesis, the following research objectives have been set:

- To quantify the temporal trend in the ionosphere during a period of solar maximum, over the State of Victoria;
- To analyse the suitability of four typical global empirical ionospheric models for providing ionospheric corrections in a Network-RTK environment;
- To provide a means of modelling the temporal double differenced ionospheric bias in a Network-RTK environment, by testing a number of different extrapolation techniques, together with different data sampling rates; and
- To develop temporal ionospheric correction models; using GPSnet as a test bed.

The associated research questions are:

- How often does the ionosphere need to be sampled to meet a $\pm$5cm accuracy criteria, within the mid-latitude Victorian region?
- How quickly do the model estimations diverge from the truth? How far forward in time is the model capable of predicting the double differenced ionospheric bias?
- Is it feasible to use global empirical ionospheric models to produce ionospheric corrections of suitable accuracy for Network-RTK applications?
- How does the ionospheric bias behave at different times of the day, and does the efficiency of the proposed ionospheric model vary during these times?

1.3 Project rationale

The research will aid the surveying and mapping industry and wider GPS user communities by enabling more accurate positioning, by optimising the use of the current GPSnet infrastructure. It is envisaged that this research will aid in extending the current capabilities of commercially available network-based positioning systems, and will lead to a second generation of CORS networks, that operate using a sparse (+100km) configuration of reference stations.

Under constantly changing ionospheric conditions, it is essential that corrections are delivered to the user in the field with sufficient latency that they are still applicable. The research will aid in reducing the cost of Network-RTK delivery by determining the frequency with which ionospheric corrections need to be sent.

1.4 Contribution of this research

Over the last two decades, significant advances have been made in the area of real time cm-level positioning using RTK surveying techniques (Rizos, 2003). Single base station RTK surveying is however limited in range due to such distant dependent biases as orbital, ionospheric and tropospheric errors. These biases degrade the accuracies achievable as baseline length between the base station and rover increases over 10 km. In order to mitigate these biases and increase the operational length of RTK baselines the concept of using a network of GPS receivers to model these errors was first investigated in the mid-1990's (Han & Rizos, 1996; Wubbena *et al.*, 1996). Multiple reference stations are used to empirically model these distance dependent measurement biases over a user area. These corrections are then transmitted to the user in the field. Several authors have investigated the use of the system and improved RTK positioning. Their results for medium range applications have been presented in Han (1997) and Raquet (1998) amongst others.

At present there are three possible structures from which to base the implementation of Network RTK. All three methods broadcast corrections to users in the field using different approaches:

(1) generation of the virtual reference station (VRS),
(2) generation and broadcast of an Area Correction Model (ACM), as demonstrated in Leica's Master-Auxiliary Concept (MAC), and
(3) the broadcasting of raw data from each reference station in the network (see chapter 4).

The issue of signal bandwidth and transmission rates is a topic at the forefront of contemporary precise network-RTK applications. Is simply flooding the user in the field with correctional information the most efficient approach to take? Cost of correctional delivery and network computational burden are issues that need to be taken into account. This raises the issue of latency. In order to promote a more efficient network solution, how often should the corrections be sent to the user, whilst still maintaining sufficient accuracy?

In order to accurately and reliably resolve carrier phase ambiguities, the ionosphere needs to be known to an accuracy of a quarter of a wavelength or $\pm$5cm (Teunissen *et al.*, 2000). This thesis extends the current knowledge by investigating the short term temporal characteristics of the ionosphere over the Victorian region. Wu et al. (2006) has recently investigated medium to long term ionospheric variations in Victoria to understand the behaviour of the ionosphere over the region. It is therefore necessary to investigate further how the ionosphere changes from one epoch to the next over Victoria, as a means of quantifying its behaviour during different seasonal and diurnal periods. The analysis will look for any trends in the raw observational data that will aid in forward prediction. This will provide information as a precursor to predicting the ionosphere's variability (how often it needs to be sampled) and how well it can be modelled. Based on this analysis a means of modelling the temporal variability of the double differenced ionospheric bias in a Network-RTK environment will be investigated. This will be achieved by testing a number of different extrapolation techniques, together with different data sampling rates. The models investigated include such techniques as a Moving Average and Linear Polynomial approach, together with a Box-Jenkins Time Series Analysis of the double differenced ionosphere over Victoria.

1.5 Limitations and scope of the project

In order to keep the scope of the project at a manageable level, in terms of the data processing required, three GPSnet base stations, at Melbourne, Ballarat and Bendigo have been chosen as the test bed sites for the project. The model produced from the data collected at these sites, could be expanded to include the remaining stations located throughout Victoria, thus offering a state-wide coverage.

This research focuses primarily on the temporal nature of the ionosphere over Victoria, even though both the temporal and spatial variation of the ionosphere are intrinsically linked. The three GPSnet base stations used to perform the analysis of the short term double differenced ionosphere are separated at distances that are on average typical of the current GPSnet reference station separations (approximately 100km) across the state. It is assumed that the results obtained will be indicative of other triangles within the network.

The techniques developed should therefore be viewed as a recipe for temporal characterisation of the ionosphere and can be applied to other locations and time periods. It is understood that because of the variable nature of the ionosphere, it is not possible to characterise its temporal nature for all conditions and locations.

The L4 linear combination is used to produce double differenced ionospheric bias estimates that are used as 'truth' data for further analysis in this thesis. However, this observable may contain carrier phase multipath that may be responsible for some short term variability in the datasets. This multipath is very difficult to remove from the observations. Therefore, some of the conclusions drawn may be clouded by the presence of carrier phase multipath.

The determination of a network ionospheric model involves both spatial and temporal components. A prerequisite for an ionospheric model involves the estimation of carrier phase ambiguities for all satellites observed at the reference stations. Once these ambiguities are determined, the ionospheric, tropospheric and satellite orbit errors can be determined over time between the reference stations. These corrections can then be spatially interpolated and temporally extrapolated for users

within the network. However, this research will focus on the temporal correlation of the ionosphere and will not consider network ambiguity estimation and spatial ionospheric interpolation issues.

1.6 Thesis structure

The thesis has the following structure:

Chapter 2 provides an overview of the ionosphere and how it affects the GPS signals that propagate through it. The ionosphere is described in a physical sense, looking at its different structural layers in altitude and how it varies both geographically and temporally. The relationship between the Sun's activity and the Earth's magnetic field and how it influences ionospheric disturbance will also be discussed. The physics behind wave refraction and dispersion will also be presented, as this forms the basis of the ionospheric effect on the GPS signal. This chapter will provide the basis of scientific understanding of the ionosphere's physical makeup together with its different spatial and temporal characteristics. This will provide an understanding of the types of ionospheric influences that need to be considered when producing a cm-level ionospheric correction model suitable for Victorian conditions.

Chapter 3 focuses on different ionospheric probing techniques, the processes involved and the accuracies achievable, as well as GPS as a means of estimating the ionosphere. This chapter looks at ionospheric sounding using both terrestrial methods and satellite techniques. The terrestrial methods include: ionosonde, incoherent scatter radars and Faraday rotation techniques as a means of ionospheric estimation. Satellite techniques include topside sounding of the ionosphere, which includes: the Allouette program, Navstar GPS, PRARE and the TOPEX/Poseidon satellite programs. The background behind the extraction of ionospheric data from GPS measurements is also investigated. This includes how the GPS observables are used to estimate the ionosphere, and the impact of the ionosphere on GPS in high precision geodetic applications. This chapter provides a background of both historical and current methods of measuring the ionosphere, and the types of accuracies associated with each procedure. This is covered as the production of an ionospheric model requires the input of raw ionospheric measurement. The use of GPS to

produce these measurements and the science behind the extraction of ionospheric data from GPS observations is investigated, as the data used to conduct the research in further chapters is gained via GPS methods.

Chapter 4 presents a review of GPS ionospheric modelling. Some of the well established and internationally accepted empirical models that have been developed over the last three decades are described. These models include: the Bent Model, the Broadcast GPS Model, the International Reference Ionosphere (IRI) 2001 and the Centre of Orbit Determination in Europe (CODE) Global Ionospheric Maps (GIMs). The application of GPS measurements in the formulation of ionospheric models and corrections is also investigated. Such modelling concepts as grid-based approaches, ionospheric tomography, GPS augmentation systems and the application of RTK corrections within a CORS network are discussed. The accuracies achievable and applications of these different systems are also examined. This chapter is presented as a means of gaining an understanding into the types of ionospheric modelling procedures that are currently available, and the applications associated with each procedure. The use of CORS networks to produce ionospheric corrections that can be used to improve the positional accuracy of users within the network coverage area is also introduced. This is introduced as the improvement of current modelling techniques within this environment is the focus of further research in upcoming chapters.

Chapter 5 provides an introduction to Victoria's CORS network (GPSnet) and its current operational status. The global ionospheric models described in the previous chapter, are tested against each other, to see how they perform in a more regional sense. Their ability to predict the double differenced ionospheric bias over Victoria is investigated as a means of testing their usefulness in providing corrections in a Network-RTK environment. This was carried out as a first step towards understanding the variability of the ionosphere over Victoria, and to provide further insight into the issues that need to be addressed in order to model the ionosphere to cm-level accuracy. Victoria's GPSnet infrastructure is used to carry out this investigation.

Chapter 6 investigates the temporal variation of the ionosphere over Victoria. This is undertaken by firstly looking at the variation of the actual ionospheric TEC over Victoria, then refining the study to quantify the temporal characteristics of the differential ionospheric bias over the same region. The research is undertaken to give an insight into Victoria's ionospheric conditions as a precursor to the development of an ionospheric model suitable to support state-wide Network-RTK enhancement for the currently operating GPSnet infrastructure.

Chapter 7 investigates ionospheric modelling in a differential sense, and provides the means of computing ionospheric corrections through the use of an ionospheric model within a Network-RTK environment. This model will provide a prediction method for the ionospheric bias, which would allow the roving GPS receiver to interpolate forward, thus reducing the need for constant network corrections. The level of predictional accuracy produced by the model would allow for the precise resolution of the integer cycle ambiguity at the roving receiver. Three different modelling approaches are tested and investigated.

Chapter 8 provides a summary and the conclusions of the thesis. Recommendations for future research are also given.

Chapter 2 The Earth's ionosphere and GPS signal propagation

This chapter provides an overview of the ionosphere and how it affects the GPS signals that propagate through it. The ionosphere will be described in a physical sense, looking at its different structural layers in altitude and how it varies both geographically and temporally. The relationship between the Sun's activity and the Earth's magnetic field and how it influences ionospheric disturbance will also be discussed. In addition, the physics behind wave refraction and dispersion will be investigated, as this forms the basis for the ionospheric effect on the GPS signal.

This chapter also provides the basis of scientific understanding of: the effect that the ionosphere has on GPS signal propagation and the ionosphere's physical makeup, together with its different spatial and temporal characteristics. This understanding will provide an awareness of the types of ionospheric influences that need to be considered when implementing a cm-level ionospheric correction model suitable for Victorian conditions.

2.1 The Earth's ionosphere

Sir Robert Watson-Watt, in 1929, was the first to use the term "ionosphere" for defining the ionised layers that encircle the Earth. During the period 1932-1934 the

expression came into wider use when Watson-Watt, Appleton and Ratcliff, amongst others, used it in numerous papers and books.

Early speculation about a conductive layer in the Earth's atmosphere by Gauss in 1839 was given credibility with the successful transmission of a radio signal across the Atlantic by G. Marconi in 1901. This successful transmission implied that the signal was being reflected around the Earth by the atmosphere. The discovery of the electron by J.J. Thompson around 1900, supplied the theory behind the still theoretical conductive layer. In 1902 a British physicist, Oliver W. Heaviside, and an American electrical engineer, Arthur Edwin Kennelly, were both speculating that the free electrons in the Earth's upper atmosphere could reflect radio waves and the link between the Sun's ultraviolet emissions and this conductive layer was being suggested. It was not until some 20 years later that the existence of the ionosphere was proven, via experiments undertaken by Appleton & Barnett (Appleton & Barnett, 1925a;, 1925b) and Breit &Tuve (Breit & Tuve, 1925; 1926) using reflecting radio wave techniques (Rishbeth & Garriott, 1969).

Within the terrestrial environment, the correlation between the Sun's activity, and disturbances in the near Earth magnetosphere, ionosphere and neutral atmosphere have been extensively researched and documented. The ionosphere has a complex structure, which evolves due to a number of various physical processes that govern its makeup. The ionosphere must be considered in both a spatial and temporal sense. Its structure can be broken down into a number of layers in altitude, into three zones in latitude, and further to this, the day and night ionosphere need to be looked at individually (Gorney, 1990). The structure and electron densities of the ionosphere are very closely linked with time, geographical location and solar activity.

2.1.1 Chapman profile

As a background to electron production in the ionosphere, it is useful to understand the basic theory of photoionisation in the atmosphere. The Chapman function (Rishbeth & Garriott, 1969; Davies, 1990) derives a general formula for the rate of ion production as a function of height h and solar zenith angle α. Although Chapman's results were based on a number of assumptions and simplifications, his overall

theory captured the fundamentals of the problem, and can be used as a useful reference (Tascione, 1988). In the simplest case we consider the rate of production of ion pairs produced by a parallel, monochromatic beam of solar radiation that is ionising a horizontally stratified, one component isothermal gas.

$$q(h,\alpha) = q_0 e^{\left(1 - z - \sec\alpha e^{-z}\right)} \qquad \text{where } z = \frac{h - h_0}{\Delta h} \tag{2.1}$$

where:

$q(h,\alpha)$	is the ion production rate,
h	is the altitude,
α	is the solar zenith angle,
q_0	is the ion production rate at $z = 0$,
z	is the scaled altitude,
h_0	is the reference height of maximum ion production when the Sun is at zenith ($\alpha = 0$), and
Δh	is the pressure scale height; and
e	is the base of the natural exponential function.

The rate of ion production q_0 is given by:

$$q_0 = \frac{\varnothing(\infty)\eta}{\Delta h.e} \tag{2.2}$$

where:

$\varnothing(\infty)$	is solar flux density outside the atmosphere in photons per unit area, and
η	is the number of ion pairs produced per photon.

To obtain the altitude of maximum ion production $h_{\max}$ the Chapman function (2.1) is differentiated, which yields:

$$h_{\max} = h_0 + \Delta h.In\sec\alpha \tag{2.3}$$

The vertex of ion production in the atmosphere is:

$$q_{\max} = q_0 \cos\alpha \tag{2.4}$$

As the ion-electron recombination rate is proportional to the square of the electron density N_e, the rate at which the electron density changes within the ionosphere is simply the difference between production and loss (recombination) rates (see section 2.1.4). By removing the transportation term, the following continuity equation holds:

$$\frac{dN_e}{dt} = q - \Omega N_e^2 \tag{2.5}$$

where:

Ω is the effective recombination coefficient for molecular ions.

It is important to note, that equation (2.5) is not valid at higher altitudes in the ionosphere with low electron densities, as the electron density N_e has a more linear relationship with loss rates (Davies, 1990).

In quasi-equilibrium, that is where $\frac{dN_e}{dt} = 0$, the electron density distribution at any height using the Chapman function (2.1) is:

$$N_e(z,\alpha) = N_{e,0} e^{1/2(1-z-\sec\alpha e^{-z})} \text{ where } N_{e,0} = \left(\frac{q_0}{\alpha}\right)^{1/2} \tag{2.6}$$

where:

$N_{e,0}$ is the electron density at $z = 0$.

The altitude of the maximum electron density and that of maximum ion production (2.3) are the same. The peak of electron density $N_{e,\max}$ is:

$$N_{e,\max}(\alpha) = N_{e,0} \cos^{1/2} \alpha \tag{2.7}$$

Figure 2.1 provides a graphical view of how the electron density varies with altitude according to the Chapman profile. It is produced assuming a reference altitude of h_0 = 350km, a scale height of Δh =100km and the solar zenith angle α =0. This conveys that the altitude of maximum ion production $h_{\max}$ (which can be clearly seen on the graph at 350km) is equal to the reference altitude h_0. The vertical electron density distribution was calculated using zenith angles α =0-85° in steps of 5° as in Schaer (1999).

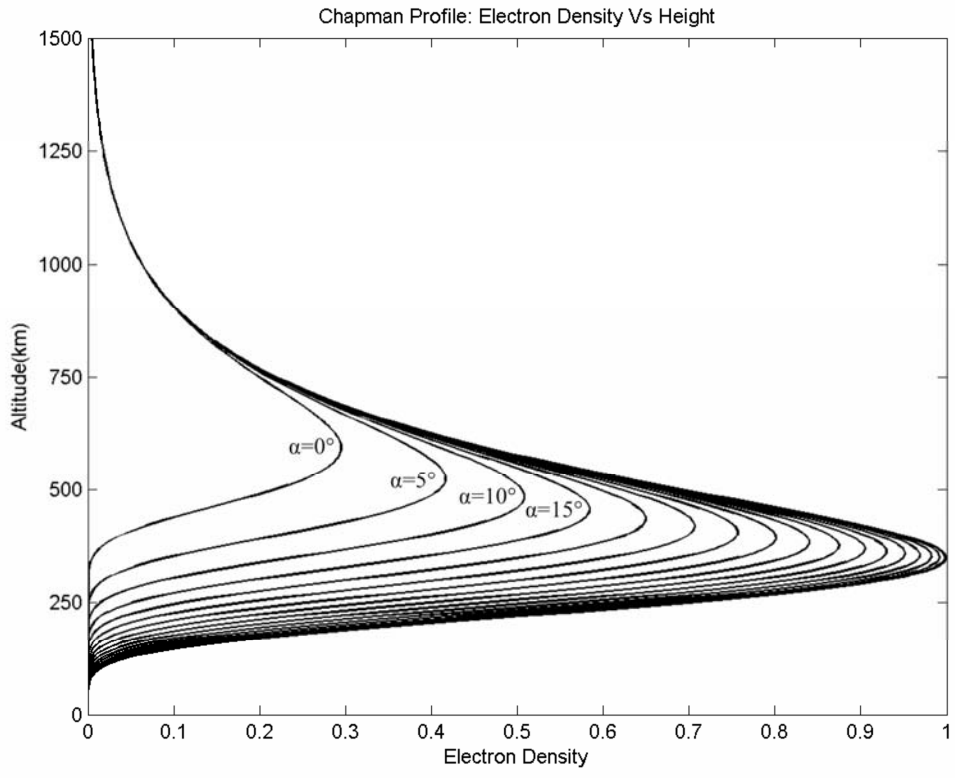

Figure 2.1 The vertical electron density distribution of a Chapman Layer for solar zenith angles of 0° through to 85°, in steps of 5°. (after Schaer, 1999)

From equation (2.7) it can be seen that the electron density is strongly correlated with the Sun's position and the solar zenith angle α. This indicates that both local time and season have a pronounced effect on electron concentrations (see section 2.1.2).

2.1.2 Integrated electron density

The electron density N_e within the ionosphere and its effect on electromagnetic waves that propagate through it has the most pronounced effect on GPS signals. The number of electrons encountered by an electromagnetic wave travelling through the ionosphere is commonly known as the total electron content (TEC), and is the integrated electron density along the signal path between the satellite and GPS receiver expressed in units of electrons per cubic metre (see Figure 2.2). The TEC is commonly expressed in TEC units (TECU), where one TECU corresponds to 10^{16} electrons contained in a cylinder with a one square metre cross section, that extends along the line of sight between the satellite and receiver. One TECU is equal to approximately 0.163m of range delay on the GPS L1 signal (Klobuchar, 1996). The typical TEC value experienced along the signal path between satellite and receiver has a low of 10^{16} and a high of 10^{19} electrons per m^2. A value of TEC greater than 10^{19} electrons per m^2 has never been recorded, even from a low elevation angle satellite during solar maximum conditions (see section 2.2). The TEC can either be expressed as the line of sight TEC (TEC along signal path) or it can be reduced to vertical TEC (VTEC) using a mapping function (see section 4.2.5). The line of sight TEC or slant TEC E is the integral:

$$E = \int N_e(\rho)\, d\rho \tag{2.8}$$

where

E in TECU is the number of electrons per square metre,

$N_e(\rho)$ denotes the electron density along the signal path,

The TEC is not a constant and is highly variable in both space and time, as it is linked to the varying electron density within the ionosphere (see section 2.1.5). The TEC

also depends strongly on the elevation angle of the satellite, as at low elevations the GPS signal has to pass through more ionosphere to reach the receiver.

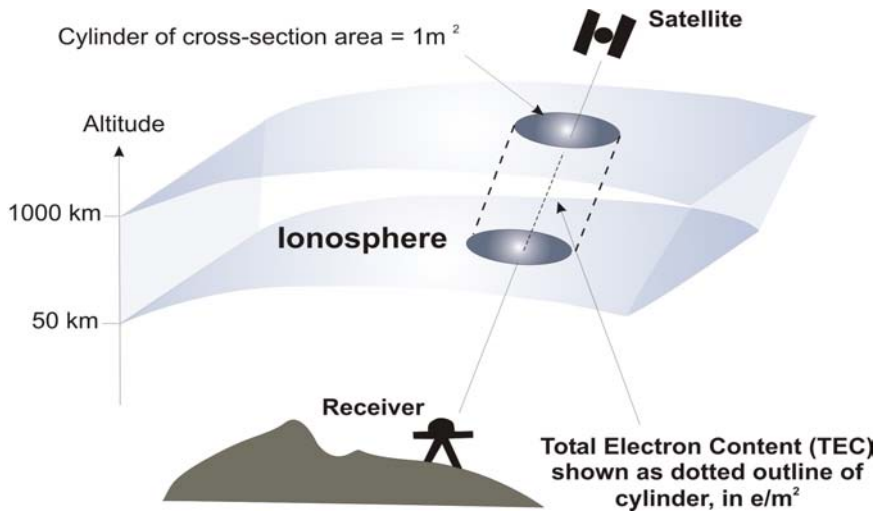

Figure.2.2 Illustration of concept of Total Electron Content (TEC) (after Komjathy,1997)

During solar maximum conditions, the VTEC may reach as high as 200 TECU. When applying the factor of 3 conversion (Spilker, 1980) or obliquity factor for low elevation angle GPS satellites, the slant range error due to the Earth's ionosphere can be as high as 100m.

2.1.3 The Earth's magnetic field

The Earth's magnetic field to first order approximation is that of a sphere, uniformly magnetised in the direction of a dipole axis (see Figure 2.3). This axis cuts the Earth's surface at points known as the boreal (north) and austral (south) dipole poles. The dipole axis is inclined at approximately 11° to the axis of rotation. Therefore, the geomagnetic equator, which is the plane through the centre of the Earth perpendicular to the dipole axis, will not coincide exactly with the geographic equator, which is why it is important to use geomagnetic field coordinates to describe or model the ionosphere. Scientists use dipole or dip latitude to describe the Earth's geomagnetic field. The dip poles are defined where the geomagnetic field lines are vertical and the dip equator where the field lines are horizontal with respect to the Earth's surface. The interested reader is referred to Tascione (1988) and McNamara

(1991) for a more detailed description of the relationships between geographic, geomagnetic and dip latitude.

The formation of the Earth's ionosphere is greatly affected by the Earth's magnetic field. The Earth is constantly being bathed in a steady stream of ionised plasma from the Sun. Much of this plasma, being transported by solar winds, is deflected by the Earth's magnetic field. However, some of this energised solar wind finds its way into the ionosphere and upper atmosphere via the auroral regions where ionisation takes place by energetic particle impact on neutral gases (see section 2.1.6.3). The Earth's magnetic field lines create a vast circulating system of ionised plasma in and around the Earth's nearby space environment. For a more detailed description of the interaction between the Earth's magnetic field and the ionosphere, the interested reader should look at such texts as Hargreaves (1995) and Kelley (1989).

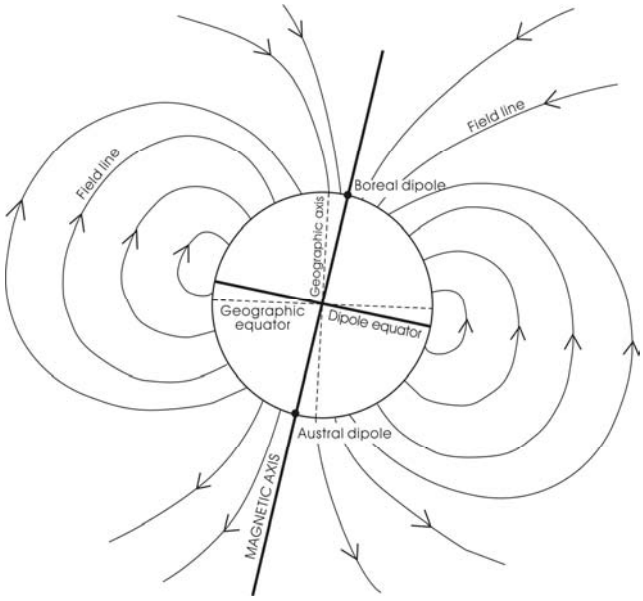

Figure 2.3 Simple Model of the Earth's Magnetic Field

2.1.4 The ionosphere in profile

Detailed explanations of the physical and chemical processes within the ionosphere are numerous and can be found in McNamara (1991), Davies (1990) and Kelley (1989) amongst others. This section will provide a short summary of these processes.

The ionosphere is that part of the Earth's atmosphere that lies between approximately 50-1000km above the Earth's surface. The ionospheric layer or plasma is formed by the interaction of the Sun's extreme ultraviolet (EUV) and X-ray radiation with different chemical regions within the Earth's atmosphere. This interaction has an ionising effect on the atoms or molecules in the atmosphere that causes the production of an abundance of free electrons, that affect the propagation of radio waves that pass through it (Langley, 1998). The extent of ionisation is dependent on temperature. If the temperature is low, the majority of the atoms within the plasma will remain neutral, however, if exposed to radiation (in the form of solar illumination), the atoms will absorb this energy and an ionising effect will take place (Ohanian, 1989). The temperature within the ionosphere can vary from 300°C in the lower regions, through to between 480-1230°C in the upper regions, depending on solar activity (Ivanov-Kholodnyi & Mikhailov, 1986).

In terms of altitude, the ionosphere may be subdivided into a number of different regions. These regions, known as the D, E, F1 and F2 regions are formed by their chemical components and their ability to absorb different wavelengths of radiation emitted from the Sun (Klobuchar, 1996), which causes a heterogeneous spread of ions and electrons in the upper atmosphere (see Figure 2.4). The two main emissions from the Sun that produce ionisation within the Earth's atmosphere (the breaking away of electrons from atoms and molecules) are that of Extreme Ultraviolet (EUV) and X-ray radiation (Rishbeth & Garriott, 1969). The more penetrating X-ray radiation has more of an effect on the lower regions of the ionosphere, whilst the EUV radiation, which is less intense, produces ionisation in the upper areas (Klobuchar, 1996). Ionisation can also be countered by a process known as recombination, where the ions and electrons rejoin to again form neutral atoms and molecules. As the absorption of EUV increases with decreasing altitude combined with the increasing number of neutral atmospheric molecules respectively, this results in the formation of a layer of maximum electron density. However, due to the different molecules and atoms within the atmosphere and their different rates of absorption, a series of defined layers exist with different electron densities.

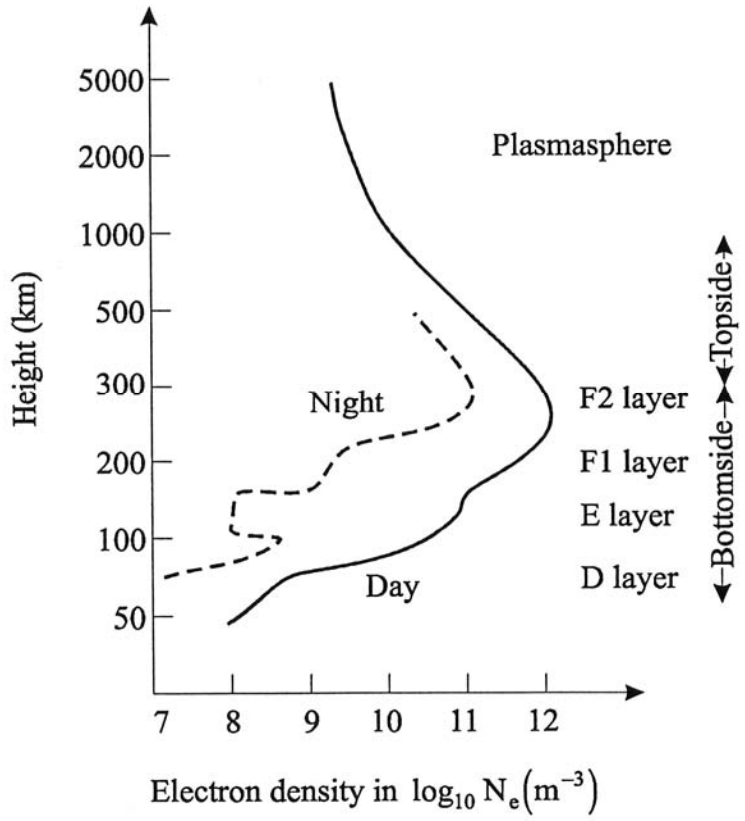

Figure 2.4 Typical vertical profile of the ionosphere (after Davies,1990).

The degree of ionisation caused by the Sun's electromagnetic radiation is also a function of path length through the atmosphere, which is related to the zenith angle. The Sun's rays can penetrate deeper into the atmosphere at zenith, therefore the process of ionisation will take place lower down into the atmosphere. This also means that there will be a concentration of ionised particles present around the Earth's equatorial region.

The critical frequency of an ionospheric layer is the minimum frequency of an electromagnetic wave that can penetrate a particular layer when vertically incident upon it (Hargreaves, 1995). These frequencies are denoted by foD, foE, foF1, and foF2 as representative of each layer. The maximum electron density of an ionospheric layer is linearly proportional to the square of the critical frequency, and are denoted by NmD, NmE, NmF1 and NmF2 respectively.

The solar zenith angle plays a primary role in the existence of the D, E and F1 regions, as this regulates the length of penetration of the Sun's rays into the Earth's atmosphere. These regions also show a strong diurnal, seasonal and latitudinal variation. In a diurnal sense, the D, E and F1 regions practically disappear or are greatly diminished during the night. This is due to the ceasing of the photoionisation process, and the taking over of recombination. The F2 layer is able to survive the night, although in a somewhat depleted fashion. During the winter months, the F1 layer completely disappears. The 11 year solar cycle has an enormous effect on the critical frequencies of each layer, by regulating the intensity of solar radiation that coincides with the period within each cycle. For a more detailed explanation the interested reader is refered to (McNamara, 1991), (Davies, 1990) and (Rishbeth & Garriott, 1969).

2.1.5 Ionospheric layers

The particular characteristics of each of the ionospheric layers, and their potential effects on GPS radio wave transmission are described as follows:

The D region, approximately 50-90km above the Earth's surface, forms the lower limits of ionisation within the Earth's atmosphere. It is formed by the absorption of hard solar X-ray emissions and solar Lyman radiation from the Sun. As the density of the air is still relatively high at this altitude, the ions and electrons present will recombine rather quickly. This means that the D layer shows a strong diurnal variation in electron density. It is present during the day-time hours, but disappears at night. Typical values at midday in the mid-latitude region range between 6.1×10^8 and 13.1×10^8 electron/m^3 according to solar activity. Therefore, this layer has little to no effect on GPS signal wavelengths.

The E region, is located approximately 90-140km above the Earth's surface. Its behaviour almost entirely depends on the zenith angle of the Sun and current solar conditions. This region is known for its normal E and sporadic-E region behaviour. The normal E behaviour is produced by the absorption of soft X-ray radiation from the Sun. This area of the ionosphere has been thoroughly studied over past decades, with vast amounts of vertical-incidence ionosonde data collected. Its behaviour can

be fairly well predicted in the context of current solar conditions, showing distinct solar cycle, seasonal and daily variations. The E layer practically disappears during the night.

Sporadic-E is the predominant variable feature in the otherwise quiet E-region. It is a transient slab of ionisation that is usually 1 to 2 km thick, with an electron density up to two to three times greater than that of the normal E layer. This phenomena can cause irregularities in the ionosphere and is often present in the auroral regions or areas of intense solar particle precipitation. Sporadic-E in the mid-latitudes is often associated with meteor showers and large thunderstorms, however, little is known about its connection with the latter. Apart from the possible scintillation effect of sporadic-E, this region also has little effect on GPS signal frequencies. Typical values at midday in the mid-latitude region range from $1.3x10^{11}$ to $1.7x10^{11}$ electrons/m^3.

During the daytime hours the F region is split in two, and produces the F1 and F2 regions. The F1 region is located approximately 140-210km above the Earth's surface. It is slightly less predictable than the previous E layer, however its density can be fairly well defined from known solar conditions. Ionisation at this altitude is caused by the absorption of EUV radiation by the molecular species found in this region. The F1 region is only present during the day, as the electron densities are primarily derived from the zenith angle of the Sun. Typical values at midday in the mid-latitude region range from between $2.3x10^{11}$ to $3.3x10^{11}$ electrons/m^3. This layer accounts for approximately 10% of the delay experienced by GPS frequencies (Klobuchar, 1996).

The F2 region is located approximately 210-1000km above the Earth's surface. Its peak density lies somewhere between 250-400km under normal conditions. The principle constituent of the atmosphere at this height is atomic oxygen. The F2 layer is formed by the ionisation of this chemical species via EUV radiation. This layer provides us with the maximum electron density within the ionosphere due to the combination of the absorption of EUV light and the increase of the neutral atmospheric density as altitude decreases. This region is highly variable and unpredictable. The F2 region provides most of the delay experienced by GPS frequencies. Typical values at midday in the mid-latitude region range from $2.8x10^{11}$

to $5.2x10^{11}$ electrons/m^3. The regions below the F2 layer (D, E and F1) are collectively known as the bottomside of the ionosphere, and the region above is called the topside.

The area above these layers is known as the Plasmasphere (or Protonosphere). This region extends out to approximately the height of the GPS satellites (about 20,000km above the Earth's surface) and is composed principally of ionised hydrogen. During the daytime hours, it is estimated that it contributes approximately 10% of the delay on GPS frequencies. However, it may contribute up to approximately 50% during the night time period, which coincides with the density of the F2 region being somewhat depleted (Kelley, 1989).

2.1.6 The ionosphere in zones of latitude

Globally, the ionosphere can be separated into three major regions, these being the equatorial, middle and high latitudinal regions. The following sections will give a brief overview of each region and their characteristic effects on GPS signals.

2.1.6.1 The equatorial region

It is in this region that the highest values of TEC are encountered as a result of stronger incident solar radiation that produces enhanced ionisation, along with the most disturbed ionospheric conditions, due to amplitude and phase scintillation effects (Fu *et al.*, 1999) (see section 2.3.3). In the equatorial and mid latitudes the process of *Photoionisation* is the primary source of ionisation (Rishbeth & Garriott, 1969). This process involves the creation of ion-electron pairs by the absorption of solar extreme ultraviolet and X-ray radiation from the Sun, by neutral atoms and molecules.

A significant feature of this region is the equatorial or Appleton anomaly (Appleton, 1954). This anomaly is characterised by two electron density maxima, located approximately 10° to 20° degrees either side of the magnetic equator. This is due to a zonal electric field being produced at the equator by global tidal winds that travel in

an east-west direction. This results in the equatorial plasma being lifted away from the magnetic equator due to *E* x *B* forces (*E* being the electric field vector and *B* the magnetic field vector) to higher than normal altitudes. This upward lift is eventually turned by gravity, which pulls the plasma down along the magnetic field lines, thus depositing plasma to the north and south of the magnetic equator. This results in large concentrations of ionised plasma in these regions. The daily equatorial anomaly generally starts to develop around 0900 local time, reaching its maximum at approximately 1400-1500 hours. During solar maximum periods however, this peak may occur at approximately 2100 hours local time, with scintillation effects occurring predominantly in the post sunset periods between 2000 – 0200 local time (Basu *et al.*, 1988).

2.1.6.2 The mid-latitude region

The mid-latitude ionosphere is the most studied region of all the ionospheric regions, as most of the ionospheric observations are taken by instruments located in countries situated in this region. The mid-latitude ionosphere is also the most undisturbed and least variable of all the regions, it acts as a buffer between the high-latitude processes and low-latitude phenomena (as previously discussed). The diurnal variation of the total electron content (TEC) in this region is characterised by a minimum just before sunrise and a maximum between approximately 1400-1500 hours local time. The most noticeable characteristic of the TEC is the large day-to-day fluctuation around the monthly mean values. This value can reach 20% during the day and 25% during the night-time periods (Klobuchar, 1978).

2.1.6.3 The high-latitude region

The high-latitude ionosphere can be divided up into the auroral and polar cap regions, with another region also existing on the equatorward side of the auroral zone, known as the ionospheric trough (Kunitsyn & Tereshchenko, 2003). The divisions in this area are brought about by the structure of the Earth's geomagnetic field.

Photoionisation by ultra violet and x-ray radiation is not the only source of ionisation in the ionosphere. At high latitudes, ionisation by energetic particle impact on neutral gases plays an important role (Kelley, 1989). Energetic particles emitted from the Sun are trapped within the Earth's magnetic field, and travel towards the high latitude ionosphere along magnetic field lines. On impacting with the ionosphere, small scale irregularities in electron concentrations are experienced (Nichols *et al.*, 1999). This phenomena results in optical and UV emissions that are commonly known as the aurora borealis/australis (northern and southern lights respectively) and are usually confined within a narrow band of approximately 65°-75° geomagnetic latitude, but can extend several degrees equatorward under severely disturbed ionospheric conditions. Therefore, the electron density at high latitudes does not just depend on the position of the Sun in the sky, but also on what particles are arriving from the Sun. Ionospheric activity in this region can be regarded as an interaction between the magnetosphere, ionosphere and atmosphere. Scintillation effects are also common in this region due to the irregularities in the electron densities caused by the localised energetic particle interaction with the ionosphere's neutral gases. The strength of high latitude scintillation is directly correlated with solar activity (see section 2.3) and the 11 year solar cycle (see section 2.2).

The polar cap region lies at latitudes of approximately 75° and above and is enclosed by the auroral rings. Not a lot is known about this region of the ionosphere due to a lack of available data. Suffice to say that the morphology of the ionosphere in this region is linked to the Earth's magnetospheric process and solar inputs. This makes the polar ionosphere largely affected by solar events. Polar region scintillation activity is a relatively poorly researched area.

There is a region of depleted electron density located on the equatorial side of the auroral regions, which is known as the *mid-latitude trough.* This trough appears in both hemispheres in all seasons and is essentially a night-time occurrence (Hargreaves, 1995). The trough serves as a boundary between the mid-latitude and high-latitude ionospheric regions (Thomas & Dufour, 1965). It is characterised by a drop in electron density by a factor of two or more (Komjathy, 1997), due primarily to increased recombination resulting from shorter daytime ionisation periods at high latitude (Tascione, 1988).

2.2 The solar cycle

As the ionisation of the ionosphere is predominantly driven by the interaction of the Sun's emissions with the Earth's atmosphere, solar activity plays a key role in this process. The regular variation of solar activity or intensity is known as the solar cycle. The solar cycle has an average period of eleven years, with each cycle being defined as starting with a solar minimum and lasting until the following solar minimum. The typical solar cycle takes four years to rise from solar minimum to solar maximum, and then approximately seven years to fall back to solar minimum. Sunspots (see section 2.2.1.2), first noticed by Theophrastus around 325 BC, are a very noticeable phenomena on the solar surface, and the periodic variation of their numbers, that coincides with the eleven year solar cycle (see Figure 2.5), historically characterises solar activity.

It can be clearly seen from Figure 2.5 that all solar cycles do not have the same number of sunspots at solar maximum. It varies from cycle to cycle. Solar cycle number 19, that peaked in 1957 was the highest ever observed, with a sunspot number of approximately 200. Higher numbers of sunspots relate to other significant physical quantities that have a direct effect on the ionosphere and subsequently the GPS signals that pass through it. The rate of Coronal Mass Ejections (CMEs)(see section 2.3.1) and the level of extreme ultraviolet flux are both a function of sunspot counts. Both of these phenomena cause variations and disturbances in the Earth's ionosphere, that affect a GPS receiver's ability to track satellites and remove ionospheric range delay (Bishop *et al.*, 1996). At a typical mid-latitude station the daily variability of TEC at solar minimum is in the order of 10 TECU, whilst at solar maximum that variability may get up to 100 TECU (Kunches, 2000).

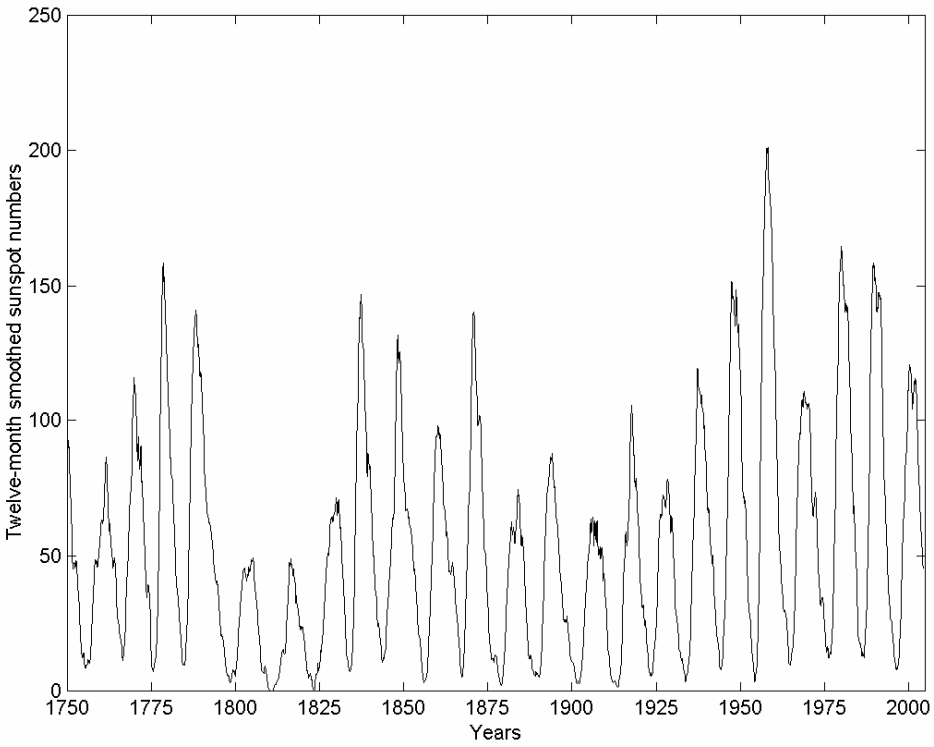

Figure 2.5 Solar cycles 1 through to 23

2.2.1 Solar-Terrestrial indices

Solar and geomagnetic indices, which are adopted internationally, are used as a means of measuring the current disturbance levels in the atmosphere. Most empirical or physical ionospheric models require the input of solar indices as an indicator of current ionospheric conditions. These indices can either be derived from ground based measuring equipment that probe the atmosphere on a continual basis, or they can be derived from continuously monitored parameters.

2.2.1.1 Kp and Ap indices

The K and A indices, are the two indices that are used to determine the level of geomagnetic activity. They relate the severity of magnetic fluctuations within the Earth's atmosphere, and hence the disturbance to the ionosphere.

The K index is designed to measure the irregular variations within the Earth's magnetic field. Each observatory measures the differences in the X, Y, and Z components of the Earth's magnetic field, at three hourly intervals during the day, starting at 00 hours UT, on a scale from 0 to 9. These measurements are associated with variations from a quiet day curve for a particular observatory, with the range R between the largest and smallest deviations of the three geomagnetic field components (the most disturbed element) measured in gammas defining a particular K value. The Kp index is a planetary average of the K index. It is derived from 13 observatories located between 46° and 63° north and south geomagnetic latitude, that all measure the ranges in the geomagnetic field components at three hourly intervals. Each observatory adopts its own K scale, which differs between observatories. This planetary three hour Kp index is designed to give a general indication of the world wide level of geomagnetic activity. The Kp index is expressed in 28 intervals from 0 (quiet) through to 9 (highly disturbed) with its fractional parts being expressed in thirds of units.

In some instances a daily average of geomagnetic activity may be required. As the K index is quasi-logarithmic, it is not suitable for averaging. In order to gain a daily average of geomagnetic activity, the "equivalent planetary amplitude" of the geomagnetic field variation "Ap" is derived from Kp, using Table 2.1 below. The daily Ap index is derived from the average of eight Ap values. A 12 month time series, from August 2001 to July 2002, of Ap index data can be seen in Figure 2.6. A strong seasonal variation of the geomagnetic field can be clearly seen, with peaks forming in the March-April and September-October periods. The data was obtained from the National Oceanic and Atmosphere Administration (NOAA) National Geophysical Data Center (NGDC).

Table 2.1 Equivalent range Ap for a given Kp

Kp	0o	0+	1-	1o	1+	2-	2o	2+	3-	3o	3+	4-	4o	4+
Ap	0	2	3	4	5	6	7	9	12	15	18	22	27	32
Kp	5-	5o	5+	6-	6o	6+	7-	7o	7+	8-	8o	8+	9-	9o
Ap	39	48	56	67	80	94	111	132	154	179	207	236	300	400

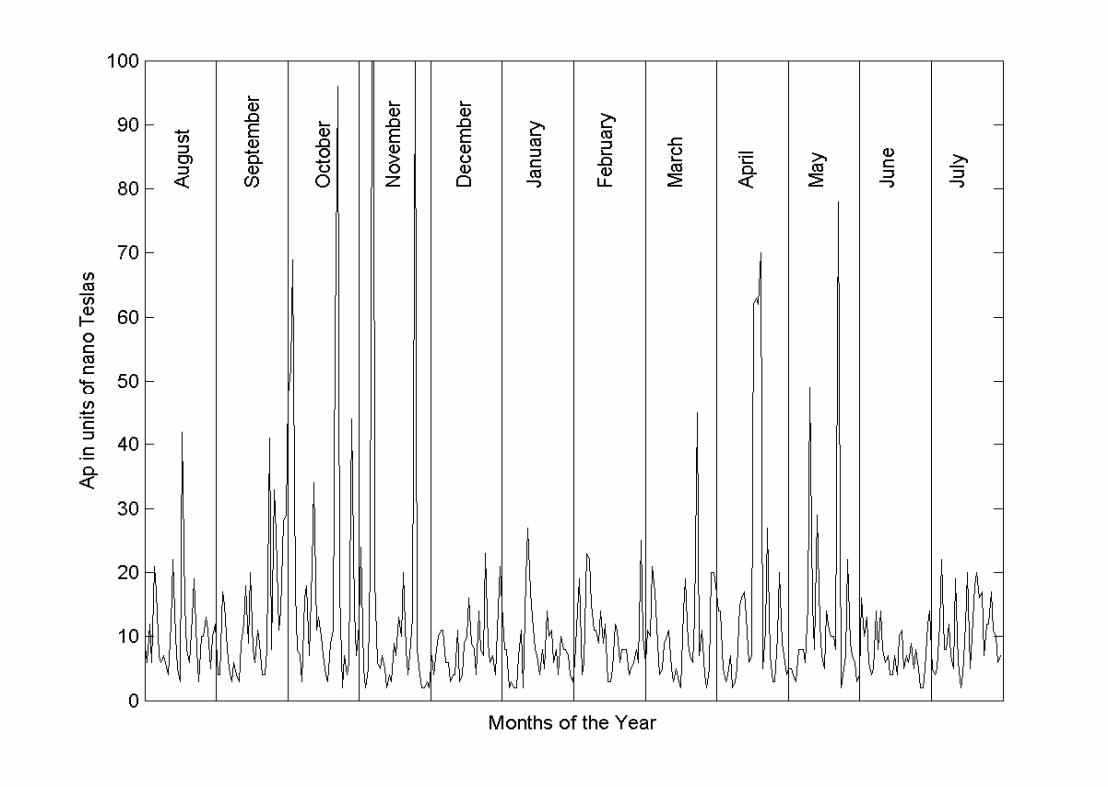

Figure 2.6 Ap index August 2001 to July 2002

2.2.1.2 Zurich sunspot number

A sunspot appears as a dark area on the visible surface (photosphere) of the Sun. Sunspots tend to group together in bipolar clusters, having both positive and negative magnetic polarities. They are also characterised by strong magnetic fields that may approach 4000 G. Sunspots appear dark because they are cooler than the surrounding photosphere. As mentioned in section 2.2, the occurrence of sunspots follows a cyclical pattern that is known as the solar cycle. As sunspot numbers increase so does solar activity and the intensity of extreme ultraviolet (EUV) flux. As the number of sunspots increase at solar maximum their magnetic complexity grows, and they become the likely catalyst for such solar events as CMEs and solar flares. As for many years the solar sunspot numbers were derived from the Zurich Observatory, the daily index of sunspot activity (R) is known as the Zurich sunspot number. The daily sunspot index (R) is defined as:

$$R = k(10g + s) \tag{2.9}$$

where:

R is the daily sunspot number;
g is the number of sunspot groups;
s is the number of observed individual sunspots; and
k is an observatory factor.

At present there are two official sunspot numbers in use. The first is the daily Boulder Sunspot Number, which is computed by the NOAA Space Environment Centre. The second is the International Sunspot Number, which is published by the Sunspot Index Data Centre (SIDC) in Belgium. The same formula as above is used to compute both values, but the published values from both sites may be slightly different due to the fact that they incorporate data from different observatories.

The life-span of a sunspot is highly variable. Some sunspots only last for a few days, whilst others can survive for several solar rotations of approximately 27 days. The solar cycle activity for the last five cycles can be seen displayed in Figure 2.7 in the form of the twelve month smoothed sunspot number (SSN). Due to the large day to day variations in sunspot number, the sunspot data is smoothed over 12 months in order to emphasize the trends. This smoothing is achieved by taking the average of the sunspot values over 13 months, centred on the month of interest. At the time of writing, we are on the downward side of solar cycle 23. By measure of the sunspot number, the current solar cycle started in May 1996, with the SSN rising steadily to a peak in April of 2000 with a value of 121. However, the largest monthly value was recorded in July 2000 with a value of 171. The SSN then proceeded to decline steadily until March 2001 where it began to climb again, reaching a second peak of 116 in November 2001, still somewhat short of the April 2000 value of 121. Historical records indicate that many solar cycles have a second peak, as displayed in the current cycle. The data was obtained from the National Oceanic and Atmosphere Administration (NOAA) National Geophysical Data Center (NGDC).

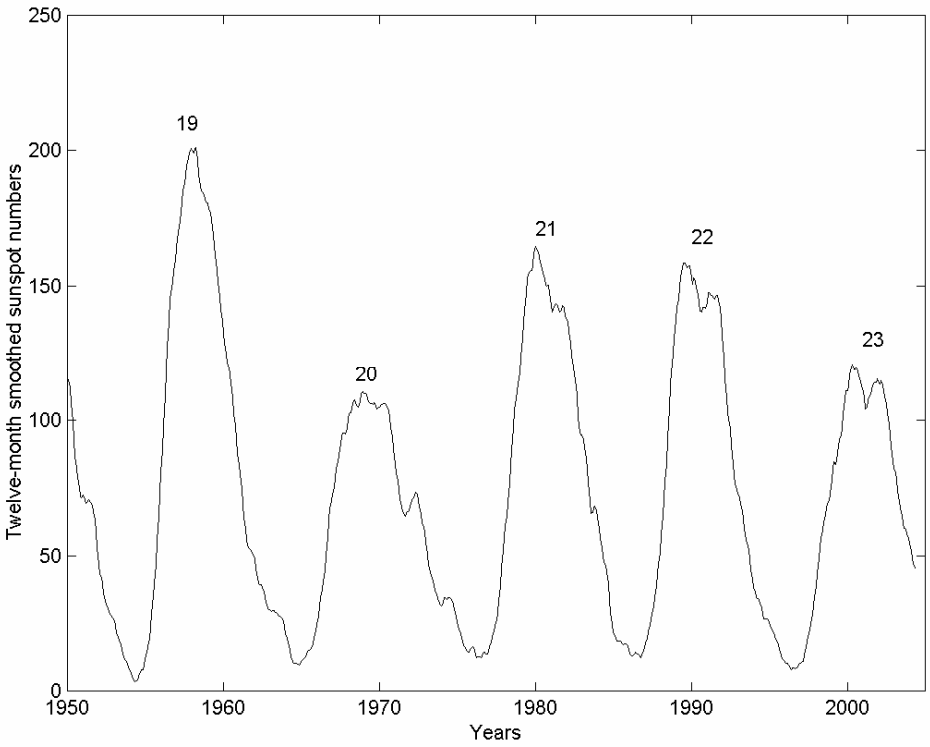

Figure 2.7 Solar sunspot activity during the last 5 solar cycles.

2.2.1.3 Ottawa 10.7cm (2800MHz) solar flux

The Sun is a source of radio noise that varies slowly in intensity. This radio flux emission from the Sun varies from day to day and tracks closely with the solar cycle and sunspot activity. The daily full disk radio flux measured at a wavelength of 10.7cm (2800MHz) is routinely monitored by radio telescopes and reported in flux units of 10^{-22} W/m^2-Hz. Its intensity varies from a minimum of 65, at low solar cycle, to approximately 200, in the solar maximum period. The observed measurements are adjusted to 1 AU (mean Earth-Sun distance). This radio flux emission is highly correlated with sunspot number, and is one of the most widely used and available indicators of the level of solar activity. Measurements of radio flux were initially taken in the Ottawa region, from 1947 through to 1990. The program was then relocated to Dominion Radio Astrophysical Observatory, Penticton, British Columbia. The daily values from August 2001 to July 2002 can be seen in Figure 2.8. The data displayed was taken during a solar maximum period. The 27 day solar rotation period can be

clearly seen in the figure. The data was obtained from the National Oceanic and Atmosphere Administration (NOAA) National Geophysical Data Center (NGDC).

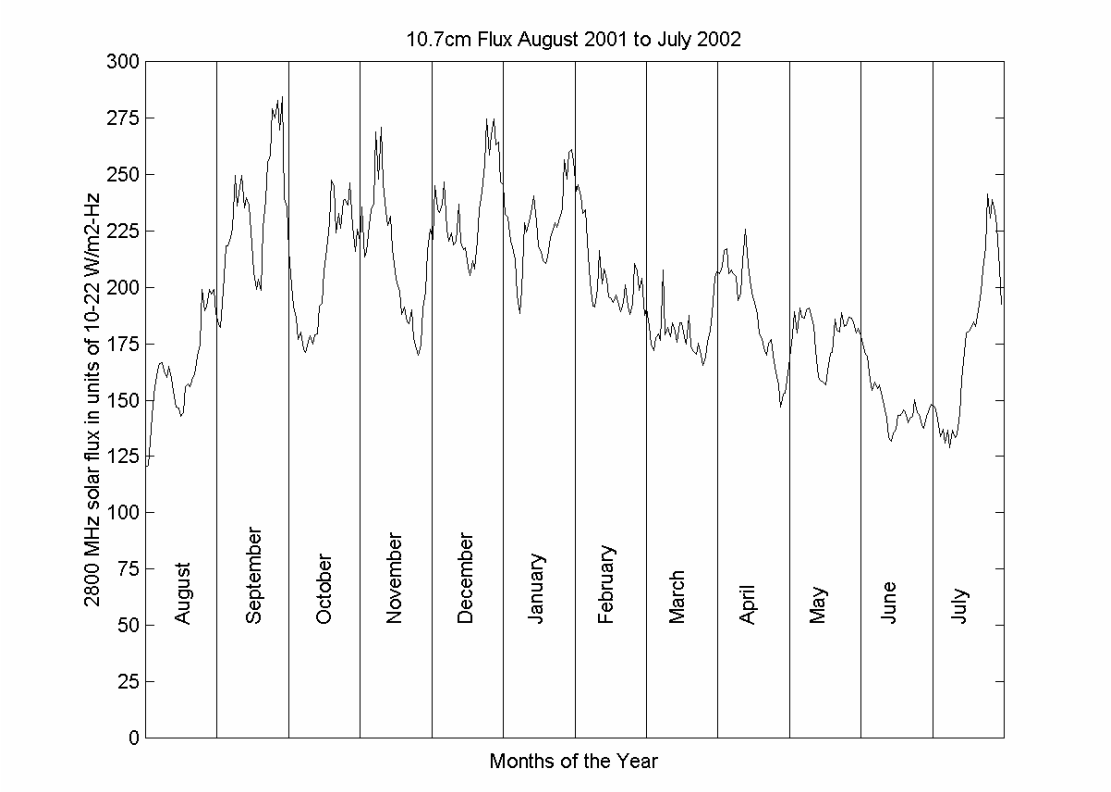

Figure 2.8 Observed daily solar flux variation

2.2.1.4 IG index

The International Global (IG) index is a derived ionospheric index that is independent of sunspot number and is referred to as the global effective sunspot number (Liu *et al.*, 1983). The IG index is computed using the observed noontime monthly median values of foF2 (F2 critical frequency), by thirteen ionosonde stations located world wide. Based on this median value, the IG index is derived by determining what value of sunspot number is required to determine the observed foF2 values from the global foF2 numerical coefficient maps supplied by the Comite Consultatif International des Radiocommunications (CCIR) (Davies, 1990). The IG index has been found to be better correlated with foF2 than sunspot number (Liu *et al.*, 1983).

These coefficient sets are based on ionosonde measurements taken between 1954-1958, for both low (12 month smoothed sunspot number of 0) and high (12 month smoothed sunspot number of 100) solar activity periods. They provide a means for making worldwide predictions of ionospheric conditions, by incorporating the relationship between solar conditions (ie. IG index or SSN) and the forecasting of foF2 (see section 2.1.4) and maximum usable frequency (MUF) values (see section 4.1.2). For a more detailed discussion on how these coefficient sets are used by ionospheric models to predict TEC values, based on geographical location, date, universal time (UT) and solar index, see Chapter 4.

2.3 Ionospheric disturbances

An ionospheric disturbance can be classifed as any deviation in the ionosphere from its usual or quiet state. These ionospheric disturbances can occur as a result of both solar or geomagnetic field disturbances. Ionospheric disturbances are linked either directly or indirectly with the events on the Sun. The Earth's magnetic field is also affected by solar events, where the geomagnetic field lines surrounding the Earth are compressed, causing geomagnetic disturbances.

2.3.1 Ionospheric storms

Large ionospheric storms occur relatively infrequently. They can be caused by intense solar eruptions that release energetic particles out into the atmosphere. These eruptions are also known as solar flares. They represent the most direct influence of solar activity on the near Earth space environment, have a large impact on ionospheric conditions that can interfere with such things as radio and satellite communications, threaten astronauts and destroy satellite electronics. Solar flares have three major effects on the ionosphere, with each effect being caused by the type of emission from the flare. Solar flares emit X-ray radiation, protons and plasma clouds. X-rays can penetrate as far down into the Earth's ionosphere as the D-region causing increased ionisation via the process of photoionisation (see section 2.1.5). Solar flares can increase the electron density in the D-region by a factor of 10 and as a result cause the phenomenon known as shortwave fadeout. Some very energetic

solar flares can emit a stream of protons that can hit the Earth if projected in the right direction. On arrival at the Earth's upper atmosphere these protons encounter the Earth's magnetic field, which causes the protons to spiral down the magnetic field lines at high latitudes deep into the ionosphere, where a dramatic increase in the D-regions electron density is produced via the process of collisional ionisation (see section 2.1.6.3). These events are known as polar cap absorption events. Solar flares can also cause ionospheric storms. When a solar flare is large enough it can release a large cloud of plasma that can hit the Earth and severely alter the state of the ionosphere. This altered state can present itself as sudden, unpredictable changes in the F2 layer critical frequency (foF2). Once the plasma cloud impacts with the Earth's atmosphere, whether the critical frequency is increased or decreased depends upon such factors as local time, season, geographical location (latitude) and the storm duration.

Coronal mass ejections that cause High Speed Solar Wind Streams (HSSWS) can be another source of ionospheric disturbance. Coronal holes are open structures in the solar corona where the Sun's magnetic field lines stretch out into interplanetary space. As ionised material can travel easily along field lines, this material can pour out into space towards the Earth, causing ionospheric storms. The impact on the ionosphere of HSSWS is not as pronounced as that of a large solar flare, partly because the HSSWS does not overtake the Earth as fast as the cloud from a solar flare hits it. Prominences or sudden disappearing filaments can be another trigger for an ionospheric storm. They are large clouds of solar material that are held above the Sun's surface by its magnetic field. When these prominences erupt, large amounts of solar material are released into space, similar to a solar flare, affecting the Earth's geomagnetic field (Tascione, 1988; Davies, 1990; McNamara, 1991).

2.3.2 Geomagnetic storms

The Earth's magnetic field is also affected by the same solar phenomena that produces ionospheric storms. Geomagnetic storms usually occur in tandem with ionospheric storms and can be caused by solar flares, high speed solar wind streams (coronal holes) and sudden disappearing filaments. The level of intensity of a geomagnetic storm can be measured using the K index (see section 2.2.1.1), which

is a measure of the level of disturbance in the Earth's magnetic field over a three hour period. Geomagnetic storms are commonly associated with an increase in the electron densities in the lower ionosphere and an increase in the absorption of radio waves. A geomagnetic storm usually begins with a sudden increase in the Earth's geomagnetic field intensity. This sudden increase is known as the initial phase and is followed by a large decrease known as the main phase, and then by a recovery phase, where the geomagnetic field returns to normal after two or three days. Geomagnetic storms that commence with a sudden increase at the start of the initial phase are typical of storms produced by a solar flare. These storms arise as a result of the shock front from the solar flare hitting the Earth's geomagnetic field and suddenly compressing it. Storms that are produced by high speed solar wind streams on the other hand, are known as gradual commencement storms. They start off gradually as the high speed solar wind stream overtakes the Earth, and tend to reoccur every 27 days or so, following the Sun's rotation (Tascione, 1988; Davies, 1990; McNamara, 1991).

2.3.3 Ionospheric scintillation

As a result of electron density irregularities in the ionosphere, that can range from a few metres to a few kilometres, radio signals that pass through the ionosphere may experience rapid fluctuations in amplitude, phase and the angle of signal arrival. These fluctuations in signal integrity, due to small scale ionospheric density irregularities, are called ionospheric scintillations (Nichols *et al.*, 1999). These fluctuations are due to both refraction and diffraction effects on the electromagnetic waves as they propagate through the ionosphere. Refraction occurs when an electromagnetic wave is bent when the wave front moves from one media to another with different propagating velocities (Serway, 1987). This can occur when a propagating wave travels through the ionosphere and comes into contact with localised ionospheric disturbances. Ionospheric scintillation effects are at their maximum during high solar activity periods in the equatorial anomaly regions (see section 2.1.6.1) during the evening hours. The auroral and polar cap regions are also significantly affected at geomagnetically disturbed periods. The mid-latitude regions will only be affected on rare occasions, during high solar activity periods and during extremely disturbed geomagnetic conditions (Doherty *et al.*, 2000). Scintillation

activity has been shown to vary with signal operating frequency, geographic location, local time, season, geomagnetic activity and the eleven year solar cycle (Aarons, 1982; Basu *et al.*, 1988; Aarons, 1993;, 1995). Amplitude scintillation, or fading, in severe cases can be at such a level that signal levels drop below a GPS receiver's lock threshold, causing the receiver to reacquire the satellite signal. The deepest fades in amplitude are experienced in the equatorial anomaly regions, where the degradation in signal strength can reach 20dB below the mean signal level. Phase scintillation occurs due to regions of small scale electron density irregularity, where rapid changes in signal phase may occur. This phenomena can cause a doppler shift in the GPS signal, which may exceed the bandwidth of the receiver's phase lock loop, that results in loss of phase lock which can produce cycle slips in GPS data.

2.4 The propagation of GPS signals in the atmosphere

This section will look into the effect the atmosphere has on the propagation of GPS signals. The concept of geometric optics is used as we are only concerned with the geometric effects of the atmosphere on electromagnetic signals. This concept assumes that any changes in the Earth's atmosphere within 1 wavelength (approximately 20cm for GPS signals) of the signal will be infinitesimal. As the GPS signal wavelength is so short the effect of signal absorption is not relevant and will not be covered.

Electromagnetic waves with frequencies below 30 MHz are reflected by the ionosphere, highlighting the importance of the ionosphere in radio communications. At frequencies above 50 MHz, electromagnetic waves are able to penetrate the ionosphere. The ionosphere in this instance is a source of nuisance for ground to satellite communications and is the reason why the developers of space based communication systems prefer to use high frequency bands in order to reduce the effect of the ionosphere.

The effect that the ionosphere has on radio signals with frequencies above 100 MHz has been studied in detail by several authors, including Hartmann & Leitinger (1984). The most relevant results are summarized below.

The refractive index n describes the ratio of the speed of propagation in a vacuum to the speed in a medium. It is defined as:

$$\mathrm{n} = \frac{\mathrm{c}}{\mathrm{v}} \tag{2.10}$$

where:

c is the speed of light in a vacuum, and
v is the speed of the electromagnetic wave in the medium.

As an electromagnetic wave travels through the atmosphere from transmitter (satellite) to receiver it is affected by atmospheric refraction, thus distorting the true geometric distance between the satellite and receiver. In a homogeneous medium, light (and electromagnetic waves) will travel from A to B based on Fermat's Principle. This principle states that when light travels between any two points, its actual path will be the one that requires the least time, this being a straight line. However, in a refractive medium, its path from A to B is bent. This excess distance in the signal path due to atmospheric refraction consists of two parts. These are, a propagation effect ($v_{\theta,j}$) and a bending effect ($\kappa_{\theta,j}$). The optical path length between the satellite and receiver using phase measurements ($l_{\theta,j}$), as derived in Gu and Brunner (1990), is given by:

$$l_{\theta,j} = \rho + v_{\theta,j} + \kappa_{\theta,j} \tag{2.11}$$

where:

ρ is the geometric distance between the satellite receiver,
$v_{\theta,j}$ is the propagation or path delay due to the ionosphere, and
$\kappa_{\theta,j}$ is a correction for curvature.

The optical path length equation for the code measurements signifying the signal group delay can also be written as above by changing the subscript θ to g.

When dealing with GPS observations, it needs to be taken into account that its signal carriers are propagating with phase velocity and the codes propagating with group velocity. In a refractive medium, we therefore need to determine a refractive index for both the carrier phase and code measurements. When considering the presence of charged particles, the problem of atmospheric refraction of GPS signals can be divided into two components: i) ionospheric refraction, and ii) tropospheric refraction. The effect of the troposphere is frequency independent of the signals that propagate through it, it has a refractive index of, $n_{trop}>1$, which means that the wave is advanced through the medium. The ionosphere on the other hand has a frequency dependent effect on the signals that propagate through it. It has a refractive index of, $n_{ion}<1$ for phase, which means that carrier is advanced, and $n_{ion}>1$ for the code, which means that the code measurements are delayed.

In order to adequately describe the behaviour of electromagnetic waves that propagate through the ionosphere we need to understand that the refractive index of the ionosphere is not constant. This is due to the fact that the ionosphere is a very complex structure that is influenced by many phenomena. The ionosphere can be described as heterogeneous, as it is made up of a number of horizontal layers with different electron densities. These layers are also subject to non-uniform irregularities (see section 2.3.3) that as a consequence vary the ionospheric refractive index in a spatial context. The Earth's non-uniform geomagnetic field, which is itself distorted by solar effects (see section 2.1.3), is a birefringent medium which means that it has the effect of splitting a propagating electromagnetic signal into two opposite rotating wave fronts. These are: a left hand circular polarised mode (extraordinary wave) and a right hand mode (ordinary wave). These waves have different refractive indexes due to their slightly different propagating velocities. On reception of GPS signals, the ordinary wave is the only one considered, as the extraordinary wave is irrelevant, due to the fact that it only contributes 0.35% of the power within the GPS antenna for L1 (Bassiri & Hajj, 1993). As the refractive index of the ionosphere is frequency dependent, this implies that it is a dispersive medium. As discussed in the previous paragraph the phase ($v_{\theta,j}$) and the group ($v_{g,j}$) velocities of a propagating wave are different within the ionosphere. The relationship between the phase and group velocities is defined by the Rayleigh equation shown below: see Hall et al.(1996)

$$v_{g,j} = v_{\theta,j} + f_j \frac{\partial v_{\theta,j}}{\partial f_j} \tag{2.12}$$

where:

f is the frequency of the electromagnetic wave.

2.4.1 The refractive index of the ionosphere

The complex refractive index n of the ionosphere is given by the Appleton-Hartree magnetoionic dispersion formula (Davies, 1990; Langley, 1996). When ignoring absorption effects due to electron collision:

$$n_{ion}^2 = 1 - \frac{2X(1-X)}{2(1-X) - Y_T^2 \pm \left[Y_T^4 + 4(1-X)^2 Y_L^2 \right]^{1/2}} \tag{2.13}$$

where:

$X = \frac{f_N^2}{f^2}$ where f is the frequency of the propagating wave, f_N is the electron plasma frequency,

$Y_L = \frac{\omega_L}{\omega}$ where ω is the angular frequency of the propagating wave (radians), ω_L is the angular gyrofrequency,

$Y_T = \frac{\omega_T}{\omega}$ where ω_T is transverse angular gyrofrequency.

The positive and negative signs in the above equation (2.13) denote the previously discussed behaviour of an electromagnetic wave propagating through a birefringent

medium (ionosphere). The wave is split into two opposite rotating wave fronts, these being that of an ordinary wave '+' and an extraordinary wave '-'.

Following the work of Bassiri & Hajj (1993) and Brunner & Gu (1991), equation (2.13) can be expanded to form a series of up to the 4th inverse power of frequency $\left(\frac{1}{f^2}\right)$. This equation includes all the terms whose magnitude is greater than one ppb (part per billion) for GPS observations.

$$n_{ion} = 1 - \frac{C_X}{2} N_e v^{-2} \pm \frac{C_X C_Y}{2} N_e H_0 \cos\theta v^{-3} - \frac{C_X^2}{8} N_e^2 v^{-4} \qquad (2.14)$$

where:

$C_X = \frac{e^2}{4\pi^2 \varepsilon_0 m_e} \approx 80.6 m^3 s^{-2}$ using the natural constants listed below,

$$C_Y = \frac{\mu_0 e}{2\pi m_e}$$

where:

N_e	is the electron density,
H_0	is the strength of the magnetic field,
θ	is the angle between the vector of the geomagnetic field and the path projected by the propagation direction of the electromagnetic wave,
e	is the charge of one electron which is equal to 1.60218×10^{-19} Coulomb,
ε_0	is the permittivity of the vacuum which is 8.85419×10^{-12} Farad/metre,
m_e	is the mass of one electron which is equal to 9.10939×10^{-31} kg,
μ_0	is the permeability in the vacuum,
v^{-2}	is the reciprocal square of the operating frequency $\frac{1}{f^2}$

As the third and fourth order terms in equation (2.14) are orders of magnitude smaller than the second term, they are usually ignored. By neglecting these higher order terms, we could introduce an error of approximately 4cm when using the 'ionospheric free' linear combination (see section 3.2.8.6.1) of GPS observables (Bassiri & Hajj, 1993). This is however, an approximation of the absolute ionospheric refraction error in the line of sight between the satellite and receiver, and is not a true reflection of the accuracies achievable when using double differenced GPS observations in the 'geometry free' linear combination (see section 3.2.8.6.2). When using GPS in differential mode (see Section 3.2.8.2) for geodetic surveying applications, it is possible to measure the change in the ionosphere to within approximately 2mm accuracy (Schaer, 1999).

By ignoring the third and fourth order terms in equation (2.14) when both electron collisions and the Earth's magnetic field are negligible, equation (2.14) can be reduced to:

$$n_{ion} = 1 - \frac{C_X}{2} N_e v^{-2} \tag{2.15}$$

Therefore, by taking into account the different refractive indices for the phase and code GPS observations, as discussed above, the refractive index for GPS observations can be defined as:

$$n_{ion}^{p} = 1 - \frac{40.3 N_e}{f^2} \tag{2.16}$$

$$n_{ion}^{g} = 1 + \frac{40.3 N_e}{f^2} \tag{2.17}$$

where:

n_{ion}^{p} is the refractive index for phase observations,

n_{ion}^{g} is the refractive index for code observations,

The geometric range between the satellite S and receiver R is given by the integration of either equations (2.16) or (2.17) along the path followed by the GPS radio signal, in the form:

$$\rho^p = \int_R^S \left(1 - \frac{40.3N_e}{f^2}\right) ds = \rho - d_{ion} \qquad (2.18)$$

or

$$\rho^g = \int_R^S \left(1 + \frac{40.3N_e}{f^2}\right) ds = \rho + d_{ion} \qquad (2.19)$$

where:

ρ is the geometric range between the satellite and receiver,

We can therefore obtain the first order ionospheric distance correction Δd_i^{ion} for GPS observations (Spilker, 1980) as a function of electron density N_e or TEC along the signal path as:

$$\Delta d_i^{ion} = \pm \frac{40.3N_e}{f_i^2} \qquad i = 1, 2 \qquad (2.20)$$

where:

Δd_i^{ion} is the ionospheric range correction for frequency i,

f_i is the operating frequency of the GPS carriers $i = 1, 2$;

$+$ is the sign for code observations, and

$-$ is the sign for phase measurements.

2.5 Summary

The ionosphere is a very complex structure that is influenced by many phenomena. In order to produce an ionospheric model, it is essential, at the very least, to have a firm understanding of the ionosphere's physical makeup, together with its spatial and temporal characteristics. In the first section, this chapter provided an overview of the ionosphere's chemical makeup, its different structural layers in altitude and how its characteristics change in a geographical and temporal sense. This overview also included an investigation into the relationship between the Sun's activity and the Earth's magnetic field and how this interaction influences the level of disturbance in the Earth's ionosphere.

The second section of this chapter described the effect the atmosphere has on the propagation of GPS signals. The physics behind wave refraction and dispersion was reviewed. The error experienced by the GPS signal is split into a propagation effect, which is estimated using a Taylor-series of third order, and an effect due to the bending of the signal.

This chapter has provided an insight into the theoretically complex nature of the ionosphere. From this, an appreciation and understanding has been gained of the types of difficulties that need to be overcome in order to produce an adequate ionospheric model, capable of cm-level corrections, that is based on Victorian conditions. Investigations carried out in future chapters have built on this understanding, by attempting to isolate the characteristics of Victoria's ionosphere, as a prelude to a temporal regional ionospheric model for the state.

The next chapter will provide an insight into the different ionospheric measurement techniques and the accuracies associated with each approach. This will provide a fundamental understanding of how the ionosphere is measured, as a prelude to using raw ionospheric observations to produce a modelling strategy for Victoria.

Chapter 3 GPS and other ionospheric probing techniques

This chapter focuses on different ionospheric probing techniques, the processes involved and the accuracies achievable, as well as the role of GPS in these techniques. This chapter examines ionospheric sounding using both terrestrial methods, including: ionosonde, incoherent scatter radars and Faraday rotation techniques, as a means of ionospheric sounding, and the satellite technique of topside sounding of the ionosphere which includes: the Allouette program, Navstar GPS, PRARE and the TOPEX/Poseidon satellite programs. The background behind the extraction of ionospheric data from GPS measurements will also be investigated, together with the GPS observables used for such activities, and the impact that the ionosphere has on GPS positioning in high precision geodetic applications.

The area of ionospheric measurement is investigated to build a good understanding of the science behind it, as the production of an ionospheric model requires the input of raw ionospheric measurement. The use of GPS to produce these measurements and the science associated with the extraction of ionospheric data from GPS observations is examined, as the data used to conduct the research in further chapters is gained via GPS methods.

3.1 Earth-Based methods for probing the ionosphere

The technique of ionospheric sounding is used as a means of determining the height of the ionospheric layer. The technique of transmitting a radio-frequency pulse vertically upward, and measuring the time taken for the echo to be received, is one of the oldest but still most important methods of ionospheric study. The principles of wave refraction in the ionosphere (see section 2.4) and ionospheric critical frequencies (see section 2.1.4) previously introduced, relate to the propagation of radio waves in the ionosphere and are used as a means of probing and determining the height of the different ionospheric layers (see section 2.1.5).

Vertical sounding has provided us with the bulk of our knowledge with respect to the electron content in the Earth's atmosphere, by providing profiles of the variations in the electron content in both a temporal and spatial sense. Spatially, with regard to altitude and latitude, and temporally as a function of diurnal, seasonal and eleven year variations.

The height of the ionospheric layer was first measured by Breit and Tuve (1925) (reported in 1926). They employed 'pulse-echo' equipment to vertically sound the ionosphere. This sounder was the predecessor to the ionosonde (see section 3.1.1), the most widely used of all ionospheric measuring instruments.

The height of the ionospheric layer is determined by measuring the time delay of the echo or time taken for the radio pulse to propagate to the ionospheric layer, where it is reflected and returns to Earth (a few milliseconds). In the first instance it is assumed that the radio pulse travels at the speed of light. The radio pulse does not however travel at the speed of light, c, due to the refractive properties of the ionosphere, but rather at the group velocity, v, (see equation 2.10) which is related to the group refractive index n_g, ie. $v = \frac{c}{n_g}$. The radio pulse therefore travels more slowly in the ionospheric layer than in free space, and causes the virtual length or height obtained to be larger than the actual height. The true ionospheric height, h_r, cannot be directly obtained by measuring the radio pulse travel time, but can be derived from the virtual height, h_v, by correcting for the group retardation as a function of the

electron density, the geomagnetic field and the wave frequency. The following integral equation derives the virtual height of an ionospheric layer as in Davies (1990):

$$h_v = \int_0^{h_r} n_g \, dh = h_0 + \int_{\varnothing_0}^{\varnothing_r} \frac{dh}{d\varnothing} n_g \left(\varnothing\right) d\varnothing \tag{3.1}$$

where:

h_r is the real height of the reflective layer;

n_g is the group refractive index;

$\varnothing$ is a function of electron density; and

$\varnothing_0$ and $\varnothing_r$ are the values of $\varnothing$ at the bottom of the ionosphere, h_0, and at height of reflection.

By neglecting the Earth's geomagnetic field and the collision frequency, we are able to obtain the true height of reflection in a relatively straight forward fashion using the integral equation (3.1). Otherwise, the inclusion of the geomagnetic field and the collision frequency terms require the use of available numerical techniques (Titheridge, 1988).

The ionosphere can also be probed using radio waves emitted at an oblique angle. Vertical incidence and oblique radio wave propagation can be related using the secant law. This law relates the vertical incidence frequency, f_v, with the oblique frequency, f_o, for radio waves reflected at the same true height and provides us with the basic theory behind the use of oblique backscatter radar (see section 3.1.2). This relationship is given in the following equation, for a radio wave incident on a plane ionosphere at an angle ϕ_o (Davies, 1990):

$$f_o = f_v \sec \phi_o \tag{3.2}$$

Equation (3.2) shows that the ionosphere can reflect higher frequencies using oblique propagation techniques rather than with vertical propagation. The reader is referred to Hunsucker (1991) and Davies (1990) for a more in-depth treatment of the relationships between vertical and oblique incidence frequencies.

3.1.1 The ionosonde

An ionosonde is an instrument that emits high frequency radio waves in order to probe the ionosphere, and is capable of obtaining echoes from the different ionospheric layers over a wide range of operating frequencies. Traditionally a sweep frequency device is used that emits radio waves from lower to higher frequencies in order to measure the virtual height of the ionospheric layer by calculating the time travelled by the reflected wave, as explained in the previous section.

As the emitted radio wave travels higher into the ionosphere, the electron density increases causing the refractive index to become smaller. A radio wave is reflected by an ionospheric layer where the plasma frequency (see section 2.1.4) equals the wave frequency. As the ionosphere contains many different layers, each layer has a critical frequency, where the wave is able to penetrate that layer. These frequencies are known as foD, foE, foF1, and foF2 as representative of each layer. As the frequency emitted by the ionosonde is increased, the time lapse or echo travel time for a vertically incident radio wave increases until the layer's critical frequency is obtained. At this stage the radio wave will penetrate the layer. As the frequency is again increased, the echo travel time will decrease somewhat, as the radio waves find it easier to penetrate the previous layer. A virtual height versus frequency record called an ionogram is obtained from this data (see Figure 3.1).

Two separate curves can be clearly seen in Figure 3.1. When taking into account the effect of the Earth's geomagnetic field and applying equation 2.12, where $Y \neq 0$ two values for the refractive index are possible. This implies that radio waves can propagate at two different speeds. These two different waves are called the ordinary and extraordinary waves (see section 2.4) and are obtained by taking the positive and negative signs respectively of their refractive indices. The curves with the higher critical frequencies f_xF1 and f_xF2 are the extraordinary waves. The phenomena known as second-hop reflection can also be observed in Figure 3.1. This occurs

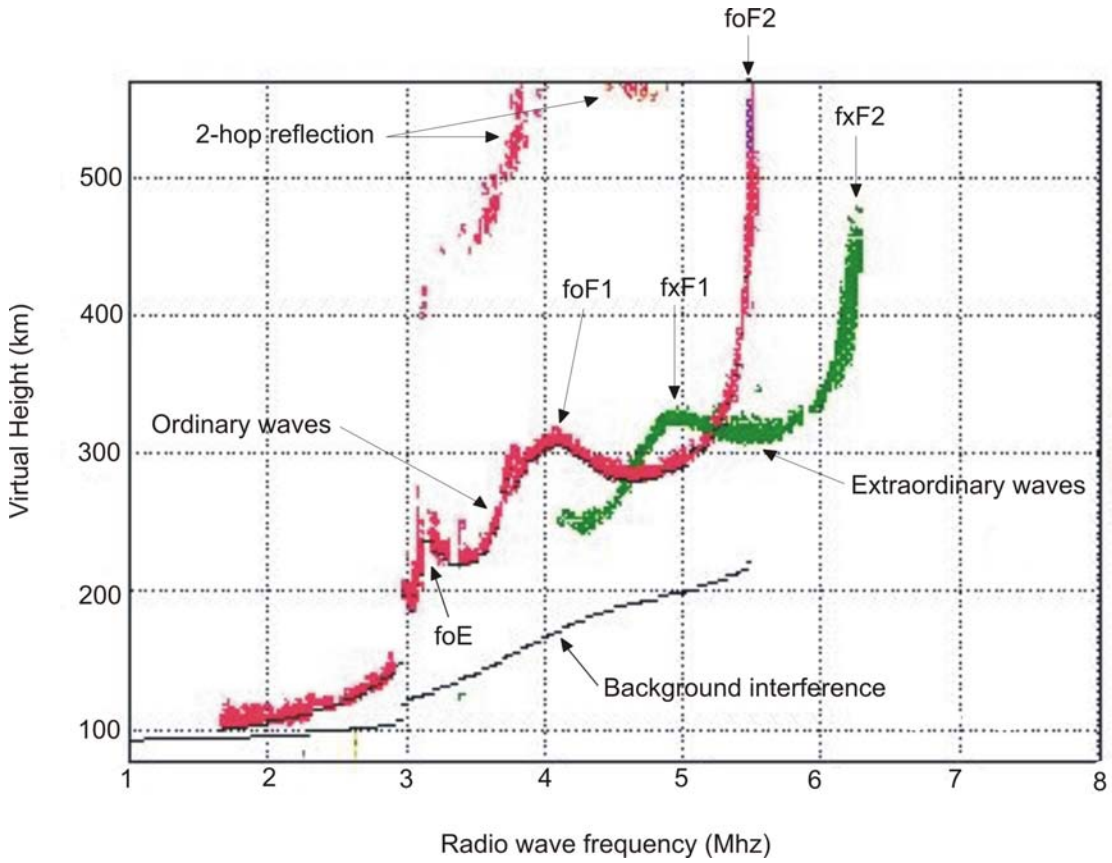

Figure 3.1 Sample ionosonde data

Obtained from image.gsgc.nasa.gov/presentations (July, 2005)

when radio waves are twice reflected from the differing ionospheric layers as a result of reflection from the ground. Background interference is also identified and characterised by a curve at the bottom of the plot (Rishbeth & Garriott, 1969).

3.1.2 Oblique backscatter radar

Sounding of the ionosphere can also be achieved by directing radio waves at oblique angles to the ionosphere. Oblique backscatter sounders are used to detect coherently backscattered radio waves from irregularities present in the ionosphere either directly or via reflection from the surface of the Earth. Using this system a train of short pulses of radio frequency energy is reflected by the ionosphere and scattered non-uniformly back to the surface of the Earth. A small percentage of the incident radio frequency energy is backscattered to the receiver over approximately

the same path. Figures 3.2a and 3.2b provide a basic illustration of the groundscatter and direct modes of ionospheric probing.

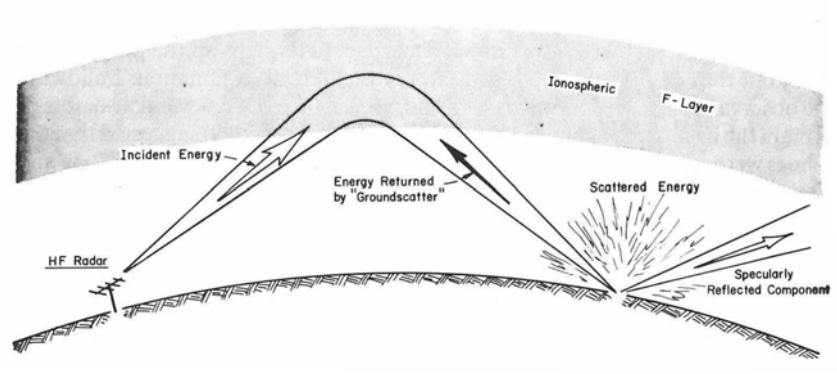

(a) Groundscatter

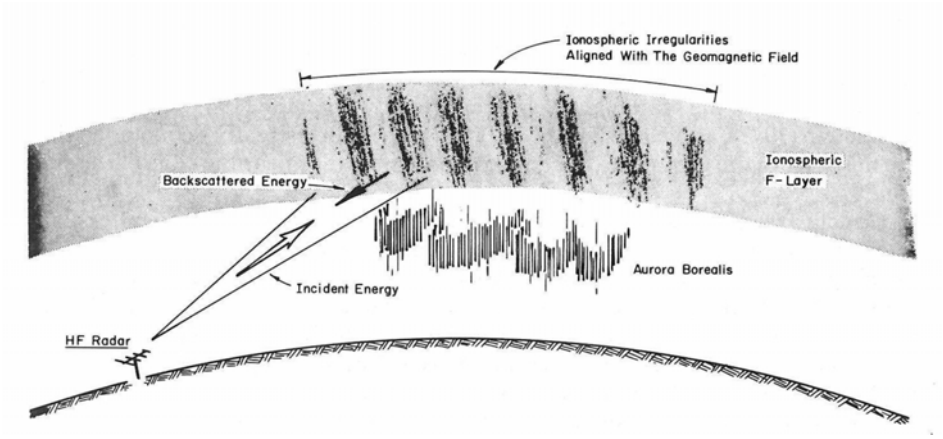

(b) Direct backscatter

Figure 3.2 Schematic diagrams of groundscatter and direct backscatter (Hunsucker, 1991)

The difference in feedback generated from groundscatter and direct modes of operation can be distinguished at the receiver. In the groundscatter mode, radio waves are reflected by the surface of the Earth and the ionosphere and some energy returns to the receiver (see Figure 3.2). The basic theory behind the groundscatter method of oblique ionospheric sounding starts with equation (3.3), which describes the secant law for the ionosphere.

$$f_{ob} = f_v \sec \phi_o \tag{3.3}$$

where:

f_{ob} is the oblique incidence frequency; and

f_v is the equivalent vertical frequency, which is approximated by $9\sqrt{N}$ Hz

For first order backscatter theory, at distances <1000km, it is sufficient to assume a plane Earth and plane-ionosphere geometry (see Figure 3.3).

Figure 3.3 Geometry of plane Earth and plane Ionosphere

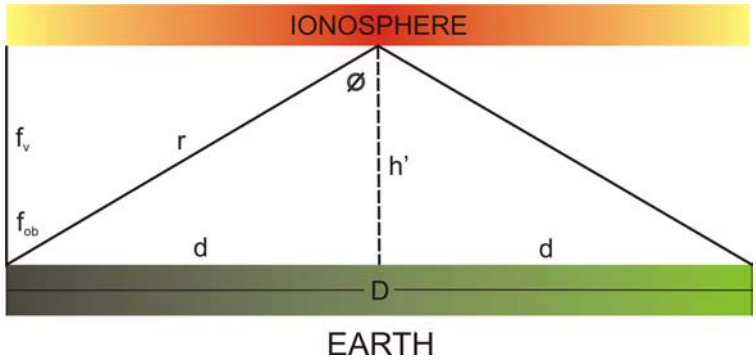

Using Figure 3.3

$$2r = \frac{2h'}{\cos\phi} \tag{3.4}$$

and

$$2d = 2r\sin\phi = 2h'\tan\phi \tag{3.5}$$

where:

r is equal to twice the oblique path length from the ground to the ionosphere.

The virtual height (h'), path length (P) and distance (D) are derived by the following equations:

$$h' = h_0 + \frac{y_m}{2} \text{ x } \cos\phi_0 ln\left[\frac{1+x\cos\phi_0}{1-x\cos\phi_0}\right] \tag{3.6}$$

then substituting equation (3.6) into equations (3.4) and (3.5) yields:

$$P = \frac{2h_0}{\cos\phi_0} + xy_m ln\left[\frac{1+x\cos\phi_0}{1-x\cos\phi_0}\right] \tag{3.7}$$

and

$$D = 2h_0 \tan\phi_0 + xy_m \sin\phi_0 ln\left[\frac{1+x\cos\phi_0}{1-x\cos\phi_0}\right] \tag{3.8}$$

where:

$$x = \frac{f_{ob}}{f_c}$$

y_m is equal to half the thickness of the parabolic layer;

h_0 is the height at the bottom of the ionospheric layer; and

ϕ_0 is the angle of incidence at the bottom of the ionospheric layer.

In the case of direct backscatter mode, the radio waves are backscattered at the ionosphere and a small portion of the incident radio frequency energy is reflected back and amplified by the receiver. As ionospheric irregularities are predominantly aligned with the geomagnetic field, the ray paths from the oblique sounders must be nearly normally incident to the irregularities, in order to obtain a reasonable backscatter echo. This means that a rather stringent sighting criteria must be observed by direct backscatter sounders. For more information on the subject the reader is directed to Hunsucker (1991) and Davies (1990).

3.1.3 Incoherent backscatter radar

Incoherent scatter radars provide ionospheric researchers with both a powerful and flexible tool for probing the ionosphere. They are able to measure many ionospheric quantities as well as provide information on the neutral atmosphere. Unlike the

ionosonde, incoherent scatter radars are not restricted to making observations to regions below the level of peak electron density. They have the capability of taking readings on both sides of the peak simultaneously and can measure the ionosphere during extremely disturbed periods, such as during large geomagnetic storms.

When making its observations, it collects its data using the principles of radar. This technique involves the detection and study of remote targets, which operates on the principle of reflected energy. The radar transmits a radio wave in the direction of the target and observes the reflection of the wave. In the case of incoherent scatter radar, the electrons that make up the ionosphere are targeted.

In 1906 J. J. Thomson showed that free electrons were capable of scattering incident electromagnetic waves (Thomson, 1906). The energy scattered by one electron is $\left(r_e \sin\psi\right)^2$ per unit solid angle per unit incident flux, where ψ is the angle between the electric vector of the incident electromagnetic wave and the path from the observer to the electron. The classic radius of an electron r_e is defined by:

$$r_e = \frac{e^2}{4\pi\varepsilon_0 m_e c^2} = 2.18\times10^{-15}\,\text{m} \tag{3.9}$$

where:

e is the charge of the electron;
m is the mass of the electron;
ε_0 is the permittivity of free space; and
c is the speed of light.

When using radar, the radar cross section (σ_R) for a single electron is required. This quantity is independent of the wavelength of the incident wave and is defined in terms of the extent to which an object will reflect a radar pulse. In the case of backscatter radar it is defined as:

$$\sigma_R = 4\pi r_e^2 = 1.0\times10^{-28}\,\text{m}^2 \tag{3.10}$$

As the amount of energy that is scattered by a single electron is well known (as described above), the strength of the return signal gathered from the ionosphere quantifies the number of electrons in the scattering volume, which in turn is a measure of the electron density. Therefore, the power of the returned signal is directly proportional to the electron density (Rishbeth & Garriott, 1969). The temperature of the ionosphere, which can be different for ions and electrons, can be gained from the width of the spectrum of the returned signal. The shape of the spectrum of the returned scattered signal is influenced by the difference between the electron and ion temperatures. Ionospheric motions can also be measured using the scatter radar technique. A detected doppler shift in the echo received from the ionosphere allows for the calculation of the speed of the ions and electrons in the plasma.

At present the currently operating incoherent radar facilities (see Figure 3.4) include:

- Jicamarca, Peru
- Arecibo, Puerto Rico
- Millstone Hill, USA
- Sondrestromfjord, Greenland
- EISCAT, Norway/Sweden/Finland
- EISCAT Svalbard Radar, Svalbard
- Kharkov, Ukraine
- Irkutsk, Russia
- MU, Japan

For a more detailed treatment on incoherent backscatter radar theory, refer to Hargreaves (1995) and Davies (1990).

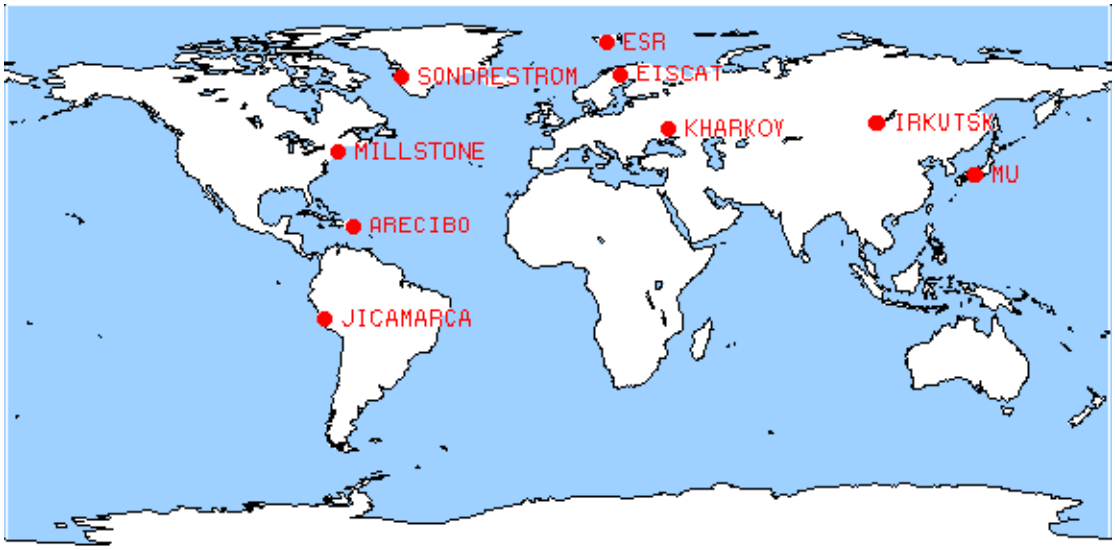

Figure 3.4 World-wide incoherent radar facilities

Obtained from http://hyperion.haystack.edu/iswg/iswg.html (June, 2005)

3.2 Satellite-Based methods for probing the ionosphere

Satellites provide a complementary method of sounding the ionosphere to that of ground-based techniques. The sounding of the ionosphere from above (topside sounding) complements the bottomside measurements in regard to both the heights within the ionosphere that are measured and also in the matter of geographical coverage. Ground-based sounders are only able to measure continuously from one place, whilst an orbiting satellite is able to cover a range of latitudes and all longitudes about twice a day. Therefore, the ground-based approach gives the best time coverage at a particular location, whereas the satellite approach gives the best geographical coverage, but only visiting at a few local times per day. Satellite techniques allow for the measurement of TEC up to the altitude of the satellite, which can be orbiting within the ionosphere or above.

3.2.1 Topside ionospheric sounders

Small ionosondes are placed on Earth orbiting satellites in order to globally probe the morphology of the topside of the ionosphere. As the ionosphere has an electron density maximum, between approximately 250 and 450km in altitude, ground based ionosondes are unable to observe the topside of the ionosphere – i.e. the region above the maximum. It is of importance to note that more than two-thirds of the

ionosphere's electron content lies above this maximum. Therefore, when considering satellite-to-ground transmissions the topside region may contain ionospheric irregularities that are hidden from ground-based ionosondes. There are only two techniques that have been used to study the topside of the ionosphere, these being the topside sounders and the incoherent backscatter radar.

The first topside sounder was the Canadian satellite Alouette 1. It was launched in 1962 into a near circular orbit of about 1000km, carrying a sweep-frequency ionosonde (Hunsucker, 1991). The Alouette 1 program was operational between 1962 and 1972. During the period 1962 through to1966 the Alouette 1 satellite contributed to the vast database of ionospheric readings complied for use in the Bent ionospheric model (Bent & Llewellyn, 1973; Bent *et al.*, 1975). The data came in the form of electron density profiles from approximately 1000km down to the height just above the maximum electron density (F2 peak). This data was also used to improve the topside profile of the International Reference Ionosphere (Bilitza, 1996).

3.2.2 Faraday rotation technique

Another technique of computing electron density which has been widely used by the ionospheric research community is that of Faraday rotation. When a linearly polarised radio wave emitted from a satellite travels through the ionosphere and is exposed to the Earth's magnetic field, the wave undergoes rotation of the plane of this linear polarisation. The rotation of the radio wave can be described as a result of the difference between the characteristics of the ordinary and extraordinary waves. The amount of rotation experienced depends upon the electron content encounter along the signal path, the strength of the Earth's magnetic field and the inverse square of the waves operating frequency (Davies, 1990). Using frequencies of 100MHz and higher, the amount of polarisation rotation experienced can be described as:

$$\Omega = \frac{k}{f^2}\int B\cos\theta\, Ndl, ..., \ (\text{radians}) \qquad (3.11)$$

As the quantity inside the integral is a product of the electron density times the longitudinal component of the Earth's geomagnetic field, integrated along the signal

path, this phenomena has allowed ionospheric researchers to extract TEC measurements from Faraday rotation data. The above equation can be rewritten as:

$$\mathrm{TEC} = \left(\frac{\Omega f^2}{k B_L} \right) \tag{3.12}$$

where:

N	is the electron density;
B_L	is $\overline{B\cos(\theta)}$ which is taken at the mean ionospheric height, which is usually approximately 400km;
k	equals 2.36×10^{-5}; and
TEC	is simply $\int Ndl$.

This is due to the fact that the Earth's longitudinal geomagnetic field strength, $B\cos\theta$, has a slower rate of change with altitude than does the electron density of the ionosphere.

As the Faraday rotation is directly affected by the strength and direction of the geomagnetic field, and the geomagnetic field decays approximately at a rate that is inversely cubed to the radial distance, the electrons at altitudes of 2000km or above have little to contribute to Faraday rotation. This means in essence that the technique of Faraday rotation can not be used to detect electron densities above the aforementioned distance. The calculation of TEC using the Faraday rotation technique is far from an exact science. The weighting of the geomagnetic field can be affected by variations in the height of ionisation, causing errors in the derivation of the electron content by as much as 10-20% (Hargreaves, 1995). The assumption of the height of electron concentration can also cause an error in the spatial distribution of the mapped vertical TEC values.

The effect of Faraday rotation is not a problem for users of the GPS signal, as GPS signals are transmitted with right-hand circular polarisation. For a more complete

study of gaining electron content values via Faraday rotation refer to Titheridge (1972).

3.2.3 Transit

It was found in the early years of the space age that observations taken from satellites that emitted continuous stable frequencies could be used to determine their orbital positions using Doppler measurements. When this scenario is reversed, the position of a user on the Earth can be determined, when the satellite position is known. As a precursor to today's modern satellite-based positioning systems, the Transit system also known as the Navy Navigational Satellite System (NNSS) was developed in a cooperative effort between the Applied Physics Laboratory (APL) of John Hopkins University and the US Department of Defense (DOD). Transit's primary function was the precise navigation and coordination of aircraft and vessels for the U.S. military. Based on the principle of differential doppler, the Transit system was also used for various geodetic purposes. Transit has been providing the ionospheric research community with data for nearly 40 years.

The first Transit satellite was launched in 1962, with the data from the satellites becoming available for civilian use in 1967. They orbit in nearly circular orbits at an altitude of approximately 1100km. When using a line of receiving stations, the polar type orbits of the Transit satellites make them an ideal investigative tool for measuring the variations of the ionosphere in a latitudinal sense. In order to maintain a good global coverage, about seven satellites were usually available. Integrated doppler measurements can be used to compute the line of sight TEC between a Transit satellite and Earth based receiver. Two harmonically related carrier frequencies are transmitted by each satellite, one at 400MHz, the other at 150MHz. The measurement of the line of sight TEC can be achieved by differencing the phase measurements between the two different frequencies. The actual line of sight TEC value can not however be directly measured without knowing the initial phase value. The initial phase value can not be evaluated without some additional data or by making some assumptions about the structure of the ionosphere. Strategies to obtain the initial phase value include comparing TEC values from Faraday rotation data (see section 3.2.2), by means of the simultaneous evaluation of the differential doppler

measurements from two suitably located stations ("two-station method") or by making assumptions about the variations of TEC in the spatial structure of the local ionosphere.

Using a network of receiving stations in Europe, the Transit system was able to detect and monitor large scale TEC variations in both latitude and longitude during a major geomagnetic storm (Leitinger *et al.*, 1984). It was stressed that the system has a role of major importance in the area of ionospheric research. The data collected from the Transit system during this period was compared with Faraday rotation data obtained from a geostationary satellite. In late 1991 the Transit system was used to gain electron density profiles for a tomographic model (see section 4.3.1) over North America (Pakula *et al.*, 1995).

The Transit satellite program officially terminated its navigational service on December 31, 1996. However, as of January 1, 1997, a new system was developed, with several Transit satellites remaining operational for ionospheric monitoring purposes. The old Transit satellite network became known as the Navy Ionospheric Monitoring System (NIMS).

For further information on the Transit program refer to Seeber (2003) and Wells et al (1987).

3.2.4 TOPEX/Poseidon

The TOPEX/Poseidon satellite mission is a joint venture undertaken by NASA and the French Space Agency (CNES). The space vehicle was successfully launched into a circular orbit at an altitude of approximately 1340km, on the 10th August, 1992. TOPEX stands for Ocean TOPography EXperiment. The satellite's primary mission is to explore ocean circulation and how it interacts with the atmosphere.

The satellite's sensor system consists of its primary instrument - a dual frequency radar altimeter operating at 5.3 GHz and 13.6 GHz simultaneously, a second single frequency altimeter operating at 13.65 GHz, a microwave radiometer, a laser reflector array, a dual frequency GPS receiver and a DORIS dual frequency Doppler receiver.

The dual frequency GPS receiver allows the satellite's position to be known within 10cm. By taking advantage of the dispersive nature of the ionosphere, the dual frequency radar altimeter can be used to provide highly accurate TEC measurements over the world's oceans. It was shown by Anderson and Johnson (1996) that the TEC maps derived from TOPEX/Poseidon data compared well with existing global ionospheric models such as IRI-95 and PRISM. Based on measurements taken from a global network of GPS receivers, Ho et al (1997) compared GPS derived global ionospheric maps with TEC data obtained from TOPEX/Poseidon. It was found that in general, the difference between the GPS derived maps and TOPEX/Poseidon data was very small, only 1.5 TEC units (this equates to approx. 0.25m of delay on the L1 GPS frequency) using data derived from within 1500km of the GPS receiver. Codrescu et al. (2001) has compared the TEC measurements derived from both the dual frequency altimeter and the DORIS derived TEC values aboard the TOPEX/Poseidon satellite. It was found that on average the difference between the dual frequency altimeter TEC and the DORIS TEC data was in the region of 4 TEC units (approximately 0.65m on the L1 GPS frequency). The differences between the altimeter TEC and DORIS TEC where found to be greatest in ionospheric disturbed areas, such as the equatorial and auroral regions. The altimeter TEC values were also compared with the Bent model (see Chapter 4) and International Reference Ionosphere (IRI) TEC results. It was found that the TEC values from the Bent model were on average 2.2 TEC units (approximately 0.36m on the L1 GPS frequency) lower and the IRI model values where on average 1.7 TEC units (approximately 0.28m on the L1 GPS frequency) lower than the dual frequency derived altimeter data.

The follow on mission to the ageing TOPEX/Poseidon satellite is Jason-1. It was launched on the 7th of December, 2001, and is again a joint venture between NASA and CNES. It was launched into a similar circular orbit, at an altitude of 1336km carrying updated versions of the same instruments. The main objective is to continue the mission for TOPEX/Poseidon by monitoring the world's ocean circulation and to study the interactions of the oceans and the atmosphere. For further information on TOPEX/Poseidon and Jason-1 refer to TOPEX/Poseidon (2007).

3.2.5 PRARE

The PRARE (Precise Range and Range-rate Equipment) system has been mounted on several satellite platforms. It was first launched on ERS-1 (First European Space Agency (ESA) remote Sensing Satellite) on July 17 1991, into a Sun-synchronous orbit at an altitude of approximately 800km. Unfortunately, the PRARE system could not be activated after launch. The system was included on successful missions such as the Russian Meteorological satellite METEOR-3/7 and ERS-2. The PRARE system was developed by the Institut fur Navigation, University of Stuttgart, the Deutsches Geodatisches Forschungsinstitut, Munchen, and the Geoforschungszentrum, Potsdam. Its primary objective is to provide accurate orbit determination for satellite missions, using a global network of ground stations. An orbital accuracy of better than 10cm has been achieved (Seeber, 2003). Further contributions were made in the areas of: absolute and relative ground station positioning, sea surface topography, the modelling of the Earth's gravity field, precise time transfer and clock synchronisation and the study of the Earth's ionosphere.

PRARE is a discontinued technology, and is unlikely to be included in any future space missions. The PRARE system itself however, offers a very powerful and versatile tool in the area of ionospheric data collection, and is worth further explanation. The measurement principle used by PRARE can be explained as follows. Two pseudorandom noise (PRN) code microwave signals are sent simultaneously to Earth from the space segment, where they are collected by ground stations. One signal is transmitted in the S-band at 2.2GHz and the other in the X-band at 8.5 GHz. At the receiving ground station the time delay between the two simultaneously transmitted signals is measured to a very high accuracy, less than 1 ns (Lechner *et al.*, 1989), then retransmitted back to the space segment for the calculation of the ionospheric correction. Tropospheric corrections are also transmitted to the space segment from meteorological parameters (temperature, humidity and atmospheric pressure) collected at the ground stations. The line-of-sight TEC can be estimated by PRARE using either one of two techniques. Firstly, the one way code travel time difference between the simultaneously transmitted X and S-band signals can be used, or it can be computed using the two-way ranging measurements, which is based on the different propagating velocities (group delay vs. phase advance).

An outline of the two different methods of computing line-of-sight TEC is given in Fletchner et al, (1997), in which an investigation into the accuracy of PRARE derived TEC values is undertaken. PRARE TEC values were found to compare favourably with TOPEX/Poseidon, DORIS and IRI-95 values. For further information on the PRARE system refer to GeoForschungsZentrum (2007).

3.2.6 Radio occultation

Sounding of the Earth's atmosphere using radio occultation (RO) methods has gained interest since the advent of the GPS/MET mission on board the Microlab-1 satellite. Low Earth Orbiting (LEO) satellites can take advantage of the constant illumination of the Earth by transmitting GPS satellites, to provide a means of thoroughly sounding the Earth's surrounding atmosphere and ionosphere. As a GPS satellite starts to descend towards the Earth's limb, the signals that are received by the LEO satellite have traversed the Earth's atmosphere (see Figure 3.5) and are refracted by the ionosphere according to Snell's law. Using inverting techniques, such as the Abel integral transformation (Melbourne *et al.*, 1994) and assuming spherical symmetry of refractivity at the locality of occultations, the signal delay can be measured. From this signal delay, TEC profiles can be computed from the height of the LEO satellite down to the Earth's surface. The GPS/MET mission showed proof of the usefulness and potential of this concept by providing globally distributed, all-weather atmospheric soundings with high accuracy and high vertical resolution (Melbourne *et al.*, 1994; Rocken *et al.*, 1997).

The following is a brief description of some satellites that use the RO technique to sound the ionosphere. The GPS/MET satellite mission spanned from its launch on the 3rd April, 1995 through to March of 1997. Its primary objectives were numerical weather prediction and long-term monitoring of the Earth's climate. GPS/MET was an experiment managed by the University Corporation for Atmospheric Research (UCAR) (Ware *et al.*, 1996) and consists of mounting a space quality GPS receiver onto a Microlab-1 satellite, launched into a circular orbit at 730km. The GPS/MET mission was the first to demonstrate how LEO satellites can be used in conjunction with GPS satellites to probe the ionosphere using RO techniques. GPS/MET data

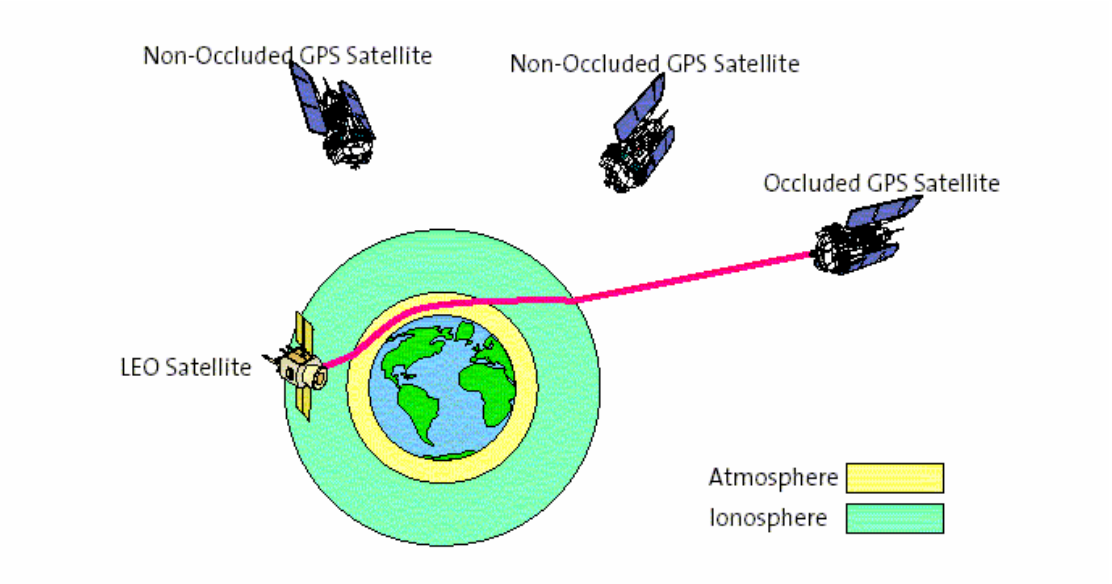

Figure 3.5 Sounding the ionosphere using GPS occultation

Obtained from www.cpar.qinetiq.com (June, 2005)

has been tested against nearby ionosonde measurements by Hajj and Romans (1998) and found to agree within approximately 20%. In a latter study by Tsai et al (2001) it was found that a correlation coefficient of >0.8 exists between data derived from the GPS/MET satellite and nearby ionosonde measurements.

The Challenging Mini-Satellite Payload for geophysical research and application (CHAMP) (Reigber *et al.*, 2000) was launched on July 15, 2000, into an approximate near circular orbit of about 450km, with an inclination of about 87.3°. The satellite was launched under the responsibility of the GeoForschungsZentrum (GFZ), Potsdam, Germany. CHAMP's main objectives are the mapping of the Earth's gravity field, the mapping of the Earth's magnetic field and the profiling of the ionosphere and troposphere (Seeber, 2003). CHAMP's sensor payload consists of a 16 channel dual frequency GPS receiver connected to a multi-antenna array, a three axis accelerometer, a laser-retro reflector (backup satellite tracking), a magnetometer and a digital ion drift meter. The GPS receiver on the CHAMP satellite can be used to position the satellite in its orbit to an accuracy of a few centimeters, when used in differential mode. The first results obtained from CHAMP occultations are reported in Wickert, et al. (2001) and indicate a successful start to the mission. These dual frequency signals provide a valuable source of information on the state of the topside

of the ionosphere, and provide a global ionospheric monitoring platform (Heise *et al.*, 2002).

The GRACE (Gravity Recovery and Climate Experiment) satellite mission is a joint venture between NASA and the German Space Agency (DLR) (GRACE, 2007). The mission consists of two identical satellites that were launched on March 17th, 2002, into a near polar orbit of approximately 500km. The mission's primary objective is the high resolution mapping of the Earth's gravity field, with a secondary scientific objective of limb sounding for the determination of tropospheric and ionospheric parameters using its onboard GPS receiver. The two identical satellites fly in the same orbital plane approximately 220km apart. The Earth's gravity field is mapped by continuously measuring the distance between the two satellites using the microwave ranging system and GPS receiver. As the microwave ranging system onboard each satellite transmits carrier phase signals to the other satellite at two frequencies (24 and 32 GHz), ionospheric corrections to the range between the two satellites can be computed.

The SAC-C satellite mission is an international co-operative mission, with its senior partners being NASA and the Argentine Commission on Space Activities (CONAE), with contributions from Brazil, Denmark, France, Spain, and Italy. SAC-C was launched on the 21st of November, 2000, into a circular Sun-synchronous orbit at an altitude of approximately 700km. The SAC-C missions major objectives are: the provision of multispectral imagery of the Earth's coastal and terrestrial environments, to use the onboard GPS receiver to measure such atmospheric phenomena as ionospheric TEC and tropospheric parameters in a bid to further our knowledge of the Earth-Sun relationship, to enhance our understanding of the Earth's magnetic field and to measure the atmosphere's high energy radiation environment so as to further understand the degradation of advanced electronic components (SAC-C, 2007).

FEDSAT is a research microsatellite that was launched on the 14th of December, 2002, into a circular Sun-synchronous orbit of approximately 800km, as the first major project undertaken by the Cooperative Research Centre for Satellite Systems (CRCSS) as an Australian Government initiative under the Commonwealth Cooperative Research Centres Program. The mission is a joint venture of four

Australian companies, six universities and two government agencies. FEDSAT's payload consists of: a dual frequency GPS receiver for satellite orbit positioning and atmospheric monitoring, the NewMag magnetometer which is a very sensitive device designed to measure the strength of the Earth's magnetic field, a Ka-band transponder that provides a 20 GHZ downlink and a 30GHz uplink which is intended for use in digital communications experiments in the area of determining the reliability and efficiency of high speed internet connections using this band and a UHF communications payload. FEDSAT's dual frequency GPS receiver will be used to support the accurate measurement of the satellite's position as well as furthering research into precisely determining satellite orbits. The GPS receiver will also be used to support research into the ionosphere, by taking dual frequency measurements to higher orbiting GPS satellites, and using occultation methods to measure the ionosphere below FEDSAT's orbit (Essex *et al.*, 1997).

FEDSAT's onboard GPS receiver has been operational since March of 2003, on a duty cycle basis, where the receiver operates for 20-30 minutes per orbital period, providing effective data sets of 10-15 minutes each orbital period. The initial results have been generally poor, due to the poor satellite geometry, which is a result of: the rear looking GPS antenna only being able to see two thirds of the hemisphere, rather high measurement noise and the observational periods only being 10-15 minutes during each orbit. On average, it has been found that FEDSAT's ranging errors have been comparatively higher than CHAMP and SAC-C. For example the RMS error for FEDSAT is nearly two times that of CHAMP and three times that of SAC-C (Feng *et al.*, 2003).

3.2.7 GLONASS

The GLobal Orbiting NAvigation Satellite System (GLONASS) is the Russian equivalent of GPS. There are many similarities between GPS and GLONASS, both offer dual frequency satellite-based positioning, with both pseudorange and carrier phase measurements available. In addition, both point positioning and relative positioning is possible, at similar levels of accuracy to GPS.

GLONASS has been fully operational, with a complete constellation of 24 satellites since January of 1996. The systems primary use is that of military application, but like GPS it has been offered to the civilian population through several declarations of the Russian Federal Government. The complete GLONASS satellite constellation consists of 24 satellites that are equally spaced in 3 orbital planes, 120° apart, orbiting in near circular orbits at altitudes of 19100km. The GLONASS satellites offer a one way ranging system, like GPS, but in contrast the broadcast carrier frequencies are satellite specific. The individual carrier frequencies in the L-band are defined as follows:

$$\begin{aligned} \phi_{L1}^{i} &= 1602.0000\ MHz\ +\ (i \times 0.5625\ MHz) \\ \phi_{L2}^{i} &= 1246.0000\ MHz\ +\ (i \times 0.4375\ MHz) \end{aligned} \qquad (3.13)$$

Where $i = 1,.....24$ is the channel number assigned to each GLONASS satellite (Kleusberg, 1990). Both carrier frequencies, L1 and L2, are modulated by two binary codes and the navigation message. As each GLONASS satellite broadcasts a satellite-specific carrier frequency, all satellites are able to use the same codes. The C/A code is modulated onto the L1 frequency only, with a chipping rate of 0.511 MHz and a period of 1 ms. The P-code is modulated on both carriers, with a chipping rate of 5.113 MHz and a period of 1 s and is not accessible by the public. The GLONASS system provides both a standard and precise navigational signal, as does GPS. The SP or Standard Precision signal is continually available to the public, and has a specified accuracy of between 50-70m horizontally and 70m vertically (Seeber, 2003). The HP or High Precision signal is restricted.

The GLONASS navigation message is different to that of GPS. Every half an hour, the satellite's transmit their position in space, along with their acceleration and velocity vectors. Users are therefore required to interpolate the satellite's position between these half hour broadcasts. The satellite coordinate system is based on a geocentric datum known as PZ-90 (Parametry Zemli 1990).

Due to a lack of funding and new launches, the GLONASS satellite constellation has decreased dramatically over the last decade, from 24 satellites at the beginning of 1996 down to only 7 operational satellites at the end of 2002. The Russian

Government, in 2001, approved the Federal GLONASS Program for 10 years, with a program directive of sustainment and development of the system, that included a minimum operational capability of 18 satellites by 2007, and full operational capability of 24 satellites by 2010 (Revnivykh, 2006). On the 25th December, 2006, Russia successfully launched 3 new GLONASS satellites into orbit. This presently brings the total number of operational satellites in the constellation to 10 (May, 2007) out of the 19 currently orbiting. Two launches are expected in 2007, with a total number of 6 more satellites. Refer to Seeber (2003), Hoffmann-Wellenhoff et al. (1997) and GLONASS (2007) for a more indepth description of the GLONASS system.

Danaher et al (1993) showed how GLONASS dual frequency P-code receivers could be used to accurately measure the ionosphere using a number of different methods. Beser & Balendra (1994) discuss the advantages of using GLONASS dual frequency P-code ionospheric measurements to improve integrated GLONASS / GPS positional accuracy for commercially available receivers. Zarraoa et al (1995) presented a detailed study on the application of GLONASS for ionospheric monitoring, in a stand alone sense or combined with GPS measurements. The GLONASS TEC results were compared with those derived from GPS measurements and found to be in agreement to within 1.6 TECU (r.m.s). Based on a single day's worth of data, the differences between GLONASS derived TEC and GPS derived TEC were approximately 4 TECU. It was found that the data quality of the GLONASS P-code measurements was comparable to GPS, with the added advantage of not being effected by Anti-Spoofing. When combining GLONASS and GPS measurements, the number of observables is increased by over 50% with an increased improvement in general satellite geometry. The Global Ionospheric Maps (GIMs) produced by CODE (See Chapter 4) as of day 117, 2003 (GPS week 1215) use combined GPS/GLONASS receivers to produce ionospheric information from data collected from some 200 IGS and other sites (AIUB, 2007).

3.2.8 Global Positioning System

The NAVSTAR GPS (NAVigation System with Time And Ranging Global Positioning System) is an all weather, space-based radio navigation system that provides three dimensional position, navigational capabilities and timing information for suitably equipped users. The GPS satellites are deployed and operated by the United States for civilian and military purposes.

Fundamentally, GPS consists of three major segments: the control segment, the user segment and the space segment. The control segment is responsible for maintaining the operational integrity of the system. It consists of five monitoring stations (Hawaii, Kwajalein, Ascension Island, Diego Garcia and Colorado Springs) that passively track all satellites in view, accumulating such information as the exact altitude, position, speed and overall health of the orbiting satellites 24 hours a day. Once this data is processed at the Master control station, the satellite orbital position and clock bias, drift and drift-rate can be predicted for each satellite. This information is then transmitted to each satellite for re-transmission back to the users in the form of the navigation message that is modulated on both GPS signals. The user segment consists of all GPS receivers used in a variety of civilian and military applications. The space segment consists of the satellite constellation itself.

To date, six generations of GPS satellites have been launched, these being, the Block-I, Block-1A, Block-II, Block-IIA, Block-IIR (see Figure 3.6) and Block-IIR-M satellites. A new generation of satellite, known as the follow-on Block-IIF satellites are currently under construction, and a Block III next generation program has begun initial development in recent years.

GPS has been under development since 1973 with the first GPS satellite, PRN 4, being launched on the 22nd of February, 1978. This launch marked the start of the deployment of the first of eleven so-called Block-I satellites, known as the concept validation satellites, used to initiate the system. The orbital planes of the Block-I satellites were inclined at about 63º with respect to the Earth's equator, making them more accessible to the North American region for testing purposes. These Block-I

prototypes where launched up until 1985 and had a design life span of five years, which was exceeded in most cases.

Figure 3.6 GPS Block-IIR Satellite in orbit

The first of the Block-II or production satellites was launched in February of 1989. The Block-II satellites are arranged in six orbital planes A to F, which are separated by about 60º in longitude and inclined by approximately 55º with respect to the Earth's equator. There orbits are close to circular, at an altitude of approximately 20200 kilometres above the Earth's surface. In November of 1989, a slightly modified version, the Block-IIA satellite, carrying more capable and reliable systems was introduced. A total of 28 Block-II and IIA satellites have been launched to support the GPS constellation. The first Block-IIR or replenishment satellites were launched in July of 1997. These satellites have the capability of being able to measure between satellites and compute their own on-board ephemeris. The design life of an operational Block-II satellite is 7.5 years, which has been proven to be much longer in reality.

As part of the GPS modernisation program, eight Block-IIR satellites are being upgraded to radiate the new military (M-code) signal, to be broadcast on both the L1 and L2 frequencies, together with a more powerful civil signal (L2C) on the L2 frequency. The M-code on the L1 and L2 frequency will be confined to military users and is designed to replace the existing P-code. The M-code will be ground-selectable providing the user with increased security and anti-jamming capability. The new L2C

civilian signal will also be ground-selectable, allowing the user the option of either the L2 C/A code or a new L2C code. This will provide the civilian user with the ability to directly correct for the ionosphere. Three of these new upgraded Block IIR-M satellites have been launched in recent years with the last being deployed in November of 2006.

The new generation, Block-IIF or follow-on satellites, are scheduled to begin launching sometime in 2008. These satellites will be equipped with all of the capabilities of the previous blocks, together with improvements that include an extended design life of 12 years, more memory and faster processors, together with a new civil signal on a third frequency (L5). The new L5 frequency will provide a higher power level than other signals and longer band width, making it easier to acquire and track weak signals. The introduction of this third frequency has many advantages, including the feasibility of instantaneous ambiguity resolution for a broad range of applications and enhanced system availability and reliability (Vollath *et al.*, 2003). On the topic of GPS modernisation, refer to Ward *et al.* (2006) for a more in-depth treatment of the subject.

The nominal GPS constellation consists of 24 satellites, at present (May, 2007) however, there are currently 30 deployed. When in full constellation, as of 1995, there are four slots assigned to each orbital plan with provision for an extra six on the basis of need for active spares. Table 3.1 lists the active GPS space vehicles as of May, 2007. The constellation consists of 1 Block-II, 16 Block-IIA and 12 Block-IIR satellites. The arrangement of the satellites in the constellation has been planned in such a way that at least four satellites can be seen by a user at any point on the Earth, 24 hours a day. Within these orbits, the satellite completes an orbital revolution in 11 hours and 58 minutes which is almost precisely half a sidereal day. This means that the satellites will complete two orbital revolutions while the Earth rotates by 360º with respect to inertial space. This will also mean that a particular satellite will rise approximately 4 minutes earlier each solar day. This particular orbital period implies that all GPS satellites are in a deep 2:1 resonance with the Earth's rotation and are therefore subject to pronounced secular or long-periodic perturbations in certain orbital elements (Beutler *et al.*, 1998).

Table 3.1 Active GPS space vehicles as of May, 2007

PRN	SVN	Plane/Slot	Block	PRN	SVN	Plane/Slot	Block
1	32	F6	IIA	17	53	C4	IIR-M
2	61	D1	IIR	18	54	E4	IIR
3	33	C2	IIA	19	59	C3	IIR
4	34	D4	IIA	20	51	E1	IIR
5	35	B4	IIA	21	45	D3	IIR
6	36	C1	IIA	22	47	E2	IIR
7	37	C5	IIA	23	60	F4	IIR
8	38	A3	IIA	24	24	D6	IIA
9	39	A1	IIA	25	25	A5	IIA
10	40	E3	IIA	26	26	F2	IIA
11	46	D2	IIR	27	27	A4	IIA
12	58	B5	IIR-M	28	44	B3	IIR
13	43	F3	IIR	29	29	F5	IIA
14	41	F1	IIR	30	30	B2	IIA
16	56	B1	IIR	31	52	A2	IIR-M

NAVSTAR GPS is a one way ranging system, i.e. signals are only transmitted from the satellites and received on Earth by the user. Each GPS satellite carries an ensemble of highly accurate oscillators, in the form of two cesium and rubidium atomic clocks (Van Melle, 1990). These clocks are used to generate two coherent frequency standards in the L-band, L1 and L2. The two carrier frequencies f_1 and f_2 are coherently derived from the fundamental 10.23 MHz frequency (f_0):

$$f_1 = 154 f_0 = 1575.42\ MHz \quad \text{where } \lambda_1 = \frac{c}{f_1} \approx 190mm \tag{3.14a}$$

$$f_2 = 120 f_0 = 1227.60\ MHz \quad \text{where } \lambda_2 = \frac{c}{f_2} \approx 244mm \tag{3.14b}$$

where:

λ_1 and λ_2 denote the corresponding wavelengths; and

c is the speed of light in a vacuum (299 792 458 m/s).

The carrier frequencies (f_1, f_2) are modulated with two pseudorandom noise (PRN) codes as a means of providing position in real time. These are: a) The coarse/acquisition (C/A) code and b) The precision (P) code. The C/A code is modulated onto the L1 carrier and generated with a chipping rate of 1.023 MHz, which equates to one tenth of the fundamental frequency f_0. It has a corresponding wavelength of approximately 300m. The C/A code is accessible to all users and provides the basis for supporting the Standard Positioning Service (SPS). The P code or its encrypted version the Y-code is the primary code used for navigation and positioning by the military, and is restricted to non authorised users. It provides the basis for supporting the Precise Positioning Service (PPS). The P code is modulated on both the L1 and L2 carriers and generated with a chipping rate of 10.23 MHz, with a corresponding wavelength of approximately 30m. In addition to these codes, a navigation message is also attached to both carrier frequencies. This message is modulated onto the carrier frequencies at a rate of 50 bits per second (bps) and is repeated every 30 seconds. The data in the navigation message provides such information as satellite clock and positional (ephemeris) information, system status information as well as GPS time. At present the quality of this broadcast ephemeris is 2-4 metres.

As the GPS is a one way ranging system, the fundamental observable is the signal travel time between the satellite and the receiver. This travel time is converted to a range measurement using the signal propagation velocity. In order to measure the signal propagation time, the signal reception time, at the receiver, is compared with the time of transmission from the satellite. This is achieved by the receiver generating a replica of the code generated by the satellite, and determining the time offset between the received satellite generated code and the receiver code at time of reception. As the satellite and receiver clocks are generally not strictly aligned, and distortions in range due to the signal propagation media (atmosphere) exist, one can not directly derive ranges from code measurements as a bias exists. These ranges are therefore known as pseudo-ranges. The basic principle of GPS point positioning requires the simultaneous observation of four pseudo-ranges: three pseudo-ranges to derive the three co-ordinates of the user position, and the fourth to estimate the clock synchronisation error.

As the GPS is primarily a military system, to prevent unauthorised civilian users from taking full advantage of the system's capabilities, the GPS signals have been intentionally degraded for the civilian population, via two methods: a) Selective Availability (SA), which is the artificial degradation of the satellite clocks, and b) Anti-spoofing (AS), which involves the encryption of the P-code. SA was first introduced in March of 1990 and permanently deactivated in May of 2000, by Presidential decision (White House, 2000). AS on the other hand, involves the encryption of the P-code into the Y-code, as a means of preventing an adversary from generating a copy of the GPS signal as a way of intentionally misleading or 'spoofing' a receiver. AS has been continuously active on all of the Block-II satellites.

3.2.8.1 GPS observables

GPS measurements can be derived using two fundamental observations: pseudorange and carrier phase. Both of these measurements are subject to errors of a systematic or random nature. Systematic errors for example, come in the form of the delays experienced by GPS signals when traversing the ionosphere and troposphere, thus causing a range error to occur between the satellite and receiver. Random errors can come in the form of receiver noise. As described above, the code derived geometric range (pseudo-range) between the satellite and receiver is measured by the time difference between the epoch of signal transmission and the epoch of its reception at the receiver. This delay is equal to the travel time, and is then converted to a range measurement by multiplying it by the speed of light.

The precision of these measurements can be partly related to the wavelength of the chip in the PRN code, indicating that the shorter the wavelength, the more precise the measurement. The P-code has a wavelength of 30m, which assuming a receiver measurement precision of 1% equates to a measurement precision of 0.30m, approximately 10 times higher than that of the C/A code.

For C/A or P-code transmitted from satellite k at time t^k and received by receiver i at time t_i equation (3.15) defines the fundamental pseudo-range observation equation:

$$P_i^k = c\left(t_i - t^k\right) = c\tau_i^k \tag{3.15}$$

where:

P_i^k is the code derived measurement (pseudo-range) in units of length;

c is the speed of light;

t_i is the reception time of the GPS signal at the receiver;

t^k is the transmission time of the GPS signal at the satellite; and

τ_i^k is the GPS signal time difference, or travel time of the GPS signal, ignoring receiver and satellite synchronisation clock errors.

Equation (3.16) relates the pseudo-range measurement P_i^k to the actual geometric (slant) range ρ_i^k between satellite k at time $t^k - \Delta t^k$, and receiver i at time $t_i - \Delta t_i$, taking into consideration the delays experienced on the signal due to the Earth's atmosphere and multipath, together with satellite orbital ephemeris errors:

$$P_i^k = \rho_i^k + c\left(dt_i - dt^k\right) + d_{i,orb}^k + d_{i,trop}^k + d_{i,ion}^k + c\left(b^k + b_i\right) + mp_i^k + \varepsilon \tag{3.16}$$

where:

ρ_i^k is the geometric range between the satellite *k* and receiver *i*;

dt_i, dt^k the receiver and satellite clock offsets with respect to GPS time;

$d_{i,orb}^k$ is the satellite orbit error;

$d_{i,trop}^k$ the delay experienced by the GPS signal due to the troposphere;

$d_{i,ion}^k$ the delay experienced by the GPS signal due to the ionosphere;

b^k, b_i are the satellite and receiver hardware biases, in units of time;

mp_i^k effect of multipath; and

ε indicates a random error or residual.

The ρ_i^k term also includes such errors as the periodic relativistic effect, that is present as a result of slight eccentricities in each satellite orbit which causes a clock offset error that varies with the satellite's orbital position, and the fact that the receiver and satellite are moving relative to each other in differing gravity fields (Ashby & Spilker, 1996). The effect of antenna phase offset also needs be considered (Schupler & Clark, 1991; Rothacher *et al.*, 1995).

The satellite and receiver hardware biases b^k and b_i are a result of hardware delays in the L1 and L2 signal paths. As these biases can not be separated from the clock offsets, dt_i, dt^k, they are usually assumed to be zero. As a result, the clock offsets compensate for the hardware bias delays.

Multipath (mp_i^k) is the phenomenon whereby a signal arrives at a GPS receiver via multiple paths due to reflection. It is a highly localised phenomenon that can severely distort both code and phase measurements, and is a genuine error source in GPS. For a more detailed discussion on multipath and its effect on ionospheric measurements, see section 3.2.8.4.

The GPS carrier phase is defined as the difference between the received Doppler-shifted carrier signal and the constant receiver generated reference frequency. When the receiver first establishes acquisition of the GPS signal, it can only measure the fractional phase within one wavelength, with the initial integer ambiguity (or whole wavelengths) between the satellite and receiver being unknown. As long as the signal tracking remains continuous, the integer ambiguity (N) will remain constant. Once the integer ambiguity has been resolved, the receiver is able to count the number of integer cycles that are being tracked. The carrier phase observable can therefore be described as the sum of the fractional part, and the number of whole wavelengths between the satellite and receiver. Special ambiguity resolution techniques are used to resolve the initial ambiguity (see section 3.2.8.7). As the wavelength of the L-band carriers approximates 0.20m and again assuming a receiver measurement precision of 1%, a measurement precision of approximately 2mm is obtained. This allows for highly accurate measurement of a user's position,

which can be adopted for high precision geodetic and surveying applications, making the carrier phase the primary GPS observable.

To produce the carrier phase observation equation, equation (3.16) can be re-written as equation (3.17), with ϕ_i^k expressed in units of length:

$$\phi_i^k = \rho_i^k + c\left(dt_i - dt^k\right) + \lambda N_i^k + d_{i,orb}^k + d_{i,trop}^k - d_{i,ion}^k + c\left(b^k + b_i\right) + mp_i^k + \varepsilon \qquad (3.17)$$

where:

λ is the wavelength of the GPS carrier; and

N integer cycle ambiguity.

The carrier phase observation equation (3.17) is very similar to the pseudo-range equation (3.16), with the major difference being the introduction of the ambiguity term (N). It can also be seen when comparing equations (3.16) and (3.17) that the group delay and phase advanced due to ionospheric refraction ($d_{i,ion}^k$) are of equal size but have opposite signs (see section 2.4).

As the main aim of this research is the quantification of the relative ionospheric delay, the primary focus will be on the parameter ($d_{i,ion}^k$), which holds the ionospheric information. As the ionospheric delay experienced by the GPS signal is frequency dependent, and can be defined as being inversely proportional to the square of the frequency $\left(\frac{1}{f^2}\right)$, it is possible to simplify the observation equations for a dual frequency GPS receiver, into a frequency dependent notation using (Schaer, 1999):

$$\rho_i^{'k} = \rho_i^k + c\left(dt_i - dt^k\right) + d_{i,trop}^k \qquad (3.18)$$

The ionospheric delay term I_i^k is also introduced. It represents the ionospheric delay related to the first frequency f_1. Therefore:

$$\phi_{i,1}^{k} = \rho_i^{'k} - I_i^k + \lambda_1 N_{i,1}^k + c\left(b^{k,1} + b_{i,1}\right) \quad (3.19a)$$

$$\phi_{i,2}^{k} = \rho_i^{'k} - \xi I_i^k + \lambda_2 N_{i,2}^k + c\left(b^{k,2} + b_{i,2}\right) \quad (3.19b)$$

$$P_{i,1}^{k} = \rho_i^{'k} + I_i^k + c\left(b^{k,1} + b_{i,1}\right) \quad (3.19c)$$

$$P_{i,2}^{k} = \rho_i^{'k} + I_i^k + c\left(b^{k,2} + b_{i,2}\right) \quad (3.19d)$$

where:

$\phi_{i,1}^{k}, \phi_{i,2}^{k}$ are the carrier phase observations on both frequencies;

$P_{i,1}^{k}, P_{i,2}^{k}$ are the code observations on both frequencies;

$\rho_i^{'k}$ is the geometric range between the satellite *k* and receiver *i* that includes the clock offsets dt_i and dt^k and troposheric delay $d_{i,trop}^{k}$;

I_i^k is the ionospheric delay related to the L_1 frequency in units of length;

ξ is the factor that relates the ionospheric delay on L_2 to that of the first frequency L_1, the quantity is 1.647, for a pair of GPS frequencies; and

$$\xi = \frac{f_1^2}{f_2^2},\ \text{i=1,2}$$

$b^{k,z}$, $b_{i,z}$ are the satellite and receiver biases respectively, where z=1, 2.

3.2.8.2 Relative positioning

It can be seen from the above equations (3.16) and (3.17), that many errors affect the accuracy of the observed GPS signal. In order to eliminate, or greatly reduce these errors, the technique of relative (or differential) positioning is used. This technique involves the differencing of code or phase data collected simultaneously from the same satellites, at two different receivers (see Figure 3.7). This practice hopes to take advantage of the fact that the errors affecting the observed signals at both receivers will exhibit some correlation or similarity, and therefore cancel out (Wells *et al.*, 1987).

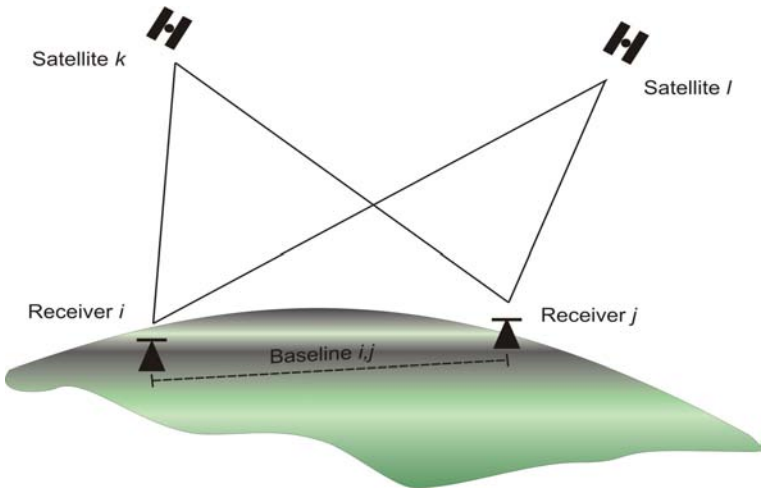

Figure 3.7 Relative positioning concept

The basic principle behind relative positioning is the determination of co-ordinates of an unknown point with respect to a known point. The relative positioning technique is able to produce highly accurate vectors (or baselines) between two GPS receivers as most of the error sources are highly spatially correlated over short distances.

Taking simultaneous readings from two receivers to multiple satellites, allows for the formation of linear combinations of the code and phase observables (see section 3.2.8.6). These combinations lead to single differences, double differences and triple differences, which are used by most GPS software packages as their basic mathematical modelling approach for high accuracy positioning.

3.2.8.3 Ionospheric effects on GPS baseline solutions

When looking at relative geodetic GPS surveying, it is the change in the ionosphere, or difference in the delay experienced at both ends of the baseline, that is of primary interest (Georgiadou & Kleusberg, 1988a). Dual frequency GPS receivers can exploit the dispersive nature of the ionosphere by forming linear combinations (see section 3.2.8.6) of the original L1 and L2 carrier phase observations to eliminate the effects of ionospheric delay over a baseline. This method provides the most effective means of eliminating the differential ionospheric bias, especially in disturbed ionospheric conditions, but also has the effect of amplifying the noise levels (see section 3.2.8.6) of the original carrier phase observations (Kleusberg, 1986). Single frequency

observations, over short baselines, can provide superior results to dual frequency solutions when processed in tandem with a localised ionospheric model (see Chapter 4). Whilst the accuracy of single frequency receivers is comparable to that of dual frequency receivers over shorter baselines of 10km in length (Henson & Collier, 1986), the differential solution starts to break down over longer distances as the ionospheric effect experienced at one end of the baseline may be significantly different to that experienced at the other end. Therefore, single frequency receivers, relying on the eight parameter broadcast ionospheric model (see Chapter 4), are unsuitable for geodetic applications over long baselines, where high accuracy results are required (Kleusberg, 1986; Lachapelle & Cannon, 1986).

The change in ionospheric delay or bias experienced between two GPS receiving stations, using single frequency observations, has the effect of shortening the baseline vector computed. The amount of baseline shortening is governed by the difference in satellite geometry experienced by co-observing GPS receivers, along with the change in TEC over the observation area (Janes, 1991). This shortening due to ionospheric biases over baseline lengths leads to a consistent scale factor between single and dual frequency results, which may be calculated using the following formula (Beutler *et al.*, 1987):

$$\frac{\Delta l_{ion}}{l} = -\frac{C_x}{2} \bullet \frac{TEC_{AV}}{R \cos z_{\max}} \bullet \frac{1}{f^2} \qquad (3.20)$$

where:

Δl_{ion}	is the distance bias induced by the relative ionosphere;
l	is the length of the baseline vector;
$\frac{C_x}{2}$	is a proportionality factor $\approx 40.3 \times 10^{16} ms^{-2} TECU^{-1}$;
TEC_{AV}	is the average vertical TEC above the baseline;
R	is the approximate Earth radius;
$z_{\max}$	is the maximum satellite zenith distance used in the processing (the lowest satellite elevation angle used); and
f	is the frequency of the GPS signal used in the processing.

Both Beutler *et al* (1989) and Santerre (1991) have investigated what affects different satellite geometry, at either end of the baseline, will have on the ionospheric bias. Differing satellite geometry will mean that the signals received at the two stations would have passed through the ionosphere at slightly different elevation angles, therefore the TEC encountered along each path would also be different, even if the vertical ionospheric profile is the same at both receiving stations. Based on the above equation, with an elevation mask of 10°, a parts per million scale bias of -0.15 for every TECU not accounted for over the baseline would be experienced. Based on the above estimate, at a typical mid-latitude site, experiencing a 10 TECU ionosphere, a bias of -1.5ppm would be experienced, leading to an error of approximately 0.01m over 5km and approximately 0.06m over 40km. These errors can be much larger when influenced by such things as: increasing baseline length, different regions of the Earth, and an increase in solar activity. Wanninger (1993) analysed the effect that the equatorial ionosphere has on relative single frequency GPS measurements. It was found that during the previous solar maximum, the ionosphere was changing by as much as 30 TECU per 100km, which introduced a 48ppm scale bias over this distance.

Under moderate and homogeneous ionospheric conditions, when processing data from small network GPS baselines, ionospheric TEC models derived from one or more dual frequency GPS receivers located in the vicinity, can remove or greatly reduce the effect of the ionospheric induced scale bias (Georgiadou & Kleusberg, 1988a). This approach can often yield results superior to dual frequency data over short baselines (Rocken *et al.*, 2000), as the ionospheric-free L3 observable (see section 3.2.8.6.1) is three times as noisy as the basic L1 observable, and also greatly amplifies such systematic errors as multipath (see section 3.2.8.4).

In addition to correcting single frequency data, ionospheric models can be used to help in the fixing of carrier integer ambiguity parameters (see section 3.2.8.7). The estimation of integer carrier phase ambiguities is usually based around a least squares adjustment of a single baseline model. It is well known that the ionosphere decorrelates over baselines of significant length, therefore the change in the ionosphere can have a significant effect on the performance of these ambiguity resolution models. If a prior knowledge of the ionospheric bias is known, this would

enhance the ambiguity resolution process, by decreasing the size and shape of the ambiguity search space (Teunissen, 1997).

3.2.8.4 Multipath and its effects on ionospheric measurements

As previously mentioned, multipath is a highly localised phenomena that occurs when a received GPS signal is composed of a direct line of sight signal and one or more indirect signals that have been reflected by objects in the receiver's vicinity. Multipath effects depend on a number of factors. These include: satellite geometry, reflective surfaces in the vicinity of the receiving antenna and the position of the antenna itself. Purely from a geometrical stand point, signals that are received from low elevation angle satellites are more susceptible to the effects of multipath than signals received from higher elevations.

Over shorter time spans (several minutes) multipath can be considered a systematic error. Its effect on the pseudo-range measurement is much greater than on the carrier phase, where P-code multipath observational errors are two orders of magnitude larger than on carrier phase observations, and can reach the decimetre to metre level. The multipath effect on the carrier phase measurements introduces a phase shift that degrades the range measurement by several centimeters due to a periodic bias. The maximum error on the L1 carrier signal due to a phase shift of 90º corresponds to approximately 5 cm. As the satellites change geometry in the sky, multipath displays a cyclical error on the carrier phase observations, with a classical period of between 15 to 30 minutes, depending on site characteristics (Holden, 2002; Seeber, 2003).

One error source that can not be removed via relative positioning is the effect of multipath (Georgiadou & Kleusberg, 1988b). Multipath is very much a site specific phenomena which means that no connection (or correlation) exists between the multipath errors occurring at either end of the baseline. Over short baselines, less than 10km, multipath is the predominant limitation to precise GPS positioning, as atmospheric effects can be eliminated, due to the fact that the signals pass through essentially the same atmosphere to reach both ends of the baseline. These errors should however not amount to anything much greater than 1cm with good satellite

geometry and a reasonably long observational period (Counselmann & Gourevitch, 1981).

As baseline lengths increase, the multipath error is no longer the dominant error source. Relative ionospheric refraction caused by the change in the ionosphere from one end of the baseline to the other produces larger errors. The effect of multipath on the determination of station co-ordinates can be minimised by averaging over long observational periods (of at least one of the effective cycles). The effect of the relative ionospheric bias can be almost eliminated on longer baselines by using the ionospheric free linear combination (see section 3.2.8.6.1). As the ionosphere is removed, it is only the multipath error that remains. Linear combinations of the original code and phase measurements play an important role in precise relative positioning, in the areas of ambiguity resolution and the estimation of co-ordinates. However, forming these differences amplifies the effect of multipath by a factor of approximately three when compared with the original code and phase observations (Wanninger & May, 2000).

When dealing with the measurements themselves, typical variations in the ionospheric bias at mid-latitudes during medium scale ionospheric disturbances cause variations in relative positioning with periods ranging from 10 minutes to 1 hour. This puts the ionospheric error in the same frequency domain as multipath, and therefore makes the separation of these two effects very difficult (Wanninger & May, 2000).

Multipath also has a serious effect on ambiguity resolution (see section 3.2.8.7), especially for satellites at low elevation angles (Leick, 2004). Measurement biases such as multipath can lead to incorrect ambiguity resolution that may pass unnoticed. This can result in unacceptable positional errors as well as biases in the estimation of such parameters as the relative ionosphere (Teunissen *et al.*, 2000). As mentioned in the last paragraph, the separation of the multipath error and the residual ionosphere is a very difficult task. This research will therefore consider multipath to be part of the measurement error or noise, and accept that it is a limiting factor in the accuracy of ionospheric measurement (Parkinson & Enge, 1996).

3.2.8.5 Forming differences

It can be seen that both the code and carrier phase observations produce pseudorange measurements on both the L1 and L2 carrier frequencies. These measurements can be used to form different linear combinations of the phase observations, in order to extract information from, or take advantage of certain properties that affect the accuracy of GPS observations. For example, this practice can greatly reduce the atmospheric errors (particularly the ionosphere) affecting the GPS observables.

Errors that are present in the original observations can be eliminated or reduced when differences are formed between these observations (see Figure 3.7). Linear combinations of the original phase measurements play a key role in the resolution of carrier phase ambiguity and the estimation of station co-ordinates, as part of high precision relative positioning applications, such as geodetic surveying. The formation of these different linear combinations however, comes at a price, as the noise level of the measurement can be significantly increased (Wubbena, 1989).

Referring to Figure 3.7, the line connecting two GPS receivers is known as a baseline. The fundamental single difference equation involves two points and one satellite. It is the difference between two phase (or code) measurements acquired simultaneously from satellite *k* at receivers *i* and *j.* Figure 3.7 shows four one way observations that can be used to form two single and one double difference respectively, of the code and phase observables.

$$\phi_{ij}^{k} = \phi_{i}^{k} - \phi_{j}^{k} \tag{3.21}$$

The single difference between receiver technique removes or greatly reduces any errors associated with the satellite. Equation (3.21) almost completely eliminates the satellite clock offset dt^k and also removes the satellite hardware delay b^k.

The difference between two simultaneously acquired phase (or code) single differences from satellites *k* and *l* at receivers *i* and *j:*

$$\phi_{ij}^{kl} = \phi_{ij}^{k} - \phi_{ij}^{l} = \left(\phi_{i}^{k} - \phi_{j}^{k}\right) - \left(\phi_{i}^{l} - \phi_{j}^{l}\right) \tag{3.22}$$

Equation (3.22) forms the double difference observation equation. Based on this equation the observation equations in (3.19) can be rewritten as:

$$\phi_{ij,1}^{kl} = \rho_{ij}^{'kl} - I_{ij}^{kl} + \lambda_1 N_{ij,1}^{kl} \tag{3.23a}$$

$$\phi_{ij,2}^{kl} = \rho_{ij}^{'kl} - \xi I_{ij}^{kl} + \lambda_2 N_{ij,2}^{kl} \tag{3.23b}$$

$$P_{ij,1}^{kl} = \rho_{ij}^{'kl} + I_{ij}^{kl} \tag{3.23c}$$

$$P_{ij,2}^{kl} = \rho_{ij}^{'kl} + \xi I_{ij}^{kl} \tag{3.23d}$$

where:

$\rho_{ij}^{'kl}$	represents the double differenced geometric term, which consists of the geometric range ρ_{ij}^{kl} and tropospheric refraction $d_{ij,trop}^{kl}$; and
$N_{ij,1}^{kl}$, $N_{ij,2}^{kl}$	represent the double differenced cycle ambiguities on both frequencies.

As the observations are acquired simultaneously at receivers *i* and *j*, the receiver clock error dt_i and dt_j cancel out completely along with the satellite hardware delays b^k and b^l. As multipath is a site specific phenomena, it can not be removed in the double difference observable. The successful resolution of the integer ambiguities N_{ij}^{kl} plays an important role in double differencing. Fixing the ambiguities to integers via a least squares estimation is the preferred option. This adds strength to the baseline solution by reducing the number of parameters and correlations. The double difference observation forms the basic observable in many geodetic GPS processing software packages.

Taking it a step further, triple differences can be formed by taking the difference between two double differences over two different epochs:

$$\phi_{ij}^{kl}\left(t_2, t_1\right) = \phi_{ij}^{kl}\left(t_2\right) - \phi_{ij}^{kl}\left(t_1\right) \tag{3.24}$$

The main advantage of the triple difference observable is that the initial cycle ambiguity (N) is cancelled from the observation equation. This observable can be used in the initial processing of data to establish a good estimate of position and to help detect and repair phase cycle slips in preparation for the double difference solution.

Geodetic relative positioning uses single, double and triple differences to produce highly accurate relative positions between simultaneously operating GPS receivers. Typically, one station of known co-ordinates is held fixed, whilst the 3D baseline components ΔX, ΔY and ΔZ are computed along the baseline to estimate the position of the roving receiver. The technique of relative positioning has become popular in surveying, because by forming these differences, both clock errors and hardware biases are cancelled out, and the remaining errors due to inaccurate satellite orbits, mismodelled troposphere and unmodelled ionosphere are also greatly reduced.

3.2.8.6 Linear combinations

It is possible to form different linear combinations of the original phase (or code) observations, in order to extract information from, or take advantage of certain properties that affect the accuracy of GPS observations. For example, this practice can greatly reduce the atmospheric errors (particularly the ionosphere) affecting the GPS observables and enhance the resolution of carrier phase ambiguities for precise relative positioning. However, there are some disadvantages associated with forming differences, and these mostly centre around the measurement noise produced by the combinations (see Table 3.2). The purpose of this section is to derive the equations of certain linear combinations of GPS measurements, that were used by the Bernese GPS software as part of the baseline processing carried out in this research (see Chapter 5).

In the general form, the linear combination L_x of two phase measurements ϕ_1 and ϕ_2 is formed using:

$$L_x = a_x \bullet \phi_1 + b_x \bullet \phi_2 \quad (3.25)$$

where:

a_x, b_x are coefficients.

The above coefficients are used to form the new observable. There are a variety of different linear combinations of the L1 and L2 observations that can be used in GPS data processing algorithms (Wubbena, 1989). In particular the ionospheric-free, wide-lane and narrow-lane linear combinations are commonly used. The wide-lane and narrow-lane observables are commonly used to support the rapid resolution of phase ambiguities (Talbot, 1992). The ionospheric-free linear combination is used in the estimation of baseline co-ordinates by removing the frequency dependent ionospheric delay.

Table 3.2 summarises the characteristic values of the linear combinations. The information includes: the linear combination or LC, the description or name of the linear combination, the coefficients used to form the new observable (*a,b)*, the wavelength in metres (λ), the measurement noise (σ) in metres along with the ionospheric amplification factor (IAF).

3.2.8.6.1 Ionospheric-Free linear combination

The Ionospheric-Free linear combination (L3) (Leick, 2004), is used widely as a means of greatly improving the accuracy over baselines greater than approximately 10km, by removing the ionospheric parameters I_{ij}^{kl} from the double difference observation equations. It relies on the fact that the ionospheric delay is frequency dependent and comes in the form:

$$L_3 = a_{1,3} \bullet L_1 + b_{2,3} \bullet L_2 \quad \text{(For the phase observations)} \quad (3.26)$$

where the coefficients are:

$$a_{1,3} = \frac{f_1^2}{\left(f_1^2 - f_2^2\right)} \approx +2.546 \qquad (3.27a)$$

$$b_{2,3} = \frac{-f_1 f_2}{\left(f_1^2 - f_2^2\right)} \approx -1.984 \qquad (3.27b)$$

Similar coefficients can be derived for the code observations (Leick, 2004). The above combination eliminates the ionospheric refraction terms I and ξI from the code and phase observation equations (3.19) and the double difference observation equations (3.23), which is why it is referred to as the ionospheric free observable (L3). Using the undifferenced observation equations (3.19), together with equation (3.18) and neglecting the satellite and receiver hardware biases (b), the following carrier phase equation is obtained when including the above coefficients from equation (3.26):

$$\phi_{i,3}^k = \rho_i^{'k} + a_{1,3}\lambda_1 N_{i,1}^k + b_{2,3}\lambda_2 N_{i,2}^k \qquad (3.28)$$

where:

λ_1, λ_2 are the L1 and L2 wavelengths, 0.19 and 0.24 metres respectively; and

$N_{i,1}^k$, $N_{i,2}^k$ are the real valued ambiguity parameters, for the L1 and L2 wavelengths.

Unfortunately, the integer nature of the ambiguities has been lost, as the coefficient multipliers $a_{1,3}$ and $b_{2,3}$ are not integers. Expressed using the double difference observation technique (see Figure 3.7), equation (3.28) reads:

$$\phi_{ij,3}^{kl} = \rho_{ij}^{'kl} + a_{1,3}\lambda_1 N_{ij,1}^{kl} + a_{2,3}\lambda_2 N_{ij,2}^{kl} \qquad (3.29)$$

In this form, the satellite and receiver biases (b) cancel out through the differencing. The ionospheric free L3 combination is used to eliminate the effects of the ionosphere over baselines greater than 10 km in length, and is certainly the most

frequently used observable. Forming these differences, however, has the effect of amplifying the random measurement error (ε) of the observations. The standard deviation of this measurement error is known as noise (Takac *et al.*, 1998). The law of the propagation of variances is used to compute this value, as shown in the general equation (3.30) below. The ionospheric free linear combination leads to a measurement noise that is amplified by a factor of three, when compared to the original L1 and L2 observations:

$$\sigma_{L3} = \sqrt{a_{1,3}^2\sigma_1^2 + b_{2,3}^2\sigma_2^2} = \left(\sqrt{a_{1,3}^2 + b_{2,3}^2}\right)\bullet\sigma_1 \approx 3\sigma_1 \qquad (3.30)$$

When looking at the biases present in the $\rho_{ij}^{'kl}$ term, providing that dual frequency data is used in tandem with the double differencing technique, most of the error associated with the satellite and receiver clocks $\left(dt_i, dt^k\right)$ will cancel out, along with any orbital errors ($d_{i,orb}^k$) associated with the satellites when precise ephemerides are used in a post processing scenario. Any un-modelled tropospheric error that may have been present in the baseline solutions produced for this research, was mitigated by estimating site specific tropospheric parameters using the DRY_NIELL mapping function in the Bernese GPS software package (see Chapter 5).

3.2.8.6.2 Geometry Free linear combination

When looking at relative geodetic GPS surveying, it is only the change in the ionosphere, or difference in the delay experienced at either end of the baseline, that is of primary interest (Georgiadou & Kleusberg, 1988a). The L4 linear combination known as the geometry-free combination, is capable of measuring the change in the ionosphere to within a few millimetres of accuracy (Schaer, 1999). It is used to form the 'truth data', using the Bernese GPS Software Version 4.2, to assist with the research in upcoming chapters.

The geometry-free linear combination (L4) is formed by subtracting the phase observable of the second frequency (L2) from the phase observable of the first (L1).

The geometric term $\rho^{'}$, which includes clock offsets $\left(dt_i, dt^k\right)$ and tropospheric delay $d^k_{i,trop}$ is eliminated when using the geometry-free linear combination:

$$\phi_4 = \phi_1 - \phi_2 = a_{1,4}\phi_1 + b_{2,4}\phi_2 \tag{3.31}$$

where:

$a_{1,4}$ is equal to +1; and

$b_{2,4}$ is equal to –1.

Neglecting the satellite and receiver hardware biases (b), this combination only contains the ionospheric correction term I and the integer cycle ambiguity parameters N for both frequencies, and comes in the form:

$$\phi^k_{i,4} = -\xi_4 I^k_i + a_{1,4}\lambda_1 N^k_{i,1} - b_{2,4}\lambda_2 N^k_{i,2} \tag{3.32}$$

where:

ξ_4 is the ionospheric correction factor, that converts the L4 ionospheric delay to that of the first frequency L1; and

$$\xi_4 = 1 - \xi = 1 - \frac{\mathrm{f}_1^2}{\mathrm{f}_2^2} \approx \text{-}0.647$$

$N^k_{i,1}$, $N^k_{i,2}$ are ambiguity parameters with an undefined wavelength

To the corresponding double difference:

$$\phi^{kl}_{ij,4} = -\xi_4 I^{kl}_{ij} + a_{1,4}\lambda_1 N^{kl}_{ij,1} - b_{2,4}\lambda_2 N^{kl}_{ij,2} \tag{3.33}$$

When applying the double differencing technique to the geometry-free linear combination, the satellite and receiver hardware biases (b) cancel out. Furthermore, once the L1 and L2 ambiguity parameters are fixed to integers, the only remaining unknown parameter is that of the double differenced or relative ionosphere (I_{ij}^{kl}) between two receivers *i* and *j*, which can be determined with a high degree of accuracy. The geometry-free linear combination allows for a detailed analysis of the change in the ionosphere in a temporal sense, and is also helpful when applied to ambiguity resolution strategies.

Table 3.2 Characteristics of the linear combinations of carrier phases used in baseline processing

LC	Description	*a*	*b*	λ (m)	σ (m) L_1	*IAF (m)*
L_1	Basic Carrier	1	0	0.19	1.000	1.000
L_2	Basic Carrier	0	1	0.244	1.000	1.647
L_3	Ionospheric-free LC	2.546	-1.984	0.107	3	0.000
L_4	Geometry-free LC	1	-1	0.054	1.414	-0.647

3.2.8.7 Ambiguity resolution

GPS carrier phase observations are affected by an initial unknown ambiguity term (N), which can be defined as the number of complete wavelengths between the satellite and receiver. In order to exploit the full accuracy potential of the GPS carrier phase observations, the initial ambiguity has to be determined.

The resolution of the unknown carrier phase ambiguities provides a testing problem in the area of precise geodetic surveying. Once these ambiguities are resolved or fixed, their integer nature provides highly accurate range measurements between the satellite and receiver, that support the accurate positioning of station co-ordinates using the relative positioning technique.

Resolution of the initial unknown integer ambiguity in the L1 and L2 phase observations has been a much researched area over the last two decades. Some of the more prominent contributions include: Counselman & Gourevitch (1981) who

introduced the ambiguity resolution function, which was one of the first resolution strategies devised, Brown & Hwang (1983) for early work on a multiple hypothesis scheme, Hatch (1990) for introducing rapid ambiguity resolution techniques and Frei and Beutler (1990) who showed that it was possible to resolve phase ambiguities within a few minutes over short baselines using a sequential ambiguity resolution strategy, as a means of rapid real-time baseline recovery using single frequency GPS data. A significant contribution to this area of research has been made by Teunissen (1995) with the introduction of the now widely used computationally efficient and powerful LAMBDA (Least Squares Ambiguity Decorrelation Adjustment) method of ambiguity resolution.

The technique of double differencing plays a vital role in the resolution of phase ambiguities. When using the single difference technique, the receiver clock offset is still present and this can not be effectively separated from the integer ambiguities. The receiver clock offset cancels out however, when using the double differencing technique, which allows for the effective isolation of the ambiguities. Ambiguities must by fixed to their correct integer values, as one cycle on the L1 signal, translates to 0.19m of positional error.

Baseline length plays a critical role in the ability to resolve ambiguities to their correct integers. It is assumed that over short baselines of less than 10km, when using the double differencing technique, the effect of the ionosphere, troposphere and satellite orbital errors will cancel out to provide the following equation:

$$\lambda\phi_{ij}^{kl}(t) = \rho_{ij}^{kl}(t) + \lambda N_{ij}^{kl} + \varepsilon \qquad (3.34)$$

However, any residuals present in these neglected terms can affect the positional accuracy of the solution and the integer nature of the ambiguities. This is more likely to occur as baseline length increases.

Ambiguity resolution can also be affected by poor satellite geometry (Talbot, 1991b). The ability of a GPS receiver to track as many satellites as possible allows for redundancy in the ambiguity resolution process which aids in the efficiency and reliability of the solution. The length of baseline occupation time also has an

important effect on the performance of the ambiguity resolution result (Frei, 1991; Teunissen, 1998). In recent years, significant advances in ambiguity resolution strategies, software and GPS receiver design have significantly reduced the amount of time required to correctly resolve ambiguities. Depending on the application, the time taken to fix ambiguities for precise determination of position, can range from a few seconds to a couple of minutes (Euler & Landau, 1992; Teunissen, 1995; Euler & Ziegler, 2000).

The presence of multipath can have a detrimental effect on the ambiguity resolution process (Joosten *et al*., 2002; Kubo & Tasuda, 2003). Baseline length has no impact here, as multipath is purely a site specific phenomena, therefore its effect may be significant over short baselines. Just as in the case of atmospheric errors and satellite orbital errors over long baselines, multipath can also degrade the accuracy of station co-ordinates by contaminating the ambiguities.

There are two major steps in the ambiguity resolution process (Langley, 1984). Firstly, for consideration in the processing algorithm, an estimate of the potential integer ambiguities for each combination in the double difference solution must be produced. This is achieved by constructing a search space, which contains the level of uncertainty relating to the approximate coordinates of the unknown antenna position. In static positioning applications, this search space can be gained by estimating the antenna's position using the so-called float ambiguity solution. The size of this search space, containing the possible integers that need to be assessed, will dictate the computational load and thus the efficiency of the process. The search space therefore needs to be conservative, whilst still being mindful of computational load.

The second step in the ambiguity resolution process is to identify the correct integer ambiguity combination. Many ambiguity resolution strategies revolve around a least squares adjustment, where an ambiguity combination which minimises the sum of the squared residuals is chosen to be correct. It has been found that the least squares approach to ambiguity resolution, maximises the probability of the correct integer estimation (Teunissen, 2003). This approach relies on the theory that the combination that best fits the data is the correct one. When using the least squares

approach, it is assumed that the data being used is normally distributed. However, due to the systematic effects of such errors as those brought about by the atmosphere, orbital irregularities and multipath, this is not always the case, and this is the reason why ambiguity resolution over longer baselines can fail.

Using dual frequency data can be very advantageous as it allows for the use of many possible linear combinations to resolve ambiguities. Such combinations include the wide-lane and narrow-lane approaches, with their corresponding wavelengths of 86.2cm and 10.7cm respectively (Wubbena, 1989). The wide-lane technique with its increase in wavelength from the original L1 and L2 signals provides easier resolution of the ambiguities. The ionospheric error on the wide lane frequency is three times smaller than on L1. Therefore, it is possible to ignore the ionospheric error in the wide-lane, on baselines up to approximately 100km (depending on ionospheric conditions) and still successfully resolve integer ambiguities (Hungentobler *et al.*, 2001). As the baseline length increases, however, especially in times of disturbed ionospheric conditions, the ambiguity resolution process can be severely hindered by the ionosphere, and the wide-lane approach may fail. In this case it is possible to use a deterministic ionospheric model, based on the results obtained from the Geometry-Free linear combination (see section 3.2.8.6.2), to help reduce the effect of the ionosphere to a manageable level. Once the wide-lane ambiguities are fixed, the narrow-lane technique can be used to gain high precision results, due to its smaller wavelength and low measurement noise (Seeber, 2003).

An alternative to the above approach, is to use the Quasi-Ionospheric-Free (QIF) ambiguity resolution strategy (Mervart, 1995). This technique estimates the ionospheric error for every satellite, at every epoch, then resolves the L1 and L2 ambiguities directly (see section 3.2.8.7.1).

3.2.8.7.1 Quasi-Ionospheric-Free (QIF) resolution strategy

The resolution of ambiguities N_1 and N_2 directly over long baselines is possible using the QIF ambiguity resolution strategy (Mervart, 1995). The L1 and L2 phase observations are processed together using equations (3.23a) and (3.23b). The

ionospheric error is estimated using one parameter per satellite per epoch. The estimation of these ionospheric parameters using the ordinary least squares approach, would lead to the inversion of an extraordinarily large matrix, which would make the task unfeasible, even with today's modern computing power. In order to make this technique viable, a process of pre-eliminating the ionospheric parameters epoch by epoch is used, which is based on the equivalence of the mathematical and stochastic models (Blewitt, 1998). This means that a parameter can be estimated explicitly within the mathematical model, or alternatively, implicitly through the variance co-variance model (Brown, 2003). On computing and removing the ionospheric influence using the pre-elimination technique, it is possible to gain good real valued estimates of the ambiguities using a float solution. The most likely pairs of L1 and L2 ambiguities are then estimated in the QIF strategy using the float ambiguities and their co-variance matrix. Using the ambiguity estimates from the float solution, the ionospheric bias is then calculated for every double difference combination. The computed ambiguity sets are then ordered from most to least precise, using the root-mean-square (RMS) of the ionospheric bias, which is computed via the ambiguity co-variance matrix. In order to fix the correct ambiguities, within the search space a test is carried out to find the set of estimated ambiguities that produce the smallest deviation from the true value, based on the following equation:

$$\Delta\eta = N_{ij,5}^{kl} - N*_{ij,5}^{kl} \tag{3.35}$$

where:

$\Delta\eta$ is the difference between the estimated $N_{ij,5}^{kl}$ and true value $N*_{ij,5}^{kl}$. This value should be very close to zero.

If $\Delta\eta$ is within a preset limit, the ambiguity set is held fixed to the integer values. The ambiguity process is then recomputed until no other ambiguity sets can pass the criteria. The QIF ambiguity resolution strategy within the Bernese GPS Software was used to fix the baseline solutions that are used as truth data to assist the research discussed in further chapters.

3.2.8.8 Absolute ionospheric measurement with GPS

The use of ground based GPS receiving stations or networks for the measurement of ionospheric TEC has been extensively researched and quantified within the GPS scientific fraternity. GPS provides a very versatile system for taking ionospheric measurements, on either a local, regional or global scale. Dual frequency GPS receivers can be used to measure and model the ionosphere in order to provide corrections to single frequency GPS receivers in the vicinity or to aid in the fast resolution of integer ambiguity parameters (see section 4.3). The use of one or a network of GPS receivers to measure the ionospheric effect over a region has proven to be an effective approach for correcting the ionospheric range error and improving GPS positional accuracy (Liu *et al.*, 2005).

However, the line of sight ionospheric measurements derived from differencing dual frequency GPS delays are corrupted by instrumental biases in both the GPS receiver and GPS satellite (Lin & Rizos, 1996). These delays are commonly known as differential hardware biases. In the case of the GPS receiver, the L1 and L2 signals must travel through different internal circuitry paths, which introduces a hardware delay. The GPS satellite signals (L1 and L2) are synchronised to transmit simultaneously. However, absolute synchronisation is not possible, therefore the time difference in transmission between the two signals introduces a satellite hardware bias. Therefore, the line of sight ionospheric delay can be described as the sum of the receiver and satellite hardware biases, plus the actual ionospheric delay along the signal path (Wilson & Mannucci, 1993). When using GPS measurements to compute line-of-sight TEC values, ignoring the satellite and receiver hardware biases may result in an error of $\pm$9 and $\pm$30 TECU respectively (Wilson & Mannucci, 1993).

In order to gain absolute TEC readings, from dual frequency line-of-sight GPS measurements, the estimation of the receiver and satellite biases is required. It is possible to compute the receiver bias via direct calibration for some receivers. As an example, the Allen Osbourne Associates Rogue receiver can be calibrated, with the receiver differential delays usually lying within the range of $\pm$10 nanoseconds (ns) with an uncertainty of 0.2 ns (Wilson & Mannucci, 1993). The satellite hardware bias is also calibrated prior to launch, however Cohen et al. (1992) found that these

estimates were not accurate enough for precise TEC determination. A number of modelling schemes have been developed to estimate the combined receiver and satellite hardware biases (Mannucci *et al.*, 1993; Wilson & Mannucci, 1993; Lin & Rizos, 1996). Hernandez-Pajares (2003) reported on the comparisons in estimating the satellite and receiver hardware biases for the International GNSS Service (IGS) analysis centres (COD, EMR, ESA, JPL, UPC). It was found that the agreement between the different analysis centres was at the 1 ns level. Note that 1 ns of delay corresponds to 0.30m of range error on the L1 frequency. These biases have been found to be very stable over time, over a period of days to months, and are therefore treated as constants during ionospheric modelling (Gao *et al.*, 1994; Schaer, 1999).

A number of different modelling approaches have been developed that provide TEC estimates to an average accuracy of approximately one to several TECU (Komjathy, 1997; Gao & Liu, 2002). These approaches include such methods as the use of: a 2D Taylor series polynomial, spherical harmonic functions or 3D ionospheric tomography to describe TEC values over a region.

As a means of quantifing the ionospheric behaviour over Victoria during different seasonal periods, the ionosphere over Victoria is modelled in Chapter 6 using the spherical harmonic approach. This analysis provided information on the overall stability of the ionosphere over the region.

3.3 Summary

In order to model the ionosphere over Victoria, a means of physically measuring it is required. This chapter has provided an overview of the various approaches that are available to measure the ionosphere and the types of accuracies that are achievable. This involved an investigation into traditional Earth based probing techniques, which include the ionosonde, oblique backscatter radar and incoherent backscatter radar methods. Terrestrial probing methods including satellite-based approaches were also covered.

The global positioning system was also introduced as a means of gathering ionospheric measurements. The effect that the ionosphere has on GPS geodesy was

presented along with methods used to mitigate its influence. A description of the GPS observables was given and how these observables can be used to form different linear combinations that can be used to extract ionospheric information from the observations taken. This ionospheric information can be used as input for absolute TEC models or as a means of quantifying the change in the ionosphere through the double differenced ionospheric parameter.

This chapter has presented a background into both traditional and modern means of gathering ionospheric information. The use of GPS to provide this information was established, as GPS networks provide an accurate and continuous method of data collection. This chapter has provided an understanding of how ionospheric information is gathered and how GPS can be used to fulfil this role. An appreciation of the precise nature of GPS measurements and the types of errors that influence its accuracy has been gained. This understanding will help form an appreciation of the strengths and weakness associated with the use of GPS networks to adequately model the ionosphere over Victoria. The source of all ionospheric information used to conduct the research in further chapters was derived from GPS observations taken in Victoria.

The next chapter will give a background into how ionospheric information gained via GPS observations can be manipulated to model its effect. The types of modelling approaches being currently used and the accuracies achievable will be investigated. This is undertaken as a means of gaining insight into the current models available and their suitability for producing real-time cm-level corrections over Victoria.

Chapter 4 Ionospheric modelling, GPS Augmentation and Correctional Services

This chapter presents up to date research in the area of ionospheric modelling within the GPS community. Some of the more well established and internationally accepted models developed over the last three decades will be described. These models include the Bent Model, the GPS Broadcast Model, the International Reference Ionosphere (IRI) 2001 and the Global Ionospheric Maps (GIMs) produced by the Centre of Orbit Determination in Europe (CODE). The application of GPS measurements in the formulation of ionospheric models and corrections is also investigated. Modelling concepts such as grid-based approaches, ionospheric tomography, GPS augmentation systems and the application of RTK ionospheric corrections within a CORS network are discussed. The accuracies achievable and applications of these different systems are also examined.

This chapter is presented as a means of gaining an understanding into the types of ionospheric modelling procedures that are currently available, and the applications associated with each procedure. The use of CORS networks to produce ionospheric corrections that can be used to improve the positional accuracy of users within the network coverage area is also introduced. The improvement of current modelling techniques within a network RTK environment is the focus of further research in upcoming chapters.

4.1 Ionospheric modelling approaches

Since the advent of radio and satellite communications, the effect of the ionosphere on radiowave propagation has been of much interest, and in more recent times, a concern for the users of GPS. A number of ionospheric models are available to the GPS user to correct for ionospheric signal delay, where dual frequency receivers are not available, and to assist in the resolution of carrier phase ambiguities in precise geodetic surveying applications. The majority of these models fall into two categories (Klobuchar, 1996):

1) Empirical models, that are derived from actual ionospheric observations, usually compiled over a number of years. They are typically global in nature and attempt to describe ionospheric variation with respect to daily, seasonal and even yearly time scales. Examples of these models include the Bent Ionospheric Model (Bent & Llewellyn, 1973), the International Reference Ionosphere (IRI) (Bilitza, 2001) and the Global Ionospheric Maps (GIMs) produced by the Centre of Orbit Determination in Europe (Schaer, 1999).

2) Theoretical models, that attempt to model the ionosphere by solving a set of equations that describe the physics and chemistry of the ionospheric plasma. These models are computationally intensive, and require a large amount of computer time. A good reference for information about theoretical models is the STEP, *Handbook of Ionospheric Models* (Schunk, 1996). Examples of ionospheric models contained in this handbook include, the Utah State – Time Dependent Ionospheric Model (TDIM)(Schunk & Sojka, 1996) and the Phillips Laboratory – Global Theoretical Ionospheric Model (GTIM) (Anderson *et al.*, 1996).

It should be noted that no available model can do it all, and that the selection of model to be used is dependent on the type of information required by the user, the computational resources available and type of ionospheric input parameters at hand (Cander *et al.*, 1998).

4.1.1 Models and solar indices

Solar indices (see section 2.2.1), over extended periods, show a high correlation with the eleven year solar cycle and the variation in solar radiance that accompanies it. Ionospheric models such as the Broadcast, Bent and IRI, use solar indices as a way of reproducing these variations. Solar indices such as sunspot number and 10.7cm solar flux are widely used by ionospheric models, as long data records exist for both. Correlation analysis shows that the solar flux value is a better predictor for regions of strong solar control, below the F-layer peak, and that for regions above, where dynamic influences compete with solar influences, the sunspot number is a better indicator. A 12-month running mean of these solar indices has been found to produce a higher correlation with ionospheric parameters than either monthly or daily averages (Klobuchar & Doherty, 1992). The IRI model also uses a global ionospheric index (IG) as an alternative to the 12 month running mean sunspot number (Liu *et al.*, 1983). This index is ionospherically based, and intended for use with the existing CCIR model coefficients (see section 2.2.1.4). The IG index is derived from observed noontime monthly median values of foF2 from 13 mid-latitude ionosonde stations, located throughout the world. The sunspot number required to produce the observed value, is designated as the IG index for the month in question, thus the 12 month smoothed value is denoted by IG_{12}. The IG index gives a much better representation of ionospheric conditions, as it is derived directly from ionospheric parameters (Bilitza, 2001).

4.1.2 World-wide ionospheric coefficients

The CCIR and the International Union of Radio Science (URSI) global representations of ionospheric conditions are explained in the following paragraphs. These coefficient sets, of the foF2 parameter, have for many years formed the backbone of many ionospheric models, including the IRI and Bent models. The models work extremely well in representing the day-night variations of the ionosphere at low and middle latitudes, but suffer at high latitudes due to the lack of ground observations in this region (Bilitza, 2002).

The first global empirical representation of the ionosphere was constructed in 1962 by Jones and Gallet (1962), as a means of making ionospheric predictions. It was based on the foF2 parameter, which is proportional to the electron density at the peak of the F2 region. This model has become the most widely used global foF2 model, and has been adopted for international use by the CCIR. The input data for the CCIR model was gained by a worldwide network of ionosondes (about 150 stations) during the years 1954 to 1958, and is routinely scaled from ionograms. The foF2 parameter is described using a set of special functions, in terms of universal time, geographic latitude and longitude and a modified magnetic dip-latitude. In areas where no data was available (particularly ocean areas) artificial values were inserted. All of the measured and artificial data was then combined and fitted with an increasing number of terms until the optimal set of coefficients was found. The model consists of 24 coefficient maps each containing 988 parameters, one for each month of the year, and for two solar activity levels R_{12}=0 and R_{12}=100, where R_{12} is the 12 month running mean of the monthly sunspot number (see section 2.2.1.2). For intermediate levels of solar activity, interpolation is recommended.

The propagation factor M(3000)F2 is also modelled by the CCIR in tandem with the foF2 maps. The MUF factor is defined as the maximum usable frequency at which a radiowave can propagate from a given point to a height of 3000km. The M(3000)F2 is the ratio of the maximum usable frequency to the F2 critical layer frequency, foF2. The value is derived from vertical incidence ionograms by a simple process based on a simplified theory (Piggott & Rawer, 1972;, 1978). When the M(3000)F2 data was introduced to the same mapping functions devised for foF2, it was found that a smaller number of parameters (only 441) were required to produce a monthly map (Jones *et al.*, 1969). The M(3000)F2 coefficients are used as a means of determining the altitude of the F2 peak electron density (hmF2), as a strong anti-correlation exists between the M(3000)F2 parameter and the hmF2 value (Bilitza, 1979).

Based on work by Fox and McNamara (1988) the URSI set out to improve the then established CCIR global representation of foF2. A new model based on CCIR like coefficients was produced from a much larger database of ionosonde measurements (approximately 45,000 station months). In areas of no data availability, such as ocean areas, screen points were computed based on a theoretical modelling approach.

Whilst the CCIR model produced screen points via an extrapolation process, the URSI model adjusts a theoretical model to agree with measured foF2 parameters over land, then uses this model to compute observations over oceans (Rush *et al.*, 1989). This has led to the acceptance of the URSI coefficients as giving a better representation of ionospheric conditions over ocean areas (CCIR, 1966, 1990). This does not mean, however, that the URSI model gives a better global representation than the CCIR model. Both models are actually comparable in accuracy, as the same formula and number of coefficients were used in both. Whilst the URSI model improved the accuracy over ocean regions, it came at the expense of accuracy over land.

4.2 Empirical ionospheric models

The ionospheric models described below are the GPS Broadcast Model, the Bent Model, the CODE Global Ionospheric Maps and the International Reference Ionosphere 2001. They are all global empirical ionospheric models. All of these models estimate the absolute ionsopheric delay with varying degrees of accuracy. This is the result of a number of different factors, including: the complexity of the model's computational workings, the accuracy of the data (coefficient sets) used as inputs, and the fact that being a global representation of ionospheric conditions, model outputs have to be interpolated where actual ionospheric data is unavailable.

The performance of these models will be investigated in Chapter 5, by comparing their outputs against differentially derived ionospheric parameters, computed using the Bernese 4.2 Software (Hungentobler *et al.*, 2001), to see how well they evaluate the change in the ionosphere from one location to the next, as a means of evaluating their suitability for producing ionospheric corrections in a Network-RTK environment. The models will be tested over three different baselines that form a triangular network in the southern Victorian region. The base stations used are part of the state wide permanent GPS tracking network, known as GPSnet (see Chapter 5).

4.2.1 The Broadcast model

The Broadcast ionospheric model (Klobuchar, 1986), was designed to provide the GPS user with a simple time delay correction algorithm, that could remove at least 50% of the ionospheric range error, using a minimum of coefficients. This 50% correction value was established as a compromise between the number of coefficients required (that were to be sent as part of the GPS navigation message), and the fact that more powerful, state of the art, computationally intensive models, requiring many coefficients, could only remove up to approximately 80% of the ionospheric delay. The correction coefficients came in the form of eight parameters that are broadcast as part of the GPS navigation message.

The model design was based on a number of limiting factors. These include:

- the room available on the navigation message for the coefficients required by the correction algorithm;
- the need for a simple algorithm to limit user computational time and complexity;
- up to date knowledge of the ionospheric behaviour; and
- the most likely geographic user's areas on the globe.

The model developed consists of a simple half cosine representation of daily ionospheric TEC, designed to approximate the median diurnal behaviour of the ionosphere, with a night time constant value (see Figure 4.1).

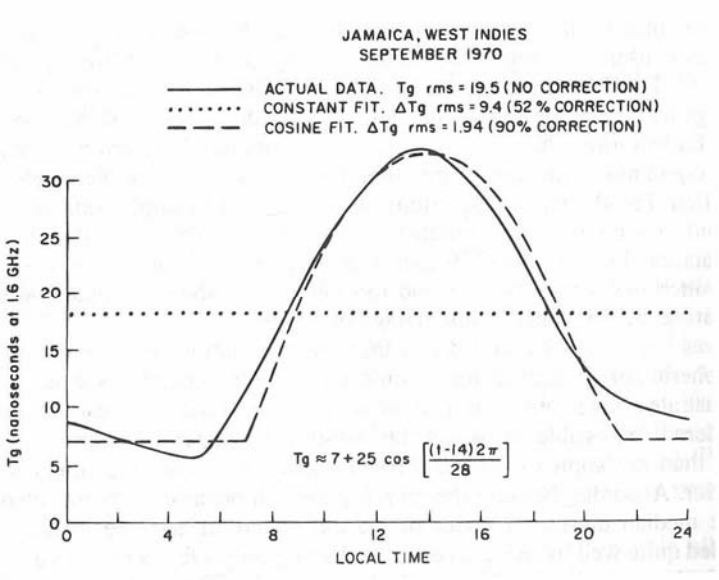

Figure 4.1 A positive half cosine shaped curve, made to fit a typical monthly average TEC diurnal variation from a station in Jamaica in Sept, 1970 (after Klobuchar, 1996)

The algorithm supports the inclusion of four potential parameters in the cosine representation of daily TEC or ionospheric delay (T_{iono}), that are represented by the eight coefficients on the navigation message:

$$T_{iono} = F \text{ x } \left\{ DC + A\cos\left[\frac{2\pi(t-\phi)}{P} \right] \right\} \tag{4.1}$$

where:

F is the slant factor, that converts line of sight delay, to vertical delay;

A is the amplitude of the cosine term;

P is the period of the cosine term;

DC is the night time constant; and

ϕ is the phase of the cosine term.

In order to decide whether any of the four cosine terms could be simplified, so as to best use the total of eight parameters available in the GPS navigation message, the Bent ionospheric model was used to produce a number of daily TEC curves, over varying latitudes, along the American longitudinal sector. It was found that on

comparison, the DC term and the phase term (ϕ) in the cosine representation, vary to a much lesser extent than the amplitude (A) and period (P) terms. According to the analysis, the DC term was then given a constant value of 5ns, and the phase term a constant peak value at 14 hours. The remaining amplitude (A) and period (P) terms are represented by a cubic polynomial, whose coefficients are transmitted via the GPS navigation message. These coefficients are updated once every 10 days, based on the mean of the previous five days 10.7cm solar flux value, or as ionospheric behaviour governs. The model's primary intent is to provide single frequency GPS users with an estimate of the ionospheric time delay.

The model has been tested and found to meet its design criteria of removing at least 50% of the ionosphere, with previous authors recording the model removing approximately 60% of the ionospheric effect (Fees & Stephens, 1986; Klobuchar, 1986; Newby & Langley, 1992)

4.2.2 The Bent model

The Bent Ionospheric Model (Bent & Llewellyn, 1973; Bent *et al.*, 1975) is a global empirical ionospheric model developed in the early 1970's, primarily for the estimation of ionospheric delay corrections for ground to satellite communications. The model is based on a vast database of historic ionospheric information. The database includes data from approximately 400,000 bottomside ionospheric soundings gathered by fourteen ionosonde stations located within the American longitudinal sector, covering magnetic latitudes N85° to 0°, during the period from 1962 to 1969. The data produced from these soundings came in the form of hourly profiles of the ionosphere up to the foF2 peak. The topside ionosphere was probed by approximately 60,000 Alouette 1 topside ionospheric soundings, covering the magnetic latitudes N85° to S75° during the period from 1962 to 1966. This data came in the form of electron density profiles from about 1000km down to the height just above the maximum electron density (F2 peak). The period from May 1967 to April 1968, which coincided with solar maximum conditions, was covered from the topside with 6000 Ariel 3 satellite electron density profile measurements which were linked to

F-peak parameters from simultaneous ground station ionosonde readings, that covered the geographic latitudes of N70° to S70°.

This data was then used to produce a model, with a primary role of mapping the electron content as accurately as possible, in order to obtain very precise estimates of the signal delay experienced, as well as the directional changes of the signal due to refraction (Kohnlein, 1978). During the process of describing the profile of the ionosphere, by analysing the aforementioned vast database of measurements, a number of assumptions were made. As the collected topside data did not represent conditions over the entire globe, and the bottom side soundings were only available for areas covered by land masses, a definitive global description was not possible. This shortcoming was overcome by the fact that local time has a far greater influence over ionospheric conditions than longitude. Therefore, the data was analysed as a function of latitude and local time. Next, in order to describe ionospheric behaviour, primarily electron density versus altitude, a theoretical profile was developed, that fit the measurements taken.

This profile came in the form of three equations that describe the electron density of the lower, middle and upper ionosphere to a height of 1000km (see Figure 4.2):

where:

N the electron density;

N_m the maximum electron density;

N_o the maximum electron density for each exponential layer;

a & b are vertical distances measured from the start of each layer;

y_m the half thickness of the lower layer;

y_t the half thickness of the upper parabolic layer; and

k the decay constant for an exponential profile.

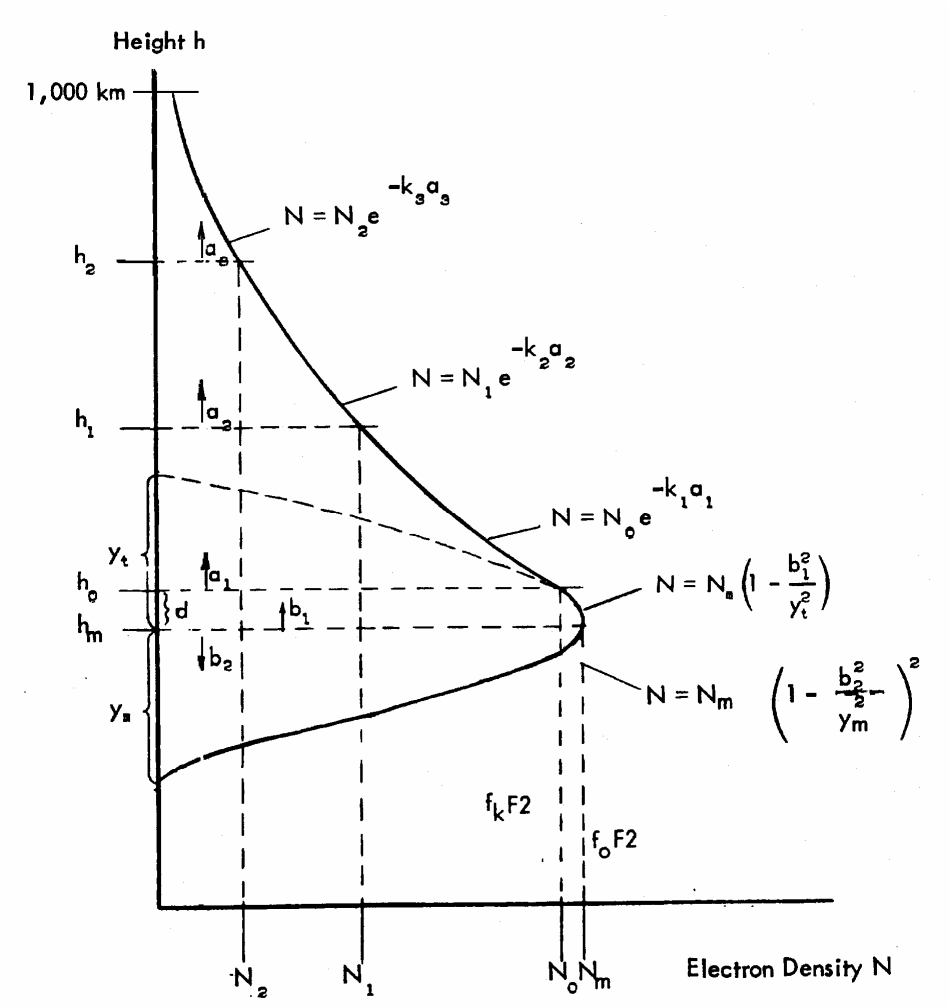

Figure 4.2 Bent Ionospheric Profile (Llewellyn & Bent, 1973).

The lower ionosphere is described by a bi-parabola, the upper described by an exponential function, with both layers fitting together using a parabola.

The total integrated vertical electron content N_T, at the derived Ionospheric Pierce Point (IPP) (see section 4.2.5), and the height of the maximum electron content (h_m) is determined using the *CCIR* generalised foF2 and M(3000)F2 coefficients (Jones & Obitts, 1970) that are derived from the present 12 month running solar flux value (10.7cm solar flux) in order to yield a specific set of foF2 coefficients. In order to estimate the value of foF2, the difference between the 12 month running solar flux value and the daily value is computed ie. $Flux_{12}$ – Flux. The total integrated vertical electron content, N_T, is defined in the following equation:

$$N_T = 1.24 \times 10^{10} \times (\text{foF2})^2 \times \left(\frac{N_T}{N_m} \right) \quad (4.2)$$

where:

$\frac{N_T}{N_m}$ is the ratio of the total integrated electron content to the maximum electron density.

The height of the maximum electron density (h_m) is derived using the following equation (Appleton & Beynon, 1940; 1947):

$$h_m = 1346.92 - 526.40 \times M(3000)F_2 + 59.825 \times \left[M(3000)F_2 \right]^2 \text{ km} \quad (4.3)$$

The M(3000)F2 values come in the form of a monthly set of coefficients, that are derived for both a 12 month running average sunspot number S_{12}=0 and S_{12}=100. These coefficient sets are adjusted against the 12 month running average sunspot number for the evaluation date through extrapolation. The final M(3000)F2 coefficient set is produced using time dependent and position dependent functions.

Initial testing carried out on the Bent model estimated that it can account for up to 75-90% of ionospheric delay (Bent & Llewellyn, 1973). The model was tested against dual frequency satellite data (Bilitza *et al.*, 1988) and it was found to overestimate the delay during the day, and underestimate it during the night. The model has also been tested against Faraday rotation data (Newby & Langley, 1992), where it was found to remove approximately 70-80% of the daytime ionosphere and approximately 60-70% of the night-time effect.

4.2.3 The CODE model

Since early 1996, the Centre for Orbit Determination in Europe (CODE) has been producing Global Ionospheric Maps (GIM's), that are derived from data collected via the International GNSS Service (IGS) network. The CODE is one of several analysis centres of the IGS, and uses the network's globally distributed GPS tracking stations to produce estimates of world wide TEC readings. These TEC values can then be used to calculate ionospheric GPS signal delay, for line of sight receiver to satellite range correction.

The IGS network was first established in 1994, as a service of the International Association of Geodesy (IAG). Its primary role is to provide support for geodetic and geophysical research activities via the production of GPS data and associated products. The network is currently made up of over 300 permanent GPS tracking stations. CODE currently uses approximately 150 of these stations as its data source.

In order to gain the raw data for the global representation of TEC, data from the IGS tracking network is used in such a way that the double difference phase observations are processed using the geometry-free linear combination (L4) (see section 3.2.8.6.2), with the Bernese GPS Software Version 5. A least squares adjustment of these globally derived parameters is then performed in order to obtain the TEC values (Schaer *et al.*, 1996). A data sampling interval of 5 minutes is used as an input, and the data is collected using a 10° elevation angle cut off (Schaer, 2003).

This procedure provides a framework to model the TEC to the vertical in a solar-geomagnetic reference system using a spherical harmonic expansion up to degree and order 15. Global TEC E(β,s) is represented as a spherical function as follows:

$$E(\beta,s) = \sum_{n=0}^{n_{max}} \sum_{m=0}^{n} \overline{P}_{nm}(\sin\beta) \bullet (a_{nm}\cos ms + b_{nm}\sin ms) \qquad \text{with } t \in [t_i, t_{i+1}] \tag{4.4}$$

where:

E is the vertical Total Electron Content (VTEC);

β is the geocentric latitude of the intersection point between the line of receiver-satellite and the ionospheric layer;

$s=\lambda-\lambda_0$ is the sun fixed longitude of the IPP or sub-ionospheric point, i.e. the difference between the Earth fixed longitude λ and the longitude of the Sun λ_0;

n_{max} is the maximum degree of the spherical harmonic expansion;

$\overline{P}_{nm} = \Lambda_{nm} P_{nm}$ are the normalised associated Legendre Functions of degree n and order m based on the normalisation factor Λ_{nm} and the classical (unnormalised) Legendre functions P_{nm};

a_{nm}, b_{nm} are the TEC coefficients of the spherical functions, ie. the GIM parameters describing the global TEC; and

t_i, t_{i+1} is the specified period of validity (of model number i).

Recent findings on the accuracy of the CODE model (Hernandez-Pajares, 2003), indicate that it can estimate TEC in an absolute sense to within 1.4 TECU (TEC units) (1 TECU ~ 0.16m delay on L1), with a standard deviation of 6.5 TECU, when compared to TOPEX dual frequency altimeter data.

4.2.4 International Reference Ionosphere (IRI) 2001

The Committee on Space Research (COSPAR) and the International Union of Radio Science recognise the IRI as being the world-wide standard ionospheric specification model (Bilitza, 2002). Several updated editions of the model have been produced since it was first released in 1978 (Rawer *et al.*, 1978). The COSPAR and URSI formed a working group in the late 1960's, with the primary objective of establishing a global empirical model, based on all of the available data sources at the time (Bilitza, 1992). Each year the models' shortcomings and suggested improvements are

discussed at annual IRI meetings, where the current IRI is evaluated and compared with data and other models.

A number of special reports have been published (Rawer *et al.*, 1978; Rawer *et al.*, 1981; Bilitza, 1990) where indepth descriptions of the models' inner workings can be found. These reports describe such model details as; its background, database, algorithms, formulas and computer program. The model released in June, 2001, has a number of important improvements and additions when compared to its predecessors (Bilitza, 2001). Its Fortran source code can be obtained from the IRI home page (IRI, 2007), along with a description of the model, member working groups and links to other web applications.

The IRI consists of global models of the D, E, F1 and F2 regions of the ionosphere (see section 2.1.4). Full electron density profiles are obtained by using mathematical functions and merging algorithms to pull the different regions together. Figure 4.3 illustrates how the ionospheric electron density profile is constructed (Bilitza, 1990). The boundaries between the subsections in the profile are marked by several characteristic points including the F2, F1 and E-layer peaks.

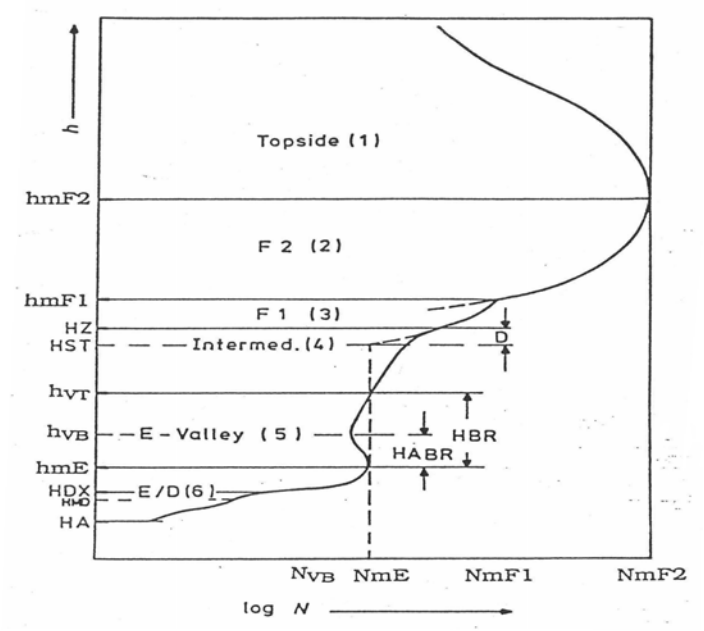

Figure 4.3 The International Reference Ionosphere, electron density profile

With certain modifications, the CCIR models are used to compute the F2, F1 and E peak densities. The CCIR coefficient sets are recommended for use over continental areas, whilst for ocean areas, the URSI-88 model is provided. The height of the F2-peak, $h_m F2$, is calculated from M(3000)F2 using the empirical formula (Bilitza, 1979):

$$h_m F2 = \frac{1490}{\left(M\left(3000\right)F2 + DM\right)} - 176 \tag{4.5}$$

Using a correction factor:

$$DM = \frac{f_1 f_2}{\left(\frac{f_0 F2}{f_0 E - f_3}\right) + f_4} \tag{4.6}$$

With solar activity functions:

$$f_1 = 0.00232 \bullet R_{12} + 0.222 \tag{4.7a}$$

$$f_2 = \frac{1 - R_{12}}{150 \exp\left(-\left(\frac{\psi}{40}\right)^2\right)} \tag{4.7b}$$

$$f_3 = 1.2 - 0.0116 \exp\left(\frac{R_{12}}{41.84}\right) \tag{4.7c}$$

$$f_4 = \frac{0.096\left(R_{12} - 25\right)}{150} \tag{4.7d}$$

where:

R_{12} is the 12 month running mean solar sunspot number; and

ψ is the magnetic dip latitude.

The IRI is based on two different coordinate systems. Geodetic coordinates are used to describe the low altitudes and a magnetic system for higher altitudes. This is due to the strong connection to the neutral gas (high collision frequency) in the lower ionosphere, and the coupling with the magnetic field lines in the middle and upper ionosphere. The CCIR foF2 model was modified to be based on magnetic latitude, rather than having a geographic orientation and the F1 layer is restricted in its appearance to non-winter months only. The peak electron density of the E-region is described by a combination of the day time CCIR model coefficients and a night time model based on incoherent scatter radar measurements (Rawer & Bilitza, 1990). The IRI recommends a constant height of 110km for the height of the E-peak density. This value has been confirmed by analysis against incoherent scatter radar measurements (Pandey *et al.*, 2000) and ionosonde data (Mosert *et al.*, 2000).

The D-region is characterised by high variability coupled with a limited database. As the region is too low for satellite readings, and the electron densities are too small for ionosonde and radar measurements, the only available data source comes from rocket experiments. The deep valley between the E and F layers, that is characteristic of the night time ionosphere and is also present to a lesser degree during the day time hours, can be seen represented on the electron density profile (see Figure 4.3). The length and width of the valley is described by parameters derived from incoherent scatter radar measurements (Kouris & Muggleton, 1973a;, 1973b), that are based on latitude and solar zenith angle. The F2 bottom side profile established by Ramakrishnan and Rawer (1972), is described by a thickness parameter, B_0, and a shape parameter, B_1, and is defined by:

$$\frac{N(h)}{NmF2} = \frac{\exp\left(-x^{B1}\right)}{\cosh(x)} \tag{4.8}$$

where:

$$x = \frac{(hmF2 - h)}{B_0} \tag{4.9}$$

The topside model of the IRI is an analytical representation of the Bent model, based on Epstein functions. The Bent model is based on data obtained from a satellite topside sounder (Alouette 1), ionosonde measurements and *insitu* measurements (Bent & Llewellyn, 1973). The parameters used to characterise this region are: the F2 peak plasma frequency, the geomagnetic latitude and the monthly 10.7cm solar flux value. The IRI model also uses these variables to describe the variation of the topside scale heights, that are derived from the Bent model (Bilitza, 1990). The Bent model provides a graphical representation of the profile parameters versus solar activity for differing ranges of foF2 values and latitudinal sectors. It was found by Rawer et al. (1978) that the Bent model displayed irregular activity and discontinuities at class boundaries. In order to avoid these discontinuities, the IRI applies analytical functions using the previously mentioned variables. This smoothed analytical representation of scale height, provides a better description of electron density. When compared with actual TEC data compiled from Faraday rotation measurements (see section 3.2.2), the IRI and Bent models were found to provide a good estimate at mid and high latitudes (McNamara & Wilkinson, 1983; McNamara, 1984;, 1985), but within the equatorial region both models performed poorly. During high solar conditions, in the equatorial region, the IRI models estimates of TEC where almost a factor of 2 below the actual measurements. This problem was partly because of the limited latitudinal resolution of the original Bent model, which only provided three sectors, being equatorial, middle and high. Bilitza (1985) produced a correction term to help reduce this problem, based on incoherent scatter radar data, and satellite measurements from AEROS, AE-C and DE-2 satellites. This correction term was added to the IRI-86 model. In a later study undertaken by Ezquer *et al.* (1998), the IRI-95 model was tested against TEC measurements gained via Faraday rotation techniques, obtained in the equatorial region during a period of high solar activity. It was concluded that the IRI-95 model overestimates TEC around the daily minimum and underestimates it the rest of the time. These disagreements were found to be mainly a result of the inadequacy of the shape of the topside model profile for describing this region. In an attempt to improve the current IRI topside model Bilitza *et al.* (1998) and Bilitza and Williamson (2000) are incorporating a large database of topside electron densities obtained from the Alouette and ISIS satellites during the period from 1965 to 1980. This data covers a longer period of solar activity than the original Bent model, and is hoped that this will overcome any shortcomings

experienced at high solar activity periods. For an indepth treatment of the improvements made to the 2000 version of the International Reference Ionosphere see Bilitza (2001). The newest version of the model has recently been released, IRI-2006. This model has implemented a number of improvements to the previous IRI-2001, including a better representation of the topside electron density profile (Bilitza *et al.*, 2006).

4.2.5 Mapping functions

In the previous sub-section, the procedures and equations used to estimate absolute ionospheric delay for each of the test models was briefly covered. In order to spatially reference these delays, each of the models uses a technique where all of the electrons present in the ionosphere are assumed to be contained within a thin shell of infinitesimal thickness. This is known as the *thin-shell* or *single layer* approach (see Figure 4.4). The height of this shell is set to approximate the height of maximum electron density. The Bent, CODE and IRI use the same mapping function, 1/cos z', where the Broadcast model uses a more simplified equation, to convert the vertical delay at the IPP to a slant delay, or delay experienced along the signal path. These mapping functions can be described as a ratio between the vertical delay and the slant delay, and are based on the zenith distance (or elevation angle) to the orbiting satellite.

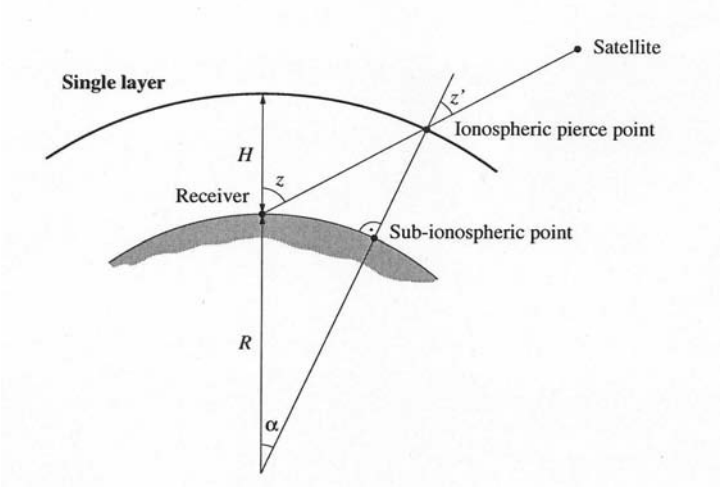

Figure 4.4: Thin Shell modelling approach (after Schaer, 1999).

Where: z, z' are the geocentric zenith distances located at the receiver and the IPP, R is radius of the Earth with respect to the station location and H is the height of the single-layer above the Earth's surface.

The Broadcast model (Klobuchar, 1986) uses the following equation to estimate the factor (F), that is used in equation (4.1) to turn vertical delay at the IPP to slant delay:

$$F = 1.0 + 16.0 \, x \left(0.53 - z\right)^3 \qquad (4.10)$$

Where, z is the elevation angle to the satellite from the ground receiver. The height (H) of the ionospheric layer is held fixed at 350km.

The Bent model converts vertical delay (in TEC units), at the IPP, into slant delay using the following equation (Bent & Llewellyn, 1973):

$$N_{TA} = \frac{N_T}{\sqrt{1 - \left(\frac{R \cos E}{R + H}\right)^2}} \qquad (4.11)$$

where:

N_T	is the vertical TEC at the IPP;
N_{TA}	is the slant TEC value;
R	mean radius of the Earth (6371200m); and
E	equates to 90°- z, which is the elevation angle of the observation.

The CODE model uses the same mapping function as the Bent model, but instead of using the elevation angle (E) as the input, it uses the zenith distance (z) (Schaer, 1997):

$$N_{TA} = F(z)\, N_T = \frac{1}{\cos z'} N_T \qquad \text{with} \qquad \sin z' = \frac{R}{R_o + H} \sin z \tag{4.12}$$

The CODE model defined the height of maximum electron density as 450km.

The IRI also uses the same mapping function as the CODE model, it uses the zenith distance to convert the vertical TEC to slant TEC (TEC along the signal path) (Bilitza, 1990). The conversion takes place based on a shell height of 400km.

For more information regarding the use and effects of different maximum electron density heights, within mapping functions, a study was undertaken by Komjathy & Langley (1996).

4.3 GPS and ionospheric corrections

Over the past two decades the use of GPS data from ground based networks to model the effects of the ionosphere has been extensively investigated (Komjathy, 1997; Skone, 1998; Fedrizzi *et al.*, 2001; Odijk, 2002). These investigations are based on the measurements of TEC using dual frequency GPS receivers that take advantage of the dispersive nature of the ionosphere. Up until recent years ionospheric models could be divided into two categories: grid-based and function-based. Early estimations of the ionosphere were mainly based on function fitting techniques such as those employed in the GPS Broadcast Model (Klobuchar, 1986), polynomial functions (Coster *et al.*, 1992; Komjathy, 1997; Coster *et al.*, 2003) and the use of spherical harmonics (Walker, 1989; Schaer, 1999). The grid-based method proposed by El-Arinin et al. (1994; El-Arinin *et al.*, 1995) has been able to produce a higher level of accuracy than that achieved by function based algorithms (Gao & Liu, 2002). This approach has been used extensively for both regional and global ionospheric modelling using GPS networks (Brunner & Gu, 1991; Webster & Kleusberg, 1992; FAA, 1997; Skone, 1998; Fedrizzi *et al.*, 2001). Both the function-based and grid-based approaches provide a 2D representation of the ionosphere by assuming that the entire effect is condensed onto a shell at a fixed height above the Earth's surface (see section 4.2.5). This assumption limits the accuracy of the model

(Komjathy & Langley, 1996) as it is only an approximation and not what is happening in reality. In order to overcome the limitations imposed by a fixed height model, in recent years tomographic modelling has received more attention. The method of ionospheric tomography is used to describe the ionosphere in a 3D sense by incorporating an altitude component (Liu & Gao, 2001) (also see section 4.3.1). This allows for a more accurate representation of actual ionospheric conditions, and hence improves the accuracy of the modelling approach.

4.3.1 Ionospheric tomography

As the ionosphere consists of many different layers (see section 2.1.4), GPS signals travelling from a satellite to a receiver will encounter varying electron densities on route. To assume that the entire ionospheric effect can be modelled to a thin shell at a fixed height is not physically true, therefore, leaving these 2D models unable to estimate ionospheric variations at different altitudes. This failure can lead to modelling errors of up to several TECU (Komjathy, 1997).

As the need for accurate ionospheric estimation increases in Earth observation related systems, such as the Global Positioning System and Radar Altimetry, the use of 3D ionospheric tomography has received more attention in recent years (Raymund *et al.*, 1990; Raymund *et al.*, 1994; Hansen *et al.*, 1997; Howe, 1997; Hernandez-Pajares *et al.*, 1999; Gao & Liu, 2002; Liu & Gao, 2004). A third dimension is added to the model by including an altitude component, which allows for a more accurate representation of ionospheric conditions (Gao & Liu, 2002). Primarily, the tomographic models developed thus far, fall into two categories: voxel-based models such as those produced by Raymund et al. (Raymund *et al.*, 1990; 1994), Hernandez-Pajares et al. (Hernandez-Pajares *et al.*, 1999; 2000), and Colombo et al. (2002) and function-based models as those produced by Howe (1997), Hansen (1998), Gao and Liu (2002), Liu (2003) and Liu and Gao (2004).

Using line of sight TEC estimates obtained from dual frequency GPS network measurements, the voxel-based tomographic models are spatially formed by a set of

cells or volume elements (voxels) (see Figure 4.5). Within these voxels the ionosphere is considered to be constant at a given time.

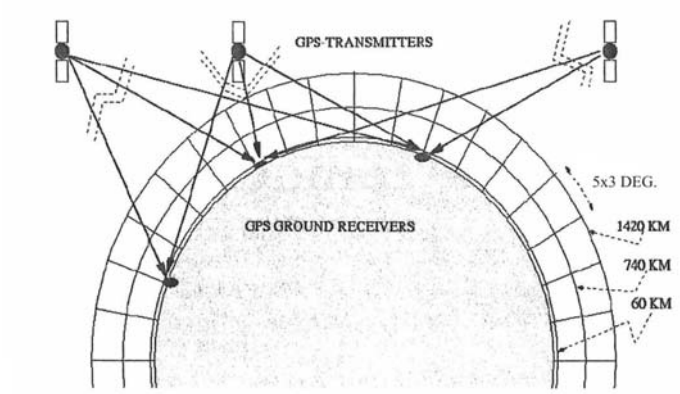

Figure 4.5 Tomographic model: Two-Layered Voxel approach (after Colombo et al., 2002)

The size of the voxels is usually set at 3º in latitude and 5º in longitude, using a two layered approach in altitude, with boundaries set, for example, between, 60-740-1420km (see Figure 4.5). The slant TEC values are formed by differencing the L1 and L2 frequencies, producing the ionospheric delays along the signal path (LI) (see equation 4.13) (Colombo *et al.*, 2002):

$$LI = \sum_{i} \sum_{j} \sum_{k} \left(N_e\right)_{i,j,k} \Delta s_{i,j,k} + \lambda_1 b_1 - \lambda_2 b_2 \qquad (4.13)$$

where:

i, j, k are the cell indices that correspond to local time, geodetic latitude and height;

$\left(N_e\right)_{i,j,k}$ the electron density;

$\Delta s_{i,j,k}$ the ray path length that crosses the i,j,k cell; and

b_1, b_2 ambiguity terms associated with the wavelengths λ_1, λ_2, which also include the instrumental delays.

The determination of the ionosphere for each voxel is performed by means of a Kalman filter (Bierman, 1977), with the estimation of the mean electron density (N_e) treated as a random walk process, with a process noise of 10^{10} electrons/m^3. This modelling approach is suitable for detecting any local trends in the electron density, and is superior to the single layer approach by significantly improving TEC estimation (Hernandez-Pajares *et al.*, 1999). The tomographic modelling approach is able to produce real time double difference residuals having a RMS value of better than 1 TECU or 10cm in L1-L2 delay (Hernandez-Pajares *et al.*, 1999; 2000). The precision of these results, allows for the model to be used in such applications as real-time GPS carrier-phase ambiguity resolution.

The function-based tomographic modelling approach, uses line of sight integral measurements between the satellite and receiver, which are inverted to obtain an estimate of the ionosphere (Howe, 1997). The 3D tomographic model can be constructed in the horizontal, using a set of spherical harmonic functions (SHFs) and in the vertical using empirical orthogonal functions (EOFs). The electron density can be estimated along the signal path using the following integral (Hofmann-Wellenhof *et al.*, 1997):

$$TEC = \int_{rx}^{sat} N_e(\lambda,\phi,z)\,ds = \int_{rx}^{sat} \left[N_e^0(\lambda,\phi,z) + \delta N_e(\lambda,\phi,z) \right] ds \qquad (4.14)$$

where: $N_e(\lambda,\phi,z)$ is the electron density at the geospatial position (λ,ϕ,z), denoting longitude (time), latitude and altitude respectively. The electron density function $N_e(\lambda,\phi,z)$ is an unknown to be estimated, and is done so by splitting it into two parts - $N_e^0(\lambda,\phi,z)$ which is the approximate estimate of the electron density function, and $\delta N_e(\lambda,\phi,z)$ which is the correction to the estimated value. The ionospheric correction term can be spatially modelled by using SHFs in the horizontal and EOFs in the vertical. In order to view the ionosphere in 3D, we integrate these two sets of functions to form:

$$\delta N_e(\lambda,\phi,z)=\sum_{k=1}^{K}\sum_{m=-M}^{M}\sum_{n=|m|}^{M}\left[a_{nk}^{m}\cos(m\lambda)+b_{nk}^{m}\sin(m\lambda)\right]\bullet\bar{P}_n^m(\cos\phi)Z_k(z) \qquad (4.15)$$

where:

$\bar{P}_n^m$ is the associated Legendre Polynomial of order *m* and degree *n*;

$Z_k(z)$ is the empirical orthogonal function (EOF); and

a_{nk}^{m} & b_{nk}^{m} are the coefficients to be estimated.

By combining equations (4.14) and (4.15) we can form the fundamental observation equation (4.16) to model the ionosphere in a 3D sense using the technique of inversion. This enables the TEC derived from a GPS network to be linked to the coefficients that define the ionospheric field (Gao & Liu, 2002):

$$\begin{aligned}TEC=&\sum_{k=1}^{K}\sum_{m=-M}^{M}\sum_{n=|m|}^{M}a_{nk}^{m}\int_{rx}^{sat}\cos(m\lambda)\bar{P}_n^m(\cos\phi)Z_k(z)\,ds\\+&\sum_{k=1}^{K}\sum_{m=-M}^{M}\sum_{n=|m|}^{M}b_{nk}^{m}\int_{rx}^{sat}\sin(m\lambda)\bar{P}_n^m(\cos\phi)Z_k(z)\,ds\end{aligned} \qquad (4.16)$$

The empirical orthogonal functions are obtained from existing empirical electron density data, which can be produced from such data sources as ionospheric models (eg. the Bent, IRI etc). This data is used to construct a height profile of the ionosphere, given such information as location, local time and solar activity (eg. sunspot number). This technique which streamlines data representation, allows a small number of EOFs to adequately describe the ionosphere, where a large amount of data was previously required (Liu & Gao, 2004).

Gao and Liu (2002) tested a function-based 3D tomographic ionospheric model in the Southern Californian area. Six permanent GPS reference stations, located between 33.9º and 34.25º in latitude, collected a total of 60 epochs of 30 second data to form the model. The proceeding 300 measurements from the same reference stations were used to test the model's accuracy. It was found that the model values compared at the 1 TECU level, with the data produced from the network of dual frequency

receivers. The slant TEC values could be estimated with a mean error of approximately 1.4%. In further research, Liu and Gao (2004) tested another function based model over a local-area, then over a wide-area GPS reference network. The model produced from the local-area GPS reference network was derived from five stations in the Southern Californian region, between 34º and 34.5º in latitude, during medium level solar conditions. Fifteen minutes of dual frequency data, at 30 second epochs, was used to estimate the model's coefficients. These coefficients were then used to predict 5 minutes in advance, and compared with dual frequency observations during the same time interval. The TEC prediction for most satellites had an average error of 3 TECU, with an average relative error of 4%.

4.3.2 GPS augmentation systems

In order to meet the navigational needs of civil aviation users, the international community has developed three classes of GPS augmentation systems: air-craft based (ABAS), satellite-based (SBAS) and ground-based (GBAS). These systems will augment the Global Positioning System in order to meet the accuracy, integrity, continuity and availability requirements of national aviation authorities worldwide.

The ABAS concept integrates the information obtained from GNSS satellites with information from other navigational sensors onboard the aircraft, to improve the navigational solution. One such ABAS is RAIM (receiver autonomous integrity monitoring). The RAIM system checks each satellite by comparing the GPS positional solution obtained from at least five satellites to various combinations of four satellites within the group (Flight Safety Australia, 2007).

The US Federal Aviation Administration (FAA) has developed an SBAS known as the Wide Area Augmentation System (WAAS). WAAS is the first SBAS certified for use in commercial aviation (see section 4.3.2.1). The WAAS produces differential corrections from a network of GPS base stations spread out over a large area. These corrections are relayed via a geosynchronous satellite to users to provide real time position correction.

GBAS systems are used to provide precision approach to landing aircraft based on the differential GPS technique. The GBAS concept has been under development since the mid-1990's. International standards and recommended practices (SARPs) have been developed by the International Civil Aviation Organisation (ICAO) Global Navigation Satellite Systems Panel for GBAS in 2000 (ICAO, 2002). World-wide, a number of aviation authorities including the FAA (USA), Air Services Australia, Brazil, DFS Germany and AENA Spain have been actively working towards GBAS implementation, and are all currently evaluating prototype systems. The FAA is currently evaluating its Local Area Augmentation System (LAAS) (see section 4.3.2.2) with the aim of producing the first certified LAAS (Murphy *et al.*, 2006).

4.3.2.1 Wide Area Augmentation System (WAAS)

The Wide Area Augmentation System (WAAS), was first proposed by the MITRE Corporation and the Air Force Phillips Laboratory (El-Arinin *et al.*, 1994; El-Arinin *et al.*, 1995) and is intended to become the primary navigational aid during all phases of flight for the US FAA (FAA, 1997). The FAA commissioned the WAAS system for operational use on the 10th July, 2003, and it has been in continuous operation since.

The WAAS was primarily designed to provide the accuracy and integrity needed for GPS aviation navigation by combining the concept of differential GPS with GPS integrity monitoring (Braff & Shively, 1985; Kee, 1996). The system achieves this by providing high integrity satellite orbit, clock and ionospheric corrections to users over the Coterminous United States (CONUS), Alaska and Hawaii. At present the WAAS is able to provide accuracy to better than 1 metre in the horizontal and 2 metres in the vertical 95% of the time (Kim *et al.*, 2006).

Based on a network of dual frequency GPS receivers, a 2D model of the ionosphere is created over the CONUS by estimating the line of sight ionospheric delay along the signal paths. The ionosphere is considered to be a thin shell at a height of 350km from the Earth's surface. The slant delays measured along the signal paths are then converted to the equivalent vertical delays using an obliquity factor or mapping function:

$$OB(elv,H)=\sec\left(\sin^{-1}\left(\left(\frac{R_E}{R_E+H}\right)\cos(elv)\right)\right) \tag{4.17}$$

where:

OB	is the obliquity factor;
elv	is the elevation of the satellite; and
H	is the height of the thin shell.

Using this data, a deterministic trend is fit to the ionosphere, whereby similar delays can be estimated for other lines of sight within the modelled area, based on a series of grid points known as Ionospheric Grid Points (IGP's). These delays, together with a confidence bound on the estimate, which is derived as a means of monitoring the integrity of the correction, are then broadcast to the user (see Figure 4.6). The Wide Area Reference Sites (WRSs) are distributed throughout CONUS and are used to collect and process data received from GPS and geosynchronous satellites. This data is then forwarded to Wide Area Master Sites (WMS), where it is processed to determine the differential corrections. These include: the GPS ephemeris, satellite clock and ionospheric corrections together with an estimate of integrity or confidence bound on the estimates. These correction estimates are then placed on the WAAS message, which is then sent to a Navigation Earth Station (NES) and uplinked to the geosynchronous satellites for distribution to the user group.

The application of the WAAS over the CONUS sector has been extensively studied over the past decade, with the published literature discussing the subject of ionospheric corrections over CONUS including Enge et al. (1996), WAAS MOPS (1999), Walter et al., (2000) and Sparks et al.,(2002). The WAAS has also been tested in various regions including the high and low latitudes (Skone, 2000; Doherty *et al.*, 2002; Skone *et al.*, 2003) and under both quiet and active solar conditions (Hansen *et al.*, 2000; Skone *et al.*, 2004; Yousuf & Skone, 2005). Alternative modelling methods to the current grid based approach have also been investigated by such authors as Hansen et al. (1997), Hernandez-Pajares et al. (2001) and Blanch et al. (2002).

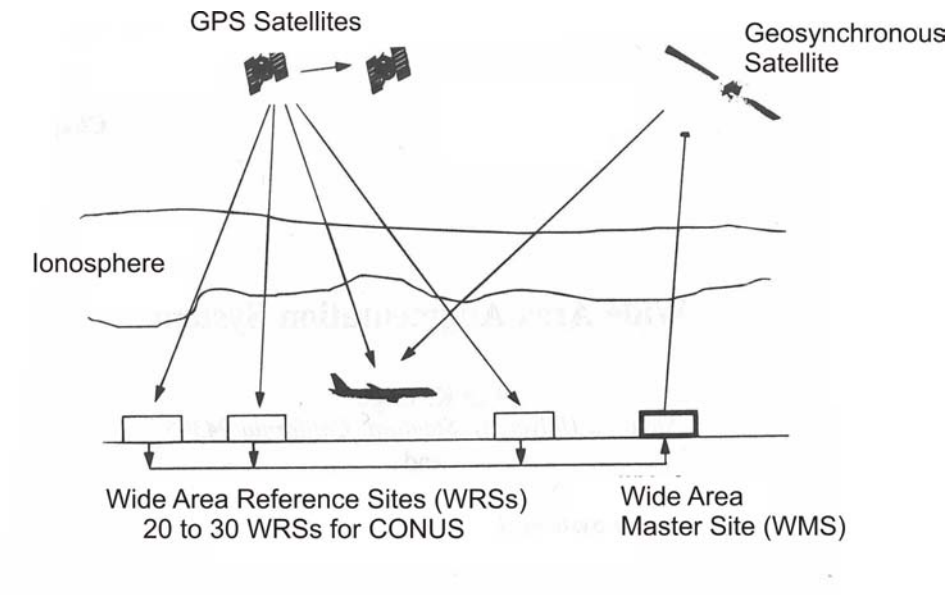

Figure 4.6 Wide Area Augmentation System (WAAS) (after (Enge & Van Dierendonck, 1996))

In order to improve the current system's integrity, accuracy and availability, the WAAS network is being expanded by placing new reference stations in Alaska, Canada and Mexico, together with the placement of an additional master station and the launching of additional geosynchronous satellites (Schempp *et al.*, 2006). The WAAS algorithms are also being enhanced with particular focus being placed on ionospheric correction.

Several other satellite based augmentation systems (SBAS) that have the same objectives as the WAAS have been developed around the world. These include: the European Geostationary Navigation Overlay Service (EGNOS) that has been produced by a combined effort from the Eurpoean Union, European Space Agency and EUROCONTROL (European Organisation for the Safety of Air Navigation) and the Multi-function transportation Satellite-based Augmentation System (MSAS) that services Japan. Canada has the Canadian-Wide Differential GPS (CDGPS) which provides metre level differential corrections, via communications satellite, in support of navigation and positioning applications, country wide. CDGPS is not intended for aviation purposes, and therefore provides no integrity monitoring. Canadian civil air navigation services provider (NAV CANADA) has participated in the development of a Canadian WAAS (CWAAS) which supplements the US WAAS by adding additional reference stations inside Canada.

4.3.2.2 Local Area Augmentation Systems (LAAS)

The US Federal Aviation Administration (FAA) is currently developing Local Area Augmentation Systems (LAAS's) in order to provide service to all three categories of precision approach (Enge, 1999). The LAAS is being developed as a means of providing highly accurate differential corrections and system integrity alerts for a particular area (radius of approximately 50km) using a VHF data link. These objectives, for precision approach applications, are being serviced by locating a small collection of GPS receivers on known surveyed control points within the bounds of an airport. The measurements taken by these reference receivers and corresponding corrections, are then broadcast to the approaching aircraft via a VHF data link from a ground based transmitter. On receiving these corrections, the aircraft's onboard GPS receiver is able to correct its position to a sub metre level of accuracy, less than 0.25m when ionospheric conditions are normal (Luo *et al.*, 2003). Also contained on the VHF broadcast is a data quality indicator that estimates the accuracy of the correction, to help ensure flight safety and warn of any system malfunctions. The distinct difference between the WAAS and the LAAS, is that the LAAS performs all its calculations, monitoring and broadcasting from a given airport. The WAAS, uses the WRS's located throughout the CONUS to collect GPS measurements that are then transmitted to WMS's where the data is processed, then transmitted to NES facilities for uplink to a geosynchronous satellite for distribution to the user group. Whilst the LAAS and the WAAS compliment each other in the pursuit of producing a precise navigational service to the aviation user, the LAAS is able to provide significantly more accurate positional corrections, as these corrections are derived for a small local region surrounding the airport (Pullen *et al.*, 2002).

Airservices Australia is currently developing and evaluating its own nation-wide concept known as GRAS (Ground based Regional Augmentation System) (Crosby *et al.*, 2000; McPherson, 2006). The GRAS concept is an integration of both SBAS and GBAS technologies. Airservices Australia decided in the mid-1990's that an SBAS system was required for en-route and non-precision approach and a GBAS system was required for airport landing precision approach. As no geostationary satellites

were available to facilitate the nation-wide SBAS, the GRAS (Ground-based Regional Augmentation System) concept was adopted. The GRAS concept employs the use of a terrestrial-based data-link to transfer data from the ground network to the user. The system works by using a number of GPS reference receivers scattered across Australia to collect dual frequency observations. These observations are sent to a Master Station for the computation of GPS integrity and differential correction information. However, instead of distributing this correctional information via geostationary satellites, the GRAS delivers its correction to a network of VHF broadcasting stations that transfers the message out to the users.

4.4 Continuously Operating Reference Stations (CORS)

Continuously operating reference stations (CORS) have been used world-wide since the 1980's, in support of scientific high accuracy global, national and regional geodetic applications (Evans *et al.*, 2002). These networks of GPS receivers are usually operated by government organisations as a free service. This means that a user in the field is able to perform high accuracy positioning by combining his observations with the data from the CORS network. This concept enabled the performance of high precision positioning with the convenience of using only one GPS receiver.

In a global context, the International GNSS Service (IGS, 2007), consists of a network of several hundred globally distributed GPS and Glonass receivers, that contribute data in support of high accuracy geodetic reference frame definition and atmospheric studies, which includes the global measurement of ionospheric TEC (Schaer, 1999). The IGS is a non-government scientific organisation that consists of over 200 voluntary world-wide agencies that support the system by providing data.

On a national and regional level many countries world-wide have established CORS networks primarily in support of high accuracy geodetic, surveying, mapping and navigational applications (Rizos, 2007). The fundamental positioning strategy for these high accuracy applications is that of relative positioning (see section 3.2.8.2). The U.S. CORS network, run by the National Geodetic Survey (NGS), is an example

of such a network (Snay, 2000). The network consists of approximately 200 receivers, which are operated by a collection of government, private, academic and commercial organisations. The CORS network provides both code and carrier phase observations in the RINEX data form, which is freely available via the internet or anonymous ftp service. In the aftermath of the 1995 Kobe Earthquake, Japan's Geographical Survey Institute (GSI) established a CORS network known as GEONET, with the primary objective of monitoring the country's crustal movement for seismic prediction. This network consists of over 1000 GPS receivers deployed across the country, which are linked to a main archive centre (GEONET, 2007). The GEONET system is also used for such scientific applications as the measurement of TEC data on a regional scale (Saito *et al.*, 1998). Other such examples of regional networks are the Canadian Base Network (CBN) and European networks such as CATNET in Spain, SWIPOS in Switzerland, SWEPOS in Sweden, SAPOS in Germany and SATREF in Norway (Hankemeir, 1996; Talaya & Bosch, 1999; Schneider *et al.*, 2000; Jonsson, 2002; Seeber, 2003; CBN, 2007).

Within Australia, the Australian Regional GPS Network (ARGN) was established in the early 1990's as a means of providing a uniform framework from which to base all geodetic applications in Australia (Steed & Twilley, 1999). The network currently consists of 16 GPS reference stations with an average receiver spacing of approximately 1000km (Roberts *et al.*, 2004). The network defines the Geodetic Datum of Australia (GDA). Some of the sites within the ARGN contribute to the world-wide IGS network. Geoscience Australia offers a free AUSPOS service based upon the ARGN and IGS receiver network. The user simply uploads at least 6 hours of high quality dual frequency RINEX data to the website, and is returned high accuracy co-ordinates in both the GDA and ITRF reference frames (Geoscience Australia, 2007).

On a regional level, in order to support an increasing demand for accurate positioning using the Global Positioning System, in the areas of surveying, mapping and high precision navigation, Victoria established a CORS network in 1994, known as GPSnet (Hale, 2000). The system currently consists of 24 permanently operating dual frequency GPS receivers with both regional and rural coverage. Users are able to download GPS RINEX files from the Land Victoria website (Land Victoria, 2007),

and combine this data with GPS data collected across Victoria in a post processing scenario, or receive network correctional information for real-time applications. For a more in-depth description of GPSnet and other CORS networks in Australia see Chapter 5.

With the increasing need for real-time accurate positioning within the GPS user community, traditionally passive CORS networks have begun actively transmitting real time data to users in the field. This provides real time positioning capability (Rizos, 2002). This application of GPS technology is known as Network-RTK.

4.4.1 Network-RTK

The last few decades have seen significant development in the area of real time cm-level positioning capability using Real Time Kinematic (RTK) surveying techniques (Rizos, 2003). There are, however, limitations associated with the application of single base station RTK techniques. The distance between the base station and the rover is the major constraint, as distance dependent biases, namely orbital, ionosphere and tropospheric biases, degrade the accuracies achievable as baseline length increases. The Network-RTK concept aims to provide cm-level positional accuracy over baseline lengths of many tens of kilometers, that can provide equivalent performance capabilities to those achieved by current single base station RTK systems over distances up to 10km. The use of multiple reference stations spread over a wide geographical area allows for the empirical modelling of these distance dependent measurement biases, thus producing corrections that can be transmitted to the user in the field. These corrections account for the normally unaccounted for distance dependent biases, allowing for the accurate resolution of carrier phase ambiguities, as baseline lengths increase (Rizos, 2002). At present more than 200 real-time CORS networks are estimated to exist world-wide (Schrock, 2006).

4.4.2 Ambiguity resolution and corrections

For high precision GPS positioning applications, carrier phase data must be used (see section 3.2.8.1). When using carrier phase data, there is however a price to pay. Carrier phase measurements are ambiguous, requiring ambiguity resolution algorithms within the data processing software to solve for the initial unknown number of wavelengths in the carrier signal between the satellite and receiver (see section 3.2.8.7). Once these ambiguities are resolved, the carrier phase observations will be transformed into highly accurate pseudo-range measurements, allowing for highly precise baseline co-ordinate estimation.

Data processing for Network-RTK positioning involves three steps. Firstly, the critical element in cm-level Network-RTK application is the capability for fast and reliable ambiguity resolution (Rizos & Han, 2003), as only observations with fixed ambiguities are used to model distance dependent biases. This requires a dense enough network to model the distance dependent biases to an accuracy that would allow the errors in the residual double difference carrier phase observable to be ignored, in the context of rapid ambiguity resolution (Rizos, 2002). From a conceptual point of view, a Network-RTK system would require a processing facility capable of fixing the integer ambiguities between all of the static stations in the network. It must be able to handle double differenced data over baseline lengths of 50-100km, in real-time. In order to enhance the prospect of timely and correct ambiguity resolution over longer baselines, all relevant a-priori information that can reduce observational errors should be used. This information comes in the form of IGS predicted satellite ephemerides, ionospheric and tropospheric corrections derived from previous network processing results, carrier phase multipath corrections obtained from previous network information and antenna phase centre corrections based on previously carried out antenna calibrations.

Secondly, once ambiguities are fixed within the network, this would enable the estimation of model correction coefficients. Within a network environment, the ionospheric and orbital biases must be modelled on a satellite by satellite basis, whilst the tropospheric bias can be estimated at each reference station. As the

ionospheric bias shows a much larger temporal variation when compared with the non-dispersive troposphere and orbital biases, commonly called 'geometric' biases, it is necessary to update the ionospheric corrections at a greater rate than the geometric corrections, therefore splitting the corrections in two (Zebhauser *et al.*, 2002).

The third step involves the transmission of correctional data to a user, to a sufficient accuracy (Rizos, 2002), using the established RTCM (see section 4.4.4) standards for data transmission. The Network-RTK system needs to be able to manage the data and provide a way of communication between the various reference stations that collect the data, and the master control stations (MCS), where all of the corrections are generated. These corrections then need to be broadcast from the MCS to the users (*ibid*). To date there are three possible structures from which to base the implementation of Network-RTK systems (*ibid*): (1) generation of the Virtual Reference Station (VRS) and associated corrections, (2) generation and broadcast of an Area Correction Model (ACM), or (3) the broadcasting of raw data from each reference station in the network. Each of these methods is described in sections 4.4.5, 4.4.6 and 4.4.7 respectively.

The major limiting factor associated with single base station RTK methods, is the distance between the reference and roving receiver as a result of distance dependent biases, such as the ionosphere, that hinder successful resolution of the phase ambiguities. When using single base station RTK positioning techniques, it is common place to ignore the ionospheric bias over short baselines of 10km or less, as the error induced by the ionosphere under normal conditions is sufficiently small. This is known as the ionospheric fixed model. As long as the ionospheric bias is less than a few centimeters, the ionospheric fixed model allows for a high success rate in ambiguity resolution being attained reasonably fast (Teunissen *et al.*, 2000). However, as baseline length increases, the ionospheric bias becomes decorrelated, thus increasing the ionospheric error experienced and hindering the accurate ambiguity resolution in real time. It then becomes necessary to include these errors into the baseline positional model as unknown parameters for estimation. This model is referred to as the ionospheric-float model (See section 3.2.8.6.1).

In order to increase the baseline length in RTK applications and still achieve the accuracies obtained under 10km, the roving receiver's observations need to be corrected for the ionospheric bias, to allow for successful ambiguity resolution and co-ordinate estimation. Networked RTK GPS surveying offers the means to provide these empirical corrections. In order to resolve ambiguities correctly, in the single frequency case, the ionosphere needs to be estimated with a maximum allowable bias derived from the following equation (*ibid*):

$$b_{\text{single}} = \tau[2\lambda_1] \tag{4.18}$$

where:

b is the allowable ionospheric error;

τ $\frac{40.3}{c^2}10^{16}TECU$, where c is equal to the speed of light; and

λ_1 is equal to the L1 operating frequency.

By setting b_{single} equal to half a cycle, it shows that the ionospheric bias should be less than a quarter of a cycle or $\lambda_1 = 4.8cm$ for reliable ambiguity resolution. However, one of the major problems associated with estimating the ionosphere is that the network derived ionospheric correction estimation may not be accurate enough, especially during disturbed ionospheric conditions, and exceed the ±5cm limit (Odijk, 2002). The issue of latency also needs to be addressed. How often does the ionosphere need to be sampled to gain this ±5cm accuracy?

4.4.3 Correctional latency

As the key to accurate Network-RTK positioning is successful ambiguity resolution, the accuracy of the atmospheric corrections (ionosphere, troposphere and orbital errors) received by the roving receiver plays a crucial role. The ionospheric error has a greater influence on ambiguity resolution as both the ionospheric delay and ambiguities are frequency dependent (Kashani *et al.*, 2004a). In order to solve the

ambiguities quickly and reliably within a network solution, the ionospheric influence needs to be known to an accuracy of greater than a quarter of wavelength or ±5cm (see section 4.4.2).

Within a network-RTK environment, the volume of data transmitted to the user in the field and the complexity of the message, provides a heavy computational burden to both the user and the MCS providing the information. The issue of signal bandwidth and transmission rates is a topic at the forefront of contemporary precise network-RTK applications.

In order to address the above issues in terms of the accuracy of the ionospheric correctional information and the efficiency of the transmitted message, it becomes critical to understand how often the ionosphere needs to be measured and corrected for, thus ensuring that the user can attain accurate results without being over loaded with additional unneeded correctional information.

An analysis has been undertaken and presented in Chapter 7 that addresses the issue of how often the ionosphere needs to be sampled to meet the ±5cm accuracy criteria, within the mid-latitude Victorian region. Predicted ionospheric delays, derived from the previously correctly resolved epochs were used to interpolate forward in the data. A number of different interpolation techniques were tried, together with different data sampling intervals. These tests were undertaken as a means of evaluating and refining different methodologies that can be used to assist in the efficient use of Network-RTK corrections.

4.4.4 RTCM standards

The Radio Technical Commission for Maritime Services (RTCM) was first established in 1947 as a US government advisory committee. It is now an independent organisation of companies that gains its support from its members all over the world. A special committee (SC-104) was first commissioned in 1983 to develop international standards in support of differential GNSS applications, then only a concept. At the time of commission, its primary objective was to support high-

accuracy positioning techniques that would provide an accuracy of a few metres over a relatively small area. Over time the concept of relative positioning was improved to provide much greater accuracy, thus providing for cm-level positioning capabilities (see section 3.2.8.2).

After considering a number of different proposals (Euler *et al.*, 2002), the RCTM subcommittee SC-104 commissioned the new standard RTCM version 3.0 (RTCM, 2007a). Up until its release, no international industry standard had been developed, that standardised the way information was to be conveyed in a Network-RTK environment. The previous RTCM version 2.3 (RTCM, 2007b) format, which is used by the VRS system (see section 4.4.5) to transmit corrections to a roving receiver via the generation of a virtual reference station, uses single reference station RTK messages such as 18/19 and 20/21 as defined in the standard. The raw carrier phase and pseudorange observations are transmitted via messages 18 and 19 respectively, whilst messages 20 and 21 contain corrections for the carrier phase and pseudorange measurements respectively. This message format was not however designed specifically for a network-RTK environment and has been subject to a number of complaints that centre around its parity scheme and data format (Kalafus & Van Dierendonck, 2003). Another system known as the FKP approach (Wubbena *et al.*, 2001), enables the roving receiver to estimate its own corrections based on a set of coefficients that model the effects of the ionosphere, troposphere and orbital errors for each satellite encountered within a specific network area. The major draw back of this area correction approach is that it uses a customised RTCM Type 59 proprietary message, which is not fully compatible with RTCM standards.

The new RTCM version 3.0 is based upon a simplified approach known as the "Master-Auxiliary Concept" (MAC) (Euler *et al.*, 2004). The concept behind the new standard is to provide the roving receiver with raw observation data from the network, in a highly compact message format, that will allow the rover control over how it uses this network data to correct for its position (Brown *et al.*, 2005)

The new standard will more readily meet the requirements of differential and real-time kinematic (RTK) GNSS applications by being extremely efficient in terms of its broadcast bandwidth. The information contained in message 1003 of RTCM 3.0 is

the same as that in messages 18 and 19 of RTCM 2.3. When transmitting this data however, RTCM 3.0 requires 1200 bits to transmit for 10 satellites dual frequency, whilst RTCM 2.3 is unable to transmit for 3 satellites at that limit. The efficiency of RTCM 3.0 also increases as the number of satellites increases. The maximum efficiency of RTCM 2.3 is 80% of the available data bits, whilst the efficiency of RTCM 3.0 increases from 88% to 98% as more satellites are transmitted (Lin, 2005).

One of the most critical problems associated with network RTK and RTCM data transmission is throughput. RTCM 3.0 has addressed the problem of data transmission volume by reducing the amount of data received at the rover. The MAC firstly, draws data from a subset of the entire network, as in a large network, the rover will not benefit from observations taken from distant stations (Leica Geosystems White Paper, 2005). Secondly, the MAC only sends full raw observations and co-ordinate information from one station, known as the 'master station'. The surrounding auxiliary stations in the network send correction differences and co-ordinate differences, which are computed between the master and auxiliary stations. These corrections take up less bandwidth than full raw data, and can be used by the rover to simply estimate the error at the user location or to reconstruct full observations from each station in the network.

The bandwidth required to transmit the corrections is further reduced by splitting the correction in two parts (Zebhauser *et al.*, 2002): dispersive (ionosphere) and non-dispersive or geometric (troposphere and orbital errors). As the geometric component of the error will change more slowly over time than the dispersive component (especially during solar maximum conditions), the geometric error will not need to be updated as often as the dispersive correction, thus saving bandwidth.

Once the ambiguities within the network have been fixed, a fundamental requirement of the MAC is that the phase ranges from the reference stations are reduced to a common level. Once this takes place, it is then possible to estimate the dispersive and non-dispersive errors on each frequency for each satellite receiver pair. Conceptually, if the integer ambiguities between two reference stations have been

adjusted, so that when double differences are formed the integer ambiguities cancel, it is said that these two stations are on a common ambiguity level.

The new version 3.0 is also very flexible in its application. It is compliant with traditional RTK operations, as well as supporting Network RTK, low bandwidth RTK, as well as all past GNSS applications.

4.4.5 Virtual Reference Station (VRS)

The VRS concept is applied within a CORS network, with an approximate spacing of 70km between reference stations. GPS data is fed to a MCS server. Once the network ambiguities are fixed, correctional models for the ionosphere, troposphere and satellite orbits are computed. The user is required to form a link with the MCS via a mobile phone, thus informing the MCS of their approximate position, estimated via a GPS navigation solution. The MCS then generates corrections for the rover's approximate position, as though there was a reference station at this location. Corrections are broadcast to the user in the format of single reference station RTK messages, such as 18/19 or 20/21 defined in RTCM Version 2.3 (RTCM, 2007b). The roving receiver is positioned relative to this VRS. The basic concept behind the VRS idea, is that an invisible, unoccupied virtual reference station is created, that simulates a base station in close proximity to the roving receiver. This will provide short baseline performance and accuracies to the user without the need to physically setup and operate a base station (Vollath *et al.*, 2000a;, 2000b). Preliminary testing of the system has seen accuracies of a few centimeters being achieved over baselines of between 30-40km (Wanninger, 1999; Vollath *et al.*, 2000b; Namie *et al.*, 2001; Wanninger, 2002). Due to server capacity issues, there are some limitations to the number of simultaneous users the VRS system can handle.

4.4.6 Area Correction Model (ACM)

Once all the carrier phase ambiguities within the network have been fixed, the ACM approach uses all of the GPS data collected by the network to form corrections for

both dispersive (ionosphere) and non-dispersive (troposphere and orbital) error sources or carrier phase measurement residuals for each satellite at each reference station. These corrections derived at the MCS are broadcast to the user via the standard RTCM format, in the form of a model, in support of accurate real-time positioning. A number of different correction algorithms, designed to derive correction terms at the user location have been proposed (Roberts *et al.*, 2003). These algorithms include: the Linear Combination Model (Han & Rizos, 1996), the Linear Interpolation Model (Wanninger, 1995; Wubbena *et al.*, 1996), the Distance Based Linear Interpolation Model (Gao & Li, 1998), the Low-order Surface Model (Raquet, 1998; Fotopoulos & Cannon, 2001) and the Least Squares Collocation Method (van der Marel, 1998). After some detailed testing of the above algorithms, Dai et al. (2003) concluded that the performance of all the methods is similar and that use of any of the methods, in a network based environment, significantly reduces the distance dependent biases in both the carrier phase and pseudorange measurements at the user location. The ACM approach has been shown to work well, with cm-level accuracies achieved at the rover location, for baseline distances up to 50km (Wubbena *et al.*, 2001). In addition, it only requires one way communication between the MCS and the user and there is no limit to the number of users that can be simultaneously attached to the system. Examples of current operational area based correctional approaches are the MAC produced by Leica Geosystems (as discussed in section 4.4.4), the GNSMART concept, produced by Geo++® (*ibid*) and the FKP approach (Wubbena & Bagge, 2006).

4.4.7 Raw data transmission

The broadcasting of raw data from either the MCS or each individual reference station in the network would enable the computation of corrections at the user location. This approach therefore shifts the computational burden to the user, allows for one-way communication only and there is also no limit to the number of users on the system. The main advantage to this approach is that the rover is completely independent of the reference station network operator (Rizos & Han, 2003).

4.5 Summary

As the production of a temporal ionospheric modelling technique that would meet the requirements of a network-RTK environment is the primary focus of this research, an understanding of the current modelling techniques and their suitability for such an environment needs to be established. The first two sections of this Chapter provided some examples of the more globally accepted empirical modelling approaches. This was done as the empirical models described will be tested for their ionospheric modelling suitability in a Network-RTK environment in Chapter 5.

The next section in this Chapter focused on current ionospheric modelling techniques used by the GPS research community to estimate the ionospheric delay as a means of correcting observations taken from GPS satellites. The methods employed by each approach and the accuracies achieved were also discussed.

The use of CORS GPS networks was discussed in the next section. Their application for producing ionospheric corrections for cm-level surveying applications within a network-RTK environment was presented. The different approaches currently available for producing these corrections were also discussed. This information was presented to provide a thorough background into what is currently available and to provide a perspective on how the research in upcoming chapters will contribute to this body of knowledge.

The next chapter provides a detailed description of Victoria's CORS network-GPSnet. This is undertaken as GPSnet was used as the test bed for the research undertaken in this thesis and the production of an ionospheric model suitable for Victorian conditions could have direct applications to the users of GPSnet.

Chapter 5 Empirical ionospheric models and GPSnet

Chapter 5 provides a general overview of the GPSnet system operating within Victoria, and how it can be used to provide ionospheric correction data using a Network-RTK solution for high precision cm-level applications. As a preliminary step towards understanding the variability of the ionosphere over Victoria, the global empirical ionospheric models described in Chapter 4 will be tested against each other, to see how they perform in a differential sense. This is undertaken as a means of investigating their usefulness in providing corrections in a Network-RTK environment. The data used to undertake this analysis is derived from GPSnet. The results may provide a better understanding of what modelling approach best suits the Victorian region.

5.1 GPSnet overview

The southern Australian state of Victoria has a population of approximately 4.8 million people and covers around 227 000 square kilometres, which equates to approximately 3% of Australia's land mass. The use of satellite-based positioning techniques forms an essential component in Location Based Services. In Victoria today, GPS is firmly entrenched in both the private sector and governmental organisations as a means of positioning in such areas as: surveying, road construction, mining, agriculture, mapping and geographic information systems. As

further satellite navigation systems are developed and GPS is modernised, it is important to provide an infrastructure that supports the co-ordinated and efficient use of Global Navigation Satellite Systems (GNSS).

The Victorian State Government has shown foresight in undertaking a GPS network (GPSnet) infrastructure program, in collaboration with both industry and academic partners, to help coordinate and expand satellite positioning activities in Victoria. Based on this framework, and in support of geodesy, mapping, surveying and high-end navigational users, the Spatial Information Infrastructure (SII) within the Department of Sustainability and Environment (DSE) has facilitated the establishment of a CORS network across the state (Hale, 2000). The network at present consists of 24 dual frequency GPS receivers which provide 24 hour online GPS data access. Users of the system are able to combine files downloaded from GPSnet with GPS data collected across the state. The data can be used for both post-processing and real-time applications to achieve cm-level accuracies. The GPSnet system has taken over ten years to fully implement since its inception in 1994, but it is now virtually complete. Some additional stations will be added to the network over the next few years to densify sparse coverage areas (Asmussen, 2006; DSE, 2007). At present, Victoria is the only state in Australia to have such a high accuracy, continually operating, state-wide network of this type.

Traditionally, for post-processing applications, the GPSnet data has been supplied over the internet in the form of 1 and 5 second RINEX files, which can be downloaded via an ftp service on the Land Victoria website (Land Victoria, 2007). In order to keep up with an ever increasing need for better accuracy, reliability and availability of positional information, a global trend has seen the evolution of conventional passive CORS networks into active networks where high accuracy real-time positioning is available (Zhang *et al.*, 2006). As a result, two new GPSnet services have been implemented in Victoria that offer real-time positioning capability to a variety of users. The first is the VICpos DGPS sub-metre positioning service across the state (see Figure 5.1), and the second, is the MELBpos high accuracy Networked RTK service that covers the Melbourne metropolitan and surrounding areas (see Figure 5.2). On the 1st of December, 2004, the DSE put into operation the VICpos system, as shown in Figure 5.1. VICpos offers sub-metre level positioning,

using a subset of 17 reference stations within GPSnet to deliver state-wide real-time differential corrections to GPS users (Gordini *et al.*, 2006). GPS data is streamed from the VICpos network to a central server based in Geelong, where differential corrections are produced. These real-time corrections are then broadcast to users in the field, wirelessly, via the internet (Hale *et al.*, 2005). In most cases, users are able to access the service using a mobile phone that is General Packet Radio Service (GPRS) capable (Millner *et al.*, 2006). This service has application in areas such as: agriculture, asset mapping, emergency response, transport, forestry and navigation.

Similar in architecture to VICpos, MELBpos which came online in January 2006, provides a real-time cm-level positional capability within Melbourne and immediate surrounding regions (Hale *et al.*, 2005). MELBpos currently (February, 2007) consists of 8 reference stations located in the Melbourne region. All MELBpos stations contribute to the internet network corrections derived and broadcast from the central server at Geelong. MELBpos represents stage 1 of the Victorian high accuracy infrastructure. It is planned that the high accuracy service will be extended state wide in the future using a full networked RTK solution (Wu *et al.*, 2006).

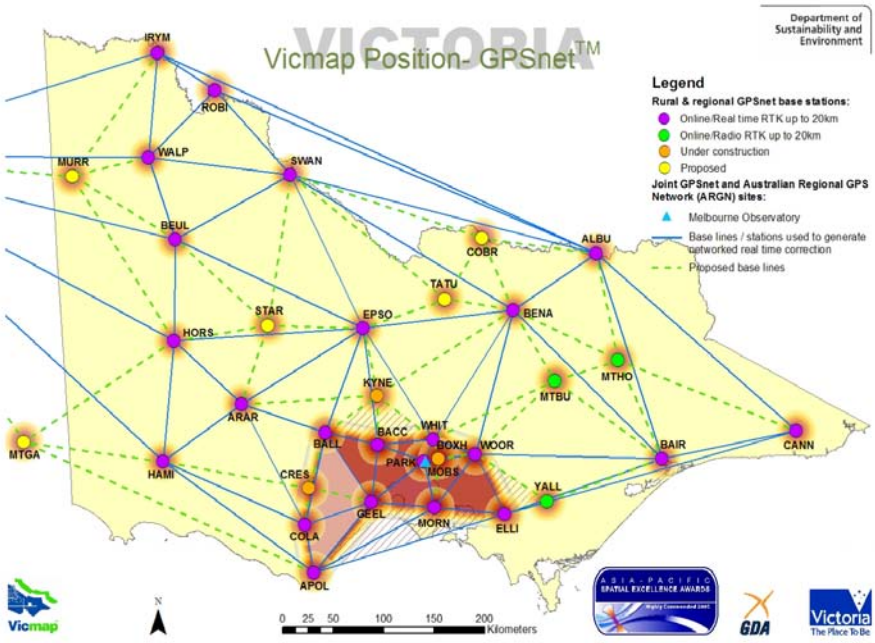

Figure 5.1 GPSnet VICpos network infrastructure (DSE, 2007)

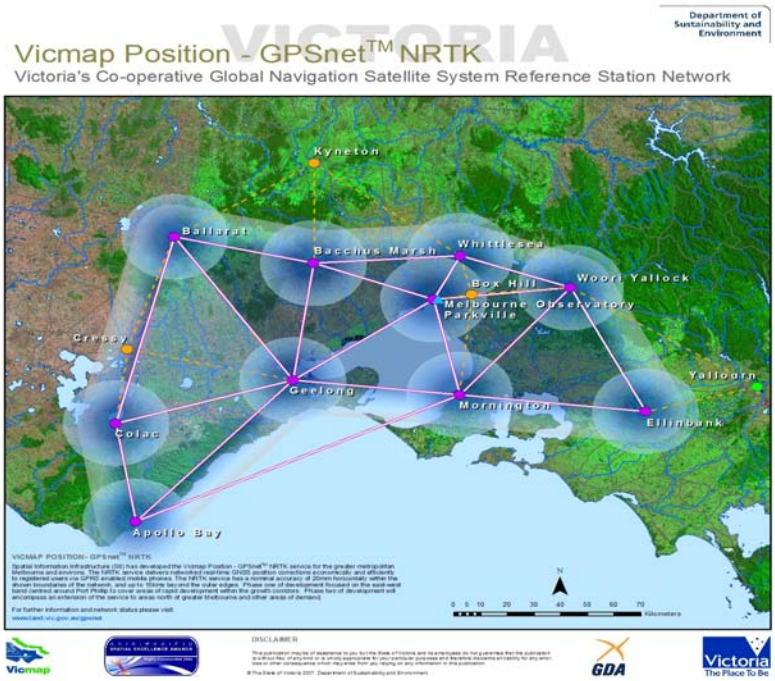

Figure 5.2 GPSnet MELBpos network infrastructure (DSE, 2007)

The current configuration of GPSnet reference stations covering the state has an average station spacing of around 100km. Internationally, most established CORS networks offering Network-RTK services for cm-level accuracy have reference station spacings of a few tens of kilometres at most. As it is not economically viable to densify GPSnet to such an extent, the question of how to increase the baseline lengths, within the Network-RTK system without sacrificing accuracy and reliability is at the forefront of both national and international research (Millner *et al.*, 2006; Zhang *et al.*, 2006). Baseline lengths within a reference station network can be increased primarily through improved methods of atmospheric bias modelling. Over the last decade, much research has gone into ways of improving reference network techniques of mapping regional atmospheric conditions (Retscher, 2002; Rizos, 2002; Dai *et al.*, 2003; Grejner-Brzezinska *et al.*, 2004;, 2005a; Grejner-Brzezinska *et al.*, 2005b; Grejner-Brzezinska *et al.*, 2006; Grejner-Brzezinska *et al.*, 2007). These network-based atmospheric bias modelling techniques are able to extend baseline lengths out to 70km or more in mid-latitude regions (Rizos & Han, 2003). Commercially however, the Trimble VRS system (see Section 4.4.5) has only been able to achieve horizontal positioning accuracies of the order of $\pm$5cm, for baseline lengths up to 35km (Higgins, 2002; Retscher, 2002).

In Australia, first generation commercial Network-RTK systems have been available for the last several years. Commercial RTK Networks are gaining momentum. In recent years the following systems have been installed: *Sun*POZ network in Brisbane, Syd*Net* in Sydney and more recently GPSnetwork in Perth.

SunPOZ was established in 2001 by Queensland's Department of Natural Resources, Mines and Water (Higgins, 2001). The network consists of a five station test bed of reference stations located in the Ipswich region south of Brisbane (Cislowski & Higgins, 2006). It uses Trimble proprietary VRS software and hardware to provide cm-level positional accuracy within the region. However, as the baseline lengths between the reference stations and user receivers are only of the order of 30km, it does not challenge the constraints that affect such CORS networks that provide Network-RTK solutions over longer baselines (Higgins, 2002).

The Syd*Net* CORS infrastructure commenced development in 2003, as a joint partnership between the NSW Department of Lands and the School of Surveying and Spatial Information Systems at the University of New South Wales (UNSW) (Rizos *et al.*, 2003). It currently consists of nine reference stations located in the Sydney basin region. At present, the network provides RINEX data for users via the internet and will soon provide real time corrections for users via the GPRS mobile phone network. The Syd*Net* infrastructure is currently being upgraded to form MetroNet, which will consist of 10-15 reference stations that will service the eastern seaboard from Nowra to Newcastle and west to Bathurst (Roberts, 2006). The Syd*Net* system will provide real time network generated corrections using software developed by UNSW and an Australia Research Council (ARC) consortium led by RMIT University (Zhang *et al.*, 2006).

More recently, in June 2006, GPSnetwork in Perth was established as the first privately owned VRS system in Australia (Trimble News Release, 2007). The system consists of 5 reference stations with plans to add two more. The Western Australian Department of Lands facilitated the new base stations into the surrounding geodetic network.

5.1.1 GPSnet test bed

The ability of the global empirical ionospheric models described in Section 4.2 to predict the ionosphere in an absolute sense has been extensively tested over the last 2 decades. Research has shown that the Bent, IRI and CODE models are able to remove approximately 80% of the absolute ionospheric effect, whilst the GPS Broadcast model is able to remove approximately 50% (see Chapter 4). As the change in the ionosphere from one end of the baseline to the next is of major importance in precise positioning applications (see Section 3.2.8.2), the ability of these existing empirical ionospheric models to derive the relative change in the ionosphere over Victoria is tested. This research is undertaken as part of a first step towards understanding the complexity of the ionosphere, and the issues that need to be addressed in order to derive cm-level ionospheric observations. The GPSnet system provides an ideal platform from which this research could be undertaken. In order to keep the testing at a manageable level, three base stations at Melbourne (RMIT), Ballarat and Bendigo were chosen as a test bed (see Figure 5.3), providing a relatively consistent network with an average baseline length of approximately 100km.

As the ionosphere can show strong seasonal variation (Gorney, 1990), it was decided to collect data at dates that coincided with the Summer Solstice and Winter Equinox periods, during the years 2001 and 2002. This period also coincided with solar maximum conditions. Data was retrieved from the DSE archives, in the form of 5 second RINEX data, that spanned the periods 22-24 September, 2001, 20-22 December, 2001, 19-21 March, 2002 and 20-22 June, 2002, (universal time) from each base station. These three particular base stations were chosen, as they have an approximate average spacing of 100km, which is indicative of the average spacing experienced throughout the network. Therefore, the ionospheric errors experienced by a user within this network would coincide with those experienced in any position within the current network configuration. Extending the analysis to include more stations would not add to or change the results in any meaningful way, as each baseline was analysed on its own merits, and the ionospheric error experienced along each line followed similar trends.

The positional solution integrity of the GPSnet network has been tested by Luton (2003), Penna *et al*. (2005) and Yousufi *et al*. (2006). Penna *et al*. (2005) used three weeks of continual dual frequency data from 16 stations within the network. The analysis carried out, compared the difference in results obtained for each 24 hour discrete solution. The RMS values of the differences in both the vertical and horizontal co-ordinate comparisons showed sub-centimeter accuracy, which coincided with the results obtained by Luton (2003). Yousufi *et al*. (2006) tested the stability of the GPSnet stations over short periods during changing weather conditions, and found that any detectable movement was at the mm-level. These results confirm the stability of the GPSnet stations in Victoria and the high quality of the data it produces.

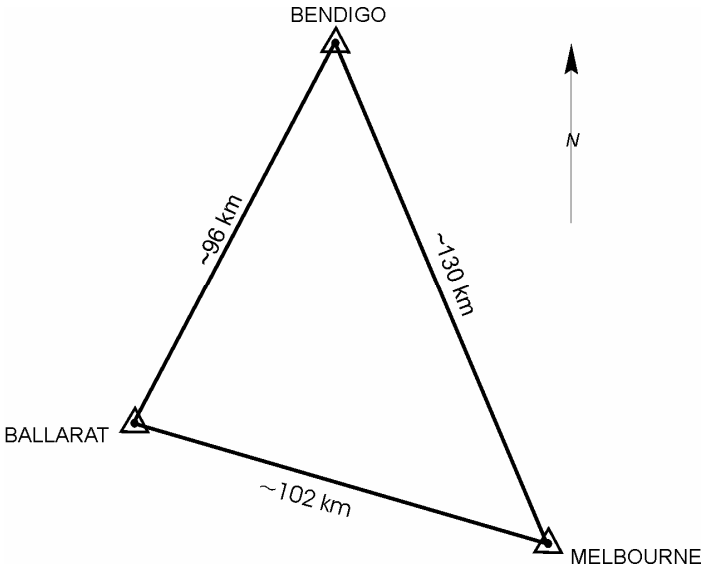

Figure 5.3 GPSnet test-bed base station network in Victoria

5.2 Solar activity during testing

The seasonal changes experienced through the year are directly associated with the Earth's revolution around the Sun (see Figure 5.4). The seasonal changes occur because the plane of the Earth's equator is inclined at an angle of 23.5º from its orbital plane around the Sun. The orbital plane is described as an ellipse, with one focus of the ellipse coincident with the Sun. The Earth completes one revolution of the Sun over the period of a year, whilst spinning on its own axis once a day. When

the Earth's inclination is directed towards the Sun, this is known as the solstices, and this occurs very near the points of perihelion and aphelion. At perihelion, the Earth has reached its closest point to the Sun, and therefore receives the greatest intensity of solar radiation, at aphelion it is at its greatest distance from the Sun, which would incur a minimum of solar heating. The difference in solar radiation experienced by the Earth at perihelion and aphelion is less than 7% (Byers, 1974).

The southern hemisphere has its greatest exposure to the Sun at the southern summer solstice. The Sun is directly over head at noon at a latitude of 23.5º S. During this period, the northern hemisphere is experiencing its winter solstice, where the northern hemisphere is tilted the farthest from the Sun. The equinoxes occur midway between the summer and winter solstice, they mark the position where the Sun shines equally in both hemispheres, therefore making the days and nights equal length. In relation to the northern hemisphere, the vernal equinox occurs in the spring and the autumnal equinox in the autumn.

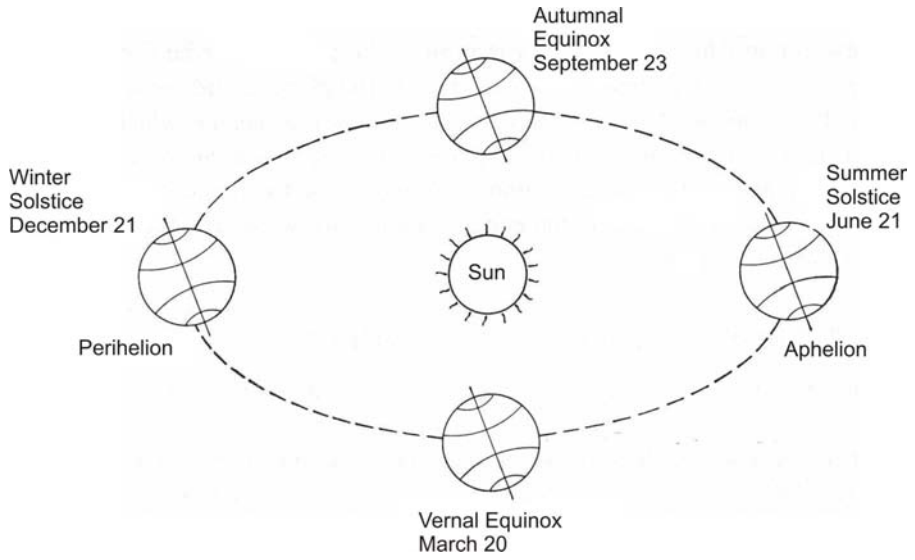

Figure 5.4 The Earth's revolution and the seasons (after (Byers, 1974)).

The solar activity during the periods of data collection have been summarised in the Table 5.1 below. The September period in 2001 shows strong solar activity, with both high solar flux and sunspot numbers recorded, as solar maximum conditions peaked. A strong solar wind disturbance, which triggered a minor geomagnetic storm (as

indicated by an Ap index of 41), was also recorded during this period. This event was brought on by a Coronal Mass Ejection (CME) that had occurred a few days earlier. The December period in 2001 showed signs of only slightly unsettled geomagnetic conditions, with the Ap index peaking at 14. The solar flux and sunspot values showed a marked decrease from the September period, with space weather agencies indicating that the Sun had been mostly quiet for a number of days. The March period in 2002 was highlighted by a number of eruptions from the Sun in the form of CMEs. These eruptions caused modest to active geomagnetic disturbances, which subsided on the last day. The solar flux and sunspot activity also subsided as solar disturbances declined from the peak. The June period of 2002 indicated moderate geomagnetic activity, with the solar flux and sunspot number again in steady decline.

Table 5.1 Solar activity during data collection periods.

Month/Year	Date	Solar Flux	SSN	Ap index
	22	255	258	8
September, 2001	23	259	293	41
	24	279	275	8
	20	221	158	4
December, 2001	21	234	171	14
	22	243	215	4
	19	175	136	19
March, 2002	20	188	119	9
	21	174	141	7
	20	145	127	5
June, 2002	21	140	122	7
	22	142	113	6

5.3 Double-differenced ionospheric delay

The Bernese GPS Software Version 4.2 (Hungentobler *et al.*, 2001) was used to individually process each baseline in the Melbourne-Ballarat-Bendigo test bed network (see Figure 5.3) to obtain precise estimates of the double differenced ionospheric bias for the satellites observed. This data was treated as 'truth', from which to compare the other empirical models.

In addition to GPS observations in the form of RINEX data, the Bernese software requires the following input data:

- precise orbit and Earth rotation parameters;
- a satellite events file;
- a phase centre eccentricities file, which contains the positions and variations of the phase centers for various antenna types,
- an antenna height translation file, which contains a translation table between the antenna heights given in the RINEX data and the antenna heights actually used in the Bernese software. This file also contains information on antenna phase centre models.
- a site name translation file, where the station names used in the RINEX files are shortened to an abbreviated form.
- a receiver/antenna translation file, where a station dependent renaming of the receiver and antenna types can be performed if necessary.
- ITRF2000 base station co-ordinates for each base station.

Once all of these files were correctly placed, the processing of each three-day block (72 hours) could take place. It should be noted that a 10º elevation mask was used during all of the baseline processing. Initially the data was run through a pre-processing step that starts with the estimation of the receiver clock offsets, based on code data, in a single point positioning mode. The input files required during this stage were the observation files, station co-ordinates and satellite orbits and clocks. Single differences of each baseline were then formed, along with a cycle slip detection and repair process.

Next, the parameter estimation section of the processing was undertaken, in which the processing involves three steps to estimate the station co-ordinates. These three steps involve the use of the float solution and error estimation, integer ambiguity resolution and validation and the use of a fixed solution to estimate the final co-ordinates. The ambiguity resolution strategy used during this processing stage was the quasi-ionospheric-free (QIF) strategy (see section 3.2.8.7.1). Firstly the ionospheric free linear combination (L3) (see section 3.2.8.6.1) was used to estimate the initial co-ordinates, holding one base station fixed. It should be noted that when

processing the Melb-Ball and Melb-Bend baselines the Melbourne base station was held fixed. When processing the Ball-Bend baseline the Ballarat base station was held fixed. During this process, tropospheric estimates and residuals were also computed. Secondly, the ambiguity resolution step was carried out. During this process the tropospheric estimates and co-ordinates calculated in the previous float solution were introduced. The L1 and L2 ambiguities were computed using the QIF strategy, whilst holding one base station fixed. Once the ambiguities had been fixed, this solution was used to compute the final station co-ordinates, by introducing the previously computed ambiguities. The L3 linear combination was used, with no base stations held fixed, but for numerical reasons, the Bernese Software requires one station to be constrained to 0.00001m (Hungentobler *et al.*, 2001).

Once the baseline ambiguities were fixed and the final station co-ordinates obtained, the Stochastic Ionospheric Parameters (SIPs) could be computed (Schaer, 1999). The SIP values provide a precise estimate of the double-differenced ionospheric delay on the L1 frequency, between a set of co-observed satellites along a particular baseline. The SIP values were computed using the L4 linear combination (see section 3.2.8.6.2). The double differenced SIP values are estimated with respect to a reference satellite, which was chosen based on the highest elevation.

The double differenced SIP values were carefully analysed to try to identify and remove any anomalies, as a number of discontinuities in the SIP values were found to exist before and after cycle slips. It was discovered that in most instances this was due to incorrect resolution of the carrier phase ambiguity, as most of the discrepancies closely resembled multiples of the L1 wavelength (0.19m). In the majority of cases, it was also found that a large portion of the problematic data was confined to satellites that were below 20º in elevation.

As a means of discovering which satellites had potential ambiguity resolution problems, an analysis was carried out on all of the data, along each baseline and season. It was found that in consecutive epochs the change in SIP value was no greater than 0.025m in 98% of the data. Therefore, any discrepancy greater than 0.025m was investigated. The data was then edited by removing erroneous data that

did not fit the overall trend of the satellite trace. This resulted in the removal of approximately 2% of the data in each 72 hour period, which equates to approximately 1.5 hours of data that was contaminated. The resulting edited data was then used as 'truth' for the model analysis.

5.4 Empirical model test methodology

In order to test the Broadcast Model, the Bent Model and the CODE model (see chapter 4), they were implemented as scripts in Matlab Version 6. The IRI-2001 was implemented in its original Fortran language form. Based on the 5 second RINEX data collected during the years 2001/2002 (see section 5.1.1), each model calculated the IPP (see section 4.2.5) for each observation, at a pre-described ionospheric shell height. The vertical delay at this point was then converted to a line of sight delay using each model's internal mapping function.

The model line of sight delays were differenced, for each baseline, to coincide with the receiver and satellite combinations used by the Bernese Software to produce the SIPs. The data produced using the models was then compared with the Bernese output, and is the source of the data being analysed in the chapter.

5.4.1 Results and analysis of model comparisons

The following Tables 5.2–5.4 summarise the statistics associated with the L1 double differenced ionospheric delay, considering each of the reference and rover satellite combinations, over the three different baselines in the network. Each of the four periods tabulated includes three days (72 hours) of data.

Table 5.2 Double differenced ionospheric delay on L1 over the Melbourne-Ballarat baseline

Date	Mean (m)	Std. Dev. (m)	Max. (m)	Min. (m)
Sept, 2001	-0.002	0.057	0.272	-0.256
Dec, 2001	-0.011	0.080	0.429	-0.475
March, 2002	-0.019	0.109	0.514	-0.731
June, 2002	-0.008	0.051	0.340	-0.296

Table 5.3 Double differenced ionospheric delay on L1 over the Melbourne-Bendigo baseline

Date	Mean (m)	Std. Dev. (m)	Max. (m)	Min. (m)
Sept, 2001	0.007	0.072	0.323	-0.303
Dec, 2001	0.003	0.092	0.400	-0.480
March, 2002	-0.004	0.100	0.636	-0.433
June, 2002	-0.002	0.066	0.324	-0.351

Table 5.4 Double differenced ionospheric delay on L1 over the Ballarat-Bendigo baseline

Date	Mean (m)	Std. Dev. (m)	Max. (m)	Min. (m)
Sept, 2001	0.008	0.056	0.360	-0.268
Dec, 2001	0.018	0.052	0.324	-0.298
March, 2002	0.012	0.080	0.496	-0.396
June, 2002	0.005	0.054	0.343	-0.336

Based on the results in Tables 5.2-5.4, the mean double differenced ionospheric delay is mostly zero, which is expected. Seasonal variation in the ionospheric bias is evident in all three tables. The variation however, shows a certain consistency from one season to the next, which is typical of mid-latitude ionospheric behaviour. Overall it can be seen that the March equinox period for each baseline shows the largest standard deviations and ranges. Generally the highest ionospheric activity occurs around the equinoxes, however, the period also coincided with active geomagnetic conditions caused by a number of Coronal Mass Ejections from the Sun, see Spaceweather (2007) for more information. Across the three baselines tested, the December period showed on average the next largest standard deviations and maxima minima results. This period coincided with the summer solstice where the southern hemisphere has its greatest exposure to the Sun. At the other end of the scale, the winter solstice in June produced the smallest variations in ionospheric bias as expected.

It can be seen that all three baselines in the network produced similar results. Hence for the purpose of brevity, the Melbourne to Ballarat baseline was chosen for further analysis in this chapter.

The comparison between the empirical model data and the actual ionospheric biases is presented next. The Bernese SIP results are treated as truth and individual model values were then compared with the Bernese data to produce model errors. Figures 5.5 and 5.6 depict the distribution of the model errors, during the high (March) and low (June) ionospheric variation periods, whilst Table 5.3 contains a summary of the respective statistics.

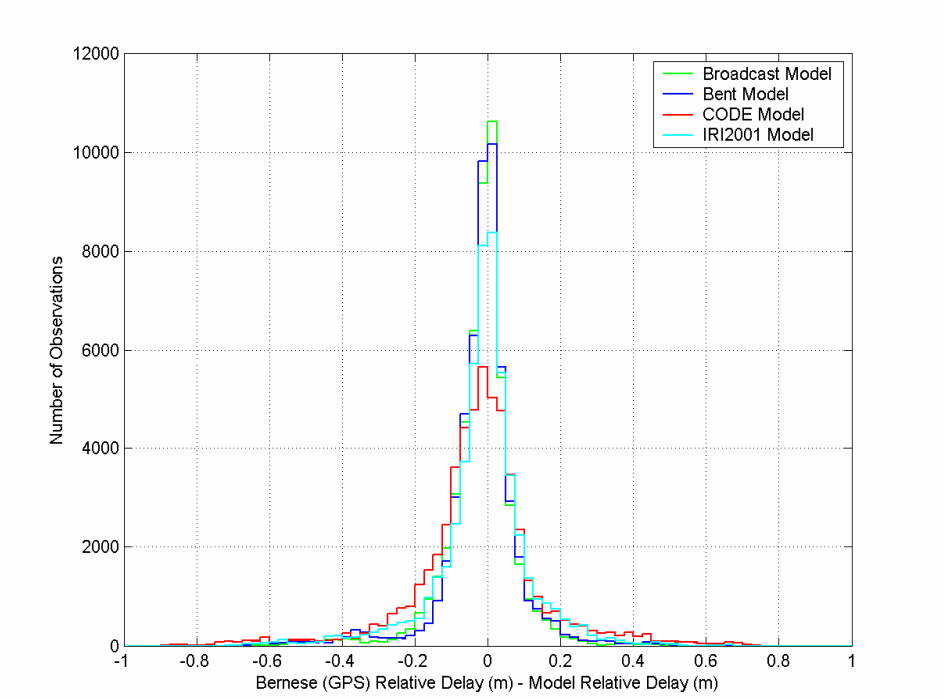

Figure 5.5 Distribution of relative delay discrepancies, between the Bernese 'truth' output and the model derived delay, over the Melbourne to Ballarat baseline, from the 19th-21st March, 2002.

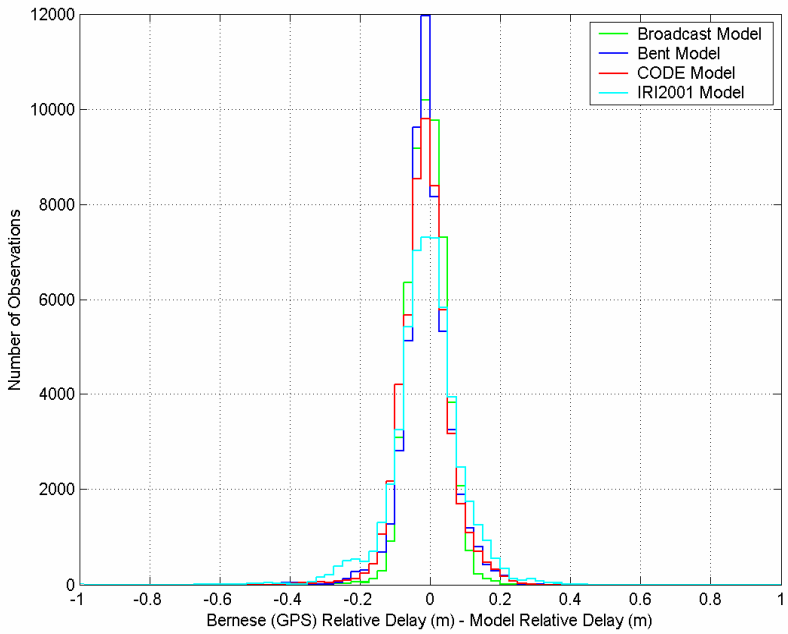

Figure 5.6 Distribution of relative delay discrepancies, between the Bernese 'truth' output and the model derived delay, over the Melbourne to Ballarat baseline, from the 20th-22nd June, 2002.

Table 5.5 Statistics of the differences between the Bernese output and model results

Melbourne-Ballarat baseline, units in metres.

Date	Model	Mean Diff.	Std. Dev.	Max. Diff.	Min. Diff.
	Broadcast	-0.006	0.072	0.449	-0.449
Sept, 2001	Bent	-0.011	0.090	0.450	-0.549
	CODE	-0.031	0.130	0.472	-1.068
	IRI2001	-0.001	0.093	0.469	-0.349
	Broadcast	-0.011	0.063	0.416	-0.487
Dec, 2001	Bent	-0.009	0.090	0.401	-0.503
	CODE	-0.024	0.137	0.536	-0.881
	IRI2001	-0.013	0.103	0.387	-0.515
	Broadcast	-0.018	0.096	0.482	-0.700
March, 2002	Bent	-0.015	0.110	0.543	-0.683
	CODE	-0.024	0.176	0.728	-0.880
	IRI2001	-0.012	0.131	0.662	-0.717
	Broadcast	-0.007	0.053	0.292	-0.371
June, 2002	Bent	-0.010	0.070	0.318	-0.568
	CODE	-0.013	0.069	0.279	-0.450
	IRI2001	-0.010	0.095	0.425	-0.658

None of the models appear to reliably estimate the actual ionospheric bias values. In fact, the standard deviations of all models (see Table 5.5), are not significantly less than the raw Bernese output results shown in Tables 5.2-5.4. In other words, an assumption of zero double differenced ionospheric bias would be as good as any of the tested models. The differential results obtained do not agree well with (undifferenced) tests of the various models that have been conducted by other investigators. Hernandez-Pajares, (2003), suggests that the CODE model out-performs both the Broadcast and Bent models, which is clearly not the case in the majority of the results found during these tests. The following Figures 5.7-5.10 graphically illustrate both the size of the actual ionospheric bias, estimated using the Bernese GPS Software, and the bias estimated by the empirical models being tested during the same timeframe.

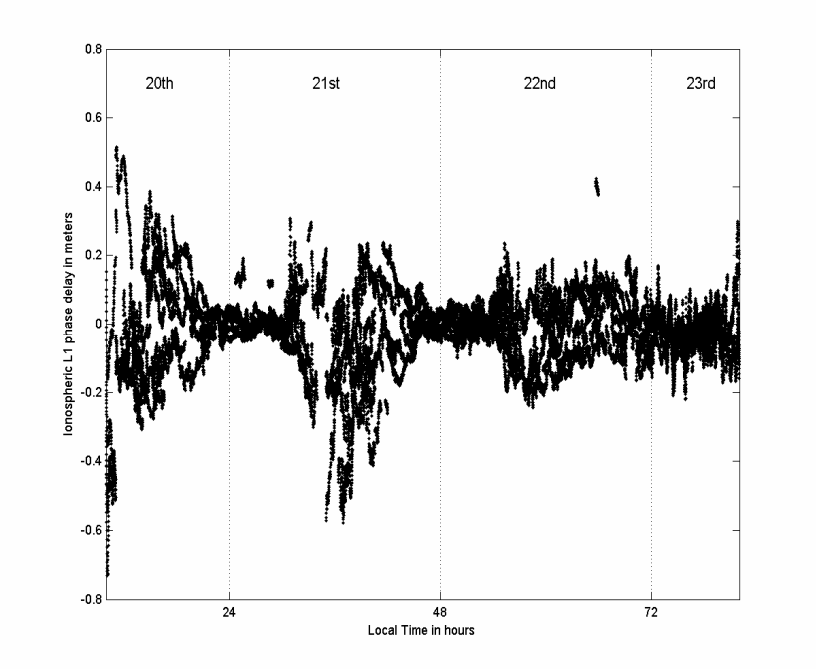

Figure 5.7 Stochastic ionospheric parameters (SIPs) from the Bernese software, describing the double differenced ionospheric delay on L1 along the Melbourne to Ballarat baseline from the 19th-22nd of March, 2002.

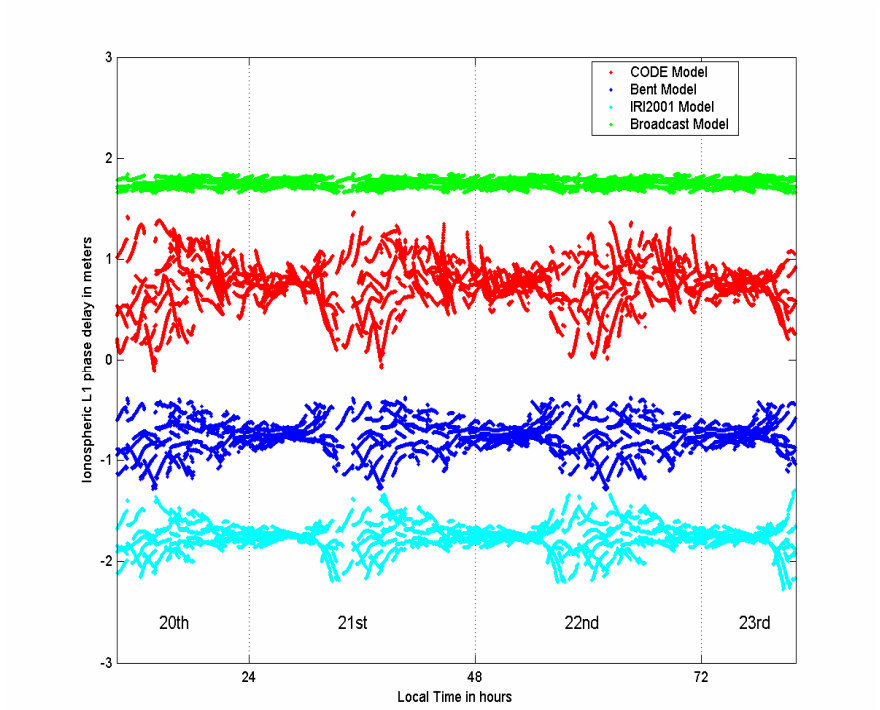

Figure 5.8 Double differenced ionospheric delay derived using the Bent, CODE, IRI2001 and the GPS Broadcast models along the Melbourne to Ballarat baseline from the 19th-22nd of March, 2002.

(The models have been offset by 0.75m for clarity)

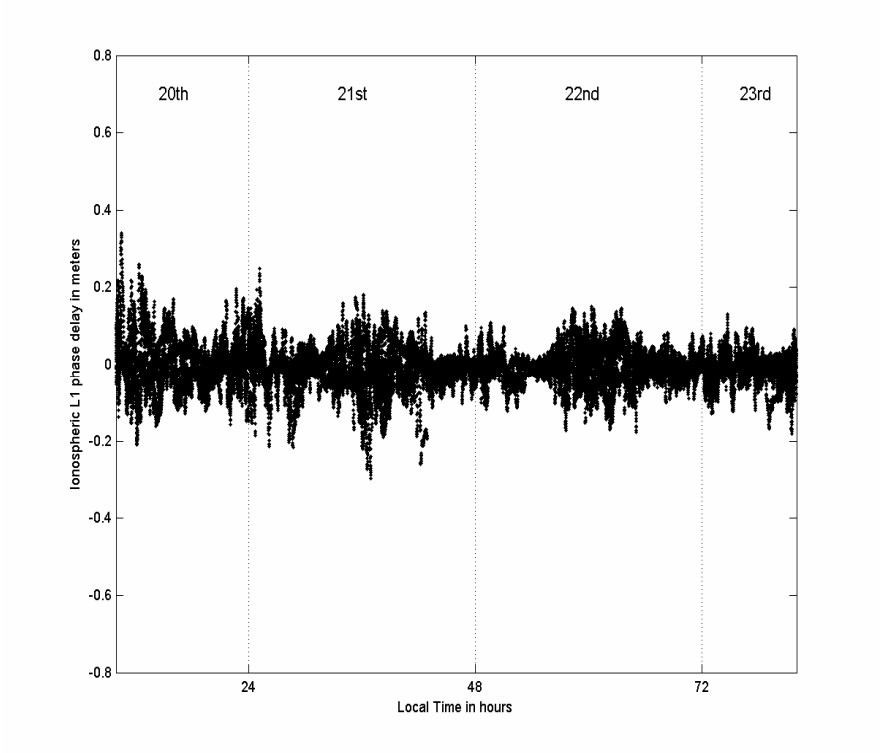

Figure 5.9 Stochastic ionospheric parameters (SIPs) from the Bernese software, describing the double differenced ionospheric delay on L1 along the Melbourne to Ballarat baseline from the 20th-23rd of June, 2002.

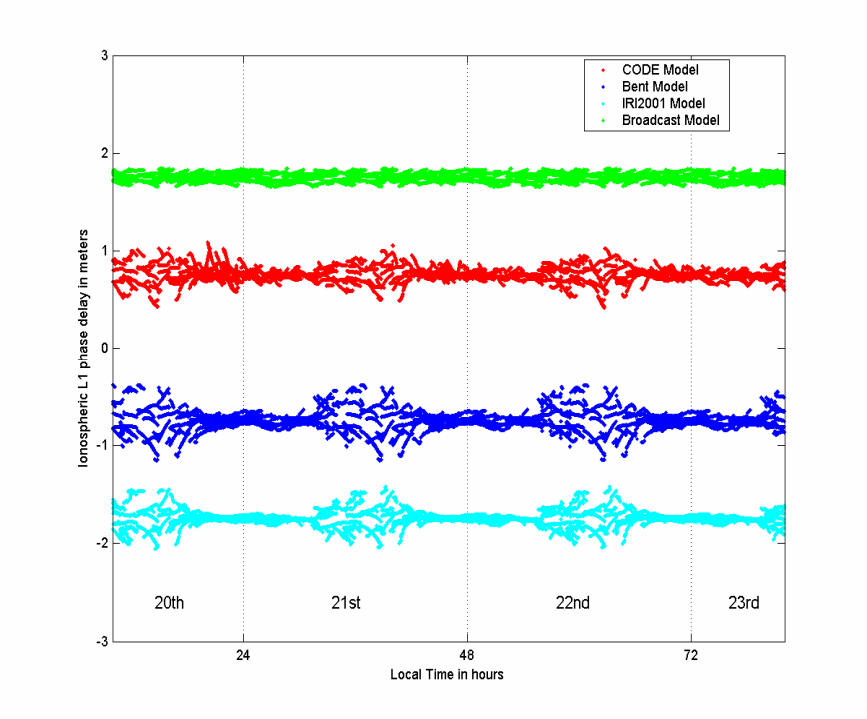

Figure 5.10 Double differenced ionospheric delay derived using the Bent, CODE, IRI2001 and the GPS Broadcast models along the Melbourne to Ballarat baseline from the 20th-23rd of June, 2002.

(The models have been offset by 0.75m for clarity)

It is useful to consider the diurnal and seasonal variation of the ionospheric bias. Figures 5.7 and 5.9 show the ionospheric bias values for each satellite tracked during the March and June timeframes respectively. The X-axis of the plots is local time – note how the ionospheric bias is quite disturbed during the March period, especially on the 20th and 21st. This coincides with active geomagnetic conditions recorded at this time, due to a number of eruptions from the Sun. The diurnal variation is also pronounced, with conditions being relatively undisturbed from approximately midnight through to 10am, then dramatically increasing to a peak at approximately 2pm. In June, where the ionosphere is less disturbed, the daily trend is not as noticeable, but still shows a maximum occurring at approximately 2pm each day. These quieter conditions during June contrast with the large ionospheric disturbance in March, showing the strong seasonal variation that is present in the ionosphere.

Figures 5.8 and 5.10, illustrate the model double differenced ionospheric delay for each 72 hour seasonal period. The Bent, CODE and IRI2001 models (Figures 5.8 and 5.10) contain a strong diurnal variation parameter and also appear to vary from

season to season, whilst the Broadcast model tends to remain relatively flat over the data collection periods shown. None of the models are able to capture the wide ionospheric bias variation in some of the satellite traces. This reflects the difficulty of modelling the dynamic and highly variable ionosphere. The simple elevation-dependent mapping function used in all models does not appear to be sufficient for estimating the non-homogeneous ionospheric delay.

Even though the models are not able to accurately estimate the actual ionospheric bias, they do provide a stochastic measure of the expected variability in the ionosphere. This information is relevant to long baseline estimation where a-priori variance must be assigned to ionospheric biases contained in the least squares estimation model.

5.4.2 Model test conclusions

Precise positioning is now a widely used GPS technique. The ionosphere introduces an unknown bias in GPS observations which must be precisely known to be able to achieve accurate ambiguity resolution in real time over baselines longer than 10km in mid-latitude regions. Four well known global empirical ionospheric models were tested against actual double difference ionospheric bias values over baselines of approximately 100km. These global models were assessed to see how they would perform in a more regional sense, in order to gain an understanding of the variability of the actual ionosphere across the state of Victoria, and test their suitability for modelling the ionosphere in a Network-RTK environment.

None of the models appeared to provide ionospheric bias estimates to an accuracy required for the correction of real time data in a Network-RTK environment. Furthermore, a user would be better off assuming that the ionospheric bias is zero, rather than use any of the ionospheric models tested. The results from the differential analysis are significantly different from absolute ionospheric delay studies where the Bent, CODE and IRI2001 models have been found to remove approximately 75-90% of the ionospheric delay (See section 4.2). Although the models were unable to determine the actual double differenced ionospheric biases, they all provided a

stochastic measure of the diurnal and seasonal variability which is important for long baseline estimation problems.

Given the fact that each model is global in nature, they are constrained to the general nature of their input coefficients, and are therefore unable to adequately estimate ionospheric behaviour in a smaller regional sense. Also the measurements used to derive the coefficient sets that are used as input for the particular models are derived predominantly from the northern hemisphere, and therefore may be biased to a certain degree when adapted for use in the southern hemisphere.

5.5 Summary

This chapter provided a general overview of the GPSnet CORS system operating in Victoria. The network in recent years has implemented two real time positioning capabilities, these being the high precision cm-level MELBpos system and VICpos the state-wide DGPS sub-metre system. The MELBpos real-time cm-level positional capability is currently restricted to Melbourne and its immediate surrounding regions due to the density of the state-wide network.

Victoria's GPSnet is currently undergoing extensive infrastructure upgrades as part of a state government initiate to implement a cm-level real time positioning service across the state. Due to the sparse (+100km) configuration of GPSnet's reference stations, the precise modelling of Victoria's ionosphere will play a key role in providing a state-wide cm-level service. This challenge is an active topic of research for both national and international researchers. As a preliminary step towards producing an ionospheric modelling approach that will enhance the capability of the GPSnet system, four well known global empirical ionospheric models were tested to assess their suitability for precise ionospheric correction in the Victorian Network-RTK environment.

The ability of the four different global empirical ionospheric models to predict the double differenced ionosphere has been tested with respect to GPS derived double differenced observations using the GPSnet infrastructure. The results indicate that

none of the models are capable of capturing the wide ionospheric bias variation to cm-level accuracy. This poor performance was thought to be due to a number of factors. Firstly, the general global nature of their input coefficients made them unable to accurately reproduce ionospheric conditions over smaller regions. Secondly, the measurements used to derive these coefficients are obtained predominantly from the northern hemisphere, which may introduce a bias when adapted for use in the southern hemisphere. Thirdly, the simple elevation dependent mapping functions used by all of the models, may not have been able to accurately estimate the non-homogeneous ionosphere.

Based on these results it would seem that in order to model the ionosphere to a sufficient level of accuracy, a model would have to be produced that used accurate input data from the immediate surrounding area. The data would also have to be collected as close to real-time as possible, due to the ever changing ionospheric conditions. In order to gain a better understanding of Victoria's ionosphere as a precursor to producing a temporal ionospheric modelling technique, the next chapter focuses on defining the variation of the absolute ionosphere over Victoria, then refines the study to investigating the temporal nature of the double differenced ionosphere over the same region during the same period.

Chapter 6 The temporal ionosphere over Victoria

The primary objective of this chapter is to investigate the temporal variation of the ionospheric bias over Victoria as a precursor to the development of an ionospheric model capable of providing corrections accurate enough to ensure precise ambiguity resolution in a Network-RTK environment. The analysis undertaken in this chapter will firstly focus on the ionosphere in its general "macro" form, then analyse its behaviour more closely ("micro" form), from one epoch to the next. A preliminary investigation that analyses the absolute TEC over the Victorian region, as a means of quantifying its behaviour over four seasonal periods will first be conducted. This preliminary study will provide an insight into the overall stability of the ionosphere over Victoria. Next, the temporal variability of the double differenced ionospheric bias will be analysed. Its behaviour from one epoch to the next will be investigated as a means of understanding how quickly it decorrelates over time.

6.1 Victoria's absolute ionosphere

In order to get an understanding of the general characteristics of the ionosphere over Victoria, an analysis of the temporal variation of the ionospheric TEC over the region was performed. This investigation focused on the diurnal and seasonal variations of

the ionosphere, based on a series of GPS-based TEC estimates. This analysis enables the characterisation of the nature and fine structure of the ionosphere over Victoria in both a local and regional sense (Yuan, 2002; Huo *et al.*, 2005). This investigation provides an insight into the most appropriate modelling strategy to use, in order to improve the precision of ionospheric correction for real-time positioning.

A subset of eight GPSnet stations located across the state were used as a test bed for this analysis. Dual frequency GPS observations were collected from each station that coincided with the same test period used in Chapter 5. The data collected consisted of 72 hours of observations that centred around the September 2001, December 2001, March 2002 and June 2002 solstice and equinox dates. The observations were recorded at the Melbourne (RMIT), Ballarat, Bendigo (now Epsom), Benalla, Geelong, Hamilton, Horsham and Yallourn GPSnet base stations (see Figure 5.1).

6.1.1 TEC estimation using spherical harmonics

It is common practice within the GPS research community to assume that the ionosphere can be represented as a very thin shell for mapping purposes (see section 4.2.5). The two dimensional modelling approach adopted for this analysis assumes the ionosphere to be concentrated on a spherical shell of infinitesimal thickness located at an altitude of 350km above the Earth's surface. Previous research in this area has confirmed that it is possible to parameterise the vertical TEC (VTEC) onto this shell using a spherical harmonic function referenced to a solar-geographical framework (Feltens & Schaer, 1998; Schaer *et al.*, 1998; Wu *et al.*, 2006). The TEC representation using spherical harmonics is expressed mathematically by equation (4.4) (Schaer, 1999).

The time series of TEC measurements were obtained using the spherical harmonic function expressed in equation 4.4, together with dual frequency GPS carrier phase data as input. In the spherical harmonic function, a degree and order $m = n = 3$ with 16 unknown parameters was adopted in the calculation. The geometry free (L4) (see

section 3.2.8.6.2) linear combination was used to eliminate the effects of satellite geometry, clocks and the troposphere. The unknown satellite and station instrumental biases (Wilson & Mannucci, 1993; Yuan & Ou, 1999) are estimated together with the unknown ionospheric parameters using the least squares technique. The instrumental biases for a particular satellite and receiver combination are considered as a constant value for a day, as both the satellite and receiver hardware is relatively stable over the course of 24 hours (Schaer, 1999; Yuan & Ou, 1999)(see section 3.2.8.8). This modelling technique has an estimated accuracy of several TECU (Gao & Liu, 2002), which equates to an equivalent model accuracy of approximately 1.1m.

A trigonometric single-layer mapping function (see equation 4.12) was used to convert line of sight TEC to VTEC at the GPS receiving station and at the IPP on the thin shell (see Figure 4.4). An elevation cut-off angle of 20° was adopted to reduce the potential effects of mulipath during these tests. A data sampling rate of 30 seconds was used.

This study involves a two step process: (1) The vertical TEC values above the Melbourne base station were calculated at 30 second intervals using 3 days worth of observations collected during each season, as described in section 6.1, (2) Line of sight TEC values, from all eight GPSnet stations used in the analysis, were converted to VTEC values at each IIP on the thin shell. This data was used to produce contour plots of the ionosphere at two hourly intervals over a 24 hour period, for each season.

6.1.2 Diurnal and seasonal ionospheric variations over Melbourne

The spherical harmonic function described in section 6.1.1 was used to produce VTEC estimates above Victoria using the Melbourne base station. As ionospheric activity is closely related to the Sun's position, a solar-geographical reference frame was adopted to estimate the TEC model parameters. Figure 6.1a-d, depicts both the diurnal and seasonal variation of the ionosphere over Melbourne during the 72 hours

(3 days) captured in each seasonal period. There are four sub-frames in Figure 6.1, each depicting 3 x 24 hours of VTEC data captured over Melbourne during the September, 2001, December, 2001, March 2002 and June, 2002 periods. The X-axis and Y-axis represent universal time (UT) of the day and VTEC value respectively.

For the sake of this analysis it is assumed that in Melbourne, local time 5:00~9:00 is morning, 9:00~17:00 hours is daytime, 17:00~21:00 is dusk and 21:00~5:00 is nighttime, respectively. Firstly, when examining the plots in Figure 6.1 in a diurnal sense, it suggests that the maximum VTEC values occur at approximately 4:00 UT or 14:00 Local Time (LT), and the minimum VTEC values occur at approximately 17:00UT or 3:00LT. On examination, it does become evident that there is a significant change in the VTEC values from day to day within each season, except for the June period, which traditionally displays a more quiet and stable ionosphere. These changes from day to day, especially during the local daytime period, can equate to as much as 20%, with the changes experienced from one season to the next as great as 50% as found between the March and June periods. The VTEC values experienced during the day are higher than those at night-time. However, the occurrence time of the maximum and minimum ionospheric values varies with season.

When comparing the plots in Figure 6.1 in a seasonal sense, significant VTEC differences can be observed in both magnitude and pattern, with the highest values occurring during the March period, and the lowest obtained in the June period. It can be seen that the daytime (23:00~7:00UT) VTEC values obtained in September (spring) and March (autumn) periods are generally greater than those obtained during the December (summer) and June (winter) periods. However, during the December period, the VTEC values remain at a higher level for a longer period than the remaining months.

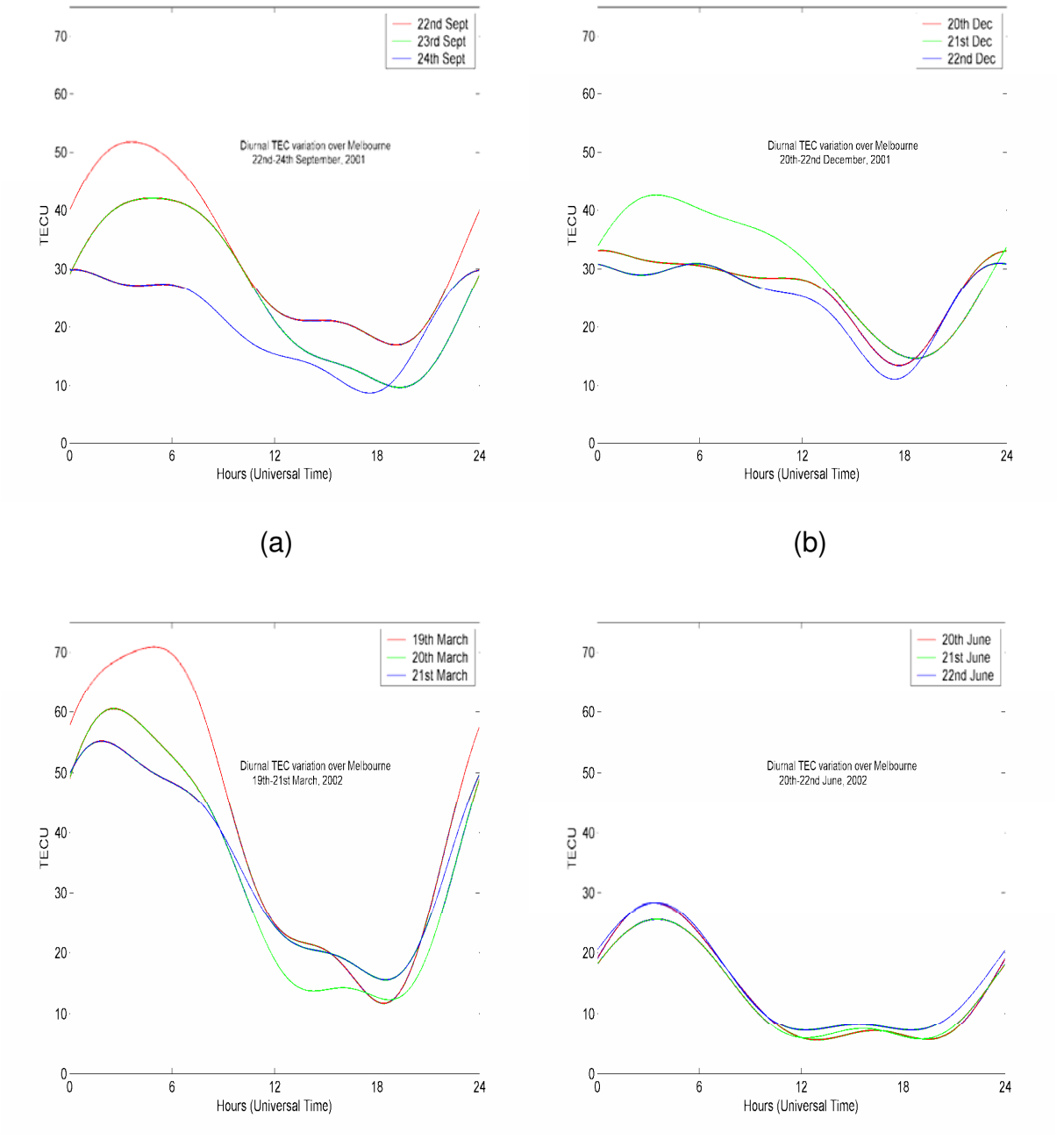

Figure 6.1 Diurnal and seasonal variations of VTEC values above the Melbourne (RMIT) GPSnet base station over 24 hours.

Based on these results, there is little evidence of consistency in observation from season to season. Whilst the general trend in the plots within each seasonal period is similar, modelling coefficients derived from one day's worth of data would not be accurate enough to describe the ionosphere from one day to the next for the purpose of cm-level Network-RTK requirements. This highlights the fact that in order to adequately describe ionospheric conditions within a Network-RTK environment,

ionospheric corrections must be derived from periods that coincide with or are as close to the period of correction as possible, due to the ionosphere's constant variability.

6.1.3 TEC variations over Victoria

A state wide analysis of the ionosphere is conducted in this section. Eight GPSnet stations scattered across Victoria were used to produce VTEC values, using the method described in section 6.1.1. Based on these results obtained, a time series of 12 x 2 hourly snapshots of VTEC over Victoria for each season was computed and compiled over two graphs. Figures 6.2-6.5 show these results in the form of 2 x 12 hours worth of VTEC contour plots. The X-axis and Y-axis denote longitudinal and latitudinal directions respectively.

On examination of Figures 6.2-6.5, the largest VTEC values were recorded during March 2002, with values as high as approximately 70 TECU during the day and as low as 10 TECU during the night in June, 2002. This equates to a delay of approximately 11.2m in the vertical, during peak daytime conditions. As a general rule, an obliquity factor of 3 is applied to low elevation angle satellites. This ratio describes the factor with which the ionospheric delay is increased relative to the delay experienced at zenith, as a product of ionospheric conditions and satellite elevation angle (Spilker, 1980). This would mean that during the peak daytime conditions in March, 2002, low elevation angle satellites would have been experiencing ionospheric delays in the order of 33m. In contrast, during June of the same year, peak values were recorded at approximately 30 TECU (4.8m vertical delay) during peak daytime conditions and down to a low of 10 TECU (1.6m) during minimum night time conditions. Therefore, during peak daytime conditions in June, low elevation angle satellites would have been experiencing delays of approximately 14m.

It can be seen that the VTEC values over Victoria vary with the time of day, and the spatial correlation characteristics of the VTEC values corresponding to each 2 hourly

epoch are quite different. Over the day time period, the figures presented show that the most significant increase in TEC between 2 hourly snap shots occurs during the morning period, where increases of approximately 50% were attained across all seasonal periods, due to the ionosphere's rapid heating as a result of its first exposure to the Sun. During the peak day time period of between 12 noon and 4pm local time, steady increases of approximately 10% occurred between each snap shot before the peak was reached. In the late afternoon and early evening, TEC values decreased at a fairly steady rate of 10-15% between 5pm and 8pm. The night time period showed fairly stable plots with little variation.

The graphs also depict many spatial anomalies or inconsistencies in VTEC across Victoria, especially during the September and December, 2001 periods. This disturbed period showed TEC gradients between 2-8ppm over the state during the peak day time period. These anomalies generally occur during the daytime hours. The more stable conditions experienced during June showed TEC gradients of approximately 0.5ppm across the state.

It should be noted that the changing patterns portrayed on each plot of the ionosphere describe the changing satellite geometry experienced over Victoria. Some of the snap shots of the ionosphere over Victoria show gaps in coverage. This means that at the time of observation, from the GPSnet stations chosen for the analysis, the satellite geometry was not sufficient to cover the whole of the state. Using the entire GPSnet infrastructure would alleviate this problem to some extent. However, in order to consistently produce a state wide ionospheric model, that covers all of Victoria, data from GPS receivers located outside of the state boundaries would enable sufficient coverage even when satellite availability was low.

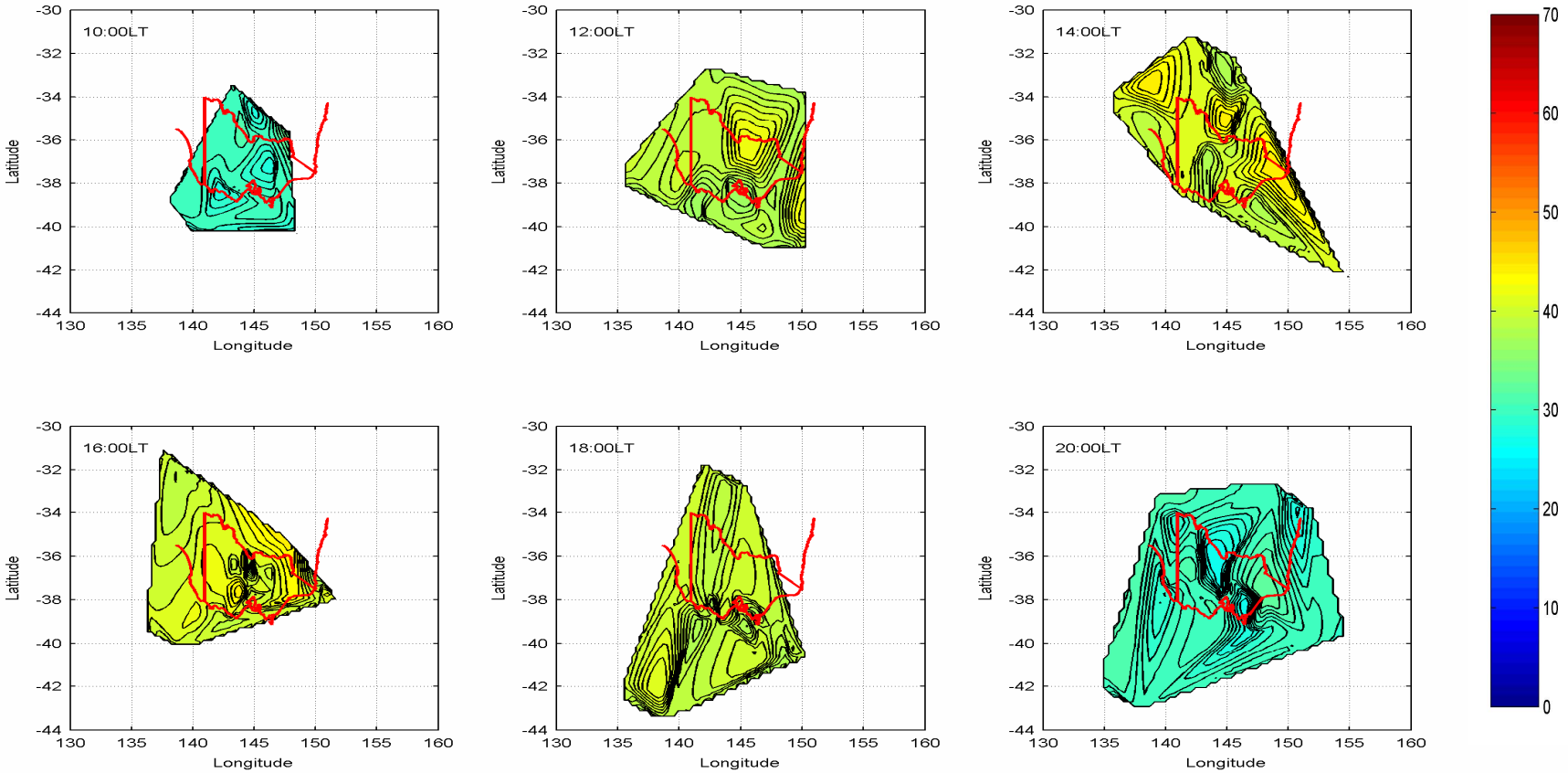
10:00LT
12:00LT
14:00LT
16:00LT
18:00LT
20:00LT
Latitude
Longitude
-30
-32
-34
-36
-38
-40
-42
-44
130
135
140
145
150
155
160
70
60
50
40
30
20
10
0

(a)

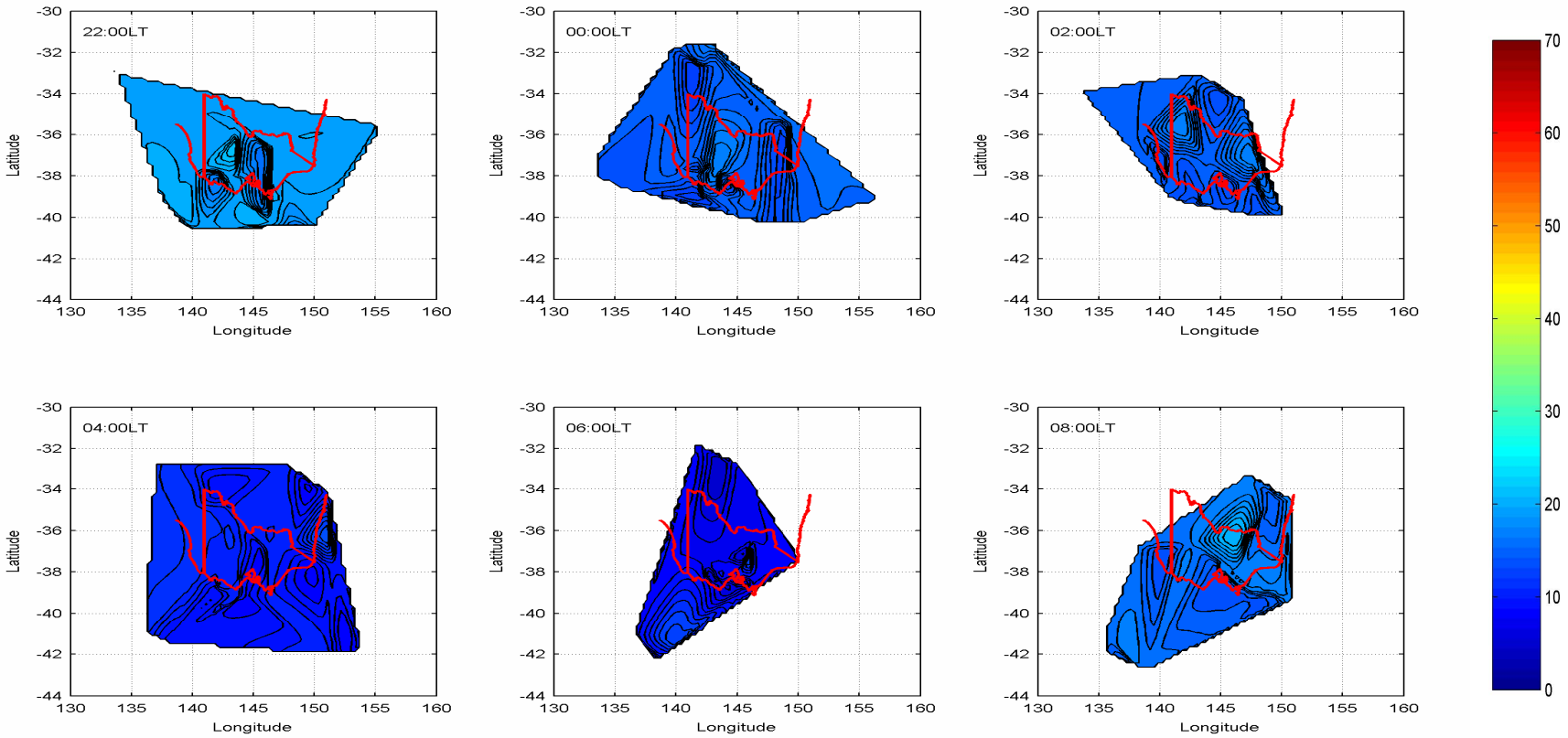

(b)

Figure 6.2: 24 hours of 2 hourly VTEC snapshots over Victoria, taken from the 23rd to the 24th of September, 2001.

(Data is shown in units of TECU and expressed in Local Time (LT))

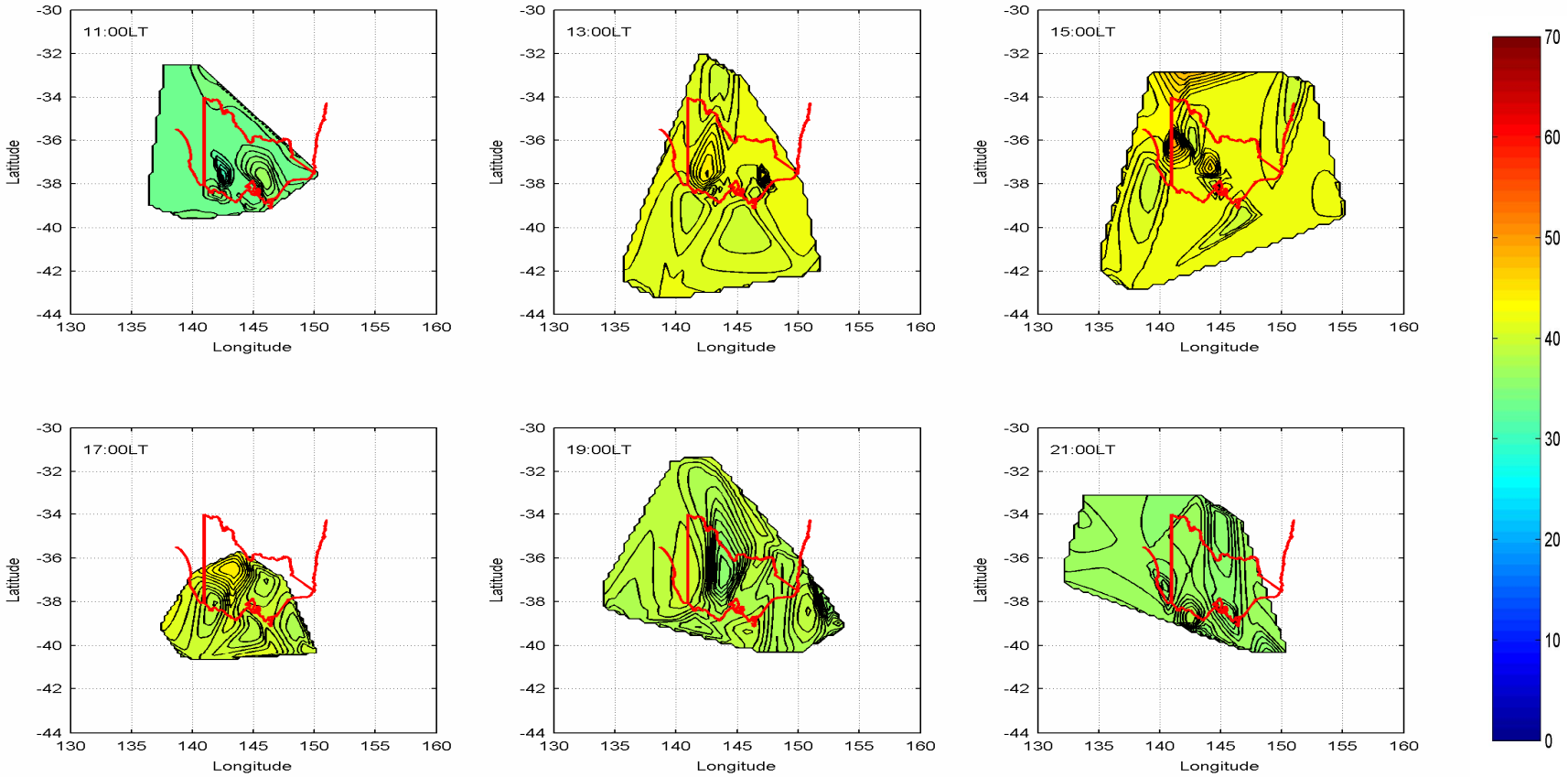
11:00LT
13:00LT
15:00LT
17:00LT
19:00LT
21:00LT
Latitude
Longitude
-30
-32
-34
-36
-38
-40
-42
-44
130
135
140
145
150
155
160
70
60
50
40
30
20
10
0

(a)

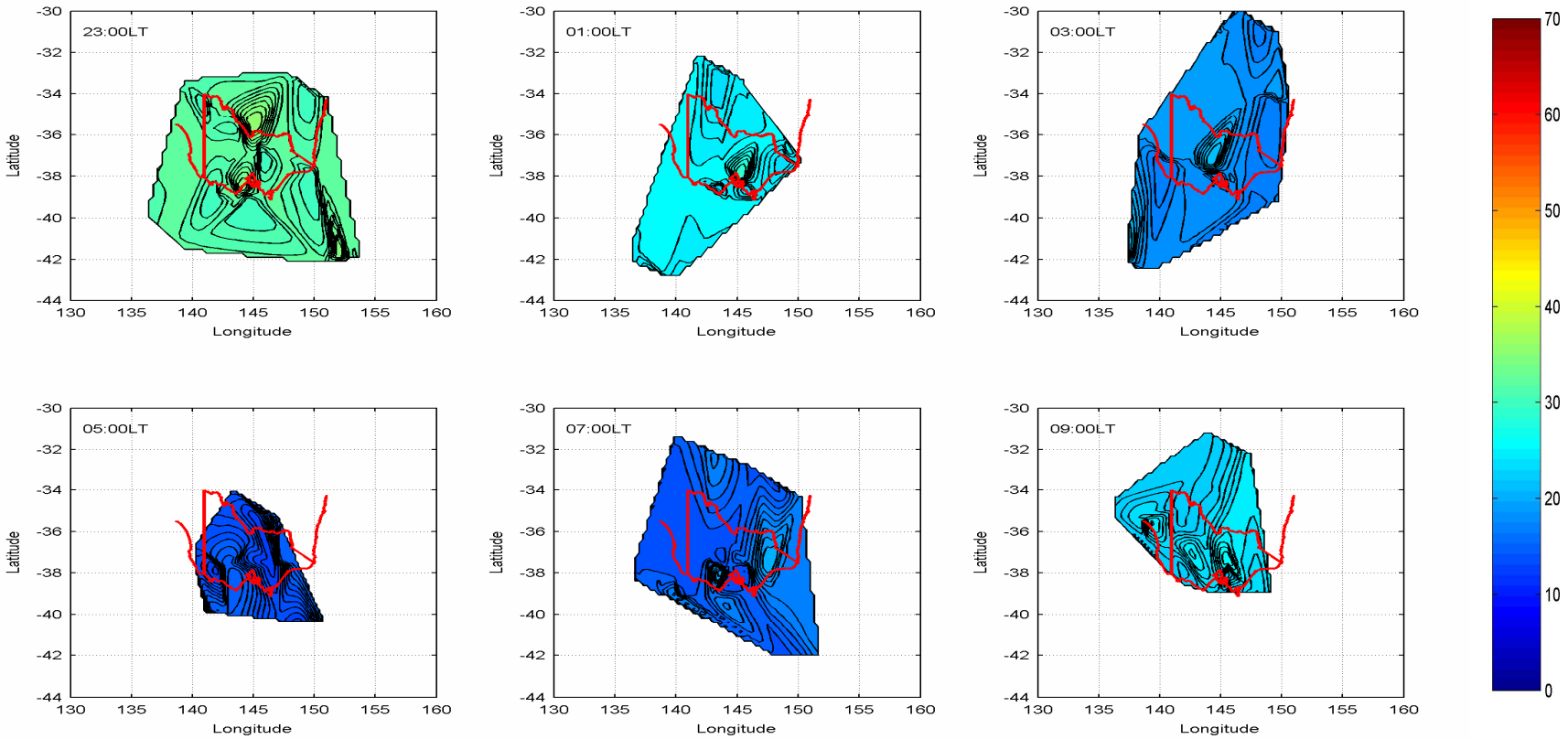

(b)

Figure 6.3: 24 hours of 2 hourly VTEC snapshots over Victoria, taken from the 21st to the 22nd of December, 2001.

(Data is shown in units of TECU and expressed in Local Time (LT+1 hour for daylight savings))

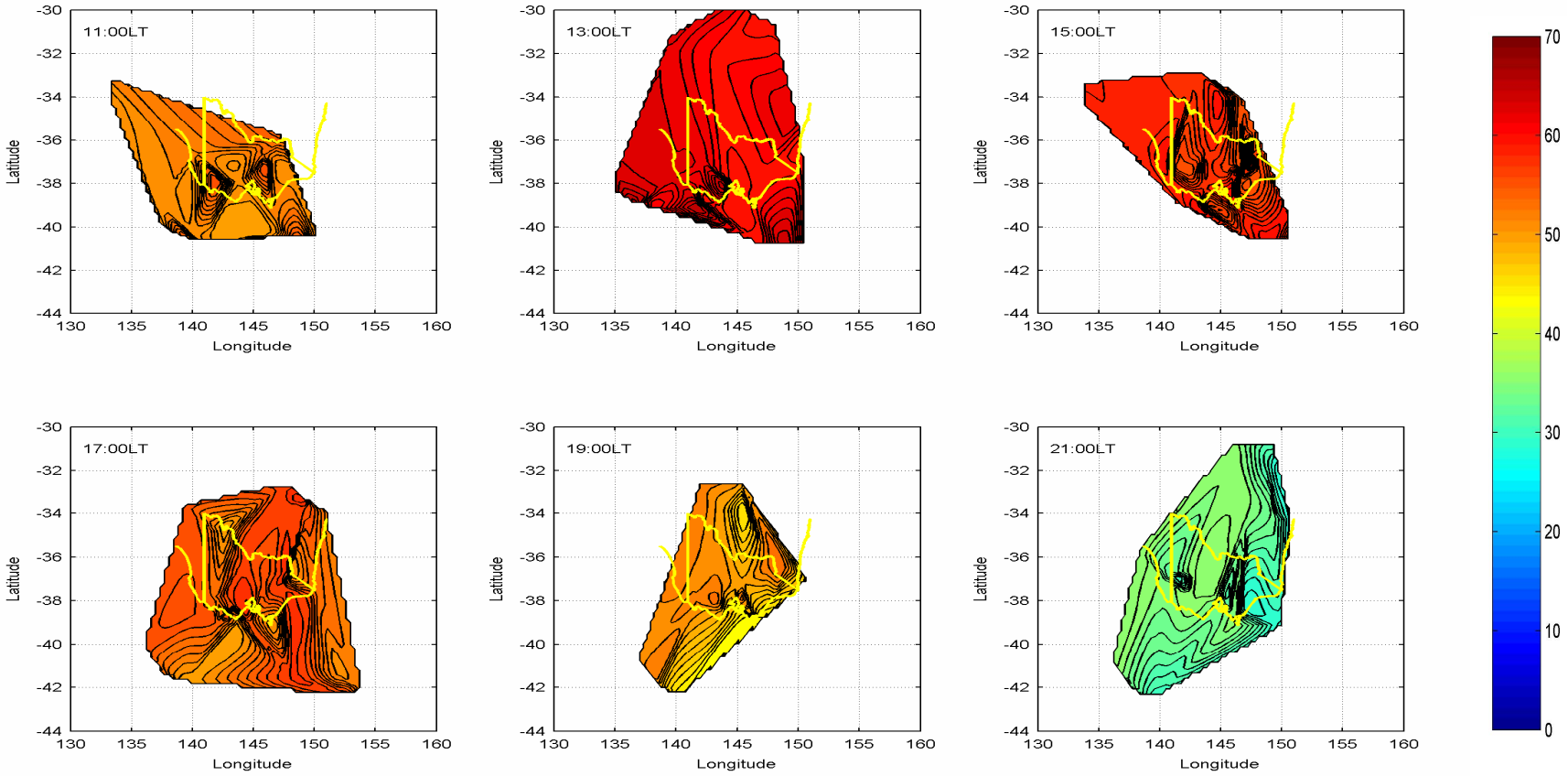
11:00LT
13:00LT
15:00LT
17:00LT
19:00LT
21:00LT
Latitude
Longitude
-30
-32
-34
-36
-38
-40
-42
-44
130
135
140
145
150
155
160
70
60
50
40
30
20
10
0

(a)

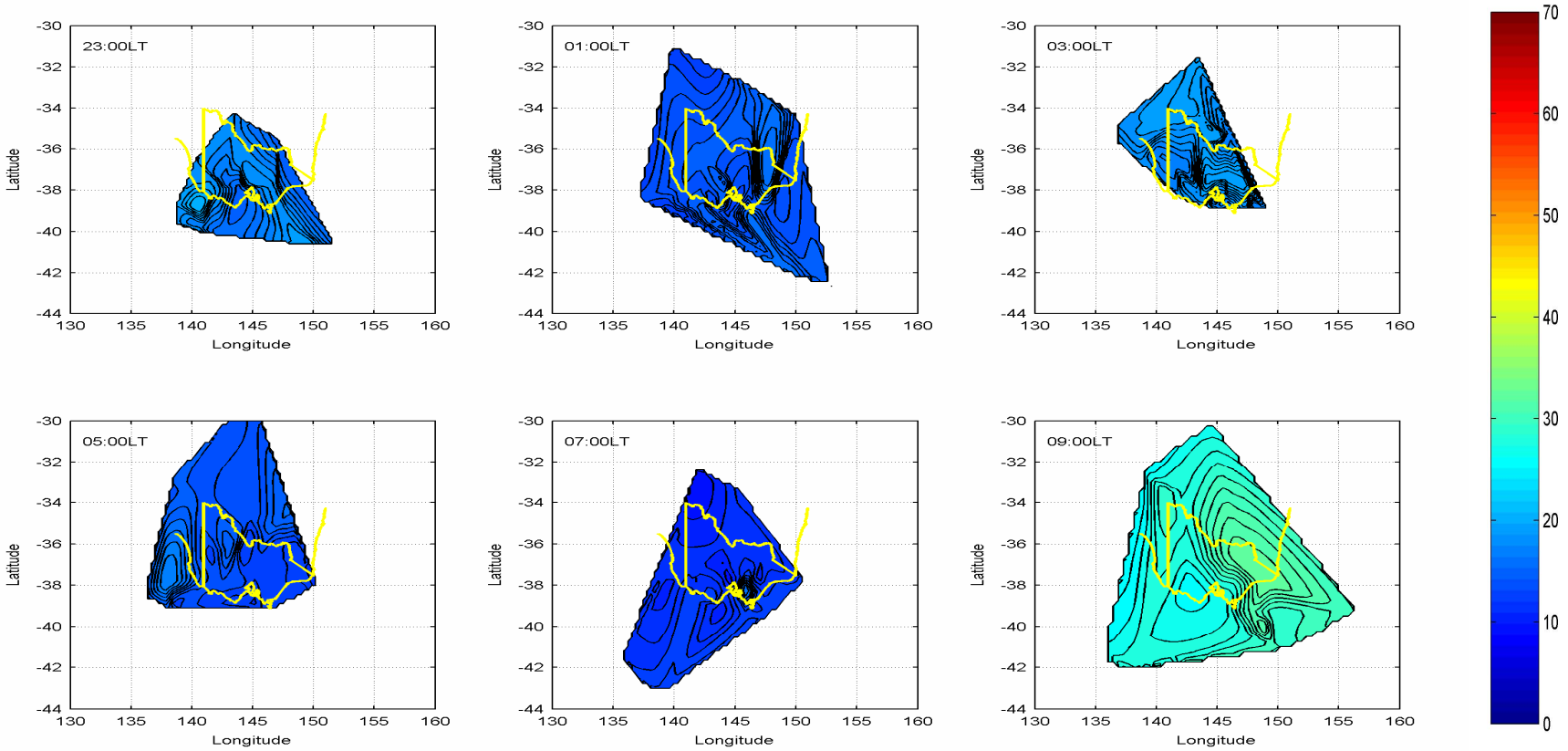

(b)

Figure 6.4: 24 hours of 2 hourly VTEC snapshots over Victoria, taken from the 20th to the 21st of March, 2002.

(Data is shown in units of TECU and expressed in Local Time (LT1 hour for daylight savings))

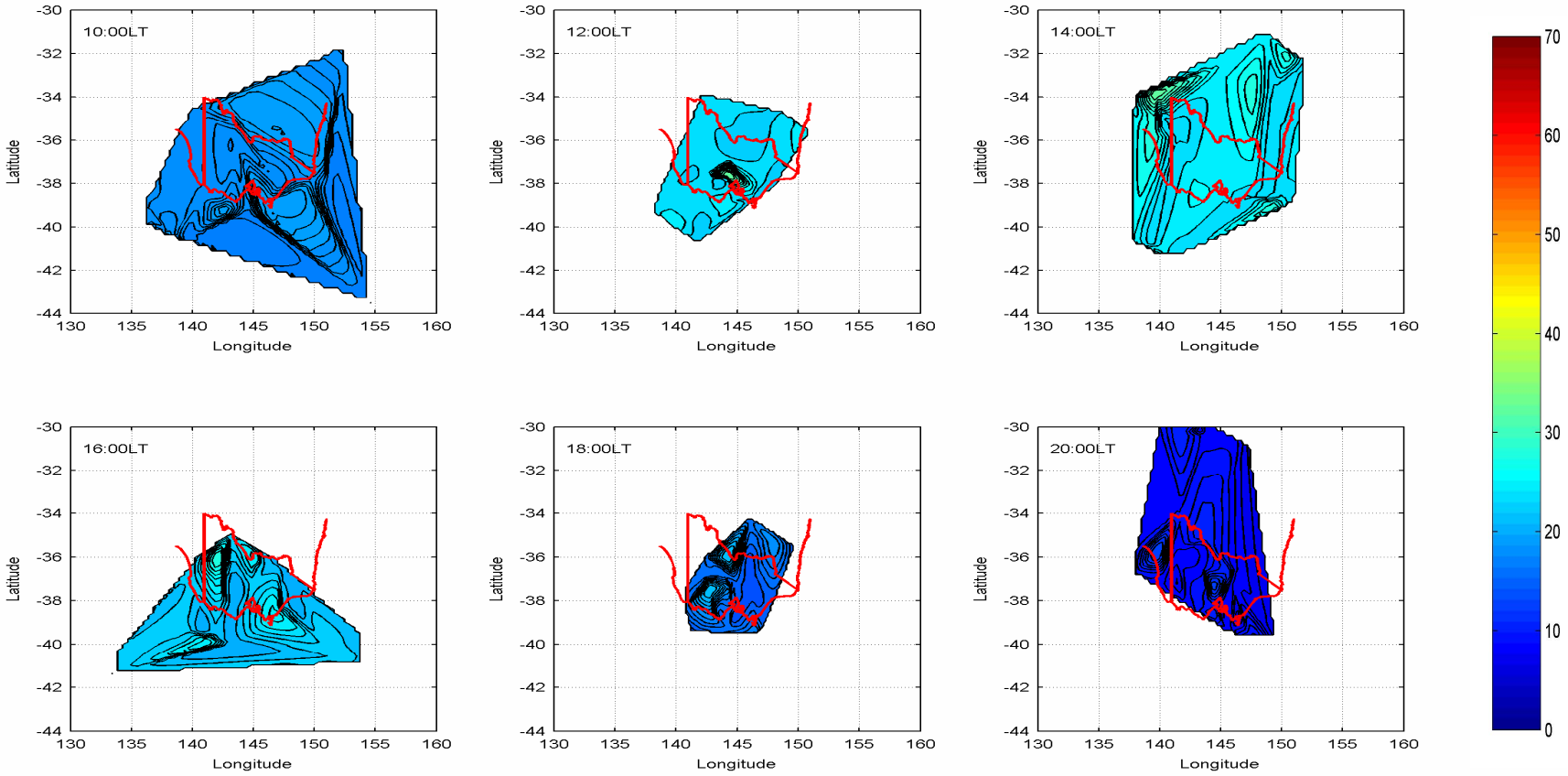
10:00LT
12:00LT
14:00LT
16:00LT
18:00LT
20:00LT
Latitude
Longitude
-30
-32
-34
-36
-38
-40
-42
-44
130
135
140
145
150
155
160
70
60
50
40
30
20
10
0

(a)

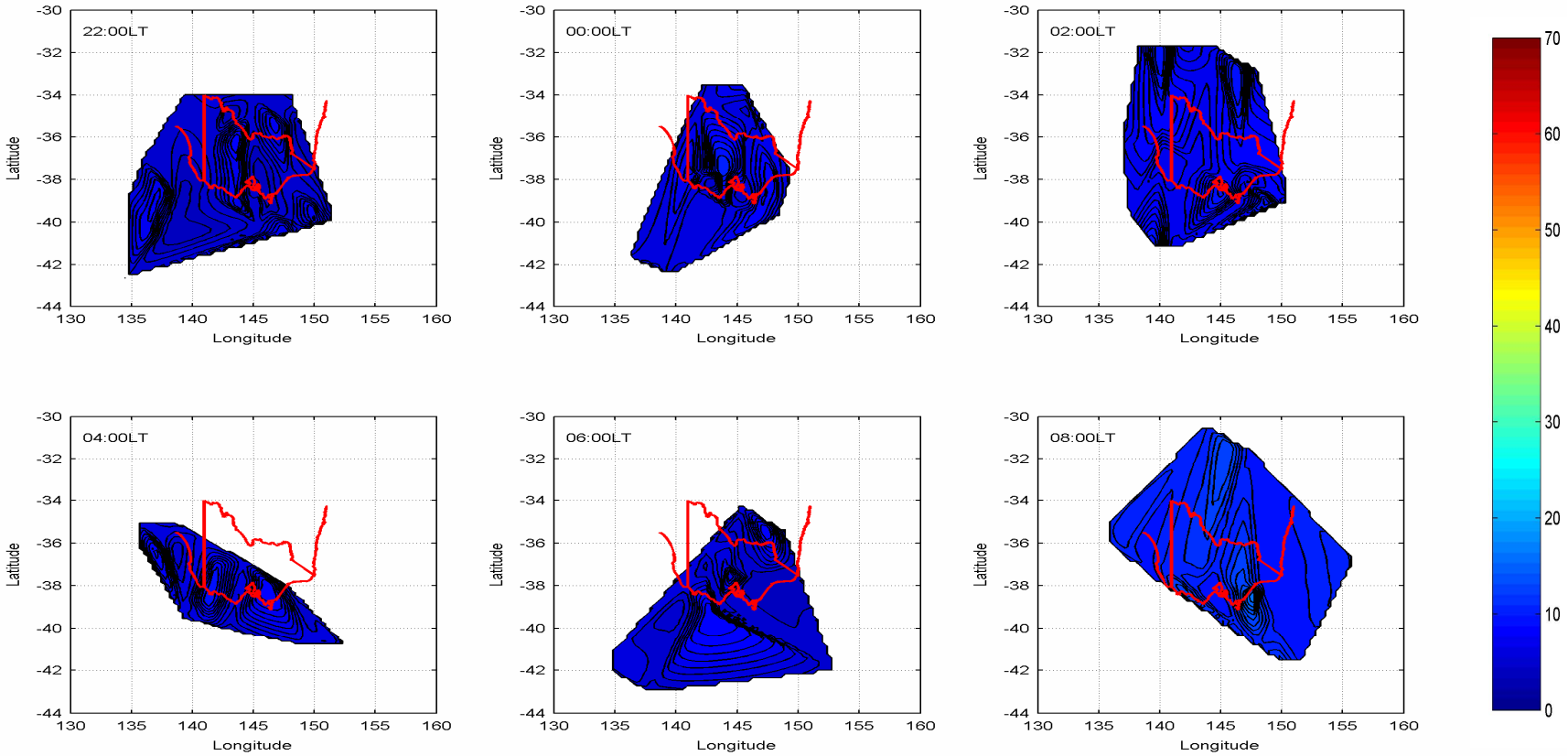

(b)

Figure 6.5: 24 hours of 2 hourly VTEC snapshots over Victoria, taken on the 21st to the 22nd of June, 2002.

(Data is shown in units of TECU and expressed in Local Time (LT))

In a Network-RTK environment accurately positioning the rover receiver depends primarily on correctly knowing the change in the ionosphere from its surrounding base station network. The double differenced phase observables are able to measure this change in ionosphere to mm-level accuracy (see section 3.2.8.6.2). As a means of quantifying the behaviour of the present ionosphere, an analysis will be undertaken in the next section that focuses on the decorrelation rates of the double differenced ionospheric bias over short periods. This will provide an insight into its stability over time.

6.2 The temporal change in the double differenced ionospheric bias

The ionosphere is not a stable and homogeneous medium. It is prone to quick variation which makes it difficult to adequately predict even over short periods (see sections 6.1.2 & 6.1.3). This complex nature makes it a challenging task to accurately represent the behaviour of the ionosphere over Victoria. In order for the rover to quickly and reliably resolve the carrier phase ambiguities over extended baselines (greater than 10km), the ionosphere over the network area needs to be estimated to an accuracy of $\pm$5cm (Teunissen *et al.*, 2000). In order to achieve this accuracy, the double-differenced ionosphere is estimated for each satellite pair along each baseline in the network, as an area fit model will not provide adequate results for precise ambiguity resolution (see Chapter 5 and Wyllie et al. (2003); Wu et al. (2006)).

In a Network-RTK environment, the ionosphere needs to be predicted forward, as real time positioning requires corrections to the rover's observations to provide instantaneous positioning. These corrections have to be computed and broadcast to the user in the field, therefore some latency is involved. Based on this approach, the amount of latency that is acceptable to ensure the accurate and efficient use of the Network-RTK system is of critical importance, as the reduction of data transmission volume will ease network computational load. In addition, it is important that the telecommunication companies providing these corrections, consider the minimum frequency required to deliver the required accuracy, as they usually charge the users of correctional information according to the amount of data traffic.

At present, the Victorian Network-RTK system (GPSnet) is undergoing an intensive upgrade (see Chapter 5) with new network reference stations being installed regularly. It is envisaged that the completed system will provide an integration of the current post-processing service and the new real time Network-RTK service across the entire state (Zhang *et al.*, 2007). One of the main limitations relating to the network's configuration is the long baseline separations, and the ionospheric errors experienced over these lines. In order to overcome this potential barrier to performance and implementation (Alves *et al.*, 2003), the key to achieving real-time state-wide centimeter level performance is the precise modelling of Victoria's ionosphere (Han, 1997; Zhang & Roberts, 2003).

The first step towards producing a regional modelling approach is to investigate and understand the behaviour of the ionosphere over the region. It is therefore necessary to investigate how the double-differenced ionosphere (DDI) changes from one epoch to the next over Victoria, and quantify its behaviour during different seasonal periods. The analysis will look for any trends in the raw observational data that will aid in predicting the ionospheric bias. This will provide information as a precursor to predicting the temporal variability of the ionosphere. The information gained from this analysis will significantly contribute to the development of adequate temporal ionospheric predictive models that can be used in a Network-RTK environment. These models will aid in the accurate resolution of network ambiguities and extend the baseline lengths used to accurately estimate user position in real-time.

6.2.1 Temporal variability of the double differenced ionosphere

The data used to conduct the investigation into the short term variation of Victoria's double-differenced ionosphere (DDI) was taken from the same three GPSnet base stations described in Chapter 5 (see Figure 5.3) during the same period. The DDI data produced by the Bernese GPS Software Version 4.2 (Hungentobler *et al.*, 2001), provides a means of investigating the ionosphere's variability as it provides a way of measuring the change in the ionosphere between a pair of co-observed satellites along a particular baseline, to a high degree of accuracy (see section 3.2.8.6.2).

However, it should be noted that some short term variability in the raw DDI estimates may be caused by carrier phase multipath. This data was treated as 'truth', from which to conduct all analyses. The Bernese Software estimates the DDI by differencing all of the observed satellites against a reference satellite (satellite with the highest elevation) over a baseline for each epoch. The GPSnet reference stations and truth data used to undertake this analysis, were the same used to test the usefulness of the empirical models in Chapter 5 (see section 5.3). This provided a continuity of results from which to base this research.

As the temporal change in the ionosphere is our primary focus, the data was processed using a 5 second epoch interval. This approach provides a set of data that is capable of picking up any short term variations in the ionosphere thus producing an accurate portrayal of what is actually happening over the three GPSnet test bed reference stations (see Figure 5.3). The average baseline length of the three test bed stations is 109km.

In order to investigate the actual temporal variability of the ionosphere over Victoria, the truth data was analysed to quantify the ionosphere's behaviour during different seasonal periods of the year (see Section 5.2). As a means of reducing the amount of data to be analysed over the 72 hour observation blocks, collected during four seasonal periods, five satellites were chosen for each seasonal period as a sample that was indicative of all satellites. The five chosen satellites consisted of three high elevation satellites and two low elevation satellites (see Figure 6.6). The high elevation angle satellites provided, on average, approximately seven hours of continuous observations, whilst the low elevation angle satellites provided approximately four hours of coverage. The validity of this sample approach was extensively tested against the results obtained from the whole sample, with comparisons being at the millimetre level.

For a particular satellite pair, the variability of the ionosphere was tested by differencing the correctly resolved raw DDI observations at different time intervals. In order to gauge the predictability of the DDI values, each continuous double-difference satellite arc was studied as follows. An initial sample epoch of data was

selected and then the DDI values for the proceeding epochs as defined in Table 6.1 were compared with the DDI sample. In order to scan the entire dataset, the sample time was moved forward 5 seconds at a time.

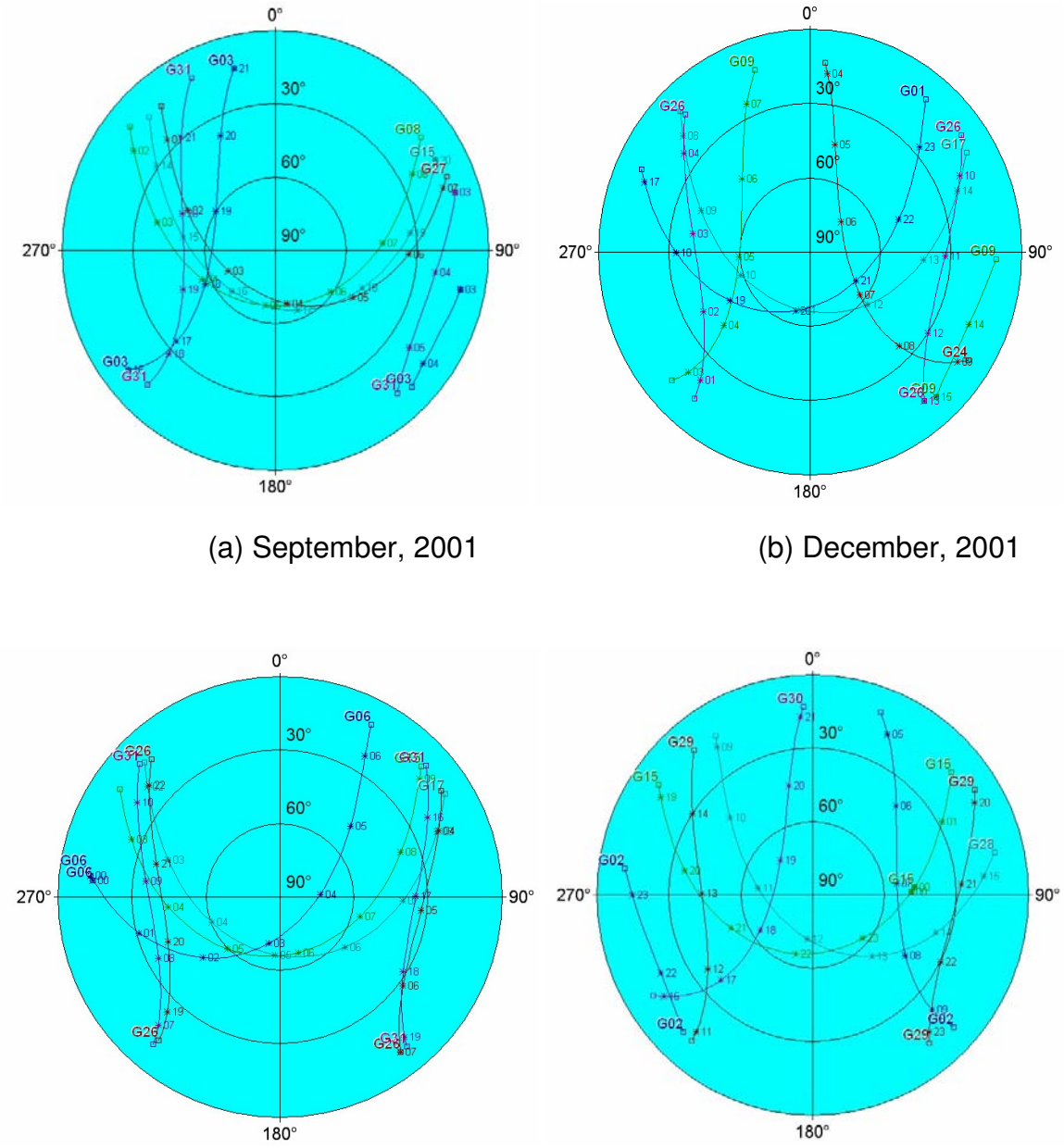

(a) September, 2001 (b) December, 2001

(c) March, 2002 (d) June, 2002

Figure 6.6 Skyplot showing satellite distribution over the periods of analysis.

Table 6.1 List of time intervals tested (up to 10 minutes)

Test Period	Interval
≤ 30 seconds	every 5 seconds
1 min. – 5 min.	every 30 seconds
5 min. – 10 min.	5 minutes

It could be expected that small time intervals would produce DDI values that agree well. The results have been presented in terms of a 99% confidence level. Figure 6.7 provides a means of graphically representing the decorrelation of the DDI for each baseline, during each seasonal period, with the x-axis showing the time interval in seconds and the y-axis showing the 99% confidence interval in metres.

All four seasonal plots along all baselines depicted in Figures 6.7(a)-(d) show very similar decorrelation trends, with a smooth increase in the difference between the DDI as the time intervals increase. This trend may be indicative of the relatively mild ionospheric conditions experienced at mid-latitudes, even though the data was collected during solar maximum conditions. As a means of further analysing the trend in the decorrelation of the DDI over Victoria, a series of histograms has been produced, see Appendix A. These histograms depict the mean and 99% confidence interval for each time difference. The histograms depicted in Appendix A, show a very symmetrical unbiased distribution centred about the mean. The results from these histograms have been tabulated and presented numerically in Table 6.2.

Table 6.2 highlights the time intervals along each baseline where the DDI residual has reached the $\pm$5cm threshold. Table 6.2 shows that the ionosphere is decorrelating at such a rate, that it reaches the $\pm$5cm threshold within a range of 60-150 seconds, giving an average of approximately 108 seconds. On further investigation, it can be seen that the results obtained along the Melbourne- Bendigo (MEBE) baseline show a significant increase in ionospheric decorrelation, with shorter correlation periods. The MEBE baseline shows an average decorrelation time of 83 seconds before it reaches the $\pm$5cm critical value, whilst the Melbourne-Ballarat (MEBA) baseline and Ballarat-Bendigo (BABE) baseline both share an average of 120 seconds.

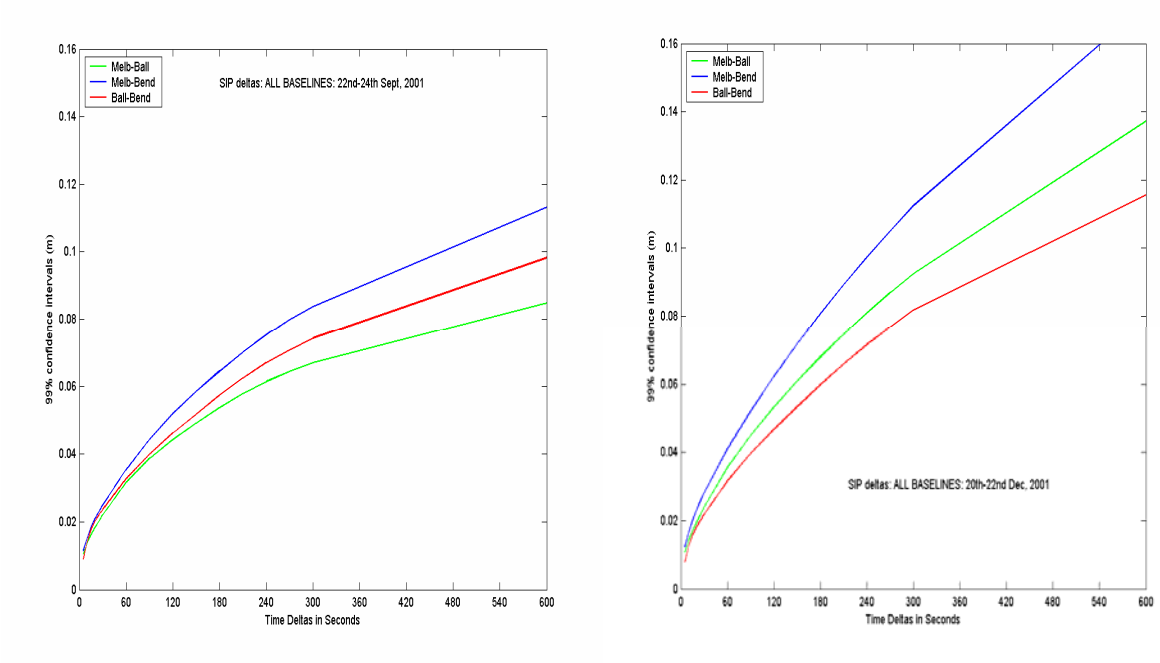

Figure 6.7:The temporal variability of the double differenced ionosphere during four seasons: (a) September, 2001; (b) December, 2001; (c) March, 2002; (d) June, 2002.

Whilst the average baseline length of the three station network is approximately 109km, when comparing the three baseline lengths the MEBE baseline is 130km, the MEBA is 102km and the BABE baseline is 96km. The decrease in correlation along

the MEBE baseline may be explained by the fact that it is approximately 24% greater in length than the other two baselines, and highlights the fact that an increase in baseline length does have significant effects on the DDI residuals.

6.2.2 Day versus night ionosphere

As the ionosphere typically displays a strong diurnal variation (see section 6.1.2), with a quieter night time and a more active day period, it was decided to investigate whether or not the day and night periods displayed any differences in temporal stability. The previous analysis undertaken in section 6.2 combined both the day and night time data sets. Six hours of data was analysed that included all of the available satellites during this period, with the night time interval positioned between 0-6 hours local time, and the day time interval positioned between 10-16 hours local time. The outcome of this analysis provided some 'surprising' results. The September and December periods showed a more active ionosphere observed during the night time, whilst the March and June periods reverted back to the more traditionally active day time period and quieter night time. Figure 6.8 shows the MEBA baseline during the September and March periods, depicting the differences observed during the night and day periods.

In an attempt to explain this phenomena, the global Kp index (see section 2.2.1.1) was studied for these particular periods. It showed that during the night time periods in September and December the Earth experienced some high solar activity, in the form of strong magnetic field fluctuations that are recorded via the Kp index. The March and June periods however displayed a much more stable atmosphere with the magnetic field disturbances being slightly higher during the day in March and constant throughout both day and night periods in June (see Table 5.1). This 'reversal' of ionospheric activity is not completely out of character as Diep Dao *et al* (2004) and Kashani et al. (2004b) have also observed increased ionospheric activity at night whilst undertaking research in a related area.

Table 6.2 The DDI differences at increasing time intervals using the 3 station test bed across four seasons

Date	Baseline	5 sec	10 sec	15 sec	20 sec	25 sec	30sec	60 sec	90 sec	120 sec	150 sec	180 sec	210 sec	240 sec	270 sec	300 sec	600 sec
	MEBA	0.011	0.014	0.016	0.018	0.020	0.022	0.031	0.038	0.044	0.049	0.053	0.057	0.061	0.066	0.080	0.083
Sept, 01	MEBE	0.012	0.015	0.018	0.021	0.023	0.025	0.035	0.044	0.052	0.058	0.064	0.070	0.075	0.080	0.084	0.113
	BABE	0.009	0.014	0.018	0.020	0.022	0.024	0.033	0.040	0.046	0.052	0.057	0.062	0.067	0.071	0.074	0.098
	MEBA	0.011	0.014	0.017	0.019	0.022	0.024	0.035	0.045	0.053	0.061	0.068	0.074	0.081	0.087	0.092	0.136
Dec, 01	MEBE	0.012	0.017	0.020	0.023	0.026	0.028	0.041	0.052	0.062	0.071	0.080	0.089	0.096	0.104	0.111	0.169
	BABE	0.008	0.012	0.016	0.018	0.020	0.022	0.031	0.039	0.046	0.053	0.059	0.065	0.071	0.076	0.081	0.114
	MEBA	0.010	0.013	0.015	0.017	0.018	0.020	0.028	0.035	0.042	0.048	0.053	0.059	0.064	0.069	0.074	0.109
Mar, 02	MEBE	0.011	0.014	0.017	0.019	0.020	0.022	0.031	0.038	0.045	0.051	0.057	0.062	0.067	0.072	0.077	0.112
	BABE	0.008	0.012	0.014	0.016	0.018	0.019	0.027	0.033	0.039	0.045	0.050	0.056	0.061	0.065	0.070	0.097
	MEBA	0.010	0.013	0.015	0.017	0.019	0.021	0.032	0.043	0.054	0.063	0.073	0.082	0.090	0.098	0.105	0.144
Jun, 02	MEBE	0.012	0.015	0.018	0.020	0.023	0.025	0.038	0.050	0.061	0.071	0.082	0.091	0.101	0.109	0.117	0.164
	BABE	0.008	0.013	0.016	0.018	0.020	0.022	0.033	0.044	0.054	0.064	0.074	0.083	0.091	0.098	0.105	0.146

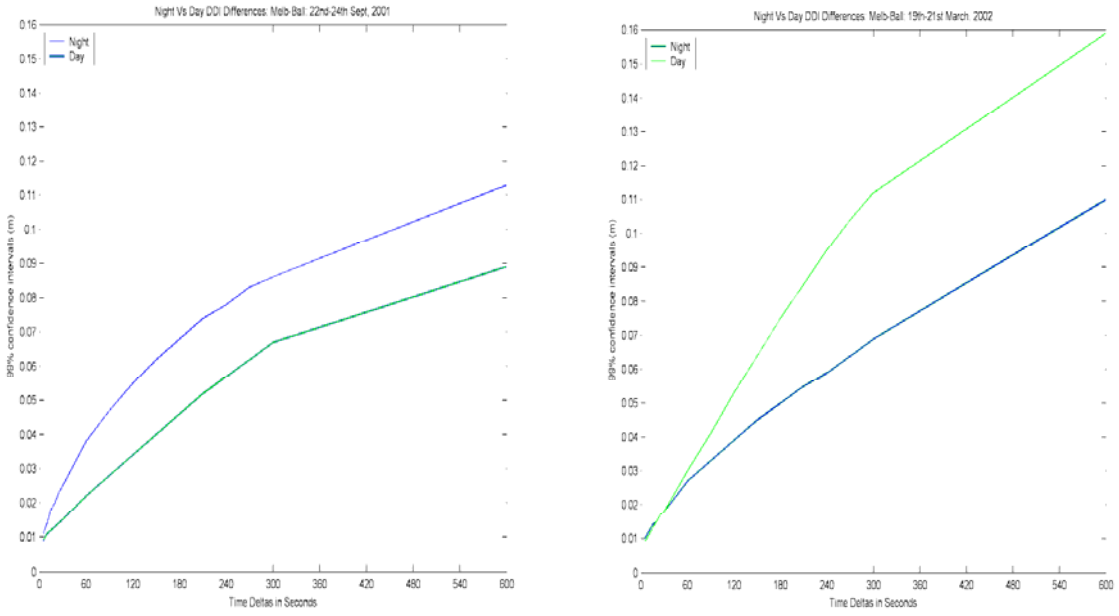

(a) (b)

Figure 6.8: The Day Vs Night double difference ionosphere differences

(a) September, 2001; (b) March, 2002.

An analysis was then undertaken to investigate how quickly the DDI residuals decorrelated during the night and day periods. Table 6.3 gives a summary of how quickly the ±5cm threshold is reached, with the values indicating the maximum temporal period achieved before the ±5cm level is exceeded. During the September and December periods, where high solar activity was experienced during the night, the length of temporal similarity under ±5cm was on average 70 seconds during the night and 155 seconds during the day. This represents a reversal of approximately 55%. Based on these results it appears that after a significant solar event during the night, the next day may offer a calm that is indicative of the night time ionosphere under more normal circumstances.

During March the length of temporal similarity under ±5cm was on average 210 seconds during the night and 90 seconds during the day. This represents a reversal of approximately 57% from night to day but in the opposite direction to the September and December periods. The June observations show the length of temporal similarity under ±5cm to be on average 90 seconds during the night and 60 seconds during the day, which represents a reversal of approximately 33%.

The results obtained from this analysis truly highlight the unpredictable nature of the ionosphere and what a challenging task it is to accurately model. The effect of solar activity has been highlighted as displayed in the September and December periods, where the night and day ionospheric activity was reversed. Further to this, the June period which lies in the southern hemisphere's winter, displays the shortest ionospheric correlation period. This is surprising, as the winter months traditionally display a quieter, more stable ionosphere, as depicted in the absolute TEC analysis in the previous section.

Table 6.3 The time intervals where the DDI residuals are below $\pm$5cm.

(For both Night and Day periods)

Date	Baseline	Night (sec)	Day (sec)
Sept, 2001	MEBA	90	180
	MEBE	60	120
	BABE	90	120
Dec, 2001	MEBA	60	180
	MEBE	60	150
	BABE	60	180
March, 2002	MEBA	150	90
	MEBE	240	90
	BABE	240	90
June, 2002	MEBA	90	60
	MEBE	90	60
	BABE	90	60

6.3 Summary

The first part of this chapter was devoted to an analysis of the absolute ionosphere or TEC values present over Victoria during four different seasonal periods. Eight reference stations within the GPSnet infrastructure were used to collect the data and spherical harmonics were used to map the ionosphere to a thin shell at a height of 350km, as a means of producing TEC maps for analysis. This study was undertaken to provide a general understanding of the characteristics and stability of the

ionosphere over Victoria, and to also provide an insight into the type of modelling strategy required to ensure accurate ambiguity resolution within a Network-RTK environment.

From the above analysis, the results suggest that the temporal and spatial TEC variations over Victoria are of a complicated nature. It suggests that any model trying to predict the absolute ionospheric TEC based on location, time of day, time of month and season, would be unable to adequately represent the complicated nature of the ionosphere to a level that would ensure fast ambiguity resolution and cm-level positional accuracy. As the ionosphere can vary significantly over a short period of time it is suggested that in order to predict the ionosphere to a high degree of accuracy, any model chosen would have to be designed to predict forward based on actual ionospheric information received up to the period of prediction.

The second part of this chapter provides an analysis of the double-differenced ionosphere over Victoria during the same four seasonal periods. The Bernese software was used to produce the double differenced values using the L4 linear combination. Three reference stations within GPSnet were used as the data source for the analysis.

In order to gain accurate instantaneous positioning within a Network-RTK environment, corrections to the rover's position have to be broadcast to the user in the field. As these ionospheric corrections have to be determined then broadcast to the user, some latency is involved. Therefore, the determination of the amount of latency that is acceptable to ensure the accurate and efficient use of the Network-RTK system is of critical importance, as any reduction of data transmission volume will ease network computational load and user download requirements. This study was undertaken as a means of quantifying the ionosphere's behaviour from one epoch to the next in order to understand how quickly it decorrelates over time.

Based on the analysis undertaken, in an overall sense, the temporal variability of the ionosphere over Victoria, out to approximately 100km, remains under $\pm$5cm out to an average of 120 seconds or 2 minutes. The traditional assumption of ionospheric

activity being higher during the day and lower at night was not always so in the test data. During the quiet ionospheric periods the ionosphere's decorrelation can remain below the ±5cm threshold for up to 3 minutes, whilst during the active solar times the ±5cm threshold was reached in less than 60 seconds.

Chapter 7 Modelling Victoria's temporal ionosphere

This Chapter focuses on the production of a temporal differential ionospheric model that is suitable for Network-RTK use in Victoria. The model will be used as a means of predicting the trend in the double-differenced residuals and needs to be sufficiently accurate to allow for the precise resolution of the integer ambiguities at the roving receiver.

This research is undertaken in order to produce a new ionospheric model suitable for Victorian conditions, which would have direct and indirect applications in the upgrading process of Victoria's current GPSnet infrastructure. It is envisaged that this model may move Victoria a step closer to achieving a state-wide Network-RTK system capable of producing cm-level accuracies within minimal CORS infrastructure requirements. The data used to test the models produced, is the same used in section 6.2.

7.1 Correcting the rover's observations

At present there are three main approaches used to broadcast corrections for atmospheric biases in a network solution (see section 4.4.1):

1) Virtual Reference Station (VRS),

2) Area Correction Model (ACM), and

3) Direct transmission of raw data from each network station.

Both the VRS and ACM systems revolve around the broadcasting of correctional models derived from a CORS network from a Master Control Station (MCS). The third option involves the transmission of raw GPS observations from each station in the network, therefore placing the computational burden on the rover. Figure 7.1 illustrates the data flow used in Network-RTK correction generation.

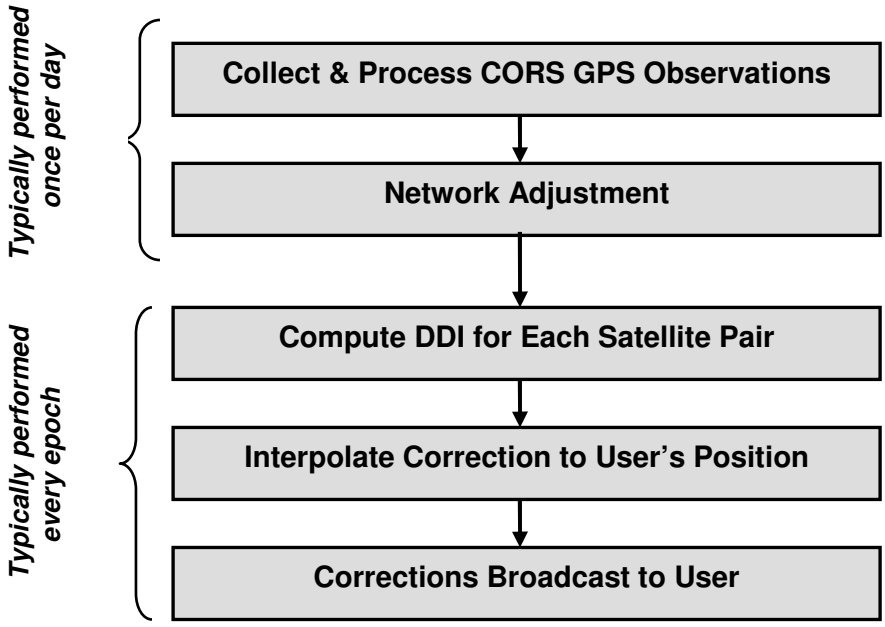

Figure 7.1: Network–RTK correction generation by permanent network (CORS) GPS stations.

The coordinates of all network stations must be very accurately known, in a well defined reference frame such as ITRF. Typically GPS data is used to estimate the network station co-ordinates once a day.

The known network station co-ordinates are held fixed and used to aid the estimation of the carrier phase ambiguities and the ionospheric and tropospheric errors for all

satellites during normal operation. The network ionospheric and tropospheric errors are then distributed to roving receivers within the network.

7.2 Temporal prediction of the ionosphere

As real time positioning in a Network-RTK environment requires the broadcasting of accurate ionospheric corrections to the user in the field, the error experienced due to the ionosphere needs to be predicted forward. This requires an accurate prediction of the ionosphere using a prescribed modelling technique.

The modelling techniques presented below can be applied to any ionospheric scenario, however, the results presented are for a specific set of ionospheric conditions.

The predictive models presented below are based on using the previously correctly resolved baseline double differenced ionosphere residuals to predict forward in the data sets on a satellite by satellite basis. This method provides a more accurate approach than corrections interpolated using observations from a network of GPS receivers (Kashani *et al.*, 2004b). The modelling methods used to predict the double-differenced ionosphere residuals over the State of Victoria include:

- Moving average;
- Linear Polynomial;
- Time series analysis – Auto Regressive Integrated Moving Average (ARIMA)

The models presented attempt to provide a compromise between complexity and accuracy achieved. The first two modelling techniques tested provide a simplistic approach to predicting a trend in a very complex ionosphere, whilst the third method (ARIMA), provides an in depth analysis of the ionosphere, to ascertain whether or not a more complex method would provide better predictive results.

7.2.1 Moving average

The moving average strategy is based on the assumption that the local time series is locally stationary with a slowly varying mean. From the analysis undertaken in the previous sections this assumption is supported out to an average of approximately 120 seconds. Within this time frame, the DDI residuals remain under the $\pm$5cm threshold. The moving average technique uses the average of a series of previously correctly resolved DDI residuals to estimate the next residual, and comes in the form:

$$R(t) = \frac{\left(z(t-1) + z(t-2) + ... + z(t-k)\right)}{k} \tag{7.1}$$

where:

$R(t)$	is the DDI residual to be estimated;
z	are the previous values in the dataset;
t	is the time at the present epoch; and
k	sample window size.

The approach is sometimes known as a 'Box-car' moving average, however, for brevity it will be known as the moving average scheme. The moving average model was used to extrapolate forward in the data, from a stationary fixed sample region. The differences between the predicted and 'truth' DDI residuals were computed, based upon the sample intervals defined in Table 6.1. Once these values were computed the sample region was moved forward 5 seconds and the process repeated again through to the end of each satellite's observation period. As a means of finding the sample size that provided the best fit to the data, the (k) value was adjusted to incorporate both 30 and 60 seconds of 5 second epoch data. This was undertaken to see which sample window provided better predictive results and to also ascertain whether a larger sample window was required.

The difference between the moving average model and the truth data was then collated, using both the 30 and 60 second sampling widows. On analysis, the difference in residuals between the two sampling sizes was negligible. Figure 7.2 provides a graphical representation of the comparison between the 30 and 60 second sampling windows, based on the residuals produced. As all of the baselines during all of the seasons displayed very similar results, the MEBA baseline during the September period was arbitrarily chosen to convey this information. The 60 second sample size provided results in all instances that were equal to or less accurate than those obtained from the 30 second sample size. This provides evidence that keeping the sample region closer to the area of estimation provides a better result. In other words, as the ionosphere is decorrelating at a steady rate, the data sample used to provide future estimates of the ionosphere needs to be as close as possible to the period of prediction.

As a means of graphically illustrating how the moving average model decorrelates as the time interval increases, a graph for each time interval and season along the MEBA baseline has been produced and included in Appendix B. As the results for each baseline were similar, the MEBA baseline was chosen as being indicative of the other two.

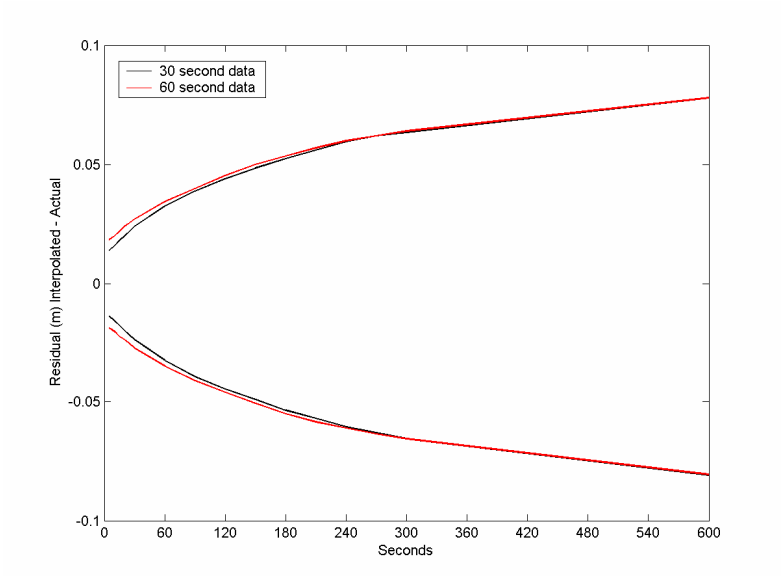

Figure 7.2 The distribution of residuals (truth-model) determined by the moving average model within a 99% confidence range along the MEBA baseline during September, 2001.

The values in Table 7.1 below indicate the maximum temporal period (in seconds) achieved before the moving average model is unable to predict the DDI residual lower than ±5cm within a 99% confidence interval. As the sample data set used to produce these results was made up of three high elevation and two low elevation angle satellites, Table 7.1 also shows how the results from each category compared, along with a comparison of the results achieved using the 30 and 60 second sampling intervals.

Table 7.1: Approximate time intervals where the moving average residuals are below ±5cm. (Showing the Low / High elevation satellites for both 30 and 60 second sample windows).

Date	Baseline	30 seconds Low/High	60 seconds Low/High
Sept, 2001	MEBA	150 / 150	150 / 120
	MEBE	120 / 120	90 / 120
	BABE	120 / 150	90 / 150
Dec, 2001	MEBA	90 / 120	60 / 90
	MEBE	60 / 120	60 / 90
	BABE	90 / 150	90 / 150
March, 2002	MEBA	180 / 150	180 / 120
	MEBE	180 / 180	180 / 150
	BABE	150 / 180	150 / 180
June, 2002	MEBA	120 / 60	90 / 60
	MEBE	120 / 60	90 / 60
	BABE	120 / 90	90 / 60

When comparing the results from the 30 and 60 second sample windows in Table 7.1, it becomes apparent that no real increase in model accuracy is achieved by using the larger sample size. The 30 second data provides results that are at worst equal to the 60 second data and on a number of occasions outperformed the larger data set.

The results produced by the Low / High elevation angle categories displayed no real difference during the September and March periods. During the September period the moving average model was able to predict the DDI residual to under ±5cm out to

an average of 130 seconds for the low elevation angle satellites and 140 seconds for the high. The March period saw a slight increase with the low elevation angle satellites producing an average of 150 seconds and the high elevation satellites achieving an average of 170 seconds. During the December period however, the results displayed a more traditional elevation dependent behaviour from the ionosphere, with the moving average model only predicting the DDI residual under $\pm$5cm out to and average of 80 seconds for the low elevation satellites. The high elevation angle satellites during this period however, met the $\pm$5cm criteria out to an average of 130 seconds, which is comparable to the results in the September and March periods. The June period however showed a complete reversal from the normal elevation dependent behaviour of the ionosphere, with the average length of predictability at 120 seconds for the low elevation angle satellites and 70 seconds for the higher elevation angle satellites. These results are again comparable with the September and March periods for the low elevation angle satellites, but completely out of character for the higher elevations. One explanation for this is that the higher elevation angle satellites during this period may have experienced some localised ionospheric activity, possibly in the form of scintillation or a travelling ionospheric disturbance (see section 2.3), that impeded the model's ability to predict forward. These results are reinforced by those produced by previous analysis, and displayed on Tables 6.2 and 6.3. The June period seems to be somewhat disturbed, with the ionosphere changing at a rate that is greater on average than the results produced from the other three periods, therefore decreasing the ionosphere's predictability with the moving average model.

A comparison of how well the moving average model was able to predict the DDI residuals over all of the seasons has been produced in Figure 7.3. The MEBA baseline in September was again chosen as being indicative of the other three seasons and baselines. On analysis, it can be seen that the June and December periods are much noisier, and less predictable than the September and March periods. All seasonal plots however, display a very smooth temporal decorrelation of the moving average model, with the model able to predict the DDI residuals in all cases to under 0.20m with a 10 minute lag.

In summary the moving average model using a 30 second sample region, was able to predict the DDI residual during the September and March periods to an average of approximately 150 seconds including both high and low satellites. The December period offered an average of 80 seconds for the low elevation angle satellites and 130 seconds for the high elevation angle satellites. The average was further decreased during the June period with an average of 120 seconds for the low elevation angle satellites and 70 seconds for the high elevation angle satellites. Discounting the June results, on average the moving average model was able to predict the DDI residual under the $\pm$5cm criteria out to an average of approximately 145 seconds, with a high of 180 seconds and a low of 120 seconds. Including all of the seasons for the low elevation angle satellites, the average predictable latency went out to 125 seconds with a high of 180 seconds and a low of 60 seconds, with this low being produced over the 130 km MEBE baseline.

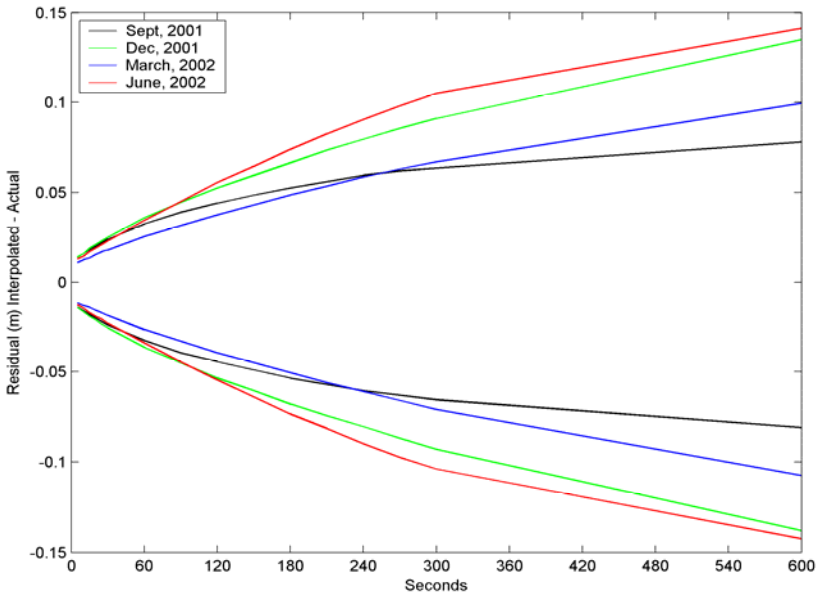

Figure 7.3: The distribution of residuals (truth-model) determined by the moving average model within a 99% confidence range using the 30 second sample window for all seasons along the MEBA baseline.

7.2.2 Linear polynomial

The linear polynomial approach attempts to model the relationship between two variables by fitting a regression line of best fit to the data. In this case the two variables are time (or latency) and DDI residuals. The method of least squares was

used to compute the best fit for the data sample by minimising the sum of the squares of the vertical deviations from each data point to the line. This technique uses a sample of previously correctly resolved DDI values to calculate a linear equation that is used to predict forward in the data. The linear equation comes in the form:

$$y = at + b \tag{7.2}$$

where:

y is the DDI value to be estimated;

t is the time at the predicted epoch;

a is the slope of the data; and

b is known as the y intercept.

The values of a and b are computed via the least squares process, using a sample of previous observations. As with the moving average model, the linear model was used to extrapolate forward in the data from a stationary fixed sample region. The differences between the predicted and 'truth' DDI residuals were computed based upon the sample intervals defined in Table 6.1. Once these values were computed the sample region was moved forward 5 seconds and the process repeated again through to the end of each satellites observation period. Once again two different sample sizes of 30 and 60 seconds were tested as a means of finding out which sample size gave the better results and to also ascertain whether a larger sample region was required.

When comparing the results obtained from the 30 and 60 second data sets, the 60 second data sample allowed the linear polynomial to predict the DDI residual under the $\pm$5cm threshold for a longer period of time. The results obtained along the MEBA baseline during September, are indicative of the other two baselines in all seasons. This shows that the longer sample region provides a better fit to the data when extrapolating forward.

As a means of graphically illustrating how the linear polynomial model decorrelates as the time interval increases, a graph for each time interval and season along the MEBA baseline has been produced using the 60 second sample interval and displayed in Appendix C. As the results for each baseline were similar, the MEBA baseline was chosen as being indicative of all baselines (see Figure 7.4).

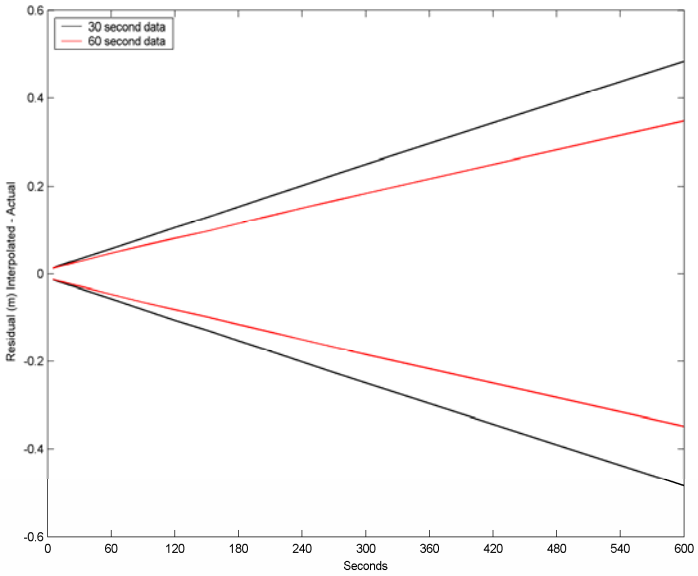

Figure 7.4: The distribution of residuals (truth-model) determined by the linear polynomial model within a 99% confidence range along the MEBA baseline during September, 2001.

Table 7.2 provides a summary of how well the linear polynomial model predicted forward in the data with the values indicating the maximum period of latency achieved (in seconds) before the $\pm$5cm threshold was reached within a 99% confidence interval. The data is again represented by showing the results obtained from the high and low elevation angle satellites, and the different data sampling times of 30 and 60 seconds.

When comparing the 30 and 60 second sample intervals in Table 7.2, the 60 second sample interval is either equal to or outperforms the 30 second data set on most occasions. The results produced by the high and low elevation angle categories within the 60 second data set are very similar for the September and December periods producing an average in both categories of 60 seconds. The March and June

periods displayed results that are not typical of an elevation dependent ionosphere. In March the linear model was able to predict out to an average of 130 seconds before crossing the ±5cm threshold with the low elevation angle satellites, whilst the high elevation angle satellites produced results out to an average of 90 seconds. The model's performance in June was again in reverse to convention. It predicted out to an average of 100 seconds with the low elevation angle satellites and to an average of 60 seconds with the high.

In summary, when looking at the results obtained from the linear polynomial with the 60 second data sample, the high elevation angle satellites can be predicted out to an average of approximately 70 seconds, with a low of 60 seconds and a high of 90 seconds, giving a relatively tight range. The low elevation angle satellites however, on average, produced an average of 85 seconds, which is approximately 20% longer than the results achieved by the high elevation angle satellites.

Table 7.2: Approximate time intervals where the linear polynomial residuals are below ±5cm.

(Showing the Low / High elevation satellites for both 30 and 60 second data samples).

Date	Baseline	30 seconds Low/High	60 seconds Low/High
Sept, 2001	MEBA	30 / 30	60 / 60
	MEBE	30 / 30	60 / 60
	BABE	30 / 30	30 / 60
Dec, 2001	MEBA	30 / 60	60 / 60
	MEBE	30 / 60	60 / 60
	BABE	30 / 30	60 / 60
March, 2002	MEBA	60 / 60	120 / 90
	MEBE	60 / 60	150 / 90
	BABE	60 / 60	120 / 90
June, 2002	MEBA	60 / 60	90 / 60
	MEBE	60 / 60	120 / 60
	BABE	60 / 30	90 / 60

The linear polynomial model's ability to predict the DDI residual over all of the seasons has been produced in Figure 7.5. Again the MEBA baseline has been

displayed as indicative of all seasons along all baselines. The results indicate that the September, December and June baselines perform at a similar level, whilst the March baseline consistently out performs these three. This is also portrayed in Table 7.2 with consistently longer latency periods than the other three seasons. All of the seasonal plots display a very linear temporal decorrelation of the model's residuals, with the model being able to predict the DDI residual in all cases to under 0.40m with a 10 minute latency. Furthermore, higher order polynomials in the form of a quadratic and cubic modelling approach were tested and found to provide no advantage.

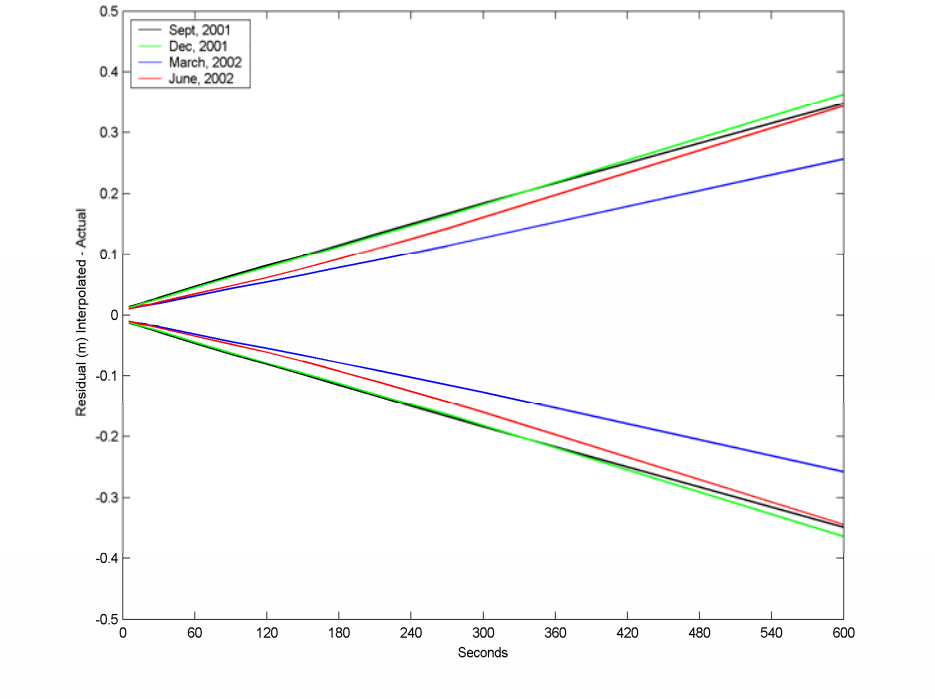

Figure 7.5: The distribution of residuals (truth-model) determined by the linear polynomial model within a 99% confidence range using the 60 second sample window for all seasons along the MEBA baseline.

7.2.3 Time series analysis

A time series can be described as a collection of observations that have an even spacing in time and are measured successively. The observation of GPS data, in this case the double differenced ionosphere between a reference and roving satellite for a given baseline, is a strong example of such a series. Time series are analysed as a means of understanding the primary structure and function that create the data. Based on an understanding of these mechanisms, a time series can be mathematically modelled in order to provide predictions of future observations. A technique created by Box and Jenkins (1976) known as the ARIMA (Autoregressive, Integrated, Moving Average) methodology, allows the production of a set of weighted coefficients that describe the ionosphere's behavior or rate of change during the sample period. These coefficients can then be used as a means of forecasting future observations. A general overview of the ARIMA technique is given in the next section. The interested reader is referred to Brockwell & Davis (1996) and Makridakis et al, (1998) for a more detailed explanation of the technique.

7.2.3.1 ARIMA modelling process

The Box-Jenkins modelling of time series observations focuses on three different phases: identification, estimation/testing, and application. Firstly, an appropriate ARIMA modelling strategy needs to be found for the particular time series, followed by the estimation and refining of the model's parameters, then finally applying the model as a means of predicting future values. In general, the model is known as ARIMA (*p,d,q*), where the autoregressive component (AR) is designated as *p.* It represents the lingering effects of previous observations. The integrated (I) component is designated *d*. It represents the degree of differencing involved. Finally the (MA) component is designated *q*. It represents the order of the moving average component. The equation for the general ARIMA(1,1,1) model is :

$$\left(1-\phi_1 B\right)\left(1-B\right)Y_t = \left(1-\theta_1 B\right)Z_t, \qquad Z_t \sim WN\left(0,\sigma^2\right) \tag{7.4}$$

where:

Y_t is the forecast variable;

B is the back shift operator, where $BY_t = Y_{t-1}$

ϕ is the autoregressive (AR) coefficient; and

θ is the moving average (MA) coefficient; and

Z_t denotes a dataset that complies with a normal distribution with mean 0 and standard deviation σ^2.

The task of identifying the most appropriate model for a given set of data can be quite bewildering as there is a huge variety of ARIMA models available. However, the following will outline a general approach to the problem.

The first step in any time series analysis is to plot the data. By graphically inspecting the data, any trends or unusual observations may be identified. Most time series forecasting methods require the time series to be stationary. That is, its mean, variance and autocorrelation properties are constant over time. This makes the time series easier to predict, as it is assumed that its statistical properties will be the same in the future as they were in the past. An examination of the raw time series data may reveal a constant trend or variation in the series' variance. If necessary, a transformation of the data may be required, to achieve '*stationarity'*. This can be done using mathematical differencing techniques. For example, if the data contains a constant trend, a curve can be fitted to the data, the residuals produced from the fit can then be used in the modelling process. Once the data appears stationary the model estimation process can begin.

The key to any time series analysis is the autocorrelation coefficient. These coefficients describe how successive values in a time series relate to each other at different time intervals and provide an insight into the estimation of the AR(*p*) and MA(*q*) components of the model. The autocorrelation coefficients r_k within a time series can be computed using the following equation:

$$r_k = \frac{\sum_{t=k+1}^{n} \left(X_t - \overline{X}\right)\left(X_{t-k} - \overline{X}\right)}{\sum_{t=1}^{n} \left(X_t - \overline{X}\right)^2} \tag{7.5}$$

where:

r_k is the autocorrelation coefficient;

X_t is the observation at time t;

$\overline{X}$ is the sample mean; and

k denotes the observation lag (number of observational separations).

Together the autocorrelation coefficients at lags 1,2,3, ……, make up the *autocorrelation function* or ACF. A plot of the ACF is used as a standard approach in exploring the characteristics of a time series before forecasting. It is used to determine whether previous values in the series contain any information about the next value, or whether no relationship exists between observations.

Another coefficient that is widely used in time series analysis is the partial autocorrelation. Partial autocorrelations are used to measure the degree of association between Y and $Y_t - k$ by removing the effect of the intervening values between these observations. These coefficients at different lags make up the *partial autocorrelation function* or PACF. Both the ACF and PACF play an important preliminary role in the prediction of future observations within a time series. They provide a measure of the degree of dependence between values at specific intervals of separation. The use of these coefficients is more widely explained in the next section 7.2.3.2.

Once the *p* and *q* values have been estimated using the ACF and PACF plots, the model can be run and residuals calculated. An examination of the model output is then undertaken to determine whether or not the model has performed adequately, or if it may be improved by a different approach. One such method of assessment is to

check the significance of the estimated model parameters, by examining the *P*-value. The *P*-value represents a decreasing index of the reliability of the result. It is a measure of the probability of error in the modelled parameters. It is conventional to conclude that the result is statistically significant if the *P*-value is less than 0.05, although this threshold is arbitrary.

The following section provides an overview of the procedures adopted and results obtained in the estimation of an adequate ARIMA model for the prediction of the double differenced ionosphere.

7.2.3.2 ARIMA – Test results

The previously tested modelling approaches were based upon trying to identify a trend in the rate of change of the DDI that could be used to predict forward in time. This section tests how well the ARIMA modelling approach is able to describe this trend. One reference and roving satellite pair was used to produce model coefficients that describe the rate of change of the DDI over the test period using the entire dataset. These coefficients were then used as a predictive model to forecast the DDI, by applying them to the observations of the remainder of the satellites in the sky during this period. Therefore, based on this philosophy, this section will investigate whether or not the ARIMA approach can adequately capture the trend in the ionosphere, by suitably predicting the rate of change of the DDI of the remaining satellites.

The data used to conduct this analysis was the same as in the previous sections. ARIMA models were produced on the 23rd of September, 2001; 21st of December, 2001; 20th of March, 2002 and the 21st of June, 2002, to coincide with the solstice and equinox periods. The test period for each of these seasons was conducted during the daytime hours, between approximately 12 midday and 4pm in the afternoon, as this was thought to be the optimum time for surveying use, coupled with maximum solar conditions. The time span for each test undertaken was between approximately 1.5 to 2.5 hours. As the span of analysis was limited in time, every satellite in view during these periods was included in the analysis.

As the ARIMA models produced were all of similar characteristics, the Melbourne to Ballarat (MEBA) baseline during the March, 2002 period is presented below as an example. Satellite 13 was chosen as the model satellite, from which the ARIMA coefficients that describe the trend in the ionosphere would be produced. The analysis took place on the 20th of March, for approximately 1.6 hours, between 12.43-13.98 hours local time, yielding 1114 observations at 5 second epochs.

Figure 7.6 below, graphically displays the time series during the March period. On analysing the graph, it can be seen that there is both a non-linear and linear trend in the data. The linear trend was removed by fitting a linear model to the data as seen in Figure 7.7. This produced a more stationary time series centred about the mean, as seen in Figure 7.8. As previously stated, the Box-Jenkins ARIMA process treats the reduction of the data to stationarity as an integral part of the model fitting technique. The removal of the non-linear component was not investigated at this stage in order to simplify the process.

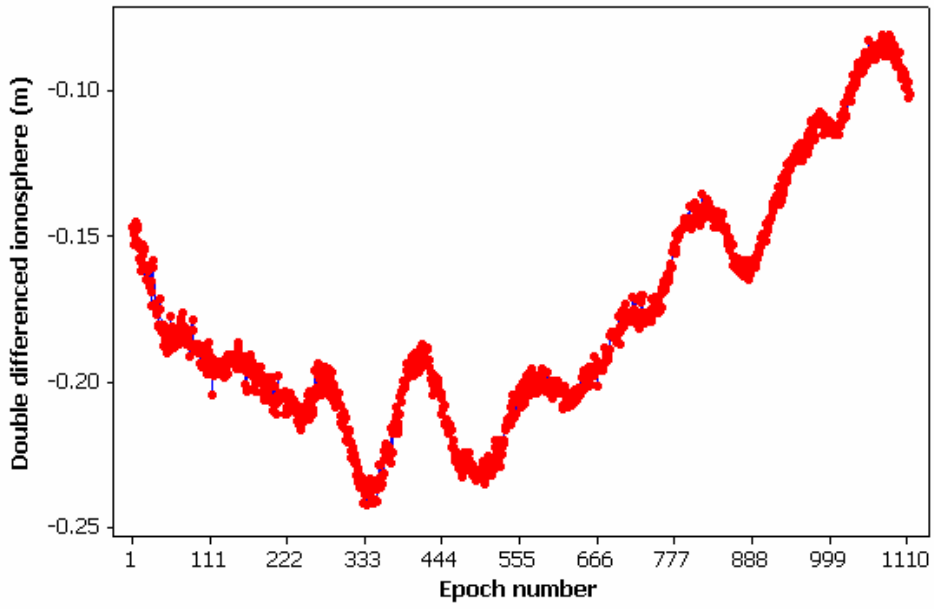

Figure 7.6: Satellite 13 raw double differenced observations along the Melbourne to Ballarat (MEBA) baseline, during 12.43-13.98 hours local time, on the 20th March, 2002.

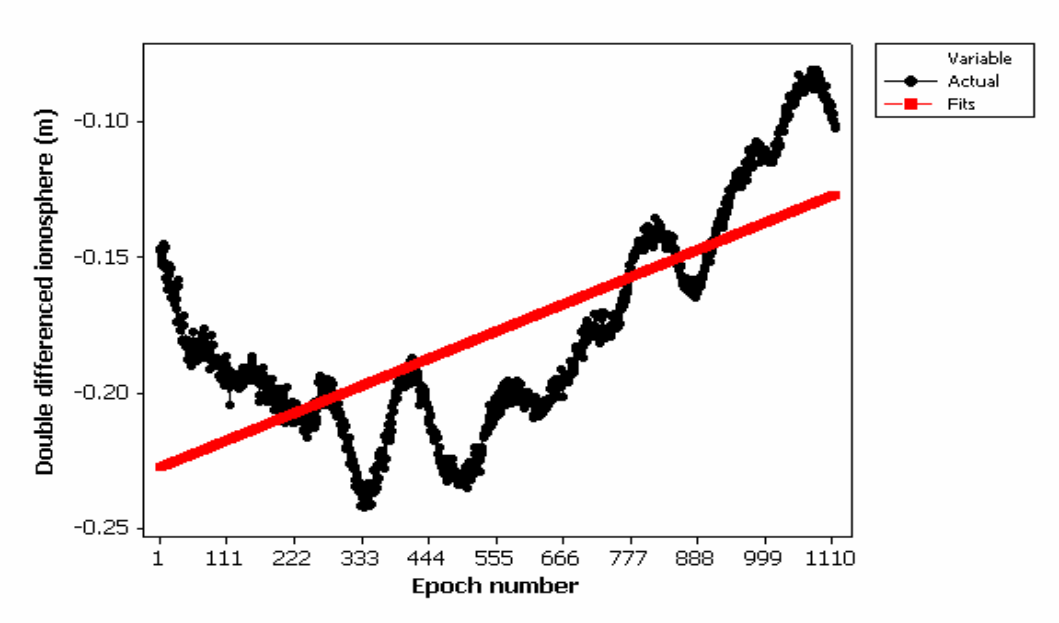

Figure 7.7: Satellite 13 linear trend analysis plot of the double differenced ionosphere. The red line depicts the linear trend model.

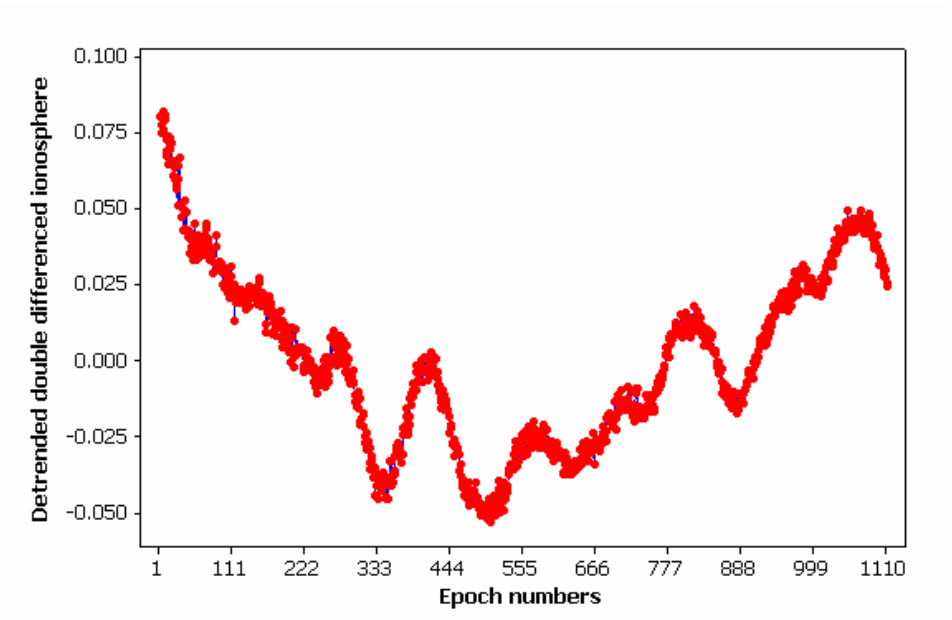

Figure 7.8: Satellite 13 detrended observations

At this stage of the process the identification of the number and type of ARIMA parameters to be estimated was undertaken. One of the major tools used in this identification phase is the PACF. The results of the PACF and how they are interpreted are in no way definitive, but give a good approximation and basis to begin

further experimentation with model combinations. Figure 7.9 displays the PACF of Satellite 13 during the March, 2002 example period.

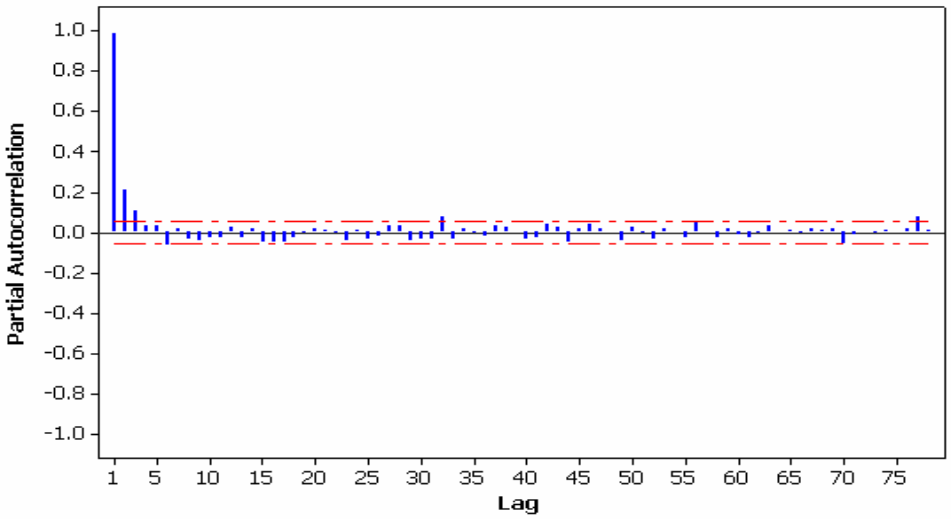

Figure 7.9: Satellite 13 Partial Autocorrelation Function (PACF) of detrended data. The red dashed lines indicate 5% significance limits for the partial autocorrelations.

On examining Figure 7.9, a high degree of short term dependence within the time series is highlighted, as the graph decays rapidly. Three statistically significant partial autocorrelations can be identified before the values drop below significance. The values at lag 32 and 77 do slightly rise above the cut off for significance; this can however be put down to chance. The three statistically significant values indicate that within the time series, only three past values have any statistical correlation to the present value. Based on the ARIMA identification criteria presented in Makridakis et al. (1998), this would indicate that an AR(3) model may be appropriate to model this data series, thus excluding any moving average component. The model coefficients were then calculated using a statistical software package known as SPSS version 14 (Statistical Package for the Social Sciences). The statistical read out including the model coefficients can be seen in Appendix D. The model coefficients produced are described in Table 7.3. It can be seen from these results that the coefficients are heavily weighted towards the first of the previous three values, therefore, placing more emphasis on the closest value in the time series, by a factor of approximately three in this instance. These results were indicative of the type of weighting experienced over the remainder of the baselines tested during the different seasons.

Table 7.3: ARIMA Auto-Regressive (AR) coefficients

AR Coefficient	Value
1	0.603
2	0.195
3	0.200

In order to assess how well the model fit the time series, the *P*-value was consulted. This value is denoted as “Approx. Sig” in the Parameter Estimates table in the statistical read out presented in Appendix D. In this instance, the *P*-values are all zero, thus indicating a good fit and a statistically significant result.

The coefficients computed were then used in the following autoregressive equation 7.6 to produce predictions forward in the time series:

$$Y_t = c + \phi_1 Y_{t-1} + \phi_2 Y_{t-2} + ... + \phi_p Y_{t-p} + e_t \tag{7.6}$$

where:

c is a constant term;

ϕ_j j_{th} autoregressive parameter; and

e_t the error term at time t.

This was the procedure used to produce coefficients for each baseline during each season. Moving average parameters were also computed and incorporated into each model, but the autoregressive-only approach produced results that were equal to or better than those produced using the combined approach. Adopting this method significantly simplified the modelling procedure, whilst still achieving optimum results.

Table 7.4 provides a summary of how quickly (in seconds) the $\pm$5cm threshold is reached using the ARIMA modelling processes described above. The time periods indicated (in seconds) reflect the model’s ability to predict the DDI residuals below the $\pm$5cm threshold to a 99% confidence level.

Table 7.4: Approximate time intervals (seconds) where the ARIMA model residuals are below the ±5cm threshold.

Date	Baseline	ARIMA (secs)
Sept, 2001	MEBA	300
	MEBE	180
	BABE	240
Dec, 2001	MEBA	150
	MEBE	120
	BABE	180
March, 2002	MEBA	90
	MEBE	90
	BABE	60
June, 2002	MEBA	60
	MEBE	60
	BABE	30

Based on the data in Table 7.4, the ARIMA modelling process was able to predict the DDI to under ±5cm out to an average of 240 seconds during the September period, 150 seconds during the December period, 80 seconds during the March period and to an average of 50 seconds during the June period respectively. The decrease in modelling performance over the four different seasons again highlights the unpredictable nature of the ionosphere. The next section directly compares the three different modelling approaches tested.

7.3 Model comparisons

Based on the analysis and the results obtained from the testing of the moving average and linear polynomial predictive models in the previous sections, the moving average model has outperformed the linear polynomial and will therefore be tested against the ARIMA modelling approach for a direct comparison. The moving average model (see section 7.2.1) was used to produce predictions of the DDI residuals during the shorter ARIMA test periods in September, 2001; December, 2001; March, 2002 and June, 2002. Table 7.5 shows a direct comparison of the results.

These results indicate that the ARIMA and moving average modelling approaches produce results that are virtually identical. This provided strong evidence that the ARIMA approach adequately described the ionosphere during the test period. As the moving average model was tested on a satellite by satellite basis whilst the ARIMA approach adopted one reference-rover satellite combination present during the entire test period to produce coefficients that described the rate of change of the DDI. Therefore the coefficients produced using the ARIMA approach were able to provide a means of predicting the DDI to a level achieved when using a moving average model.

The results presented in Table 7.5 indicate that both models are able to reproduce corrections at latencies that are consistent with the decorrelation experienced in the ionosphere itself. Both modelling schemes are able to adapt to the differing seasonal conditions and provide results that are reflective of what is actually happening in the ionosphere.

Table 7.5: A comparison of the ARIMA and moving average modelling approaches

Date	Baseline	ARIMA (secs)	Moving Average (secs)	Ionosphere (secs)
Sept, 2001	MEBA	300	300	300
	MEBE	180	180	180
	BABE	240	240	270
Dec, 2001	MEBA	150	150	150
	MEBE	120	120	60
	BABE	180	180	180
March, 2002	MEBA	90	90	90
	MEBE	90	90	90
	BABE	60	60	60
June, 2002	MEBA	60	60	60
	MEBE	60	30	60
	BABE	30	30	30

Based on these results, the ARIMA modelling approach has been very successful. It has been able to produce coefficients, using one reference and roving combination,

that describe the rate of change in the DDI residuals for the remaining satellites in the sky, regardless of azimuth or elevation, to an accuracy that corresponds to the actual decorrelation rates of the ionosphere itself and the moving average model. This is significant, as the results obtained using the moving average approach were derived on a satellite by satellite basis, modelling each satellite individually. However, the disadvantage of the ARIMA approach is that it is more complicated to compute compared to the simple moving average scheme.

The moving average scheme assumes that the DDI is a time variant bias. When compared to the linear polynomial modelling approach, the linear polynomial tends to be more affected by short-term trends in the data caused by measurement noise, multipath and real short-term ionospheric variation. Figure 7.10 highlights the differences between the moving average and linear polynomial modelling approaches, and is illustrated over a 10 minute prediction period. The first section of the data displayed is used to produce the moving average forward-prediction based on 30 seconds of data, whilst the linear modelling approach was derived from a 60 second sample size. It can be seen that the line of best fit produced using the linear model, assumes a trend in the DDI that is not present over time periods greater than one minute. The moving average approach however, provides a better fit to the data over the 10 minute prediction interval.

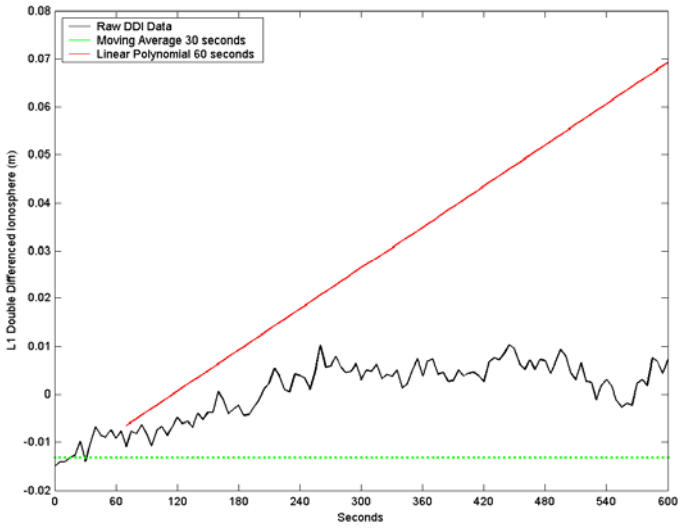

Figure 7.10: The difference between the moving average and linear modelling approaches, using the data supplied by Satellite 6, along the Melbourne to Ballarat baseline, on the 20th March, 2002.

(The time span displayed forms one predictional test period over 10 minutes)

The ARIMA approach has similar characteristics to the moving average scheme and the predictive results from both are almost identical. Due to the moving average scheme's simplicity and precision, it will be considered for further investigation in the next section. The model is tested against the data obtained from the night / day analysis undertaken in section 6.2.2.

7.3.1 Moving average model - Night and day analysis

Finally, the moving average model was tested against the results obtained for the Day Vs Night analysis in section 6.2.2. The test was designed to investigate how well the moving average model correctly predicted what was actually happening in the ionosphere during these periods. The night time period was defined as the period between 0-6 hours and the day time period was defined as the period between 10-16 hours local time. All of the available satellite observations were used for this analysis.

The results obtained in the truth data can be viewed in Table 6.2. When analysing the results gathered from the moving average test in Table 7.6 below, it can be seen that the moving average model's decorrelation periods display quite similar results. During the September and December periods, where high solar activity was experienced during the night, the average period of decorrelation of the ionosphere was 70 seconds during the night and 155 seconds during the day, before it passed the $\pm$5cm level. The results obtained from the moving average model during this same period give an average prediction latency of 65 seconds during the night and 150 seconds during the day time period, which is almost identical to the decorrelation rate of the actual ionosphere during this period. The March period decorrelated to an average of 210 seconds at night before it reached the $\pm$5cm threshold, which compares to an average prediction latency of 220 seconds. The March day time statistics reflect an average of 90 seconds against a moving average prediction latency of 90 seconds. The June results gave an actual decorrelation in the ionosphere out to an average of 90 seconds during the night and 60 seconds during the day. This was reflected with a moving average prediction of 80 seconds during the night and 40 seconds during the day.

Overall, from these results it can be said that the moving average model can predict the ionosphere to an accuracy of ±5cm on average 92% of the time during the night and 89% of the time during the day time period. These percentages would increase to an average of 94% during the night and 98% during the day if the anomalous June data was discarded.

Based on the analysis undertaken, the moving average model, using a 30 second data sample will predict the ionosphere to ±5cm to an average accuracy of approximately 90% on most occasions. However, the unpredictable nature of the ionosphere could see this accuracy fall as low as 67% as shown during the day time period in June.

Table 7.6: Testing the moving average model with 30 seconds of data. (This table shows the time intervals where the DDI residuals are below the ±5cm level for night and day periods)

Date	Baseline	Night (sec)	Day (sec)
	MEBA	90	180
Sept, 2001	MEBE	60	90
	BABE	60	90
	MEBA	60	180
Dec, 2001	MEBE	60	150
	BABE	60	210
	MEBA	180	90
March, 2002	MEBE	240	90
	BABE	240	90
	MEBA	90	60
June, 2002	MEBE	60	30
	BABE	90	30

7.4 Summary

As a means of providing an ionospheric model suitable for Victorian conditions, that would have direct applications in providing corrections to the users of Victoria's current GPSnet infrastructure, three potential modelling procedures were tested during this chapter. Based on the results obtained, the moving average model

provided both computational simplicity and accuracy when compared to the ARIMA and linear modelling approaches.

When tested over the 72-hour observational period, during all four seasons, the moving average model, using 30 seconds of previous data over approximately 100km baselines, was able to predict the DDI residuals, under the ±5cm threshold, out to an average of approximately 120 seconds, with a prediction accuracy of 89% during the day and 92% during the night when compared to the actual decorrelation rates of the ionosphere. However, disturbed ionospheric conditions (see section 2.1.9), like those experienced during the June period, and the longer 130km MEBE baseline can bring this average down to as low as 60 seconds.

The ARIMA modelling process produced results that were practically the same as those achieved by the moving average model, and coincided with the actual decorrelation rates of the raw DDI itself. This is significant, as the ARIMA approach used only one reference satellite to produce coefficients that were used to model or predict the rate of change in the double differenced ionosphere for the remainder of the satellites present during the test period. Based on these results, the ARIMA approach was able to adequately describe the ionospheric conditions over Victoria during four seasonal periods to an accuracy equal to the decorrelation rates of the ionosphere.

However, in terms of model complexity and implementation within a Network-RTK environment, the moving average model is superior to the ARIMA approach, as there is no need to produce model coefficients or assess the model's accuracy or goodness of fit.

Based on the datasets collected, the moving average modelling scheme was able to predict the DDI bias to within ±5cm over baseline lengths of 100km. The ionospheric corrections would only need to be sent every 60 seconds to achieve a ±5cm error in the DDI bias within a 99% confidence level. The latency of the corrections however, would depend on the ionospheric activity at the time. During more stable times, as observed during the September and March periods, the correctional latency could be

extended to 2 minutes between transmissions, whilst still being able to achieve the same accuracies in the field. To be able to predict the ionospheric bias at the rover, would allow the rover to be less dependent on the RTK-Network for corrections, thus making the system more efficient in terms of correction computation, data transmission volume and bandwidth efficiency.

The implications of these findings would potentially enable the most efficient use of the current GPSnet infrastructure for providing a state wide real-time cm-level positioning service. Based on the periods of analysis, and the temporal ionospheric models produced, at worst the ionospheric bias would need to be updated every 60 seconds in order to maintain a $\pm$5cm ionospheric prediction accuracy, therefore promoting the fast and reliable resolution of carrier phase ambiguities at the rover, whilst using minimal network resources. This research will also aid in reducing the cost of Network-RTK correction delivery and user costs by determining the frequency with which ionospheric corrections need to be sent to provide cm-level accuracies.

Chapter 8 Conclusions and Recommendations

At present Victoria's GPSnet is undergoing extensive infrastructure upgrades that include a recently implemented, real time cm-level positioning capability in Melbourne and surrounding areas known as MELBpos. As part of a State government initiative to implement a cm-level real time positioning service across Victoria, the network is currently being densified. One of the main limitations relating to GPSnet's configuration is the long baseline separations across the state and the ionospheric errors experienced over these baselines. Therefore, the precise modelling of Victoria's ionosphere plays a key role in overcoming this potential barrier to performance and implementation. As a result, having a better understanding of the temporal variability of Victoria's ionosphere will assist in the development of second generation Network-RTK systems that operate on sparser (+100km) base station configurations.

The aim of this thesis is to develop a high precision temporal ionospheric bias model for Network-RTK applications. The model has been developed and analysed for the state of Victoria during solar maximum conditions. Given advanced knowledge of the temporal nature of the differential ionospheric bias, it should be possible to design Network-RTK ionospheric correction messages that meet high precision GNSS user requirements. To achieve this aim, the following research objectives have been set:

- To quantify the temporal trend in the ionosphere during a period of solar maximum, over the State of Victoria;
- To analyse the suitability of four typical global empirical ionospheric models for providing ionospheric corrections in a Network-RTK environment;
- To provide a means of modelling the temporal double-differenced ionospheric bias in a Network-RTK environment, by testing a number of different prediction techniques, together with different data sampling rates; and
- To develop temporal ionospheric correction models; using GPSnet as a test bed.

High precision GPS positioning techniques use carrier phase measurements and require the resolution of the unknown integer ambiguity before precise positioning can be attained. The fast and accurate resolution of the carrier phase ambiguities is heavily reliant on the correlation of distance dependent measurement biases, such as the ionosphere, troposphere and orbital errors. As baseline lengths increase, the decorrelation of the ionospheric error has a greater influence on ambiguity resolution.

In order to mitigate the distance dependent biases that limit the application of cm-level RTK surveying, the Network-RTK concept has been developed over the last decade. This concept has been developed to provide cm-level accuracies over baseline lengths of many tens of kilometres through the use of multiple network reference stations. These reference stations are spread over a wide geographical area, and are able to empirically model the spatially dependent measurement biases, thus producing corrections that can be transmitted to users within the network. In addition to the problem of a sparse (+100km) network configuration, the issue of the reduction of data transmission volume and message complexity to the rover provides a challenge to the efficient implementation of Network-RTK resources.

The ionosphere needs to be predicted forward in a Network-RTK environment, as real time positioning requires corrections to the rover's observations to provide instantaneous positioning. The delivery of these corrections involves latencies in the order of a few seconds to ten's of seconds. It is important that the corrections are delivered sufficiently often with a small enough latency so that they are still applicable, given that the ionospheric bias is rapidly changing. Therefore, in support of promoting

efficient transmission to the rover in a Network-RTK environment, it is important to quantify the necessary update rate for the ionospheric corrections in order to maintain cm-level accuracy, thus allowing accurate rover positioning within a network. As telecommunication companies often charge users of correctional data according to the amount of data traffic, it is important to consider the minimum frequency required to deliver the required level of accuracy.

As a preliminary step towards understanding the variability of the ionosphere over Victoria and the issues that need to be addressed in order to derive cm-level ionospheric observations, four global empirical ionospheric models (Broadcast, Bent, CODE and IRI2001) were tested, to see how they perform in a differential sense in Chapter 5. This is undertaken as a means of investigating their usefulness in providing corrections in a Network-RTK environment. A test bed of three GPSnet stations was chosen that was indicative of the average spacing of the current network's configuration. The L4 linear combination of GPS measurements was used to produce the double differenced ionospheric bias information that was used as 'truth' from which the empirical models could be compared. Whilst the L4 linear combination is able to estimate the ionospheric bias to a high degree of accuracy, it should be noted that any short term variation in the double differenced ionospheric bias may be caused by carrier phase multipath. The following conclusions have been reached based on the tests:

- none of the empirical models appeared to provide ionospheric bias estimates to an accuracy required for the correction of real time data in a Network-RTK environment, as the models were unable to capture the wide ionospheric bias variation in some of the satellite traces;
- a user would be better off assuming that the ionospheric bias is zero, rather than use any of the empirical ionospheric models tested;
- the poor performance of the empirical models was due to a number of factors. Firstly, the general global nature of the input coefficients made them unable to accurately reproduce ionospheric conditions over smaller regions. Secondly, the measurements used to derive these coefficients are derived predominantly from the northern hemisphere, which may introduce a bias when adapted for use in the southern hemisphere. Thirdly, the simple elevation dependent

mapping functions used by all of the models, were unable to accurately estimate the non-homogeneous ionosphere; and

- even though the models were not able to accurately estimate the actual ionospheric bias, they do provide a stochastic measure of the expected variability in the ionosphere. This information is relevant to long baseline estimation where a-priori variance must be assigned to ionospheric biases contained in the least squares estimation model.

In order to gain an understanding of the type of modelling strategy to use, to improve the precision of ionospheric correction over Victoria for real time cm-level applications, an investigation was undertaken in Chapter 6 that focused on the diurnal and seasonal variations of ionospheric TEC over the region, during four different seasonal periods. This was undertaken by firstly studying the variation of the actual ionospheric TEC over Victoria, then refining the study to quantify the temporal characteristics of the differential ionospheric bias over the same region. This analysis helped characterise the nature and fine structure of the ionosphere over Victoria in both a local and regional sense. A subset of eight GPSnet stations located across the state was used as a test bed for this analysis. Dual frequency GPS observations were collected from each station that coincided with the same test period used in Chapter 5. The time series of TEC measurements used to quantify the ionosphere over Victoria were obtained using a spherical harmonic function and a thin shell mapping approach as described in Chapter 6. The study involved a two step process: (1) The vertical TEC values above the Melbourne base station were calculated at 30 second intervals using 3 days of observations collected during each season, (2) Line of sight TEC values, from all eight GPSnet stations used in the analysis, were converted to VTEC values at each ionospheric pierce point on the thin shell. This data was used to produce contour plots of the ionosphere at two hourly intervals over a 24 hour period, for each season. From the vertical TEC values produced at the Melbourne base station during four different seasons, the following conclusions were reached:

- the results highlighted the variability of the ionosphere in both a diurnal and seasonal sense;
- there is a significant change in the VTEC values from day to day within each season, except for the June period, which traditionally displays a more quiet

and stable ionosphere. These changes from day to day, especially during the local daytime period, can equate to as much as 20%, with the changes experienced from one season to the next as great as 50% as found between the March and June periods;

- the largest VTEC values were recorded during March 2002, with values as high as approximately 70 TECU during the day and as low as 10 TECU during the night in June, 2002. This equates to a delay of approximately 11.2m in the vertical, during peak daytime conditions. As a general rule, an obliquity factor of 3 is applied to low elevation angle satellites, therefore during peak daytime conditions during March of 2002, low elevation angle satellites would have experiencd ionospheric delays in the order of 33m;
- the VTEC values experienced during the day are higher than those at night-time. However, the occurrence time of the maximum and minimum ionospheric values varies with season; and
- based on these results, there is little evidence of consistency in observation from season to season. Whilst the general overall trend in the plots within each seasonal period is similar, modelling coefficients derived from one day's worth of data are not accurate enough to describe the ionosphere from one day to the next for the purpose of cm-level Network-RTK requirements.

The data produced from the state wide measurements of VTEC was presented in the form of 12 x 2 hourly plots that described the ionosphere during the four seasonal periods over 24 hours. The following conclusions were formulated from the VTEC analysis:

- it can be seen that the VTEC values over Victoria vary with the time of day, and that the spatial correlation characteristics of the VTEC values corresponding to each 2 hourly epoch are quite different. The data showed rapid variations of approximately 50% between snap shots during the morning periods, with a steady increase in VTEC during the day until the peak was reached, then a steady decline of approximately 10% between each 2 hourly snap shot in the late afternoon and early evening.
- the contour plots depict many spatial anomalies or inconsistencies in VTEC across Victoria, especially during the September and December, 2001

periods, which showed VTEC gradients of between 2-8ppm over the state during the day time peak. During the more stable June period, TEC gradients of 0.5ppm were experienced during the day time peak;

- as the state-wide investigation of VTEC was conducted during the same period as the analysis over Melbourne, the state-wide high and low variation of VTEC produced similar results. The high was experienced during the March 2002 period, with a value of approximately 70 TECU, with a low of approximately 10 TECU during the June 2002 period.
- it can be seen that due to the changing satellite geometry experienced over Victoria, that at certain periods, the satellite geometry was not sufficient to produce ionospheric values across the whole state, ie. there were gaps in the coverage;
- based on this temporal and spatial analysis of the ionosphere over Victoria, the results suggest that the temporal and spatial TEC variations experienced over the region are of a complicated nature. This suggests that any model trying to predict the absolute ionospheric TEC based on location, time of day, time of month and season, would be unable to adequately represent the complicated nature of the ionosphere to a level that would ensure fast and reliable ambiguity resolution, as real-time corrections would have to deliver cm-level ionospheric estimates; and
- as the ionosphere can vary significantly over a short period of time it is suggested that in order to predict the ionosphere to a high degree of accuracy, any model chosen would have to be designed to make predictions, based on actual ionospheric information received up to the period of prediction.

As a first step towards producing a regional ionospheric modelling approach that is sufficiently accurate for Network-RTK applications, Chapter 6 then produced an investigation into the variation of the DDI bias over Victoria during the same four seasonal periods previously tested. The analysis looked for any trends in the raw observational data that would aid in prediction of the DDI bias. For the purposes of this study, it was assumed that the ionospheric bias needs to be accurate to $\pm$5cm to simplify ambiguity resolution. Based on this criteria, an analysis of how quickly the DDI residuals decorrelated from one epoch to the next over Victoria was conducted. The same three GPSnet stations that were used to test the empirical models in

Chapter 5 were used to conduct the analysis over the same 72 hour period. It was found that:

- the temporal variability of the ionosphere over Victoria out to approximately 100km remains under ±5cm out to an average of 120 seconds within a 99% confidence level;
- the traditional assumption of day and night ionospheric activity being higher during the day and lower at night was not always followed in the test periods; and
- during the quiet ionospheric periods, the ionosphere's decorrelation can remain below the ±5cm threshold for up to 3 minutes, whilst during the active solar times the ±5cm threshold was reached in less than 60 seconds.

Chapter 7 focuses primarily on the production of a temporal differential ionospheric model that is suitable for Network-RTK use in Victoria. The model was used as a means of predicting the trend in the double-differenced residuals and needed to be sufficiently accurate to allow for the precise resolution of the integer cycle ambiguity at the roving receiver. The models presented attempt to provide a compromise between complexity and accuracy achieved. The first two modelling techniques tested, provide a simplistic approach to predicting a trend in a very complex ionosphere. The third method (ARIMA), provides an in depth analysis of the ionosphere, to ascertain whether or not a more complex method would provide better predictive results. The three predictive schemes were the moving average approach, the linear polynomial and the ARIMA approach. The ±5cm accuracy criteria for correct ambiguity resolution was used as a means of assessing each model's performance. Different lengths of data input were investigated in the moving average and linear polynomial approaches, to assess the optimum input window for maximum accuracy. From the tests conducted, the following findings were drawn:

- the moving average model, using 30 seconds of previous data for optimum performance, was able to predict the DDI residuals, under the ±5cm threshold, out to an average of approximately 120 seconds or 2 minutes. When compared to the actual decorrelation rates of the ionosphere, this equates to a prediction accuracy of 92% during the night and 89% during the day time

periods, over approximately 100km baselines. However, disturbed ionospheric conditions, like those experienced during the June period, and the longer 130km MEBE baseline can bring this average down to as low as 60 seconds;

- the linear polynomial model, using 60 seconds of previous data for optimum performance, was able to predict the DDI residuals, under the ±5cm threshold, out to an average of 75 seconds over approximately 100km baselines. The model's poorer performance when compared to the moving average approach was a result of it being more affected by short-term trends in the data, caused by measurement noise, multipath and real short-term ionospheric variations;
- the ARIMA modelling process produced results that were practically the same as those achieved by the moving average model, and coincided with the actual decorrelation rates of the raw DDI itself. This is significant, as the ARIMA approach used only one reference and rover satellite combination to produce coefficients that were used to model or predict the rate of change in the double differenced ionosphere for the remainder of the satellites present during the test period. Based on these results, the ARIMA approach was able to adequately describe the ionospheric conditions over Victoria during four seasonal periods to an accuracy equal to the decorrelation rates of the ionosphere;
- in terms of model complexity and implementation within a Network-RTK environment, the moving average model is superior to the ARIMA approach, as there is no need to produce model coefficients or assess the model's accuracy or goodness of fit; and
- based on the datasets collected, the moving average modelling scheme was able to predict the DDI bias to within ±5cm over baseline lengths of 100km. The ionospheric corrections would only need to be sent every 60 seconds to achieve a ±5cm error in the DDI bias within a 99% confidence level. The latency of the corrections however would depend on the ionospheric activity at the time. During more stable times, as observed during the September and March periods, the correctional latency could be extended to 120 seconds between transmissions, whilst still being able to achieve the same accuracies in the field. As a result of predicting the ionospheric bias, the rover would potentially require less frequent ionospheric correctional updates from the

network, thus making the system more efficient in terms of correction computation, data transmission volume and bandwidth efficiency.

8.1 Recommendations

This thesis recommends the following:

- a relatively simple ionospheric predictive technique such as the moving average scheme, could be used to enhance the implementation of next generation Network-RTK systems that operate on sparser (+100km) network configurations, by predicting the DDI to latencies that would enable cm-level positioning;
- the predictive approaches adopted by both the moving average and ARIMA schemes are similar, in that they both derive their corrections from observations obtained from previous epochs leading up to the prediction interval. Therefore, it is recommended that any data used as input for a temporal ionospheric predictive model should come from the period leading up to the prediction, as data from further previous observations will not enhance the model's performance, but rather impede it due to the ionosphere's rapid variation;
- the current approach of sending ionospheric corrections to users in the field every few seconds may not promote efficient use of network resources;
- in order to combine both the fast and reliable ambiguity resolution at the roving receiver and the optimum latency to which ionospheric corrections should be broadcast, the current temporal variability of the ionospheric conditions within the network needs to be considered;
- by sending ionospheric corrections to users at minimum latencies that promote reliable ambiguity resolution, the cost of providing these corrections and the cost incurred by the users of this information would be reduced, therefore encouraging a more efficient use of available resources; and
- in order to consistently produce a state wide ionospheric model, that covers the entire region, data from GPS receivers located outside of the state boundaries would be needed to enable sufficient coverage, even during periods of low satellite availability.

8.2 Future research

Outside the scope of this thesis, but warranting future research are the following topics:

- performing a detailed analysis on the most efficient means of delivering network ionospheric corrections, taking into account ionospheric model complexity, network computational load, signal bandwidth, transmission rates and data compression schemes;
- using additional base stations present in GPSnet's current configuration to perform a detailed analysis on the spatial correlation of the ionospheric bias and to test the effects that azimuth has on the ionospheric bias affecting GPS satellites;
- perform an analysis of how the developments in the next generation of GNSS satellites, including: increased satellite availability, improved signal strength and the availability of three frequencies, will influence the accuracy of ionospheric modelling techniques within a Network-RTK environment.

References

Aarons, J. (1982) 'Global Morphology of Ionospheric Scintillations', Proceedings of the IEEE, April.

Aarons, J. (1993) 'The longitudinal morphology of equatorial F-Layer irregularities relevant to their occurrence', *Space Science Review*, vol. 63, pp. 209-43.

Aarons, J. (1995), 'Fading of GPS Transmissions Due to Ionospheric Irregularities', Center for Space Physics, Boston University, report to the FAA WAAS Program Office, April,

AIUB (2007) 'Astronomical Institute University of Berne', <http://www.aiub.unibe.ch/ionosphere.html>, accessed March, 2007

Alves, P., Ahn, Y. W. and Lachapelle, G. (2003) 'The effects of network geometry on network RTK using simulated GPS data', Proceedings of ION GPS/GNSS-2003, 16th International Technical Meeting of The Satellite Division of The Institute of Navigation, Portland, Oregon, 9th-12th September.

Anderson, D. N., Decker, D. T. and Valladares, C. E. (1996) 'Global theoretical ionospheric model (GTIM)', *Handbook of Ionospheric Models*, Schunk, R. W. (ed.), Boulder, USA, Solar-Terrestrial Energy Program (STEP), Scientific Committee on Solar Terrestrial Physics (SCOSTEP), pp. 133-52.

Anderson, H. and Johnson, L. (1996), Ionospheric climatology from TOPEX/Poseidon measurements, Centre for astrodynamics research, University of Colorado, 24th-25th September,

Appleton, E. V. (1954) 'The anomalous equatorial belt in the F2-layer', *Journal of Atmospherics and Terrestrial Physics*, vol. 5, pp. 348-51.

Appleton, E. V. and Barnett, M. A. F. (1925a) 'Local reflection of wireless waves from the upper atmosphere', *Nature*, vol. 115, pp. 333-4.

Appleton, E. V. and Barnett, M. A. F. (1925b) 'On some direct evidence for downward atmospheric reflection of electric rays', Proceedings of the Royal Society, London.

Appleton, E. V. and Beynon, W. J. G. (1940) 'The application of ionospheric data to radio-communication problems - Part 1', *Proc. Phys. Soc.*, vol. 52, p. 518.

Appleton, E. V. and Beynon, W. J. G. (1947) 'The application of ionospheric data to radio-communication problems - Part 2', *Proc. Phys. Soc.*, vol. 59, p. 58.

Ashby, N. and Spilker, J. J. (1996) 'Introduction to relativistic effects on the Global Positioning System', *Global Positioning System: Theory and Applications*, Parkinson, B. W. & Spilker, J. J. (eds), American Institute of Aeronautics and Astronautics, Washington, pp. 623-95.

Asmussen, H. (2006) 'MELBpos makes its mark', *Landmark*, no. 25, pp. 19-21.

Bassiri, S. and Hajj, G. A. (1993) 'Higher-order ionospheric effects on the global positioning system observables and means of modelling them', *Manuscripta Geodaetica*, vol. 18, pp. 280-9.

Basu, S., MacKenzie, E. and Basu, S. (1988) 'Ionospheric constraints on VHF/UHF communications links during solar maximum and minimum periods', *Radio Science*, vol. 23, no. 3, pp. 363-78.

Bent, R. B. and Llewellyn, S. K. (1973), Documentation and description of the Bent ionospheric model, Laboratory, A. f. G. edition, AFCRL-TR-73-0657, Hanscom AFB, Massachusetts,

Bent, R. B., Llewellyn, S. K. and Nesterczuk, G. (1975) 'The development of a highly-successful worldwide empirical ionospheric model and its use in certain aspects of space communications and worldwide total electron content investigations', Proceedings of Ionospheric Effects Symposium, Arlington, VA, 20th-22nd January, pp. 13-28.

Beser, J. and Balendra, A. (1994) 'Enhanced ionospheric delay compensation using GLONASS', Proceedings of ION GPS-1994, 7th International Technical Meeting of The Satellite Division of The Institute of Navigation, Salt Lake City, Utah, 20th-23rd September, pp. 1609-17.

Beutler, G., Weber, R., Hugentobler, U., Rothacher, M. and Verdun, A. (1998) 'GPS satellit orbits', *GPS for geodesy*, Teunissen, P. J. G. & Kleusberg, A. (eds), Springer, Berlin, pp. 43-109.

Beutler, G., Bauersima, G. I., Gurtner, W., Rothacher, M., Schildknecht, T. and Geiger, A. (1987) 'Atmospheric refraction and other important biases in GPS carrier phase observations', *Atmospheric effects on geodetic space measurements, Monograph 12*, School of Surveying, University of New South Wales, Kensington, Australia, pp. 15-43.

Beutler, G., Bauersima, I., Botton, S., Gurtner, W., Rothacher, M. and Schildknecht, T. (1989) 'Accuracy and Biases in the Geodetic Application of the Global Positioning System', *Manuscripta Geodaetica*, vol. 14, no. 1, pp. 28-35, Jan 1989.

Bierman, G. J. (1977) '*Factorisation methods for discrete sequential estimation*', Academin Press, New York.

Bilitza, D. (1979) 'A global model for the height of the F2-Peak using M3000 values from CCIR', *Telecommunication Journal*, vol. 46, pp. 549-53.

Bilitza, D. (1985) 'Electron density in the equatorial topside', *Advances in Space Research*, vol. 5, no. 10, pp. 15-9.

Bilitza, D. (1990), International Reference Ionosphere 1990, NSSDC Report 90-22 (available from the National Space Science Data Center, Greenbelt, Maryland 20771, USA),

Bilitza, D. (1992) 'Solar-Terrestrial models and application software', *Planetary Space Science*, vol. 40, pp. 541-79.

Bilitza, D. (1996), Improved IRI model for single frequency altimeters, Centre for astrodynamics research, University of Colorado, 24th-25th September,

Bilitza, D. (2001) 'International Reference Ionosphere 2000', *Radio Science*, vol. 36, no. 2, pp. 261-75.

Bilitza, D. (2002) 'Ionospheric models for radio propagation studies', *Review of Radio Science 1999-2002*, Oxford University Press, Oxford, pp. 625-79.

Bilitza, D. and Williamson, R. (2000) 'Towards a better representation of the IRI topside based on ISIS and Alouette data', *Advances in Space Research*, vol. 25, no. 1, pp. 149-52.

Bilitza, D., Rawer, K. and Pallaschke, S. (1988) 'Study of Ionospheric Models for Satellite Orbit Determination', *Radio Science*, vol. 23, no. 3, pp. 223-32, May-June, 1988.

Bilitza, D., Koblinsky, C., Williamson, R. and Bhardwaj, S. (1998) 'Improving the topside electron density model for IRI', *Advances in Space Research*, vol. 22, no. 6, pp. 777-87.

Bilitza, D., Bodo, R. W., Radicella, S. M., Pulinets, S., Gulyneva, T. and Triskova, L. (2006) 'Improvements to the International Reference Ionosphere model for the topside electron density profile', *Radio Science*, vol. 41, April.

Bishop, G., Basu, S., Groves, K., Smitham, M., Lehneis, K., Jacobs, D., Gehred, P., Howell, D., Bainum, G. and Goldizen, D. (1996) 'Upcoming ionospheric impacts on GPS at solar max what do we know / what do we need?' Proceedings of ION GPS-1996, 9th International Technical Meeting of The Satellite Division of The Institute of Navigation, Kansas City, Missouri, 17th-20th September.

Blanch, J., Walter, T. and Enge, P. (2002) 'Application of Spatial Statistics to Ionosphere Estimation for WAAS', Proceedings of The Institute of Navigation's National Technical Meeting, San Diego, California, January.

Blewitt, G. (1998) 'GPS data processing methodology', *GPS for Geodesy*, Teunissen, P. J. G. & Kleusberg, A. (eds), Springer, Berlin, pp. 231-270.

Box, G. E. P. and Jenkins, G. M. (1976) '*Time series analysis: Forecasting and control*', Revised edn, Holden-Day, San Francisco.

Braff, R. and Shively, C. (1985) 'GPS integrity channel', *NAVIGATION : Journal of the Institute of Navigation*, vol. 32, no. 4, pp. 334-50, Winter 1985-1986.

Breit, G. and Tuve, M. A. (1925) 'A radio method of estimating the height of the conducting layer', *Nature*, vol. 116.

Breit, G. and Tuve, M. A. (1926) 'A test of the existence of the conducting layer', *Physical Review*, vol. 28, no. 3, pp. 554-75, September.

Brockwell, P. J. and Davis, R. A. (1996) '*Introduction to time series and forecasting*', Springer-Verlag, New York.

Brown, N. (2003) 'Improving ionospheric estimation in the quasi-ionosphere-free ambiguity resolution strategy', Proceedings of ION GPS/GNSS-2003, 16th International Technical Meeting of The Satellite Division of The Institute of Navigation, Portland, Oregon, 9th-12th September, pp. 2637-48.

Brown, N., Keenan, R., Richter, B. and Troyer, L. (2005) 'Advances in ambiguity resolution for RTK applications using the new RTCM V3.0 Master-Auxiliary messages', Proceedings of ION GPS/GNSS-2005, 18th International Technical Meeting of The Satellite Division of The Institute of Navigation, Long Beach, California, 13-16 September.

Brown, R. G. and Hwang, P. C. (1983) '*A Kalman Filter Approach to Precision GPS Geodesy*', vol. 2, NAVIGATION, The Institute of Navigation, Alexandria.

Brunner, F. K. and Gu, M. (1991) 'An improved model for the dual frequency ionospheric correction of GPS observations', *Manuscripta Geodaetica*, vol. 16, no. 3, pp. 205-14, August.

Byers, H. R. (1974) '*General Meteorology*', Summersgill, R. H., Harrison, B. C. & Gamer, S.(eds), 4th edn, McGraw-Hill Inc.

Cander, L. R., Leitinger, R. and Levy, M. F. (1998) 'Ionospheric models including the auroral environment', Proceedings of ESA Workshop on Space Weather, Noordwijk, The Netherlands, March, pp. 135-41.

CBN (2007) 'Canadian Base Network (CBN) - Canadian Spatial Reference System', <http://www.geod.nrcan.gc.ca/network_p/cbn/index_e.php>, accessed June, 2007

CCIR (1966, 1990), Comite Consultatif International des Radiocommunications, Report 340-1, 340-6 (ISBN92-61-04417-4), Geneva, Switzerland,

Cislowski, G. J. and Higgins, M. (2006) 'SunPoz: Enabling centimetre accuracy GNSS applications in Queensland', Proceedings of International Global Navigation Satellite Systems Society - IGNSS Symposium 2006, Surfers Paradise, Australia, 17th-21st July.

Codrescu, M. V., Beierle, K. L., Fuller-Rowell, T. J., Palo, S. E. and Zhang, X. (2001) 'More total electron climatology from TOPEX/Poseidon measurements', *Radio Science*, vol. 36, no. 2, pp. 325-33, March/April.

Cohen, C., Pervan, B. and Parkinson, B. W. (1992) 'Estimation of absolute ionospheric delay exclusively through single-frequency GPS measurements', Proceedings of ION GPS-1992, 5th International Technical Meeting of The Satellite Division of The Institute of Navigation, Albuquerque, New Mexico, 16th-18th September, pp. 325-30.

Colombo, O. L., Hernandez-Pajares, M., Miguel Juan, J. and Sanz, J. (2002) 'Wide-Area, Carrier-Phase Ambiguity Resolution Using a Tomographic Model of the Ionosphere', *NAVIGATION : Journal of the Institute of Navigation*, vol. 49, no. 1, pp. 61-9.

Coster, A., Gaposchkin, E. M. and Thornton, L. E. (1992) 'Real-Time ionospheric monitoring system using GPS', *NAVIGATION : Journal of the Institute of Navigation*, vol. 39, no. 2, pp. 191-204.

Coster, A., Foster, J. and Erickson, P. (2003) 'Monitoring the ionosphere with GPS', *GPS World*, pp. 42-9, May.

Counselmann, C. C. and Gourevitch, S. A. (1981) 'Miniture interferometer terminals for Earth surveying: ambiguity resolution and multipath with the Global Positioning System', *IEEE Trans. on Geoscience and Remote Sensing*, vol. GE-19, no. 4, pp. 244-52.

Crosby, G. K., Ely, W. S., McPherson, K. W., Stewart , J. M., Kraus, D. K., Cashin, T. P., Bean, K. W. and Elrod, B. D. (2000) 'A ground-based regional augmentation system (GRAS) - The Australian proposal', Proceedings of ION GPS-2000, 13th International Technical Meeting of The Satellite Division of The Institute of Navigation, Salt Lake City, Utah, 20th-22nd September.

Dai, L., Han, S., Wang, J. and Rizos, C. (2003) 'Comparison of interpolation algorithms in network-based GPS techniques', *NAVIGATION : Journal of the Institute of Navigation*, vol. 50, no. 4, Winter.

Danaher, J., Balendra, A., Danaher, M., Erpelding, E., Gerlach, R. and Beser, J. (1993) 'GLONASS Dual frequency ionosphere sounder', Proceedings of ION GPS-1993, 6th International Technical Meeting of The Satellite Division of The Institute of Navigation, Salt Lake City, Utah, 22nd-24th September, pp. 1363-72.

Davies, K. (1990) '*Ionospheric radio'*, Peregrinus on behalf of the Institution of Electrical Engineers, London.

Diep Dao, T. H., Alves, P. and Lachapelle, G. (2004) 'Performance evaluation of multiple reference station GPS RTK for a medium scale network', *Journal of Global Positioning Systems*, vol. 3, no. 1-2, pp. 173-82.

Doherty, P. H., Delay, S. H. and Valladares, C. E. (2000) 'Ionospheric scintillation effects in the equatorial and auroral regions', Proceedings of ION GPS-2000, 13th International Technical Meeting of The Satellite Division of The Institute of Navigation, Salt Lake City, Utah, 19th-22nd September.

Doherty, P. H., Dehel, T. and Klobuchar, J. A. (2002) 'Ionospheric effects on low-latitude space based augmentation systems', Proceedings of ION GPS-2002, 15th International Technical Meeting of The Satellite Division of The Institute of Navigation, Portland, Oregon, 24th-27th Sptember, pp. 1321-9.

DSE (2006) 'Vicmap Position - MELBpos Service*'*, DSE, Victorian Government Department of Sustainability and Environment, <http://www.dse.vic.gov.au/dse/index.htm>, accessed January 2007.

DSE (2007) 'Department of Sustainability and Environment - GPSnet information*'*, <http://www.land.vic.gov.au/gpsnet>, accessed June, 2007

El-Arinin, B., Hegarty, C. J., Fernow, J. P. and Klobuchar, J. A. (1994) 'Development of an error budget for a GPS wide-area augmentation system (WAAS)', Proceedings of The Institute of Navigation National Technical Meeting, San Diego, California, January.

El-Arinin, B., Conker, R. S., Albertson, T. W., Reagan, J. K., Klobuchar, J. A. and Doherty, P. H. (1995) 'Comparison of real-time ionospheric algorithms for a GPS wide-area augmentation system (WAAS)', *NAVIGATION : Journal of the Institute of Navigation*, vol. 41, no. 4, pp. 393-412.

Enge, P. (1999) 'Local area augmentation of GPS for the precise approach of aircraft', *Proceedings of the IEEE, Special Issue on GPS*, vol. 87, no. 1, pp. 111-32, January.

Enge, P. and Van Dierendonck, A. J. (1996) 'Wide area augmentation system', *Global Positioning System: Theory and Applications*, Parkinson, B. W. & Spilker, J. J. (eds), American Institute of Aeronautics and Astronautics, Washington, vol. 2, pp. 117-42.

Enge, P., Walter, T., Pullen, S., Kee, C., Chao, Y. C. and Tsai, Y. J. (1996) 'Wide area augmentation of the Global Positioning System', *Proceedings of the IEEE*, vol. 84, no. 8, pp. 1063-88.

Essex, E. A., Webb, P. A., Horvath, I. and Cohen, H. (1997) 'The use of microsatellites in monitoring the ionosphere/plasmasphere', Proceedings of Proceedings of the COSPAR Colloquium on Microsatellites as Research Tools, Cheng Hung University, Tainan, Taiwan, 15th-17th December.

Euler, H. J. and Landau, H. (1992) 'Fast GPS ambiguity resolution on-the-fly for real-time applications', Proceedings of The Sixth International Geodetic Symposium on Satellite Positioning, Columbus, Ohio, 17th-20th March, pp. 650-9.

Euler, H. J. and Ziegler, C. (2000) 'Advances in ambiguity resolution for surveying type applications', Proceedings of ION GPS-2000, 13th International Technical Meeting of The Satellite Division of The Institute of Navigation, Salt Lake City, Utah, 19th-22nd September, pp. 95-103.

Euler, H. J., Keenan, C. R., Zebhauser, B. E. and Wubbena, G. (2001) 'Study of a simplified approach in utilizing information from permanent reference station arrays', Proceedings of ION GPS-2001, 14th International Technical Meeting of The Satellite Division of The Institute of Navigation, Salt Lake City, Utah, 11th-14th September.

Euler, H. J., Zebhauser, B. E., Townsend, B. and Wubbena, G. (2002) 'Comparison of different proposals for reference station network information distribution formats', Proceedings of ION GPS-2002, 15th International Technical Meeting of The Satellite Division of The Institute of Navigation, Portland, Oregon, 24th-27th September.

Euler, H. J., Seeger, S., Zelzer, O., Takac, F. and Zebhauser, B. E. (2004) 'Improvement of positioning performance using standardised Network-RTK messages', Proceedings of The Institute of Navigation National Technical Meeting, San Diego, California, 26th-28th January, pp. 453-61.

Evans, A. G., Swift, E. R., Cunningham, J. P., Hill, R. W., Blewitt, G., Yunck, T. P., Lichten, S. M., Hatch, R., Malys, S. and Bossler, J. (2002) 'The Global Positioning System Geodesy Odyssey', *NAVIGATION : Journal of the Institute of Navigation*, vol. 49, no. 1, pp. 7-34.

Ezquer, R., Jadur, C. and Mosert, M. (1998) 'IRI-95 TEC predictions for the South American peak of the equatorial', *Advances in Space Research*, vol. 22, no. 6, pp. 811-4.

FAA (1997), Specification for the wide-area augmentation system, FAA-E-2892C (draft),

Featherstone, W. E. and Stewart, M. P. (2001) 'Combined analysis of real-time kinematic GPS equipment and its users for height determination', *Journal of Surveying Engineering*, vol. 127, no. 2, pp. 31-51, May.

Fedrizzi, M., Langley, R. B., Komjathy, A., Santos, M. C., De Paula, E. R. and Kantor, I. J. (2001) 'The low-latitude ionosphere: Monitoring its behavior with GPS', Proceedings of ION GPS-2001, 14th International Technical Meeting of The Satellite Division of The Institute of Navigation, Salt Lake City, Utah, 11th 14th September.

Fees, W. A. and Stephens, S. G. (1986) 'Evaluation of GPS Ionospheric Time Delay Algorithm for Single-Frequency Users', Proceedings of Position Location & Navigation Symposium - PLANS 1986, Las Vegas, Nevada, 4-7 November, pp. 206-13.

Feltens, J. and Schaer, S. (1998) 'IGS products for the ionosphere, IGS position paper', Proceedings of The IGS Analysis Center Workshop, ESOC, Darmstadt, Germany, 9th-11th February.

Feng, Y., Zhou, N. and Enderle, W. (2003) 'FedSat orbit determination: Results from daily GPS flight code observations', Proceedings of The 6th International Symposium on Satellite Navigation Technology Including Mobile Positioning and Location Services, Melbourne, Australia, 22nd-25th July.

Fletchner, F., Bedrich, S. and Teubel, A. (1997) 'Modeling the ionosphere with PRARE', Proceedings of The 3rd ERS Scientific Symposium (ESA SP-414), Florence, Italy, March.

Flight Safety Australia (2007) 'GPS Augmentation - The debate intensifies', <http://www.casa.gov.au/fsa/2007/feb/34-37.pdf>, accessed June, 2007

Fotopoulos, G. and Cannon, M. E. (2001) 'An overview of multireference station methods for cm-level positioning', *GPS Solutions*, vol. 4, no. 3, pp. 1-10.

Fox, M. W. and McNamara, L. F. (1988) 'Improved world-wide maps of monthly median foF2', *Journal of Atmospheric and Solar-Terrestrial Physics*, vol. 50, no. 12, pp. 1077-86.

Frei, E. (1991) 'Rapid differential positioning with the Global Positioning System', PhD thesis, University of Berne, Switzerland,

Frei, E. and Beutler, G. (1990) 'Rapid static positioning based on the fast ambiguity resolution approach 'FARA': theory and first results', *Manuscripta Geodaetica*, vol. 15, no. 4, pp. 325-56.

Fu, W., Han, S. and Rizos, C. (1999) 'Real-Time ionospheric scintillation monitoring', Proceedings of ION GPS-1999, 12th International Technical Meeting of The Satellite Division of The Institute of Navigation, Nashville, Tennessee, 14th-17th September.

Gao, Y. and Li, Z. (1998) 'Ionospheric effect and modelling for regional area differential GPS network', Proceedings of ION GPS-1998, 11th International Technical Meeting of The Satellite Division of The Institute of Navigation, Nashville, Tennessee, 15th-18th September, pp. 91-7.

Gao, Y. and Liu, Z. Z. (2002) 'Precise Ionospheric Modeling Using Regional GPS Network Data', *Journal of Global Positioning Systems*, vol. 1, no. 1, pp. 18-24.

Gao, Y., Heroux, P. and Kouba, J. (1994) 'Estimation of GPS receiver and satellite L1/L2 signal delay biases using data from CACS', *Proceedings of KIS-94*, 30th August-2nd September.

Geoforschungszentrum (2007) 'PRARE', <http://www.gfz-potsdam.de/pb1/op/prare/>, accessed June, 2007

GEONET (2007) 'Japan's CORS network (GEONET)', <http://mekira.gsi.go.jp/ENGLISH>, accessed May, 2007

Georgiadou, Y. and Kleusberg, A. (1988a) 'On the Effect of Ionospheric Delay on Geodetic Relative GPS Positioning', *Manuscripta Geodaetica*, vol. 13, no. 1, pp. 1-8.

Georgiadou, Y. and Kleusberg, A. (1988b) 'On carrier signal multipath effects in relative GPS positioning', *Manuscripta Geodaetica*, vol. 13, no. 3, pp. 172-9.

Geoscience Australia (2007) 'AUSPOS - Online GPS Processing Service', <http://www.ga.gov.au/bin/gps.pl>, accessed June, 2007

GLONASS (2007) 'Russian Space Agency', <http://www.glonass-ianc.rsa.ru/pls/htmldb/f?p=202:1:16454225462906441435>, accessed June, 2007

Gordini, C., Kealy, A., Grgich, P. M. and Hale, M. (2006) 'Testing and evaluation of a GPS CORS network for real time centimetric positioning - The Victorian GPSnet', Proceedings of The International Global Navigation Satellite Systems Society - IGNSS Symposium 2006, Surfers Paradise, Australia, 17th-21 July.

Gorney, D. J. (1990) 'Solar cycle effects on the near earth space environment', *Reviews of Geophysics*, vol. 28, no. 1, pp. 315-36, February.

GRACE (2007) 'Gravity Recovery and Climate Experiment', <http://www.csr.utexas.edu/grace>, accessed May 2007.

Grejner-Brzezinska, D., Kashani, I. and Wielgosz, P. (2005b) 'On the accuracy and reliability of instantaneous network RTK as a function of network geometry, station seperation, and data processing strategy', *GPS Solutions*, vol. 9, no. 3, pp. 179-93.

Grejner-Brzezinska, D., Wielgosz, P., Kashani, I., Smith, D. A., Spencer, P. S. J., Robertson, D. S. and Mader, G. L. (2004) 'An analysis of the effects of different network-based ionospheric estimation models on rover positioning accuracy', *Journal of Global Positioning Systems*, vol. 3, no. 1-2, pp. 115-31.

Grejner-Brzezinska, D., Wielgosz, P., Kashani, I., Smith, D. A., Spencer, P. S. J., Robertson, D. S. and Mader, G. L. (2005a) 'The impact of the external ionospheric models on the accuracy of RTK position', Proceedings of The Institute of Navigation National Technical Meeting, San Diego, California, 24th-26th January, pp. 462-70.

Grejner-Brzezinska, D., Wielgosz, P., Kashani, I., Smith, D. A., Robertson, D. S., Mader, G. L. and Komjathy, A. (2006) 'The impact of severe ionospheric conditions on the accuracy of kinematic position estimation: Performance analysis of various ionospheric modeling techniques', *NAVIGATION : Journal of the Institute of Navigation*, vol. 53, no. 3, pp. 203-17, Fall.

Grejner-Brzezinska, D., Kashani, I., Wielgosz, P., Smith, D. A., Spencer, P. S. J., Robertson, D. S. and Mader, G. L. (2007) 'Efficiency and reliability of ambiguity resolution in network-based real-time kinematic GPS', *Journal of Surveying Engineering*, vol. 133, no. 2, pp. 56-65.

Gu, M. and Brunner, F. K. (1990) 'Theory of the two frequency dispersive range correction', *Manuscripta Geodaetica*, vol. 15, pp. 357-61.

Hajj, G. A. and Romans, L. J. (1998) 'Ionospheric electron density profiles obtained with the global positioning system: Results from the GPS/MET experiment', *Radio Science*, vol. 33, no. 1, pp. 175-90, Jan-Feb.

Hale, M. (2000) 'The next decade', Proceedings of The Survey Conference of the Institute of Surveyors Victoria and the Institute of Engineering Surveyors Australia, Victoria Division, 27th May.

Hale, M., Collier, P. and Kealy, A. (2005) 'Developing a model for CORS network management', Proceedings of The International Symposium on GPS/GNSS 2005, Hong Kong, China.

Hall, M. P. M., Barclay, L. W. and Hewitt, M. T. (1996) '*Propagation of radio waves*', The Institute of Electrical Engineers, London.

Han, S. (1997) 'Carrier phase-based long-range GPS kinematic positioning', PhD thesis, UNISURV S-49, School of Geomatic Engineering, The University of New South Wales, Sydney, Australia, 185 pages.

Han, S. and Rizos, C. (1996) 'GPS network design and error mitigation for real-time continuous array monitoring systems', Proceedings of ION GPS-1996, 9th International Technical Meeting of The Satellite Division of The Institute of Navigation, Kansas City, Missouri, 17th-20th September.

Hankemeir, P. (1996) 'The DGPS service for the FRG - concept and status', *Freie und Hansestadt Hamburg Baudehoerde Vermessungsamt, 20302 Hamburg Postfach 300580 Germany*,

Hansen, A. (1998) 'Real time ionospheric tomography using terrestrial GPS sensors', Proceedings of ION GPS-1998, Nashville, Tennesee, 15th-18th September, pp. 717-28.

Hansen, A., Walter, T. and Enge, P. (1997) 'Ionospheric correction using tomography', Proceedings of ION GPS-1997, 10th International Technical Meeting of The Satellite Division of The Institute of Navigation, Kansas City, Missouri, 16th-19th September.

Hansen, A., Blanch, J., Walter, T. and Enge, P. (2000) 'Ionospheric Correlation Analysis for WAAS: Quiet and Stormy', Proceedings of ION GPS-2000, 13th International Technical Meeting of The Satellite Division of The Institute of Navigation, Salt Lake City, Utah, Sept. 19-22.

Hargreaves, J. K. (1995) '*The Solar-Terrestrial Environment*', Press Syndicate of the University of Cambridge, Cambridge, USA.

Hartmann, G. K. and Leitinger, R. (1984) 'Range errors due to ionospheric and tropospheric effects for signal frequencies above 100 MHz', *Bulletin Geodesique*, vol. 58, pp. 109-36.

Hatch, R. (1990) '*Instantaneous ambiguity resolution'*, Proceedings of IAG International Symposium 107 on Kinematic Systems in Geodesy, Surveying and Remote Sensing, Springer Verlag, New York.

Heise, S., Jakowski, N., Wehrenpfennig, A., Reigber, C. and Luhr, H. (2002) 'Sounding of the topside ionosphere/plasmasphere based on GPS measurements from CHAMP: Initial results', *Geophysical Research Letters*, vol. 29, no. 14.

Henson, D. J. and Collier, E. A. (1986) 'Effects of the Ionosphere on GPS Relative Geodesy', Proceedings of PLANS 1986 - Position Location & Navigation Symposium, Las Vegas, Nevada, Nov 4-7, pp. 230-7.

Hernandez-Pajares, M. (2003), Performance of IGS ionosphere TEC maps, IGS Working Group, March, pp16.

Hernandez-Pajares, M., Juan, J. M. and Sanz, J. (1999) 'Precise Ionospheric Determination and its Application to Real-Time GPS Ambiguity Resolution', Proceedings of ION GPS-1999, 12th International Technical Meeting of The Satellite Division of The Institute of Navigation, Nashville, Tennessee, Sept. 14-17.

Hernandez-Pajares, M., Juan, J. M. and Sanz, J. (2001) 'Tomographic modelling of GNSS ionospheric corrections: Assessment and real-time applications', Proceedings of ION GPS-2001, 14th International Technical Meeting of The Satellite Division of The Institute of Navigation, Salt Lake City, Utah, 11th-14th September, pp. 2507-15.

Hernandez-Pajares, M., Juan, J. M., Sanz, J. and Colombo, O. L. (2000) 'Application of ionospheric tomography to real-time GPS carrier phase ambiguity resolution, at scales of 400-1000km and with high geomatic activity', *Geophysical Research Letters*, vol. 27, no. 13, pp. 2009-12, July.

Higgins, M. (2002) 'Australia's changing surveying infrastructure from marks in the ground to virtual reference stations', Proceedings of The FIG XXII International Congress, Washington, 19th-26th April.

Higgins, M. B. (2001) 'An Australian pilot project for a real time kinematic GPS network using the virtual reference station concept', Proceedings of The FIG Working Week 2001, International Federation of Surveyors (FIG), Seoul, Korea, 6th-11th May.

Hill, C. D. (1999) 'A method for combining satellite positioning and terrestrial surveying', PhD thesis, Department of Land Information, RMIT University, Melbourne, Australia, 173 pages.

Ho, C. M., Wilson, B. D., Mannucci, A. J., Lindqwister, U. J. and Yuan, D. N. (1997) 'A comparative study of ionospheric total electron content measurements using global ionospheric maps of GPS, TOPEX radar, and the Bent model', *Radio Science*, vol. 32, no. 4, pp. 1499-512, July-August.

Hofmann-Wellenhof, B., Lichtenegger, H. and Collins, J. (1997) '*Global Positioning System: Theory and Practice'*, 4th edn, Springer-Verlag, Wien, New York.

Holden, L. (2002) 'The characterisation and quantification of GPS multipath error', MApps.Sci thesis, Department of Geospatial Science, RMIT University, Melbourne,

Howe, B. M. (1997) '4-D simulations of ionospheric tomography', Proceedings of The Institute of Navigation National Technical Meeting, Santa Monica, California, 14th-16th January.

Hungentobler, U., Schaer, S. and Fridez, P. (eds) (2001) 'Bernese GPS Software Version 4.2', Astronomical Institute, University of Berne, 515 p.

Hunsucker, R. D. (1991) '*Radio techniques for probing the terrestrial ionosphere*', Springer-Verlag, New York.

Huo, X. L., Yuan, Y. B., Ou, J. K., Wen, D. B. and Luo, X. W. (2005) 'The diurnal variations, semi-annual and winter anomalies of the ionospheric TEC based on GPS data in China', *Prog. Nat. Sci.*, vol. 15, no. 56-60.

ICAO (2002) 'International standards and recommended practices (SARPS), aeronautical telecommunications', Proceedings of The Convention on International Civil Aviation, Annex 10, vol.1, ICAO, November, 2002.

IGS (2007) 'The International GNSS Service', <http://igscb.jpl.nasa.gov/>, accessed January, 2007

IRI (2007) 'International Reference Ionosphere 2001-software', <http://nssdc.gsfc.nasa.gov/space/model/ionos/iri.html>, accessed February, 2007

Ivanov-Kholodnyi, G. S. and Mikhailov, A. V. (1986) '*The prediction of ionospheric conditions*', Kluwer Academic, Norwell, Massachusetts, USA.

Janes, H. W. (1991) 'An error budget for GPS relative positioning', *Surveying and Land Information Systems*, vol. 51, no. 3, pp. 133-7.

Jones, W. B. and Gallet, R. M. (1962) 'Representation of diurnal and geographical variations of ionospheric data by numerical methods', *Telecommunication Journal*, vol. 29, pp. 129-49.

Jones, W. B. and Obitts, D. L. (1970), Global representation of annual and solar cycle variations of foF2 monthly median 1954-1958, Telecommunications Special Report, OT/ITS/RR3, US Government Printing Office, Washington DC, USA,

Jones, W. B., Graham, R. P. and Leftin, M. (1969), Advances in ionospheric mapping by numerical methods, ESSA Technical Report ERL 107-ITS 75, Washington DC, USA, US Government Printing Office.

Jonsson, B. (2002) 'National report from Sweden to the meeting of the International Information Subcommittee in Brussels', *Geodetic Research Division*, Gavle, Sweden,

Joosten, P., Pany, T. and Winkel, J. (2002) 'The impact of unmodelled multipath on ambiguity resolution', Proceedings of ION GPS-2002, 15th International Technical

Meeting of The Satellite Division of The Institute of Navigation, Portland, Oregon, 24th-27th September, pp. 953-61.

Kalafus, R. and Van Dierendonck, K. (2003) 'The new RTCM SC-104 standard for differential and RTK GNSS broadcasts', Proceedings of ION GPS/GNSS-2003, 16th International Technical Meeting of The Satellite Division of The Institute of Navigation, Portland, Oregon, 9th-12th September, pp. 741-7.

Kashani, I., Wielgosz, P. and Grejner-Brzezinska, D. (2004a) 'The double difference effect of ionospheric correction latency on instantaneous ambiguity resolution in long range RTK', Proceedings of ION GNSS-2004, 17th International Technical Meeting of The Satellite Division of The Institute of Navigation, Long Beach California, 21st-24th September, pp. 2881-90.

Kashani, I., Grejner-Brzezinska, D. and Wielgosz, P. (2004b) 'Towards instantaneous network-based RTK GPS over 100km distance', Proceedings of the ION 60th Annual Meeting, Dayton, Ohio, 7th-9th June.

Kee, C. (1996) 'Wide area differential GPS', *Global Positioning System: Theory and Applications*, Parkinson, B. W. & Spilker, J. J. (eds), American Institute of Aeronautics and Astronautics, Washington, vol. 2, pp. 81-114.

Kelley, M. C. (1989) '*The Earth's ionosphere: plasma physics and electrodynamics'*, Academic Press, San Diego, USA.

Kim, E., Walter, T. and Powell, J. D. (2006) 'Optimizing WAAS accuracy/stability for a single frequency receiver', Proceedings of ION GPS/GNSS-2003, 16th International Technical Meeting of The Satellite Division of The Institute of Navigation, Fort Worth, Texas, 26th-29th September.

Kleusberg, A. (1986) 'Ionospheric Propagation effects in Geodetic Relative GPS Positioning', *Manuscripta Geodaetica*, vol. 11, no. 4, pp. 256-61.

Kleusberg, A. (1990) 'Comparing GPS and GLONASS', *GPS World*, vol. 1, no. 6, pp. 52-4, November/December.

Kleusberg, A. and Teunissen, P. J. G. (1996) '*Lecture notes in Earth sciences: GPS for geodesy'*, Springer.

Klobuchar, J. A. (1978), Ionospheric effects on satellite navigation and air traffic control systems, National Technical Information Service, Virginia,

Klobuchar, J. A. (1986) 'Design and Characteristics of the GPS Ionospheric Time Delay Algorithm for Single Frequency Users', Proceedings of PLANS - Position Location & Navigation Symposium, Las Vegas, Nevada, Nov. 4-7, pp. 280-6.

Klobuchar, J. A. (1996) 'Ionospheric effect on GPS', *Global Positioning System: Theory and Applications*, Parkinson, B. W. & Spilker, J. J. (eds), American Institute of Aeronautics and Astronautics, Washington, vol. 1, pp. 485-515.

Klobuchar, J. A. and Doherty, P. H. (1992) 'The correlation of daily solar flux values with total electron content', Proceedings of The International Beacon Satellite Symposium, Massachusetts Institute of Technology, Cambridge, Massachusetts, USA,pp. 192-5.

Kohnlein, W. (1978) 'Electron density models of the ionosphere', *Reviews of Geophysics and Space Physics*, vol. 16, no. 3, pp. 341-54.

Komjathy, A. (1997) 'Global ionospheric total electron content mapping using the global positioning system', PhD dissertation thesis, Department of Geodesy and Geomatics Engineering, University of New Brunswick, Fredericton, New Brunswick, Canada, 248 pages.

Komjathy, A. and Langley, R. B. (1996) 'The effect of Shell Height on High Precision Ionospheric Modelling Using GPS', Proceedings of the 1996 IGS Workshop, Silver City, MD, 19-21 March, pp. 193-203.

Kouris, S. S. and Muggleton, L. M. (1973a) 'Diurnal variation in the E-layer ionisation', *Journal of Atmospheric and Solar-Terrestrial Physics*, vol. 35, pp. 133-9.

Kouris, S. S. and Muggleton, L. M. (1973b), A proposed prediction method for monthly median foE, No. 6/3/07 to Interim Working Party 6/3, CCIR Report 252-2,

Kubo, N. and Tasuda, A. (2003) 'How multipath error influences on ambiguity resolution', Proceedings of ION GPS/GNSS-2003, 16th International Technical Meeting of The Satellite Division of The Institute of Navigation, Portland, Oregon, 9th-12th September, pp. 2142-50.

Kunches, J. M. (2000) 'In the teeth of cycle 23', Proceedings of ION GPS-2000, 13th International Technical Meeting of The Satellite Division of The Institute of Navigation, Salt Lake City, Utah, 19th-22nd September.

Kunitsyn, V. E. and Tereshchenko, E. (2003) '*Ionospheric tomography*', 1 edn, Springer-Verlag, Berlin Heidelberg, Germany.

Lachapelle, G. and Cannon, E. (1986) 'Single and Dual Frequency GPS results for Baselines of 10km to 500km', Proceedings of The 4th International Geodetic Symposium on Satellite Positioning, Austin, Texas, April 28-May 2.

Land Victoria (2007) 'GPSnet base station information', <http://www.land.vic.gov.au/land/lcnlc2.nsf/Home+Page/Land+Channel~Home+Page?open>, accessed March, 2007

Langley, R. B. (1984), Studies in the application of GPS to differential positioning, Technical Report 108, University of New Brunswick,

Langley, R. B. (1996) 'Propagation of GPS signals', *Lecture Notes in Earth Sciences*, Teunissen, A. K. P. J. G. (ed.), Springer, Berlin, New York, vol. 60,

Langley, R. B. (1998) 'Propagation of GPS signals', *GPS for Geodesy*, Teunissen, P. J. G. & Kleusberg, A. (eds), Springer-Verlag, Berlin, pp. 111-43.

Lechner, W., Reigber, C. and Herbert, W. (1989) 'The precise range and range rate equipment PRARE: System description and future perspectives', Proceedings of ION GPS-1989, 2nd International Technical Meeting of The Satellite Division of The Institute of Navigation, Colorado Springs, Colorado, 27th-29th September, pp. 67-70.

Leica Geosystems White Paper (2005) 'Networked Reference Stations - Take it to the MAX', <http://www.leica-geosystems.com/corporate/en/lgs_405.htm>, accessed March, 2007

Leick, A. (2004) '*GPS satellite surveying*', 3rd edn, Wiley, New York.

Leitinger, R., Hartmann, G. K., Lohmar, F. J. and Putz, E. (1984) 'Electron content measurement with geodetic doppler receivers', *Radio Science*, vol. 19, no. 3, pp. 789-97.

Lin, L. and Rizos, C. (1996) 'An Algorithm to Estimate GPS Satellite & Receiver L1/L2 Differential Delays and its Application to Regional Ionospheric Modeling', *Geomatics Research Australasia*, vol. 65, pp. 1-26, December.

Lin, M. (2005) 'RTCM 3.0 implementation in South Alberta network', Proceedings of ION GNSS-2005, 18th International Technical Meeting of The Satellite Division of The Institute of Navigation, Long Beach, California, 13th-16th September, pp. 2540-51.

Liu, R. Y., Smith, P. A. and King, J. W. (1983) 'A new solar index which leads to improved foF2 predictions using the CCIR atlas', *Telecommunication Journal*, vol. 50, no. 8.

Liu, Z. (2003) 'Development and analysis of a new ionospheric model', Proceedings of ION GPS/GNSS-2003, 16th International Technical Meeting of The Satellite Division of The Institute of Navigation, Portland, Oregon, 9th-12th September.

Liu, Z. and Gao, Y. (2004) 'Ionospheric TEC predictions over a local area GPS reference network', *GPS Solutions*, vol. 8, no. 1, pp. 23-9, April.

Liu, Z., Skone, S., Gao, Y. and Komjathy, A. (2005) 'Ionospheric modelling using GPS data', *GPS Solutions*, vol. 9, no. 4, pp. 63-6, April.

Liu, Z. Z. and Gao, Y. (2001) 'Ionospheric tomography using GPS measurements', Proceedings of KIS-2001, Banff, Alberta, Canada, 5th-8th June.

Luo, M., Pullen, S., Dennis, J., Konno, H., Xie, G., Walter, T. and Enge, P. (2003) 'LAAS ionosphere spatial gradient threat model and impact of LGF and airborne monitoring', Proceedings of ION GPS/GNSS-2003, 16th International Technical Meeting of The Satellite Division of The Institute of Navigation, Portland, Oregon, 9th-12th September, pp. 2255-74.

Luton, G. (2003) 'GPSnet data processing report, June 2002 data set', *Space Geodesy Analysis Center, National Mapping Division, Geoscience Australia*, 17th January.

Makridakis, S., Wheelwright, S. C. and Hyndman, R. J. (1998) '*Forecasting: methods and applications'*, 3rd edn, John Wiley & Sons, New York.

Mannucci, A. J., Wilson, B. D. and Edwards, C. D. (1993) 'A New Method for Monitoring The Earth's Ionospheric Total Electron Content Using the GPS Global Network', Proceedings of ION GPS-1993, 6th International Technical Meeting of The Satellite Division of The Institute of Navigation, Salt Lake City, Utah, 22nd-24th September, pp. 1323-32.

McNamara, L. F. (1984) 'Prediction of total electron content using the International Reference Ionosphere', *Advances in Space Research*, vol. 4, no. 1, pp. 25-50.

McNamara, L. F. (1985) 'The use of total electron content measurements to validate empirical models of the ionosphere', *Advances in Space Research*, vol. 5, no. 7, pp. 81-90.

McNamara, L. F. (1991) '*The ionosphere: communications, surveillance, and direction finding'*, FL : Krieger Pub. Co, Malabar.

McNamara, L. F. and Wilkinson, O. J. (1983) 'Prediction of total electron content using the International Reference Ionosphere', *Journal of Atmospheric and Solar-Terrestrial Physics*, vol. 45, no. 2/3, pp. 169-74.

McPherson, K. W. (2006) 'GRAS phases 1 and 2 development', IGNSS Symposium-2006, Surfers Paradise Australia, 17th-21st July.

Melbourne, W., Davis, E., Duncan, C., Hajj, G. A., Hardy, K., Kursinski, E., Meehan, T. and Young, L. (1994), The application of spacebourne GPS to atmospheric limb sounding and global change monitoring, Publication 94-18, Jet Propulsion Laboratory, Pasadena, California,

Mervart, L. (1995) 'Ambiguity resolution techniques in geodetic and geodynamic applications of the Global Positioning System', PhD thesis, Vol. 53 of Geodatisch-geophysikalische Arbeiten in der Schweiz, Schweizerische Geodatische Kommission.

Millner, J., Asmussen, H. and Andreola, R. (2006) 'Delivery of networked GPS corrections for machinery guidance', Proceedings of The 4th International Controlled Traffic Farming Conference, The University of Ballarat, Victoria, Australia, 27th-29th September.

Mosert, M., Ezquer, R. and Jadur, C. (2000) 'On the critical frequency and height of the E layer peak at noon', *Advances in Space Research*, vol. 25, no. 1, pp. 69-72.

Murphy, T., Ackland, J., Imrich, T., Lapp, T. and Friedman, R. (2006) 'Approach with precision - Ground augmentation proves out', *GPS World*, September, 2006.

Namie, H., Hagiwara, N., Kim, H., Nitta, N., Shibahara, Y., Imakiire, T. and Yasuda, A. (2001) 'RTK-GPS positioning in Japan by virtual reference station (VRS) system with GPS-based control stations', Proceedings of ION GPS-2001, 14th International Technical Meeting of The Satellite Division of The Institute of Navigation, Salt Lake City, Utah, 11th-14th September.

NCRIS (2007) 'National Collabrative Research Infrastructure Strategey', Geospatial Working Groups Draft Proposal, <http://www.ncris.dest.gov.au/>, accessed May 2007.

Newby, S. P. and Langley, R. B. (1992) 'Three Alternative Empirical Ionospheric Models - Are They Better Than The GPS Broadcast Model?' Proceedings of The 6th International Geodetic Symposium on Satellite Positioning, Columbus, Ohio, 17th-20th March, pp. 240-4.

Nichols, J., Hansen, A., Walter, T. and Enge, P. (1999) 'Observations of equatorial scintillation using GPS receivers', Proceedings of ION GPS-1999, 12th International Technical Meeting of The Satellite Division of The Institute of Navigation, Nashville, Tennessee, 14th-17th September.

Odijk, D. (2002) 'Fast precise GPS positioning in the presence of ionospheric delays', PhD thesis, Mathematical Geodesy and Positioning, Delft University of Technology, Delft, The Netherlands, 242 pages.

Ohanian, H. C. (1989) '*Physics*', 2 edn, Penguin Books Canada Ltd.

Pakula, W. A., Fougere, P. F., Klobuchar, J. A., Kuenzler, H. J., Buonsanto, M. J., Roth, J. M. and Foster, J. C. (1995) 'Tomographic reconstruction of the ionosphere over North America with comparisons to ground-based radar', *Radio Science*, vol. 30, no. 1, pp. 89-103.

Pandey, V. K., Sethi, N. K. and Mahajan, K. K. (2000) 'Comparing IRI E-Region peak height (hmE) with incoherent scatter data', *Advances in Space Research*, vol. 25, no. 1, pp. 65-8.

Parkinson, B. W. and Enge, P. (1996) 'Differential GPS', *Global Positioning System: Theory and Applications*, Parkinson, B. W. & Spilker, J. J. (eds), American Institute of Aeronautics and Astronautics, Washington, vol. 2, pp. 3-49.

Penna, N., Lo, J. and Luton, G. (2005) 'Geodetic GPS analysis of land Victoria's GPSnet', *Journal of Spatial Science*, vol. 50, no. 1, pp. 45-57, June, 2005.

Piggott, W. R. and Rawer, K. (1972), Handbook of ionogram interpolation and reduction, 2nd edition, Report UAG-23, World Data Center for Solar-Terrestrial Physics, NOAA, Boulder, Colorado, USA,

Piggott, W. R. and Rawer, K. (1978), Handbook of ionogram interpolation and reduction, 2nd edition, World Data Center for Solar-Terrestrial Physics, NOAA, Boulder, Colorado, USA, (revisions of chapters 1-4),

Pullen, S., Walter, T. and Enge, P. (2002) 'System Overview, Recent Developments, and Future Outlook for WAAS and LAAS', Proceedings of The Tokyo University of Mercantile Marine GPS Symposium, Tokyo, Japan, 11th-13th November.

Ramakrishnan, S. and Rawer, K. (1972) 'Model electron density profiles obtained by empirical procedures', *Space Research XII*, Akademie-Verlag, Berlin, p. 1253–61.

Raquet, J. F. (1998) 'Development of a method for kinematic GPS carrier phase ambiguity resolution using multiple reference receivers', PhD thesis, Department of Geomatics Engineering, University of Calgary, Calgary, Canada, 282 pages.

Rawer, K. and Bilitza, D. (1990) 'International Reference Ionosphere - Plasma Densities', *Advances in Space Research*, vol. 10, no. 8, pp. 5-14.

Rawer, K., Ramakrishnan, S. and Bilitza, D. (1978), International Reference Ionosphere 1978, Special Report, International Union of Radio Science, Brussels, Belgium,

Rawer, K., Lincoln, J. V. and Conkright, R. O. (1981), International Reference Ionosphere IRI-79, Report UAG-82, World Data Center for Solar-Terrestrial Physics, Boulder, Colarado,

Raymund, T. D., Bresler, Y., Anderson, D. N. and Daniell Jr., R. E. (1994) 'Model-assisted ionospheric tomography: A new algorithm', *Radio Science*, vol. 29, pp. 1493-512.

Raymund, T. D., Austen, J. R., Franke, S. J., Liu, C. H., Klobuchar, J. A. and Stalker, J. (1990) 'Application of computerised tomography to the investigation ionospheric structures', *Radio Science*, vol. 25, pp. 771-89.

Reigber, C., Luhr, H. and Schwintzer, P. (2000) 'CHAMP mission status and perspectives', *EOS Transactions, American Geophysical Union*, vol. 81, no. 48.

Retscher, G. (2002) 'Accuracy performance of virtual reference station (VRS) networks', *Journal of Global Positioning Systems*, vol. 1, no. 1, pp. 40-7.

Revnivykh (2006) 'GLONASS status update', Power Point Presentation, First Meeting of the International Committee on Global Navigation Satellite Systems (ICG), Vienna International Center, 1st-2nd November.

Rishbeth, H. and Garriott, O. K. (1969) '*Introduction to ionospheric physics*', Academic Press, New York.

Rizos, C. (2002) 'Network RTK research and implementation: A geodetic perspective', *Journal of Global Positioning Systems*, vol. 1, no. 2, pp. 144-50.

Rizos, C. (2003) 'Trends in GPS Technology and Applications', <www.gmat.unsw.edu.au/snap/publications/rizos_2003b.pdf>, accessed January, 2007

Rizos, C. (2007) 'Alternatives to current GPS-RTK services and some implications for CORS infrastructure and operations', *GPS Solutions*, vol. 11, no. 3, pp. 151-8, July.

Rizos, C. and Han, S. (2003) 'Reference station network based RTK systems-concepts and progress', *Wuhan University Journal of Natural Sciences*, vol. 8, no. 2B, pp. 566-74.

Rizos, C., Kinlyside, D., Yan, T., Omar, S. and Musa, T. A. (2003) 'Implementing network RTK: The SydNet CORS infrastructure', Proceedings of The 6th International Symposium on Satellite Navigation Technology Including Mobile Positioning & Location Services, Melbourne, Australia, 22nd-25th July.

Roberts, C. (2006) 'GNSS and the convergence of geodesy and the cadastre in Australia', Proceedings of The XXIII FIG Congress, Munich, Germany, 8th-13th October.

Roberts, C., Zhang, K., Hale, M. and Millner, J. (2003) 'Towards real-time network-based RTK corrections for Victoria's GPSnet', Proceedings of The 6th International Symposium on Satellite Navigation Technology Including Mobile Positioning & Location Services, Melbourne, Australia, 22nd-25th July.

Roberts, C., Rizos, C., Kealy, A., Ge, L., Ramm, P., Hale, M., Kinlyside, D. and Harcombe, P. (2004) 'Improved atmospheric modelling for large scale high-precision positioning based on GNSS CORS networks in Australia', Proceedings of The 2004 International Symposium on GNSS/GPS, Sydney, Australia, 6th-8th December.

Rocken, C., Johnson, J. M. and Braun, J. J. (2000) 'Improving GPS surveying with modeled ionospheric corrections', *Geophysical Research Letters*, vol. 27, no. 23, p. 3861, 1st December.

Rocken, C., Anthes, R., Exner, M., Hunt, D., Sokolovskiy, S., Ware, R., Gorbunov, M., Schreiner, W., Feng, D., Herman, B., Kuo, Y. H. and Zou, X. (1997) 'Analysis and validation of GPS/MET data in the neutral atmosphere', *Journal of Geophysical Research*, vol. 102, pp. 29849-60.

Rothacher, M., Gurtner, W., Schaer, S., Weber, R., Schluter, W. and Hase, H. O. (1995) 'Azimuth and elevation dependent phase center corrections for geodetic GPS antennas estimated from GPS calibration campaigns', *GPS trends in precise terrestrial, airborne, and spaceborne applications, IAG Symposium No.115*, Beutler, G. (ed.), Boulder Colorado, USA, pp. 333-8.

RTCM (2007a) 'Recommended standards for differential GNSS services - Version 3.0', <http://www.rtcm.org/>, accessed June, 2007

RTCM (2007b) 'Recommended standards for differential GNSS services - Version 2.3', <http://www.rtcm.org/>, accessed June, 2007

Rush, C., Fox, M. W., Bilitza, D., Davies, K., McNamara, L. F., Stewart, F. and Pokempner, M. (1989) 'Ionospheric mapping - An update of foF2 coefficients', *Telecommunication Journal*, vol. 56, pp. 179-82.

SAC-C (2007) 'SAC-C Satellite', NASA Goddard Space Flight Centre, <http://www.gsfc.nasa.gov/gsfc/service/gallery/fact_sheets/spacesci/sac-c.htm>, accessed February 2007.

Saito, A., Fukao, S. and Miyazaki, S. (1998) 'High resolution mapping of TEC perturbations with the GSI GPS network over Japan', *Geophysical Research Letters*, vol. 25, pp. 3079-82.

Santerre, R. (1991) 'Impact of GPS satellite sky distribution', *Manuscripta Geodaetica*, vol. 16, pp. 28-53.

Schaer, S. (1997) 'How to use CODE's Global Ionosphere Maps', Astronomical Institute, University of Berne, <http://www.aiub.unibe.ch/ionosphere/gimman.ps>, accessed March, 2007

Schaer, S. (1999) 'Mapping and predicting the Earth's ionosphere using the Global Positioning System', PhD thesis, Astronomical Institute University of Berne, Bern, Switzerland,

Schaer, S. (2003) 'Personal Communication', University of Berne, Berne, Switzerland, April.

Schaer, S., Beutler, G. and Rothacher, M. (1998) 'Mapping and predicting the ionosphere', Proceedings of The IGS Analysis Center Workshop, ESOC, Darmstadt, Germany, 9th-11th February.

Schaer, S., Beutler, G., Rothacher, M. and Springer, T. A. (1996) 'Daily global ionospheric maps based on GPS carrier phase data routinely produced by the CODE analysis center', Proceedings of The IGS Worshop, Silver Springs, Maryland, USApp. 181-92.

Schempp, T., Peck, S., Chou, W., Lopez, E. and Hendrich, R. (2006) 'WAAS performance improvements as a result of WAAS expansion', Proceedings of ION GNSS-2006, 19th International Technical Meeting of The Satellite Division of The Institute of Navigation, Fort Worth, Texas, 26th-29th September, pp. 921-9.

Schneider, D., Brockman, E., Marti, U., Schlatter, A. and Wild, U. (2000) 'Introduction of a precise Swiss positioning service SWIPOS and progress in the Swiss National Height Network "LHN95"', *Subcommission for the Eurpoean Reference Frame (EUREF), National Report of Switzerland, EUREF Publication No.9*, Torres, J. A. & Hornik, H. (eds), pp. 315-22.

Schrock, G. M. (2006) 'On-grid goal: seeking support for high-precision networks', *GPS World*, vol. 17, no. 10, pp. 34-40, October.

Schunk, R. W. and Sojka, J. J. (1996) 'USU model of the global ionosphere', *Handbook of Ionospheric Models*, Schunk, R. W. (ed.), Boulder, USA, Solar-Terrestrial Energy Program (STEP), Scientific Committee on Solar Terrestrial Physics (SCOSTEP), pp. 153-71.

Schunk, R. W., (eds.), (1996), Handbook of ionospheric models, Schunk, R. W. edition, Special Report, Solar-Terrestrial Energy Program (STEP), Scientific Committee on Solar Terrestrial Physics (SCOSTEP), Boulder, USA,

Schupler, B. R. and Clark, T. A. (1991) 'How different antennas affect the GPS observable', *GPS World*, vol. 2, no. 10, November/December.

Seeber, G. (2003) '*Satellite geodesy: Foundations, methods and applications*', 2nd edn, Walter de Gruyter GmbH & Co. KG, Berlin.

Serway, R. A. (1987) '*Physics for scientists and engineers*', 2 edn, Saunders College Publishing, Philadelphia, USA.

Skone, S. (1998) 'Wide area ionospheric grid modelling in the auroral region', PhD thesis, Department of Geomatics Engineering, University of Calgary, Calgary, Canada,

Skone, S. (2000) 'Wide Area Ionosphere Modeling at Low Latitudes - Specifications and Limitations', Proceedings of ION GPS-2000, 13th International Technical Meeting of The Satellite Division of The Institute of Navigation, Salt Lake City, Utah, 19th-22nd September.

Skone, S., Yousuf, R. and Coster, A. (2004) 'Performance evaluation of the wide area augmentation system for ionospheric storm events', *Journal of Global Positioning Systems*, vol. 3, no. 1-2, pp. 251-8.

Skone, S., Coster, A., Hoyle, V. and Laurin, C. (2003) 'WAAS availability and performance at high latitudes', Proceedings of ION GPS/GNSS-2003, 16th International Technical Meeting of The Satellite Division of The Institute of Navigation, Portland, Oregon, 9th-12th September.

Snay, R. A. (2000) 'The national and co-operative CORS systems in 2000 and beyond', Proceedings of ION GPS-2000, 13th International Technical Meeting of The Satellite Division of The Institute of Navigation, Salt Lake City, Utah, 19th-22nd September, pp. 55-8.

Spaceweather (2007) 'Spaceweather - News and information about the Sun-Earth environment', <http://www.spaceweather.com/>, accessed June, 2007

Sparks, L., Komjathy, A. and Mannucci, A. J. (2002) 'Sudden ionospheric delay decorrelation and its impact on WAAS', Proceedings of The 10th International Ionospheric Effects Symposium, 7th-9th May.

Spilker, J. J. (1980) '*GPS signal structure and performance characteristics*', vol. 1, NAVIGATION, The Institute of Navigation, Alexandria.

Steed, J. and Twilley, B. (1999) 'The Australian Regional GPS Network', Proceedings of The 4th International Symposium on Satellite Navigation Technology & Applications, Brisbane, Australia, 20th-23rd July.

Takac, F., Gerdan, G. P., Lemmon, T. R. and Hailes, T. A. (1998) 'A new civilian frequency: What can surveyors expect?' *The Australian Surveyor*, vol. 43, no. 1, pp. 41-6, March.

Talaya, J. and Bosch, E. (1999) 'CATNET a permanent GPS network with real-time capacities', Proceedings of ION GPS-1999, 12th International Technical Meeting of The Satellite Division of The Institute of Navigation, Nashville, Tennessee, 14th-17th September, pp. 33-9.

Talbot, N. (1991a) 'Real-Time high precision GPS positioning concepts: modelling, processing and results', PhD thesis, Department of Land Information, Royal Melbourne Institute of Technology, Melbourne, 222 pages.

Talbot, N. (1991b) 'Sequential phase ambiguity resolution for real-time static differential GPS positioning', *Manuscripta Geodaetica*, vol. 16, pp. 274-82.

Talbot, N. (1992) 'Recent advances in GPS hardware and software', Proceedings of National Conference on GPS Surveying, University of New South Wales, Sydney, Australia, 25th-26th June, pp. 59-69.

Tascione, T. F. (1988) '*Introduction to the Space Environment*', Orbit Book Company Inc., Malabar, Florida.

Teunissen, P. J. G. (1995) 'The least-squares ambiguity decorrelation adjustment: a method for fast GPS integer ambiguity estimation', *Journal of Geodesy*, vol. 70, pp. 65-82.

Teunissen, P. J. G. (1997) 'The geometry-free GPS ambiguity search space and weighted ionosphere', *Journal of Geodesy*, vol. 71, pp. 370-83.

Teunissen, P. J. G. (1998) 'Success probability of integer GPS ambiguity rounding and bootstrapping', *Journal of Geodesy*, vol. 72, pp. 606-12.

Teunissen, P. J. G. (2003) 'Theory of carrier phase ambiguity resolution', *Wuhan University Journal of Natural Sciences*, vol. 8, no. 2B, pp. 471-84.

Teunissen, P. J. G., Joosten, P. and Tiberius, C. (2000) 'Bias robustness of GPS ambiguity resolution', Proceedings of ION GPS-2000, 13th International Technical Meeting of The Satellite Division of The Institute of Navigation, Salt Lake City, Utah, 19th-22nd September.

Thomas, J. O. and Dufour, S. W. (1965) 'Electron density in the whistler medium', *Nature*, vol. 206, p. 567.

Thomson, J. J. (1906) '*Conduction of electricity through gases*', Cambridge University Press, Cambridge.

Titheridge, J. E. (1972) 'Determination of ionospheric electron content from the faraday rotation of geostationary satellite signals', *Planetary Space Science*, vol. 20, pp. 353-69.

Titheridge, J. E. (1988) 'The real height analysis of ionograms: A generalised formulation', *Radio Science*, vol. 23, pp. 831-49.

TOPEX/Poseidon (2007) 'TOPEX/Poseidon and Jason-1', <http://sealevel.jpl.nasa.gov/mission/mission.html>, accessed May, 2007

Trimble (2005) 'Support of network formats by Trimble GPSnet network RTK solution', Trimble White Paper, <http://www.trimble.com/index.aspx>, accessed August 2006.

Trimble News Release (2007) 'Perth builds first infrastructure network with Trimble VRS technology and GNSS capabilities', <http://investor.trimble.com/releasedetail.cfm?ReleaseID=202142>, accessed June, 2007

Tsai, L. C., Tsai, W. H., Schreiner, W. S., Berkey, F. T. and Liu, J. Y. (2001) 'Comparisons of GPS/MET retrieved ionospheric electron density and ground based ionosonde data', *Earth Planets Space*, vol. 53, pp. 193-205.

van der Marel, H. (1998) 'Virtual reference stations in the Netherlands', Proceedings of ION GPS-1998, 11th International Technical Meeting of The Satellite Division of The Institute of Navigation, Nashville, Tennessee, 15th-18th September, pp. 49-58.

Van Melle, M. (1990) 'Cesium and rubidium frequency standards status and performance on the GPS program', Proceedings of ION GPS-1990, 3rd International Technical Meeting of The Satellite Division of The Institute of Navigation, Colorado Springs, Colorado, 19th-21st September, pp. 123-30.

Vollath, U., Sauer, K., Amarillo, F. and Pereira, J. (2003) 'Three or four carriers - how many are enough?' Proceedings of ION GPS/GNSS-2003, 16th International Technical Meeting of The Satellite Division of The Institute of Navigation, Portland, Oregan, 9th-12th September.

Vollath, U., Buerchl, A., Landau, H., Pagels, C. and Wagner, B. (2000a) 'Multi-Base RTK positioning using virtual reference stations', Proceedings of ION GPS-2000, 13th International Technical Meeting of The Satellite Division of The Institute of Navigation, Salt Lake City, Utah, 19th-22nd September.

Vollath, U., Buerchl, A., Landau, H., Pagels, C. and Wagner, B. (2000b) 'Long-range RTK positioning using virtual reference stations', Proceedings of ION GPS-2000, 13th International Technical Meeting of The Satellite Division of The Institute of Navigation, Salt Lake City, Utah, 19th-22nd September, pp. 1143-7.

WAAS MOPS (1999), Minimum operational performance standards for Global Positioning System / Wide Area Augmentation System airborne equipment, RTCA Inc. Document No. RTCA/D0-229B, 6th October, pp225.

Walker, J. K. (1989) 'Spherical cap harmonic modelling of high latitude magnetic activity and equivalent sources with spare observations', *Journal of Atmospheric and Solar-Terrestrial Physics*, vol. 51, no. 2, pp. 67-80.

Walter, T., Hansen, A., Blanch, J., Enge, P., Mannucci, T., Pi, X., Sparks, L., Iijima, B., Bakry El-Arinin, M., Lejeune, R., Hagen, M., Altschuler, E., Fries, R. and Chu, A. (2000) 'Robust detection of ionospheric irregularities', Proceedings of ION GPS-2000, 13th International Technical Meeting of The Satellite Division of The Institute of Navigation, Salt Lake City, Utah, 19th-22nd September.

Wang, Z., Wu, Y. and Zhang, K. (2004) 'Triple frequency method for high-order ionospheric refractive error modelling in GPS moderisation', Proceedings of The 2004 International Symposium on GNSS/GPS, Sydney, Australia, 6th-8th December.

Wanninger, L. (1993) 'Effects of equatorial ionosphere on GPS', *GPS World*, vol. 4, no. 7, pp. 48-54, July.

Wanninger, L. (1995) 'Improved ambiguity resolution by regional differential modelling of the ionosphere', Proceedings of ION GPS-1995, 8th International Technical Meeting of The Satellite Division of The Institute of Navigation, Palm Springs, California, 12th-15th September, pp. 55-62.

Wanninger, L. (1999) 'The performance of virtual reference stations in active geodetic GPS-networks under solar maximum conditions', Proceedings of ION GPS-1999, 12th International Technical Meeting of The Satellite Division of The Institute of Navigation, Nashville, Tennessee, 14th-17th September.

Wanninger, L. (2002) 'Virtual reference stations for centimeter-level kinematic positioning', Proceedings of ION GPS-2002, 15th International Technical Meeting of The Satellite Division of The Institute of Navigation, Portland, Oregon, 24th-27th September.

Wanninger, L. and May, M. (2000) 'Carrier phase multipath calibration of GPS reference stations', Proceedings of ION GPS-2000, 13th International Technical Meeting of The Satellite Division of The Institute of Navigation, Salt Lake City, Utah, 19th-22nd September.

Ward, P. W., Betz, J. W. and Hegarty, C. J. (2006) 'GPS satellite signal characteristics', *Understanding GPS: principals and applications*, Kaplan, K. & Hegarty, C. J. (eds), ARTEC HOUSE, INC, Norwood, Main, pp. 113-50.

Ware, R., Exner, M., Feng, D., Gorbunov, M., Hardy, K., Herman, B., Kuo, Y. H., Meehan, T., Melbourne, W., Rocken, C., Schreiner, W., Sokolovskiy, S., Solheim, F., Zou, X., Anthes, R., Businger, S. and Trenberth, K. (1996) 'GPS sounding of the atmosphere from low earth orbit: Preliminary results', *Bulletin of the American Meteorological Society*, vol. 77, no. 1, pp. 19-40.

Webster, I. and Kleusberg, A. (1992) 'Regional Modelling of the Ionosphere for Single Frequency Users of the Global Positioning System', Proceedings of The 6th International Geodetic Symposium on Satellite Positioning, Columbus, Ohio, 17th-20th March, pp. 230-9.

Wells, D. E., Beck, N., Delikaraoglou, D., Kleusberg, A., Krakiwsky, E. J., Lachapelle, G., Langley, R. B., Nakiboglu, M., Schwarz, K. P., Tranquilla, J. M. and Vanicek, P. (1987) '*Guide to GPS positioning*', Canadian GPS Associates, Fredericton, N.B., Canada.

White House (2000) 'White House Press Release', White House, <http://gauss.gge.unb.ca/policy/policy.html>, accessed June 2005.

Wickert, J., Reigber, C., Beyerle, G., Konig, R., Marquardt, C., Schmidt, T., Grunwaldt, L., Galas, R., Meehan, T., Melbourne, W. and Hocke, K. (2001) 'Atmospheric sounding by GPS radio occultation: First results from CHAMP', *Geophysical Research Letters*, vol. 28, p. 3263–6.

Wilson, B. D. and Mannucci, A. J. (1993) 'Instrumental biases in ionospheric measurements derived from GPS data', Proceedings of ION GPS-1993, 6th International Technical Meeting of The Satellite Division of The Institute of Navigation, Salt Lake City, Utah, 22nd-24th September, pp. 1343-51.

Wu, S., Zhang, K., Yuan, Y. and Wu, F. (2006) 'Spatio-temporal characteristics of the ionosphere TEC variation for GPSnet-based real-time positioning in Victoria', *Journal of Global Positioning Systems*, vol. 5, no. 1-2, pp. 52-7.

Wubbena, G. (1989) 'The GPS adjustment software package - GEONAP - concept and models', Proceedings of The 5th International Geodetic Symposium on Satellite Positioning, New Mexico State University, Las Cruces, New Mexico,pp. 452-61.

Wubbena, G. and Bagge, A. (2006) 'RTCM message type 59-FKP for transmission of FKP version 1.1 Geo++®, White Paper Nr.2006.01', <http://www.geopp.de/download/geopp-rtcm-fkp59-1.1.pdf>, accessed June, 2007

Wubbena, G., Bagge, A. and Schmitz, M. (2001) 'RTK networks based on Geo++ GNSMART - concepts, implementation, results', Proceedings of ION GPS-2001, 14th International Technical Meeting of The Satellite Division of The Institute of Navigation, Salt Lake City, Utah, 11th-14th September.

Wubbena, G., Bagge, A., Seeber, G., Boder, V. and Hankemeirer, P. (1996) 'Reducing distance dependant errors for real-time precise DGPS applications by establishing reference station networks', Proceedings of ION GPS-1996, 9th International Technical Meeting of The Satellite Division of The Institute of Navigation, Kansas City, Missouri, 17th-20th September.

Wyllie, S., Zhang, K. and Talbot, N. (2003) 'A comparison of ionospheric models for precise positioning in Victoria', Proceedings of The 6th International Symposium on Satellite Navigation Technology Including Mobile and Location Services - SatNav 2003, Melbourne, Australia, 22nd-25th July.

Wyllie, S., Zhang, K. and Talbot, N. (2006) 'An analysis of the temporal correlation of the ionospheric bias affecting GPS carrier phase observations', Proceedings of the International Global Navigation Satellite Systems Society - IGNSS Symposium 2006, Surfers Paradise, Australia, 17th-21 July.

Yousuf, R. and Skone, S. (2005) 'WAAS performance evaluation under increased ionospheric activity', Proceedings of ION GNSS-2005, 18th International Technical Meeting of The Satellite Division of The Institute of Navigation, Long Beach, California, 13th-16th September, pp. 2316-27.

Yousufi, S., Asmussen, H., Zhang, K. and Ramm, P. (2006) 'Diurnal variation of the Victorian GPSnet base stations', Proceedings of The International Global Navigation

Satellite Systems Society - IGNSS Symposium 2006, Surfers Paradise, Australia, 17th-21st July.

Yuan, Y. (2002) 'Study on theories and methods of correcting ionospheric delay and monitoring ionosphere based on GPS', PhD thesis, Institute of Geodesy and Geophysics, Chinese Acadamy of Sciences, Wuhan, China,

Yuan, Y. B. and Ou, J. K. (1999) 'The effects of the instrumental bias in GPS observation on determining ionospheric delays and the methods of its calibration', *Acta Geodaetica et Cartographica Sinica*, vol. 38, pp. 110-4.

Zarraoa, N., Sardon, E., Klahn, D. and Jungstand, A. (1995) 'Evaluation of GLONASS performance in practical applications: Comparison with GPS-based ionospheric TEC values', Proceedings of ION GPS-1995, 8th International Technical Meeting of The Satellite Division of The Institute of Navigation, Palm Springs, California, 12th-15th September, pp. 1031-9.

Zebhauser, B. E., Euler, H. J., Keenan, C. R. and Wubbena, G. (2002) 'A novel approach for the use of information from reference station networks conforming to RTCM V2.3 and future V3.0', Proceedings of The Institute of Navigation National Technical Meeting, San Diego, California, 28th-30th January, pp. 28-30.

Zhang, K. and Roberts, C. (2003) 'Recent development of the Victorian high precision permanent GPS tracking network with real-time positioning capability', Proceedings of The 6th International Symposium on Satellite Navigation Technology Including Mobile Positioning and Location Services, Melbourne, Australia, 22nd-25th July.

Zhang, K., Wu, F. and Wu, S. (2007) 'Towards real-time high precision state-wide GNSS positioning through developing Australian regional atmospheric models', Proceedings of the Spatial Science Institute Biennial International Conference - SSC2007, Hobart, Tasmania, Australia, 14th-18th May.

Zhang, K., Wu, F., Wu, S., Rizos, C., Roberts, C., Ge, L., Yan, T., Gordini, C., Kealy, A., Hale, M., Ramm, P., Asmussen, H., Kinlyside, D. and Harcombe, P. (2006) 'Sparse or dense: challenges of Australian network RTK', Proceedings of International Global Navigation Satellite Systems Society - IGNSS Symposium 2006, Surfers Paradise, Australia, 17th-21 July.

Appendix A: Histograms of the temporal ionosphere

September 22nd – 25th, 2001 Local time

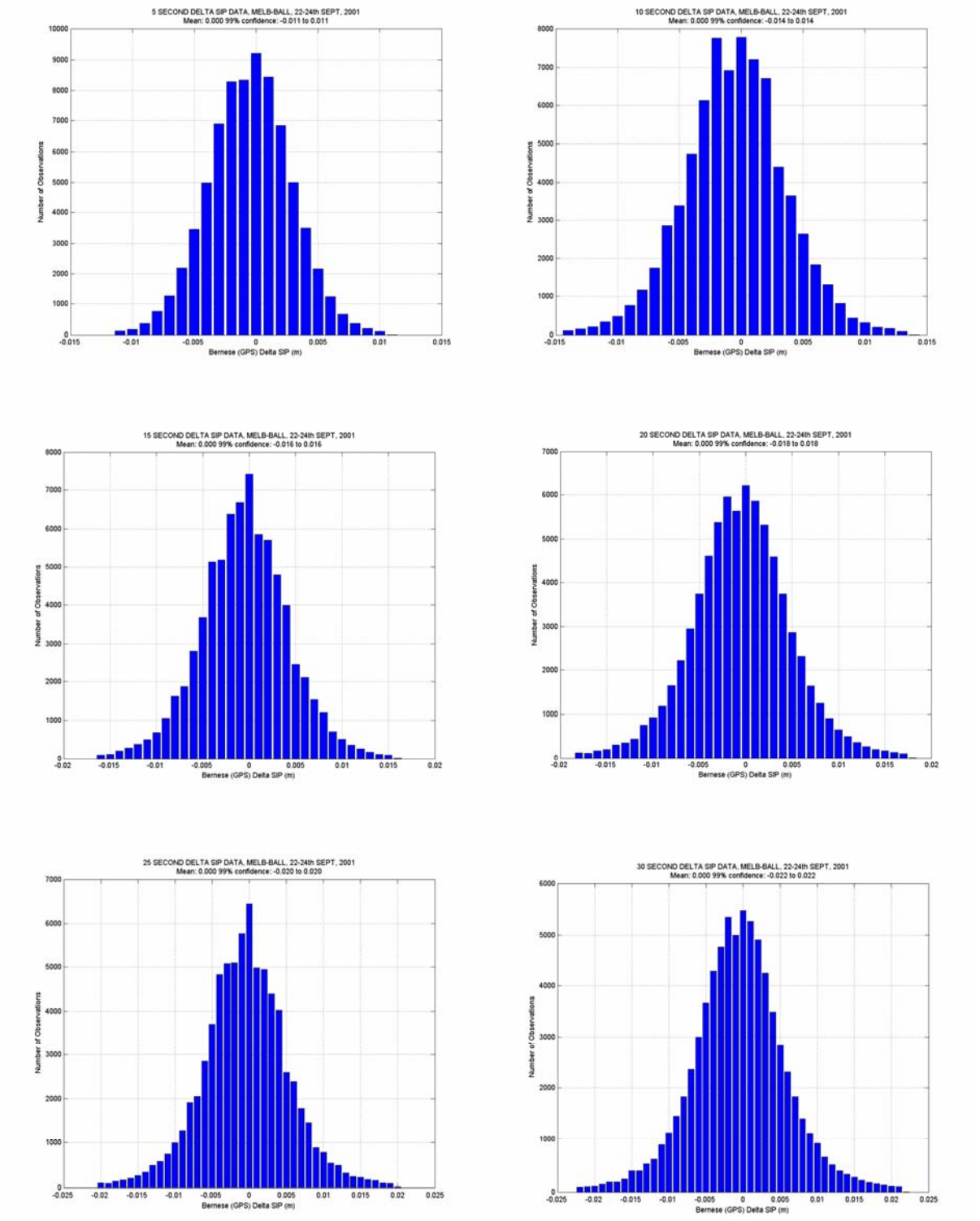

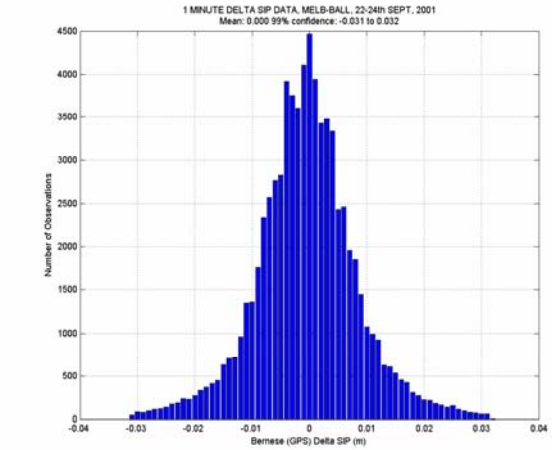
1 MINUTE DELTA SIP DATA, MELB-BALL, 22-24th SEPT, 2001
Mean: 0.000 99% confidence: -0.031 to 0.032
Number of Observations
Bernese (GPS) Delta SIP (m)

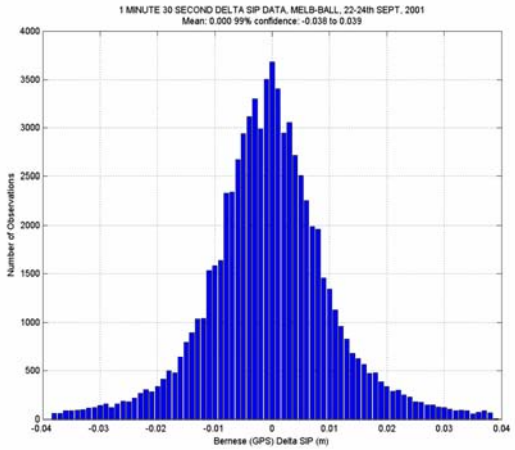
1 MINUTE 30 SECOND DELTA SIP DATA, MELB-BALL, 22-24th SEPT, 2001
Mean: 0.000 99% confidence: -0.038 to 0.039
Number of Observations
Bernese (GPS) Delta SIP (m)

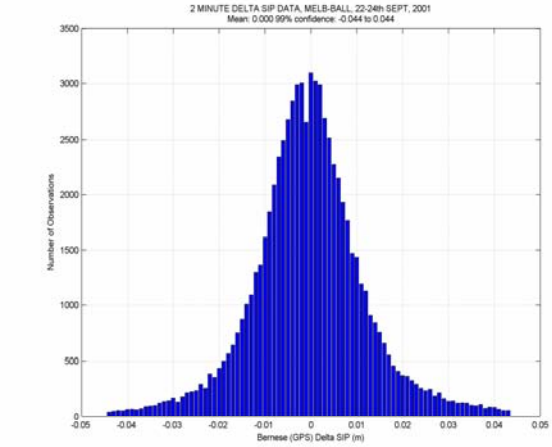
2 MINUTE DELTA SIP DATA, MELB-BALL, 22-24th SEPT, 2001
Mean: 0.000 99% confidence: -0.044 to 0.044
Number of Observations
Bernese (GPS) Delta SIP (m)

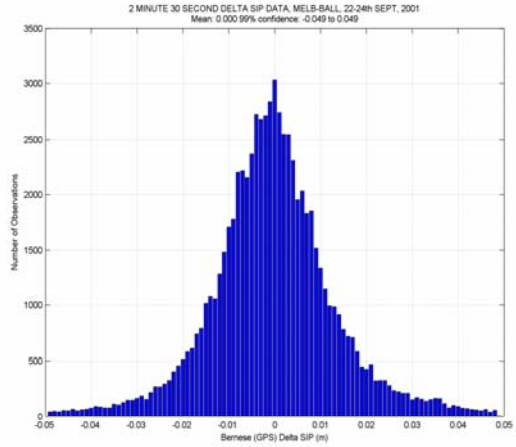
2 MINUTE 30 SECOND DELTA SIP DATA, MELB-BALL, 22-24th SEPT, 2001
Mean: 0.000 99% confidence: -0.049 to 0.049
Number of Observations
Bernese (GPS) Delta SIP (m)

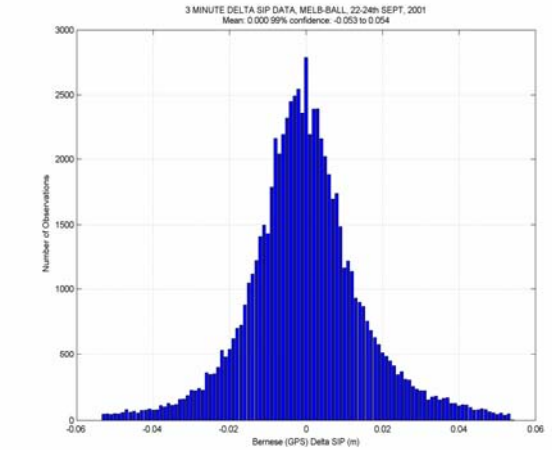
3 MINUTE DELTA SIP DATA, MELB-BALL, 22-24th SEPT, 2001
Mean: 0.000 99% confidence: -0.053 to 0.054
Number of Observations
Bernese (GPS) Delta SIP (m)

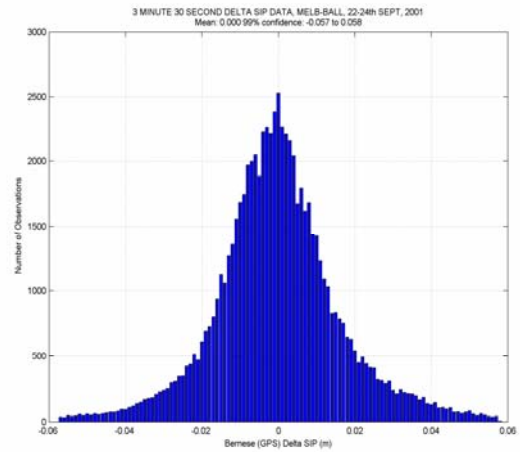
3 MINUTE 30 SECOND DELTA SIP DATA, MELB-BALL, 22-24th SEPT, 2001
Mean: 0.000 99% confidence: -0.057 to 0.058
Number of Observations
Bernese (GPS) Delta SIP (m)

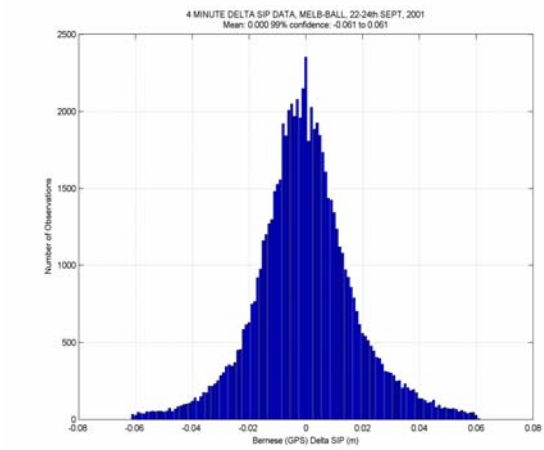
4 MINUTE DELTA SIP DATA, MELB-BALL, 22-24th SEPT, 2001
Mean: 0.000 99% confidence: -0.061 to 0.061
Number of Observations
Bernese (GPS) Delta SIP (m)

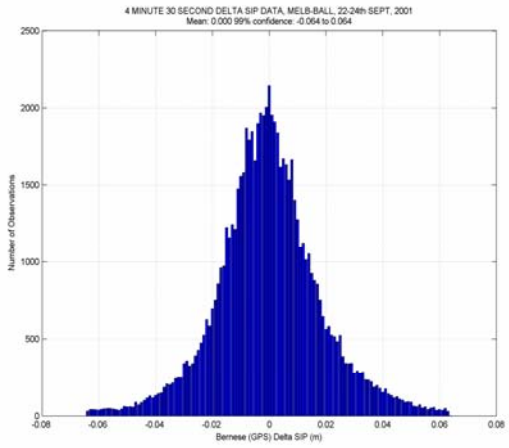
4 MINUTE 30 SECOND DELTA SIP DATA, MELB-BALL, 22-24th SEPT, 2001
Mean: 0.000 99% confidence: -0.064 to 0.064
Number of Observations
Bernese (GPS) Delta SIP (m)

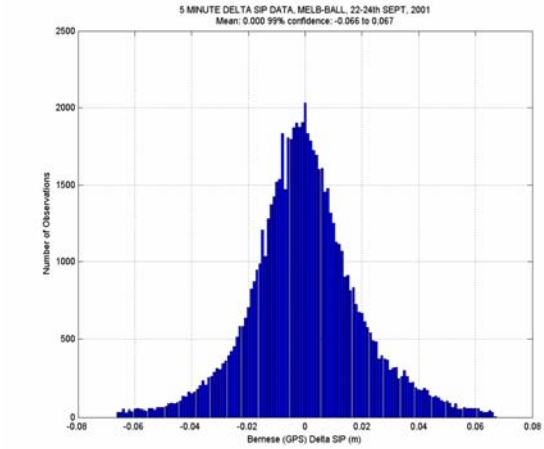
5 MINUTE DELTA SIP DATA, MELB-BALL, 22-24th SEPT, 2001
Mean: 0.000 99% confidence: -0.066 to 0.067
Number of Observations
Bernese (GPS) Delta SIP (m)

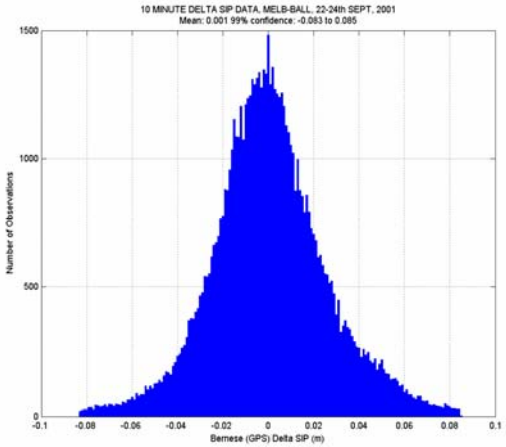
10 MINUTE DELTA SIP DATA, MELB-BALL, 22-24th SEPT, 2001
Mean: 0.001 99% confidence: -0.083 to 0.085
Number of Observations
Bernese (GPS) Delta SIP (m)

December 20th – 23rd, 2001 Local Time

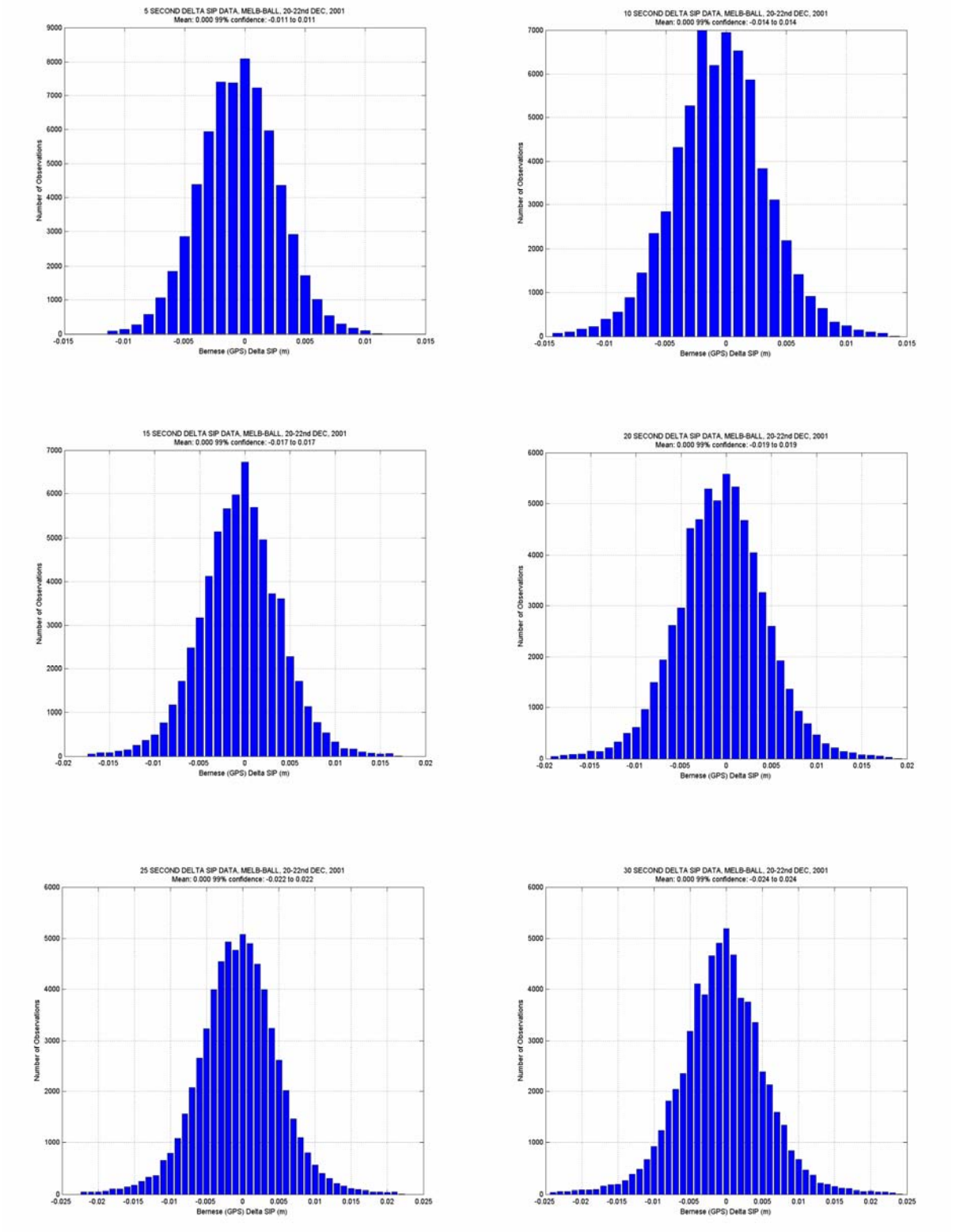

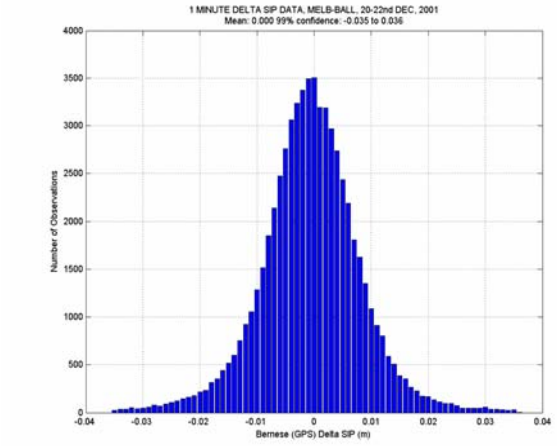
1 MINUTE DELTA SIP DATA, MELB-BALL, 20-22nd DEC, 2001
Mean: 0.000 99% confidence: -0.035 to 0.036
Number of Observations
Bernese (GPS) Delta SIP (m)

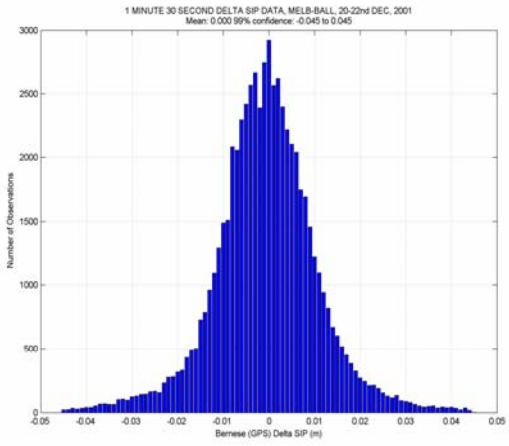
1 MINUTE 30 SECOND DELTA SIP DATA, MELB-BALL, 20-22nd DEC, 2001
Mean: 0.000 99% confidence: -0.045 to 0.045
Number of Observations
Bernese (GPS) Delta SIP (m)

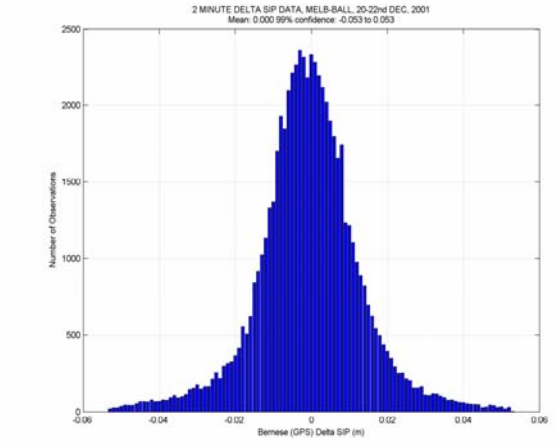
2 MINUTE DELTA SIP DATA, MELB-BALL, 20-22nd DEC, 2001
Mean: 0.000 99% confidence: -0.053 to 0.053
Number of Observations
Bernese (GPS) Delta SIP (m)

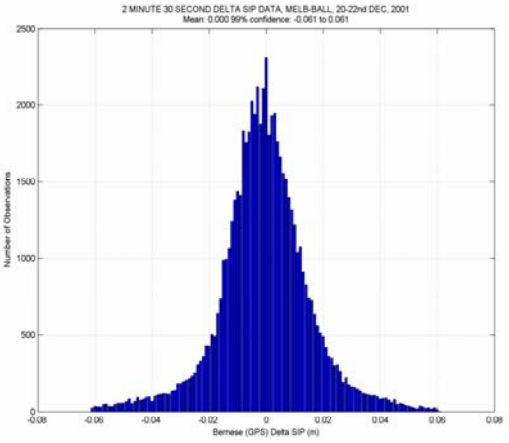
2 MINUTE 30 SECOND DELTA SIP DATA, MELB-BALL, 20-22nd DEC, 2001
Mean: 0.000 99% confidence: -0.061 to 0.061
Number of Observations
Bernese (GPS) Delta SIP (m)

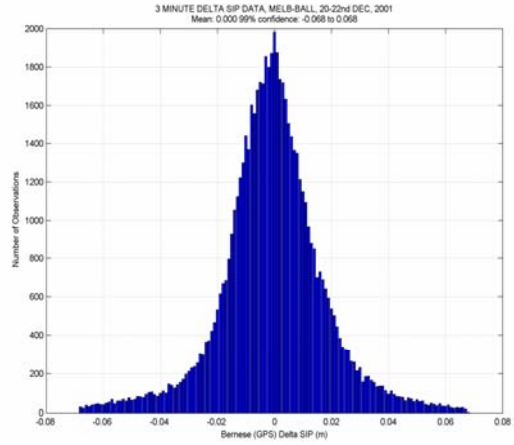
3 MINUTE DELTA SIP DATA, MELB-BALL, 20-22nd DEC, 2001
Mean: 0.000 99% confidence: -0.068 to 0.068
Number of Observations
Bernese (GPS) Delta SIP (m)

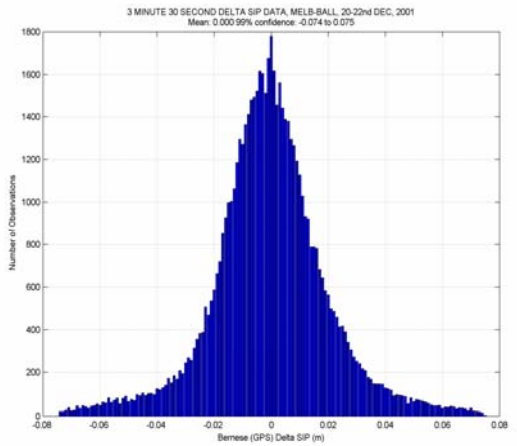
3 MINUTE 30 SECOND DELTA SIP DATA, MELB-BALL, 20-22nd DEC, 2001
Mean: 0.000 99% confidence: -0.074 to 0.075
Number of Observations
Bernese (GPS) Delta SIP (m)

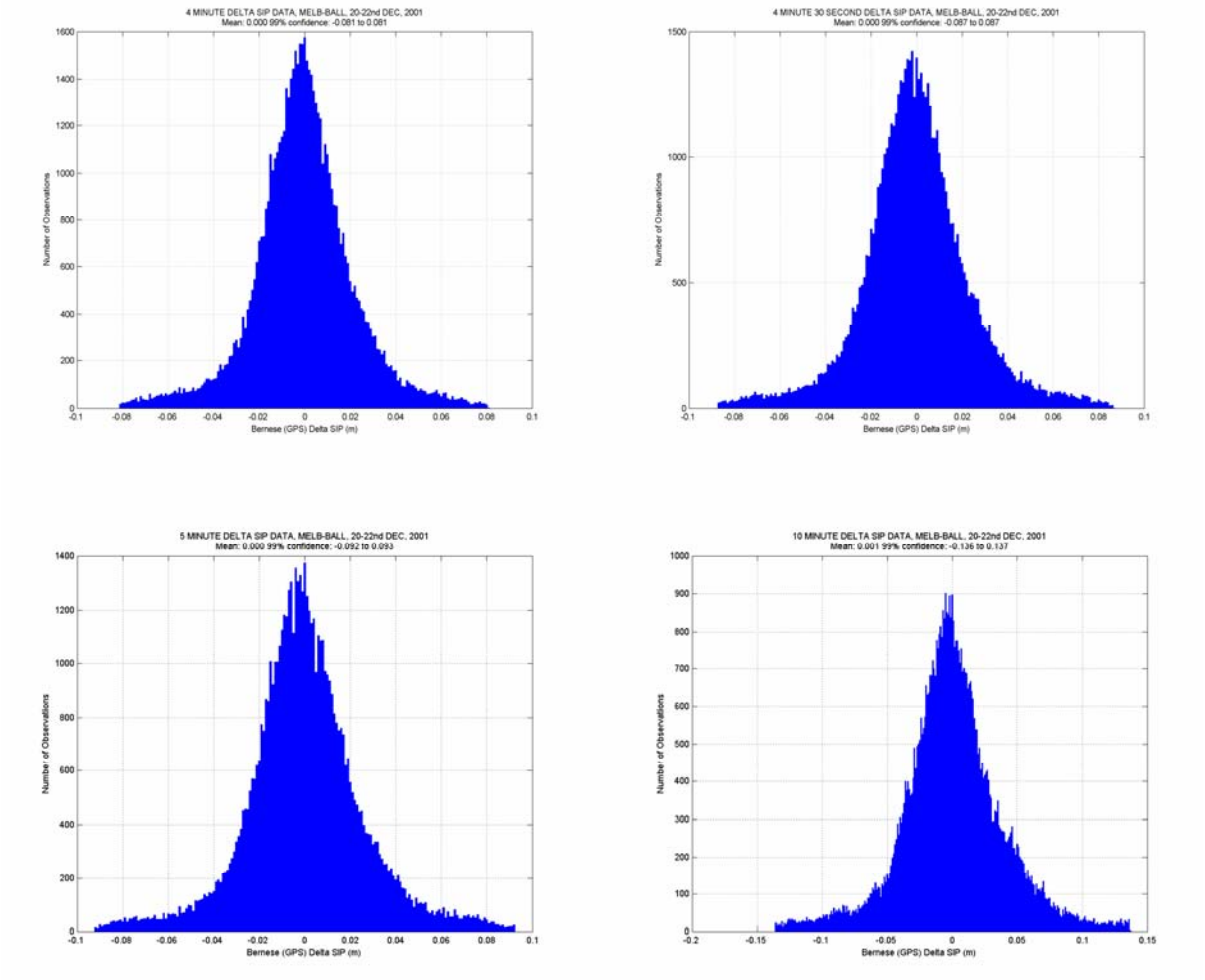
4 MINUTE DELTA SIP DATA, MELB-BALL, 20-22nd DEC, 2001
Mean: 0.000 99% confidence: -0.081 to 0.081
Number of Observations
Bernese (GPS) Delta SIP (m)
4 MINUTE 30 SECOND DELTA SIP DATA, MELB-BALL, 20-22nd DEC, 2001
Mean: 0.000 99% confidence: -0.087 to 0.087
Number of Observations
Bernese (GPS) Delta SIP (m)
5 MINUTE DELTA SIP DATA, MELB-BALL, 20-22nd DEC, 2001
Mean: 0.000 99% confidence: -0.092 to 0.093
Number of Observations
Bernese (GPS) Delta SIP (m)
10 MINUTE DELTA SIP DATA, MELB-BALL, 20-22nd DEC, 2001
Mean: 0.001 99% confidence: -0.136 to 0.137
Number of Observations
Bernese (GPS) Delta SIP (m)

March 19th – 22nd, 2002 Local Time

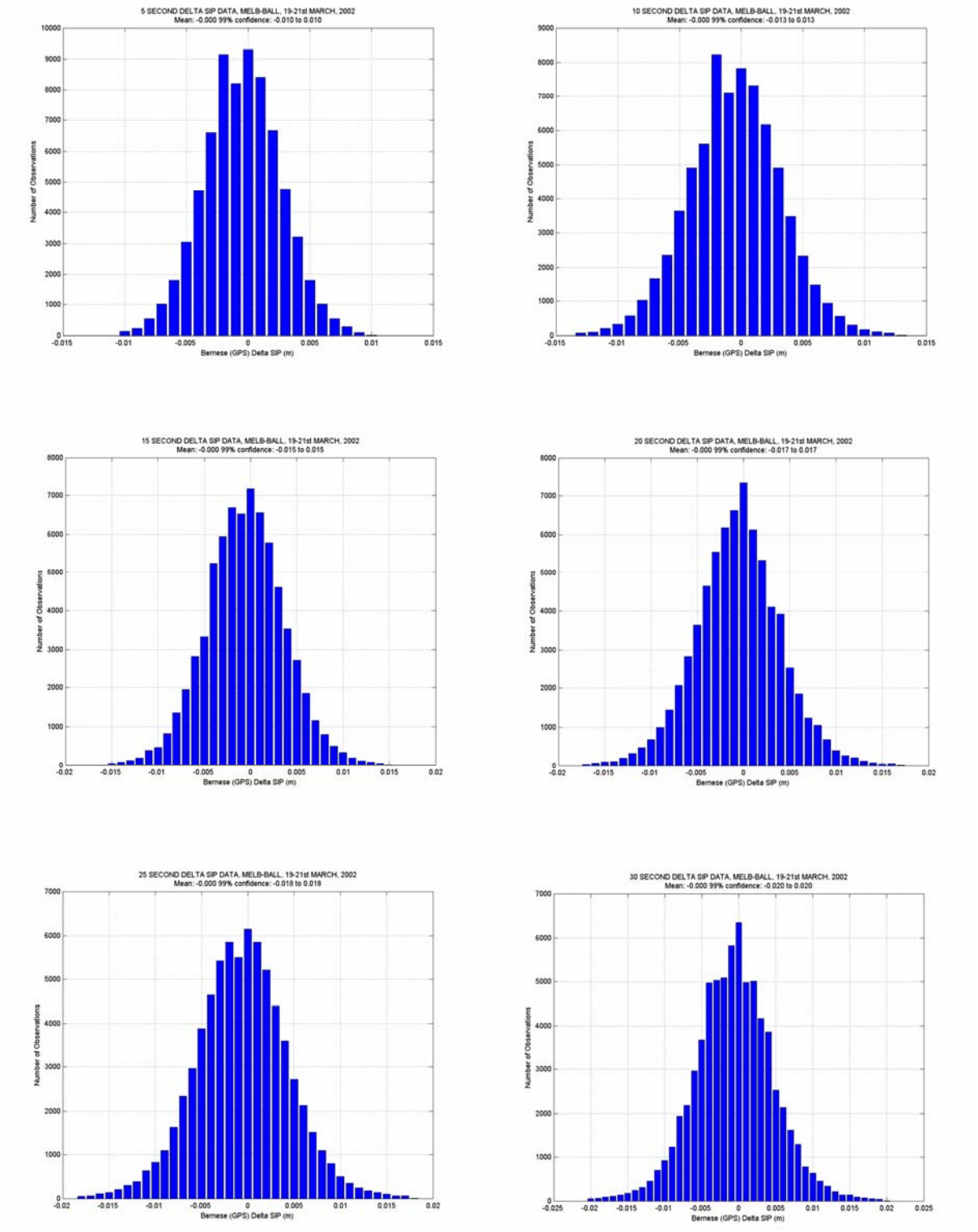

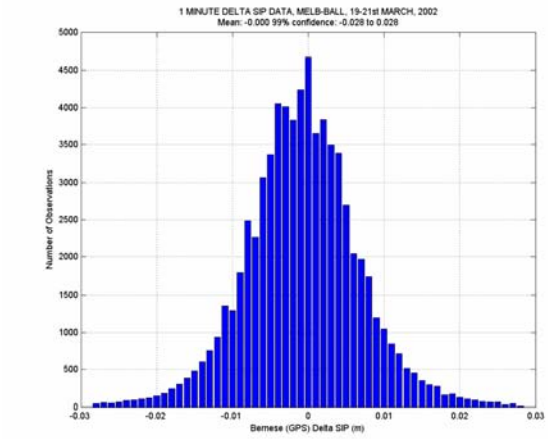
1 MINUTE DELTA SIP DATA, MELB-BALL, 19-21st MARCH, 2002
Mean: -0.000 99% confidence: -0.028 to 0.028
Number of Observations
Bernese (GPS) Delta SIP (m)

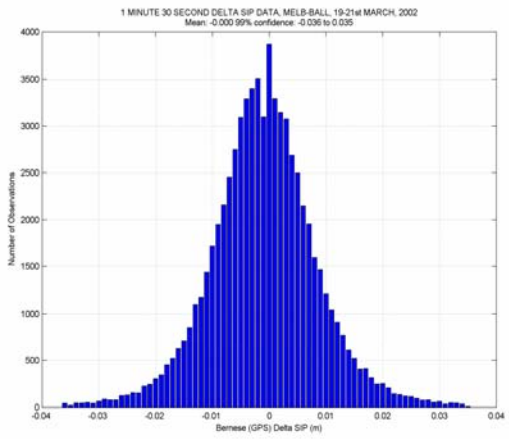
1 MINUTE 30 SECOND DELTA SIP DATA, MELB-BALL, 19-21st MARCH, 2002
Mean: -0.000 99% confidence: -0.036 to 0.035
Number of Observations
Bernese (GPS) Delta SIP (m)

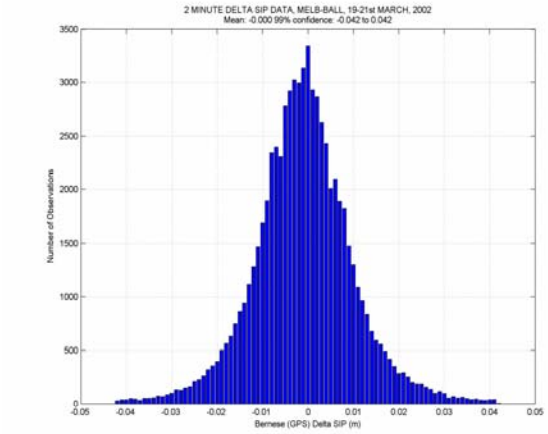
2 MINUTE DELTA SIP DATA, MELB-BALL, 19-21st MARCH, 2002
Mean: -0.000 99% confidence: -0.042 to 0.042
Number of Observations
Bernese (GPS) Delta SIP (m)

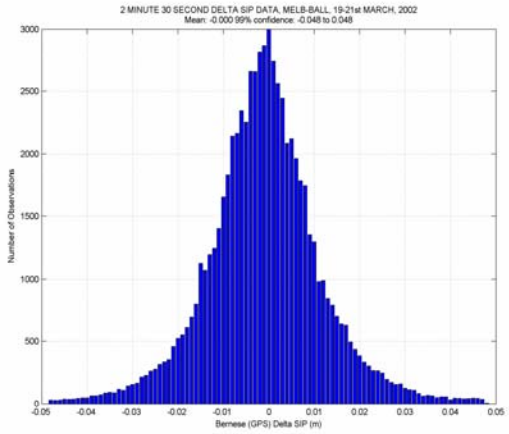
2 MINUTE 30 SECOND DELTA SIP DATA, MELB-BALL, 19-21st MARCH, 2002
Mean: -0.000 99% confidence: -0.048 to 0.048
Number of Observations
Bernese (GPS) Delta SIP (m)

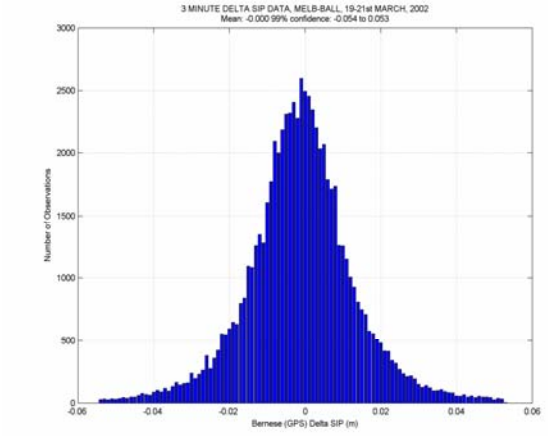
3 MINUTE DELTA SIP DATA, MELB-BALL, 19-21st MARCH, 2002
Mean: -0.000 99% confidence: -0.054 to 0.053
Number of Observations
Bernese (GPS) Delta SIP (m)

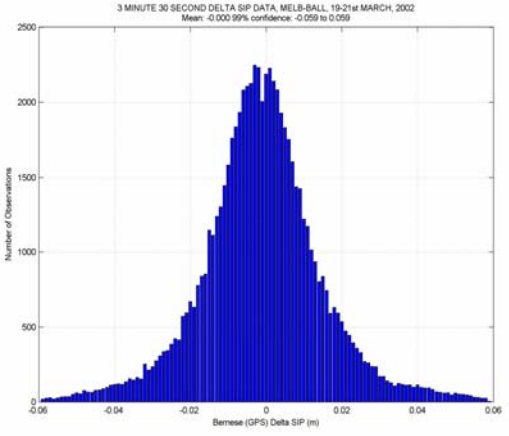
3 MINUTE 30 SECOND DELTA SIP DATA, MELB-BALL, 19-21st MARCH, 2002
Mean: -0.000 99% confidence: -0.059 to 0.059
Number of Observations
Bernese (GPS) Delta SIP (m)

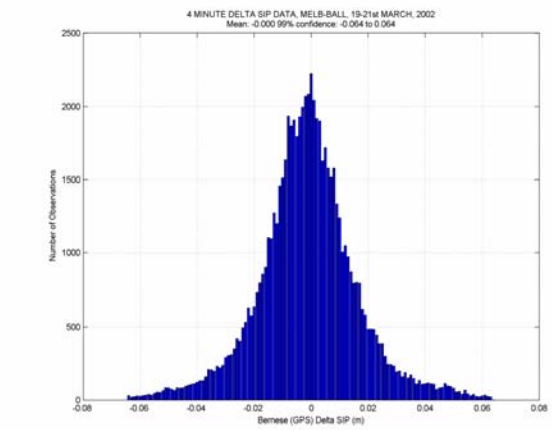
4 MINUTE DELTA SIP DATA, MELB-BALL, 19-21st MARCH, 2002
Mean: -0.000 99% confidence: -0.064 to 0.064
Number of Observations
Bernese (GPS) Delta SIP (m)

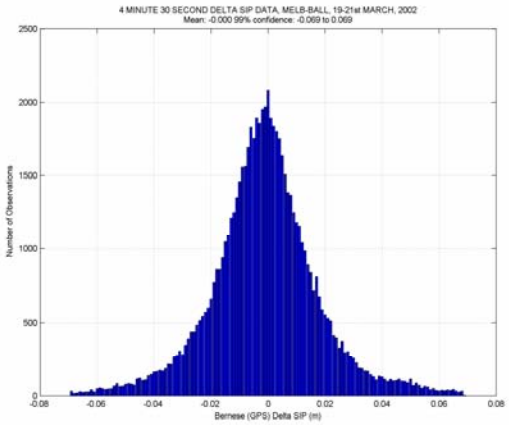
4 MINUTE 30 SECOND DELTA SIP DATA, MELB-BALL, 19-21st MARCH, 2002
Mean: -0.000 99% confidence: -0.069 to 0.069
Number of Observations
Bernese (GPS) Delta SIP (m)

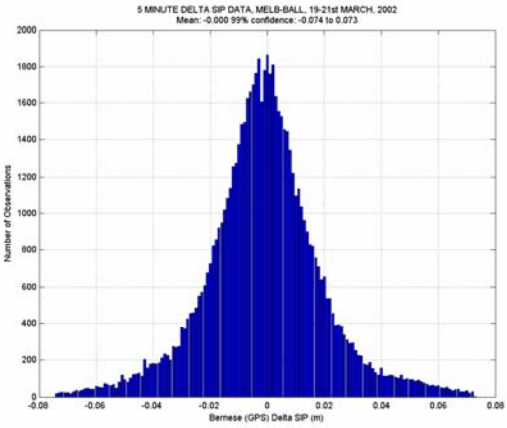
5 MINUTE DELTA SIP DATA, MELB-BALL, 19-21st MARCH, 2002
Mean: -0.000 99% confidence: -0.074 to 0.073
Number of Observations
Bernese (GPS) Delta SIP (m)

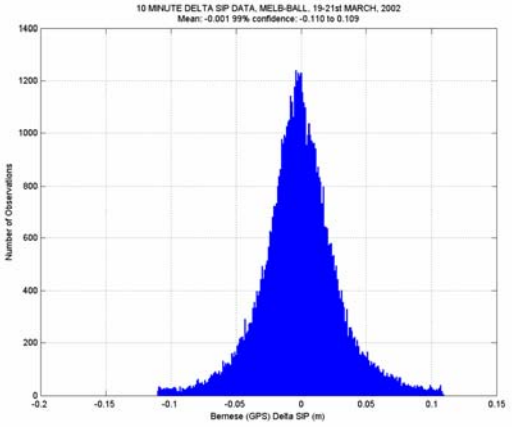
10 MINUTE DELTA SIP DATA, MELB-BALL, 19-21st MARCH, 2002
Mean: -0.001 99% confidence: -0.110 to 0.109
Number of Observations
Bernese (GPS) Delta SIP (m)

June, 20th – 23rd, 2002 Local Time

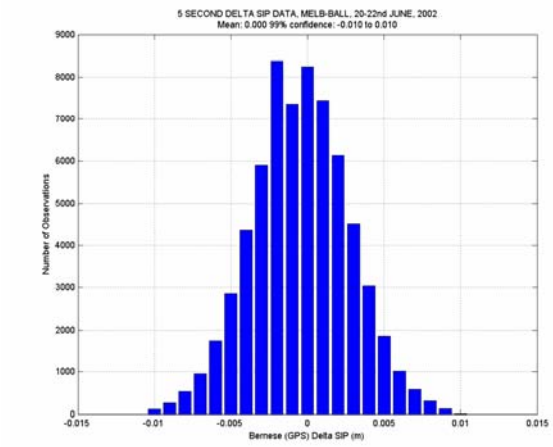

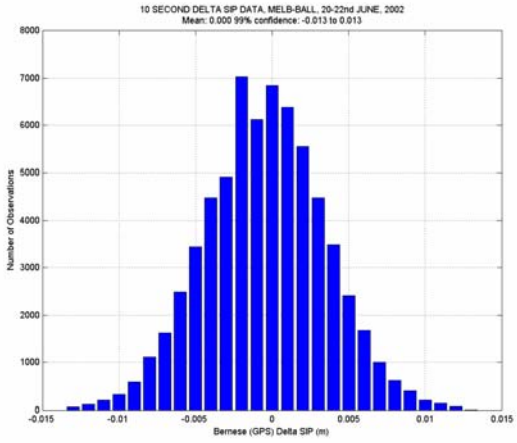

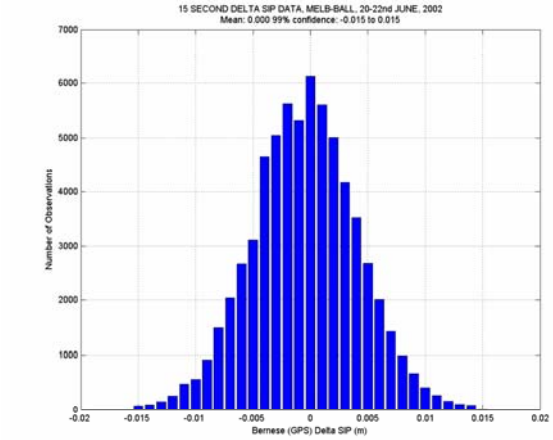

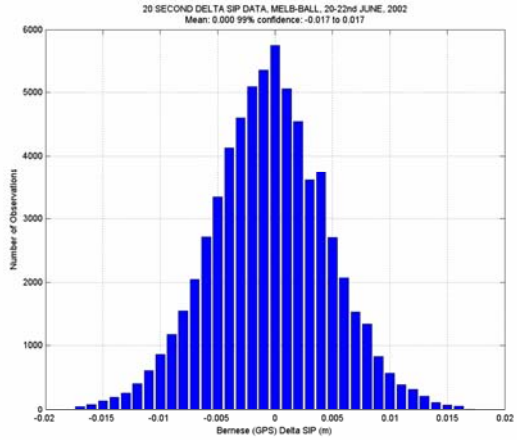

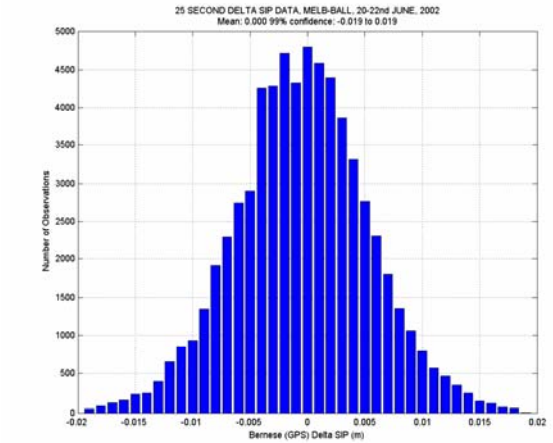

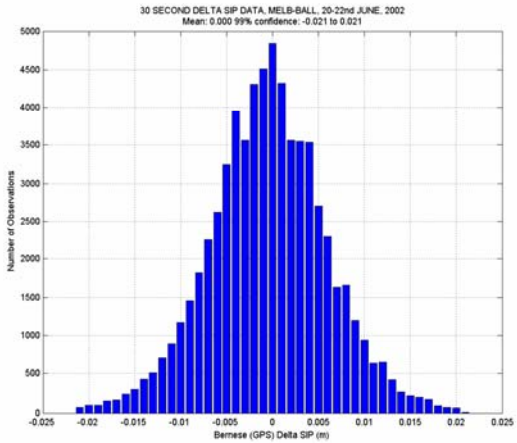

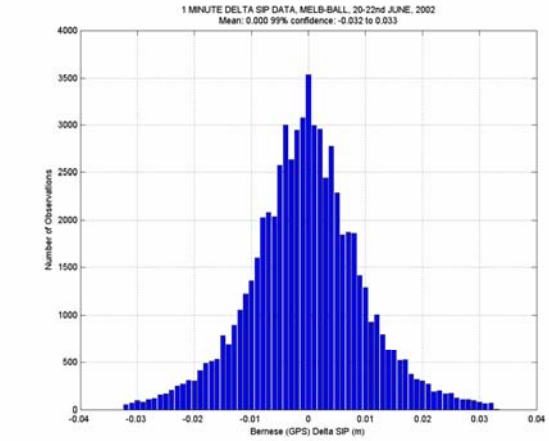
1 MINUTE DELTA SIP DATA, MELB-BALL, 20-22nd JUNE, 2002
Mean: 0.000 99% confidence: -0.032 to 0.033
Number of Observations
Bernese (GPS) Delta SIP (m)

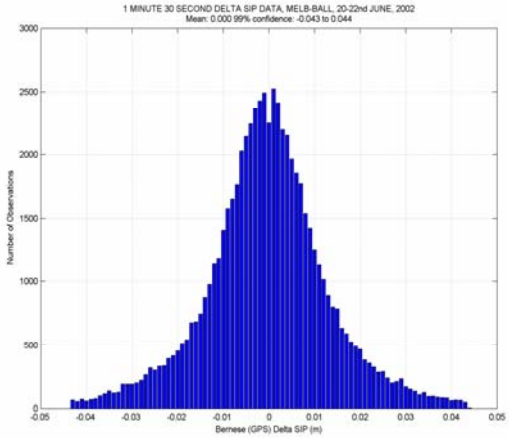
1 MINUTE 30 SECOND DELTA SIP DATA, MELB-BALL, 20-22nd JUNE, 2002
Mean: 0.000 99% confidence: -0.043 to 0.044
Number of Observations
Bernese (GPS) Delta SIP (m)

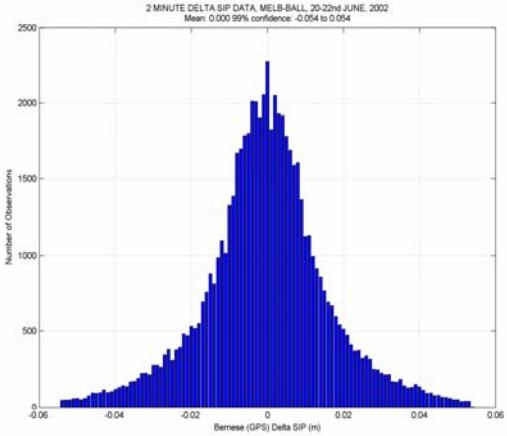
2 MINUTE DELTA SIP DATA, MELB-BALL, 20-22nd JUNE, 2002
Mean: 0.000 99% confidence: -0.054 to 0.054
Number of Observations
Bernese (GPS) Delta SIP (m)

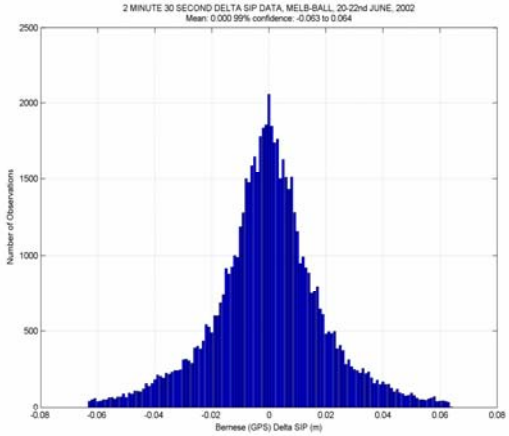
2 MINUTE 30 SECOND DELTA SIP DATA, MELB-BALL, 20-22nd JUNE, 2002
Mean: 0.000 99% confidence: -0.063 to 0.064
Number of Observations
Bernese (GPS) Delta SIP (m)

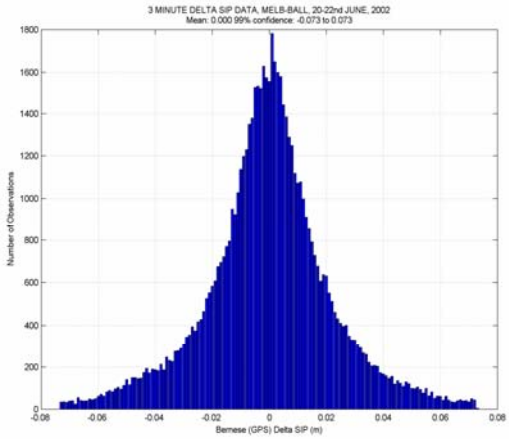
3 MINUTE DELTA SIP DATA, MELB-BALL, 20-22nd JUNE, 2002
Mean: 0.000 99% confidence: -0.073 to 0.073
Number of Observations
Bernese (GPS) Delta SIP (m)

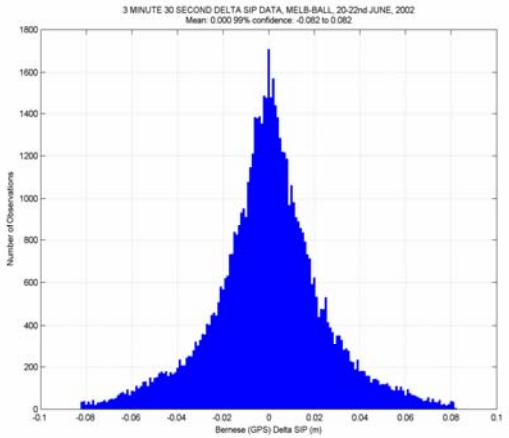
3 MINUTE 30 SECOND DELTA SIP DATA, MELB-BALL, 20-22nd JUNE, 2002
Mean: 0.000 99% confidence: -0.082 to 0.082
Number of Observations
Bernese (GPS) Delta SIP (m)

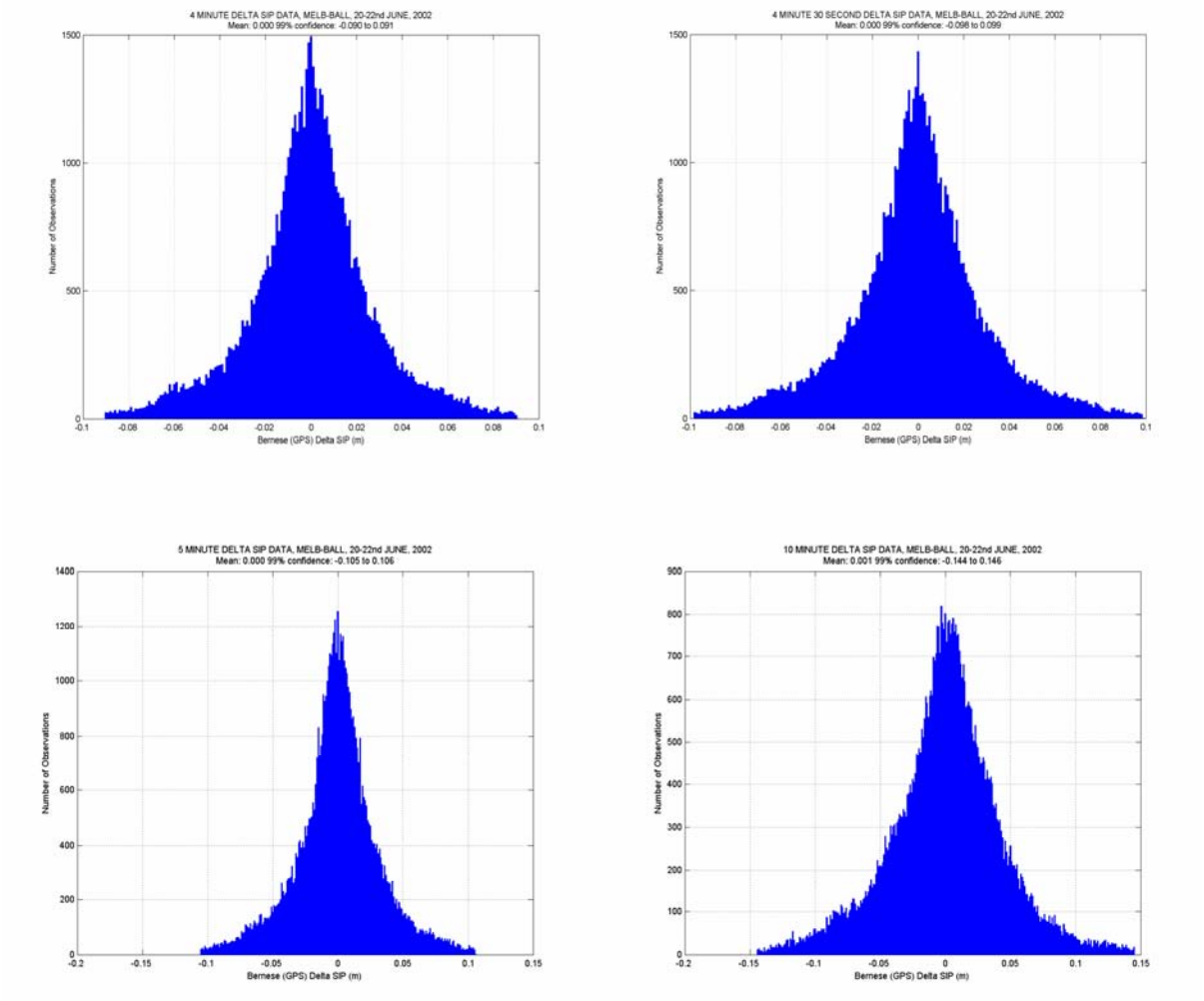
4 MINUTE DELTA SIP DATA, MELB-BALL, 20-22nd JUNE, 2002
Mean: 0.000 99% confidence: -0.090 to 0.091
Number of Observations
Bernese (GPS) Delta SIP (m)
4 MINUTE 30 SECOND DELTA SIP DATA, MELB-BALL, 20-22nd JUNE, 2002
Mean: 0.000 99% confidence: -0.098 to 0.099
Number of Observations
Bernese (GPS) Delta SIP (m)
5 MINUTE DELTA SIP DATA, MELB-BALL, 20-22nd JUNE, 2002
Mean: 0.000 99% confidence: -0.105 to 0.106
Number of Observations
Bernese (GPS) Delta SIP (m)
10 MINUTE DELTA SIP DATA, MELB-BALL, 20-22nd JUNE, 2002
Mean: 0.001 99% confidence: -0.144 to 0.146
Number of Observations
Bernese (GPS) Delta SIP (m)

Appendix B: The residuals from the moving average model

Moving average model: September 22nd – 25th, 2001 Local

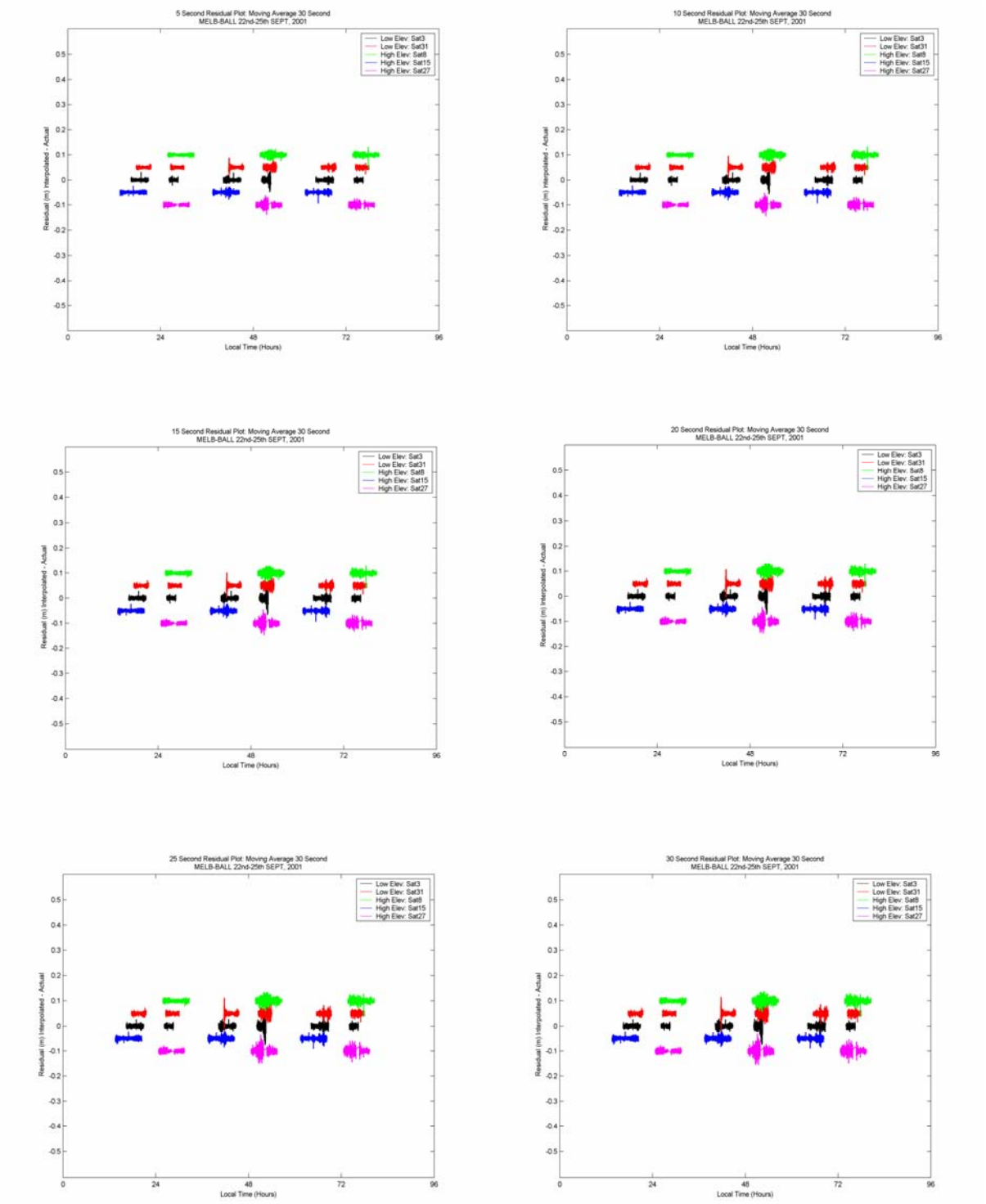

Moving average model: September 22nd – 25th, 2001 Local time

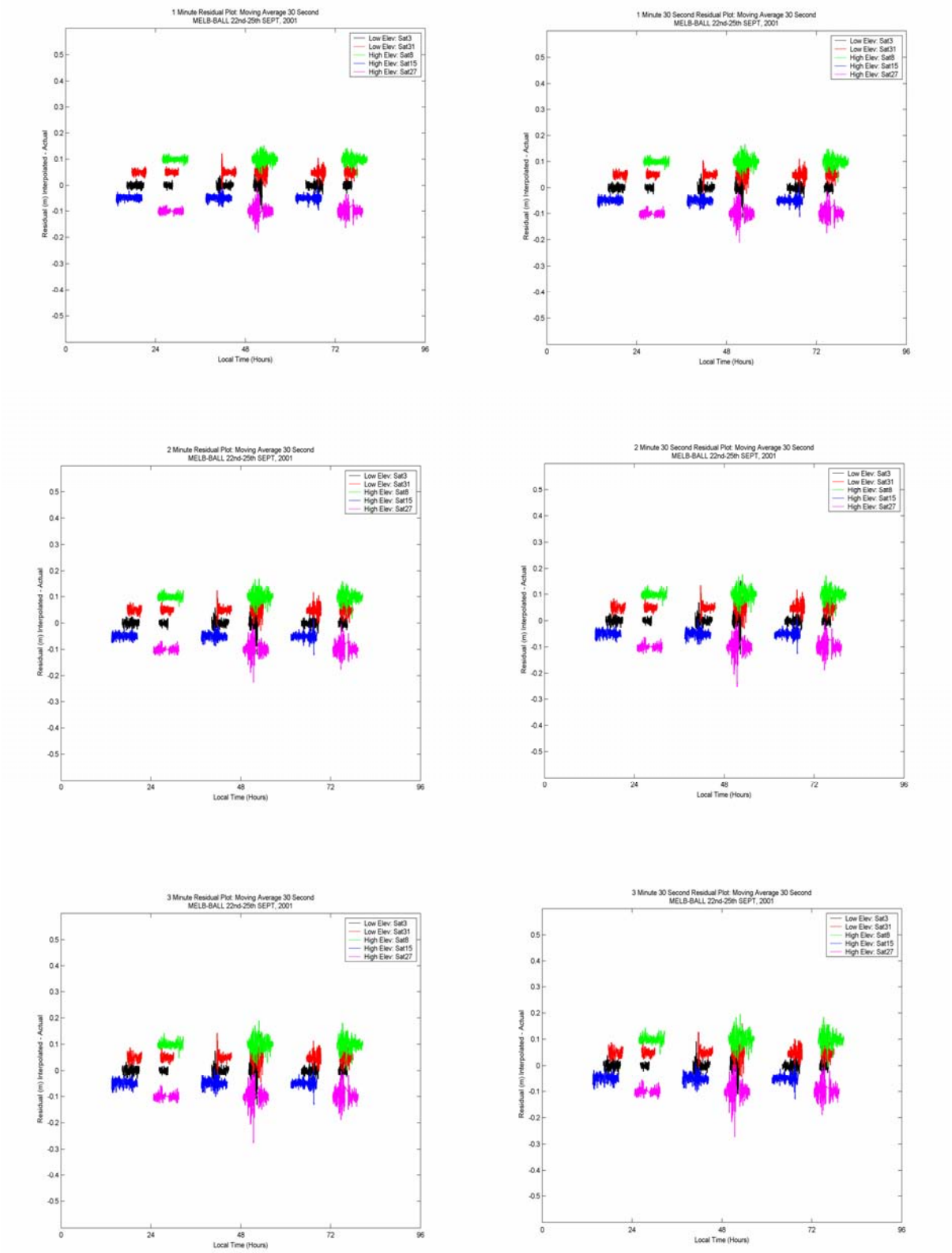

Moving average model: September 22nd – 25th, 2001 Local time

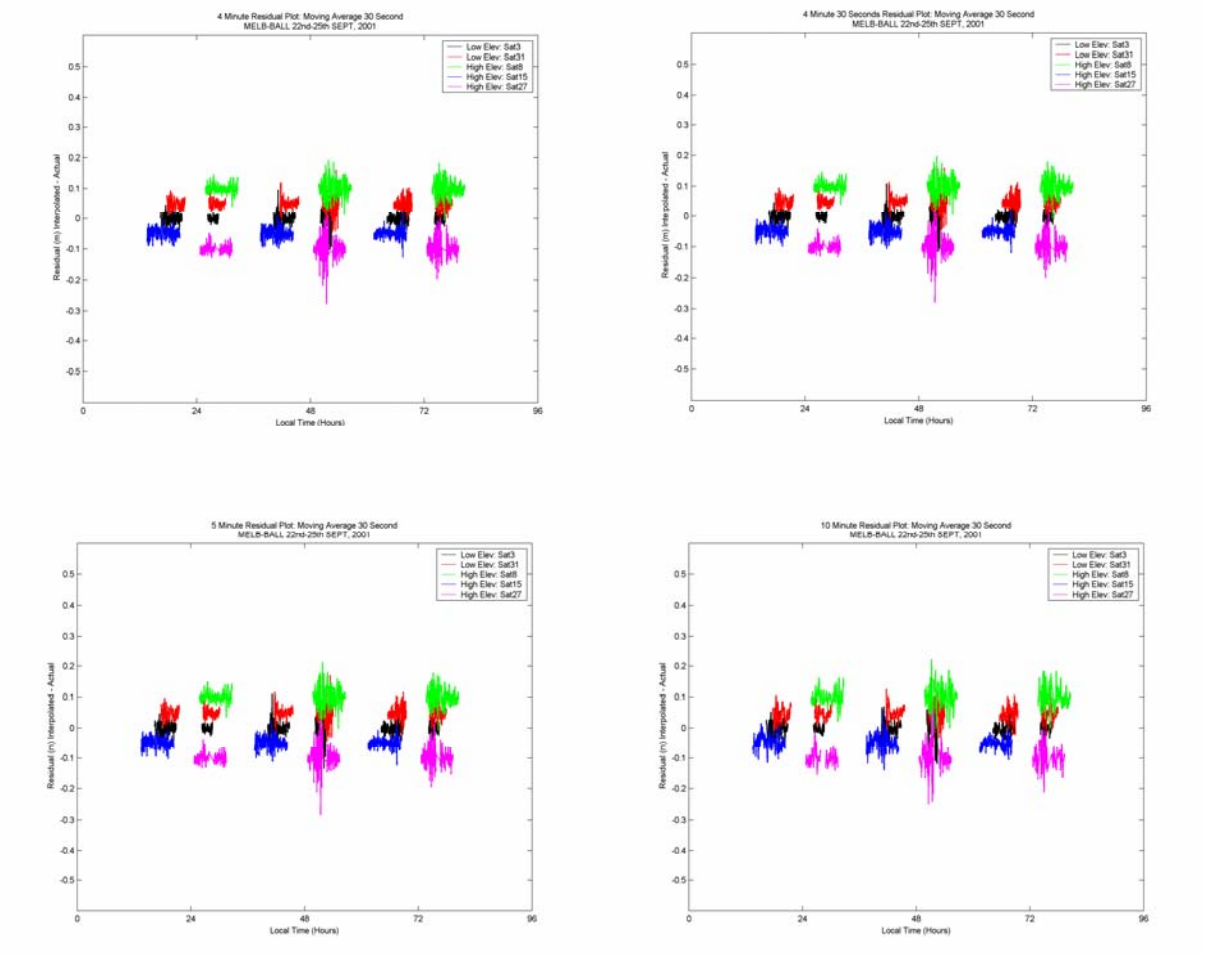

Moving average model: December 20th – 23rd, 2001 Local time

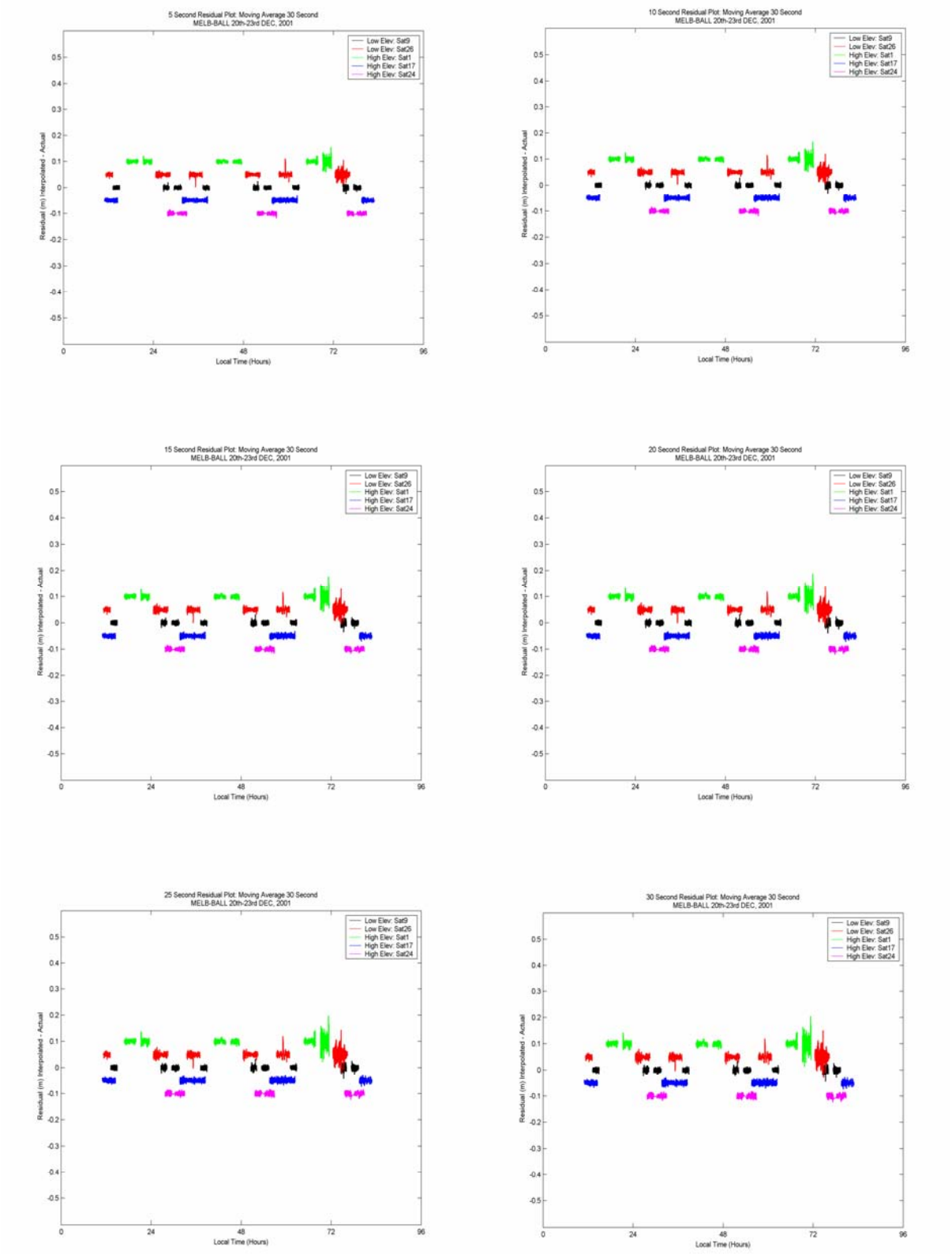

Moving average model: December 20th – 23rd, 2001 Local time

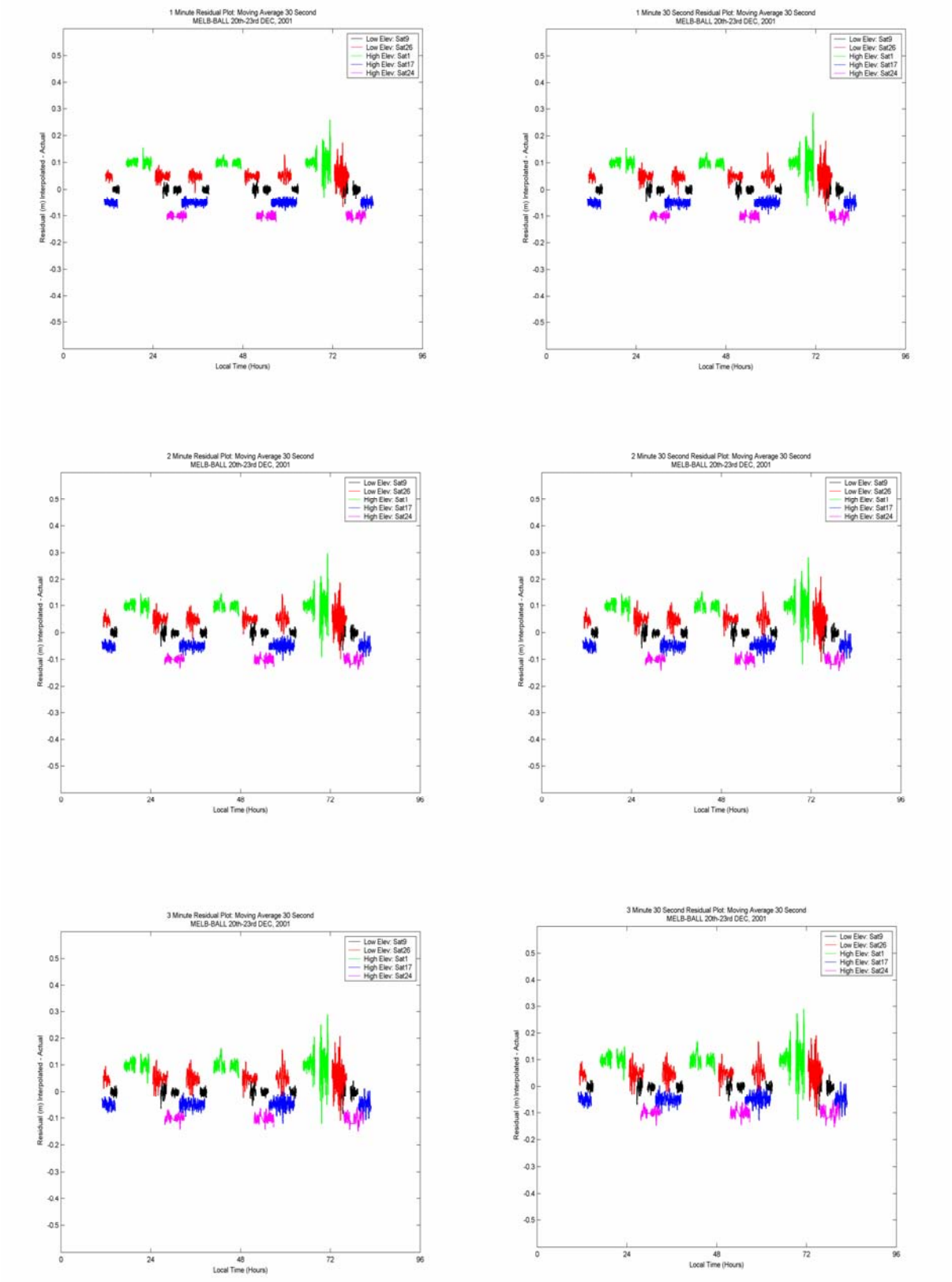

Moving average model: December 20th – 23rd, 2001 Local time

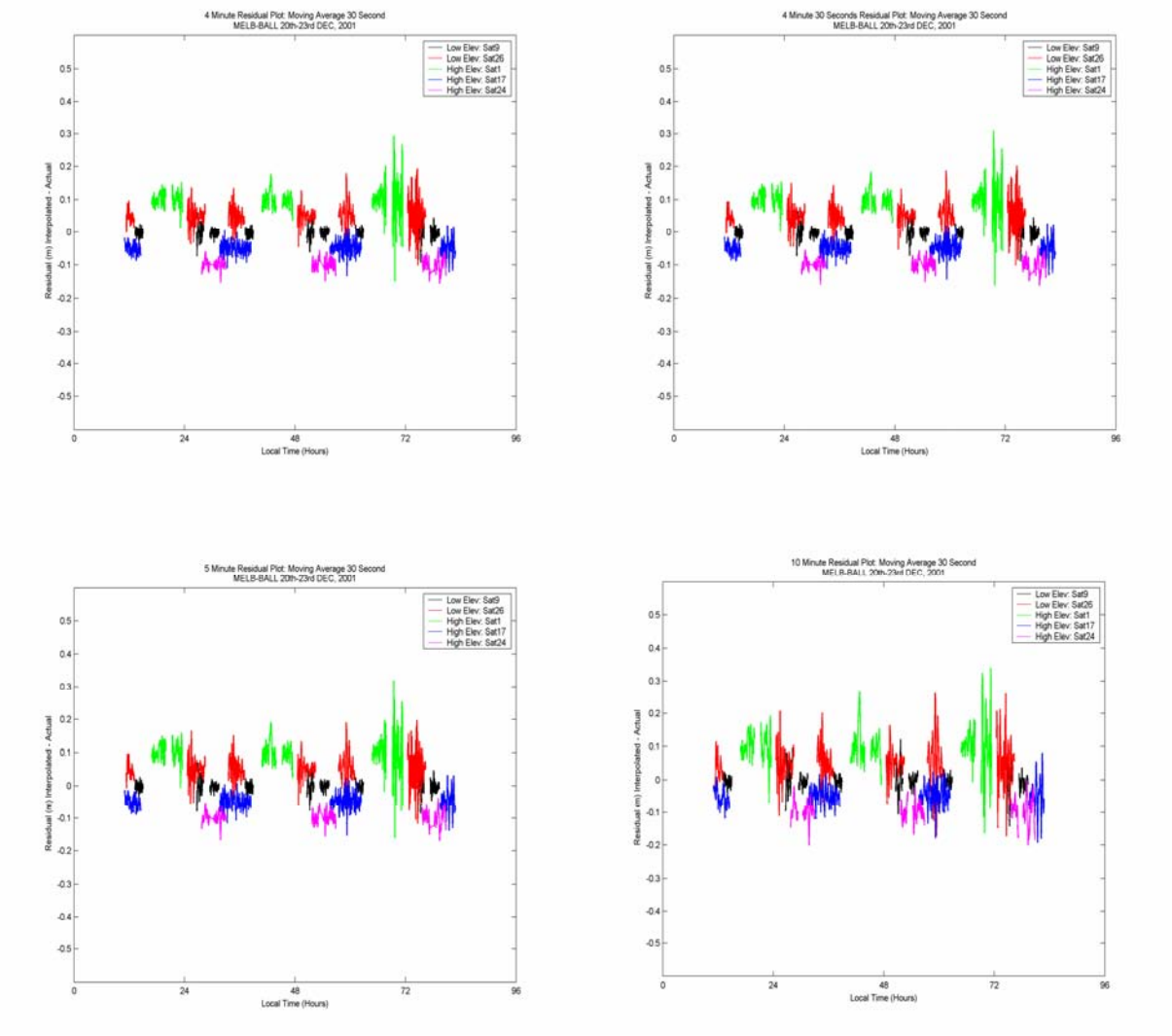

Moving average model: March 19th – 22nd, 2002 Local time

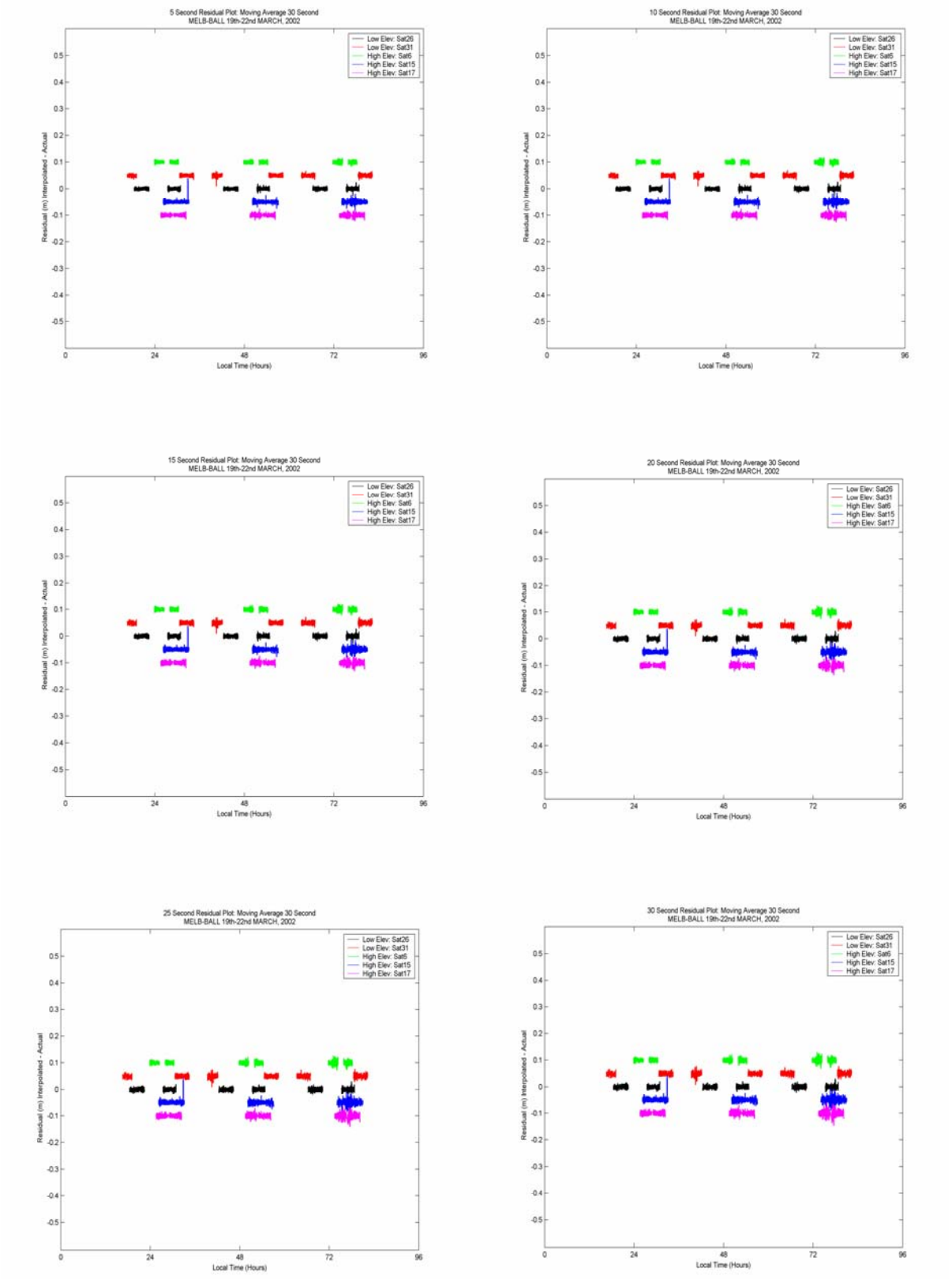

Moving average model: March 19th – 22nd, 2002 Local time

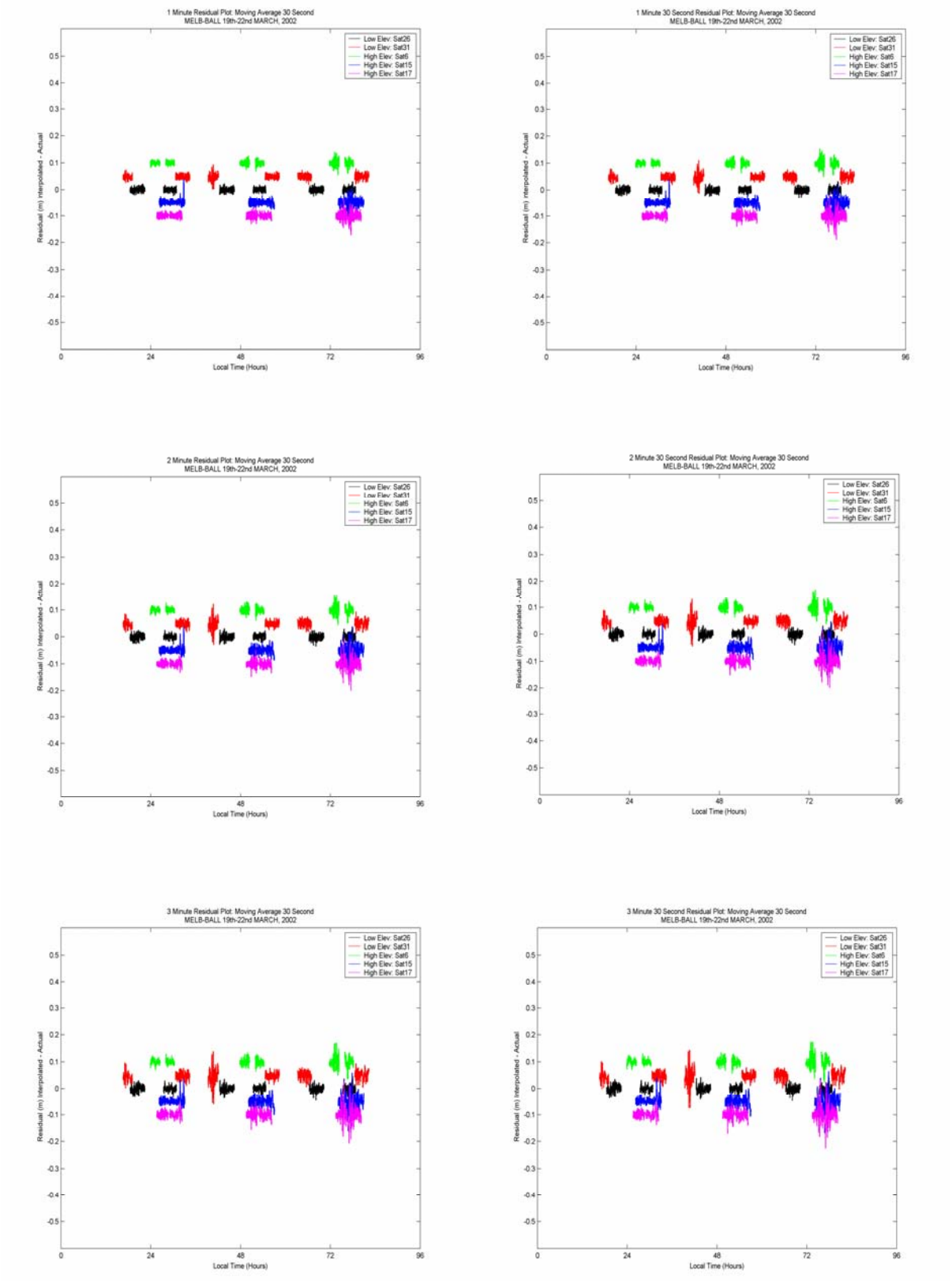

Moving average model: March 19th – 22nd, 2002 Local time

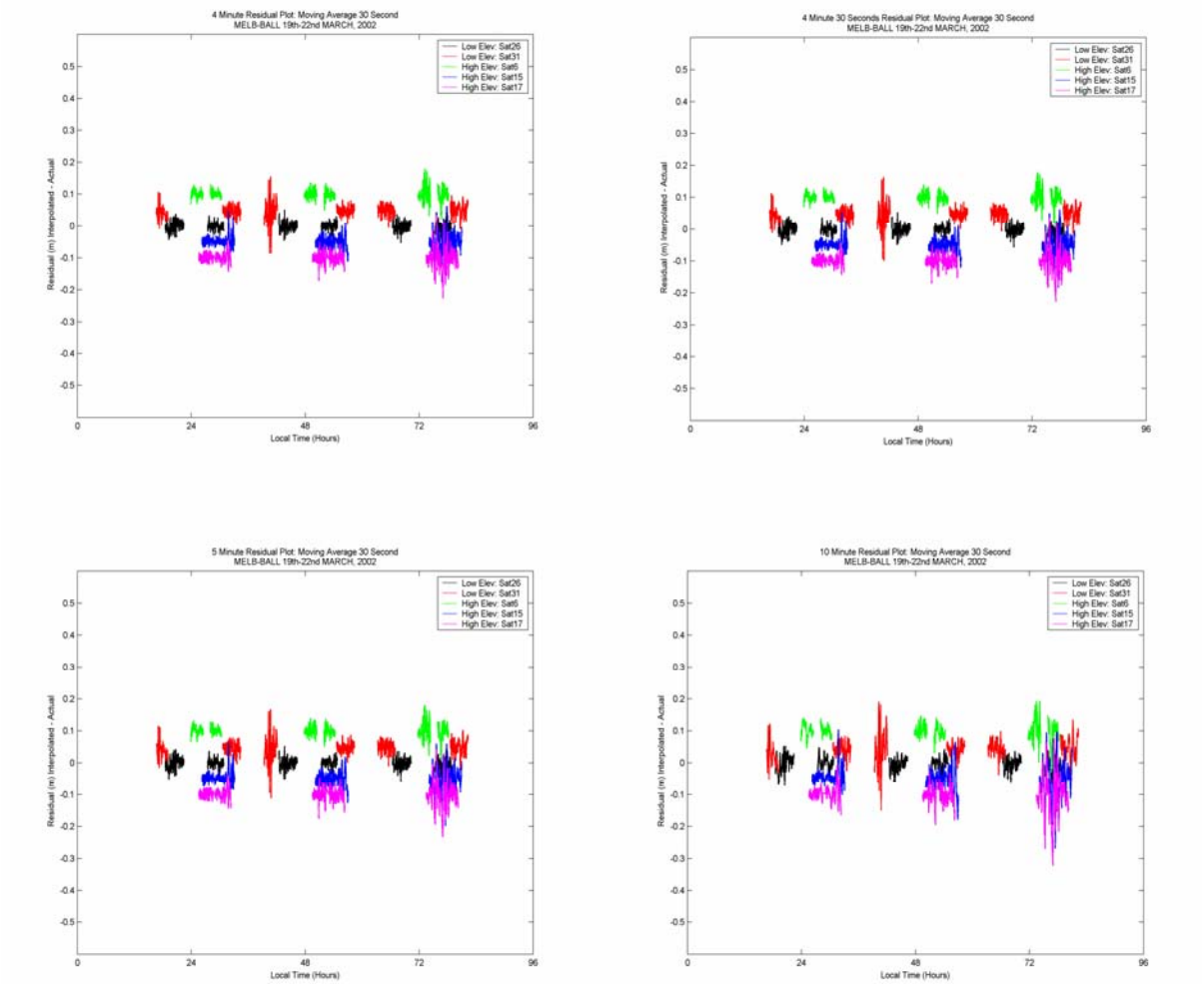

Moving average model: June, 20th – 23rd, 2002 Local time

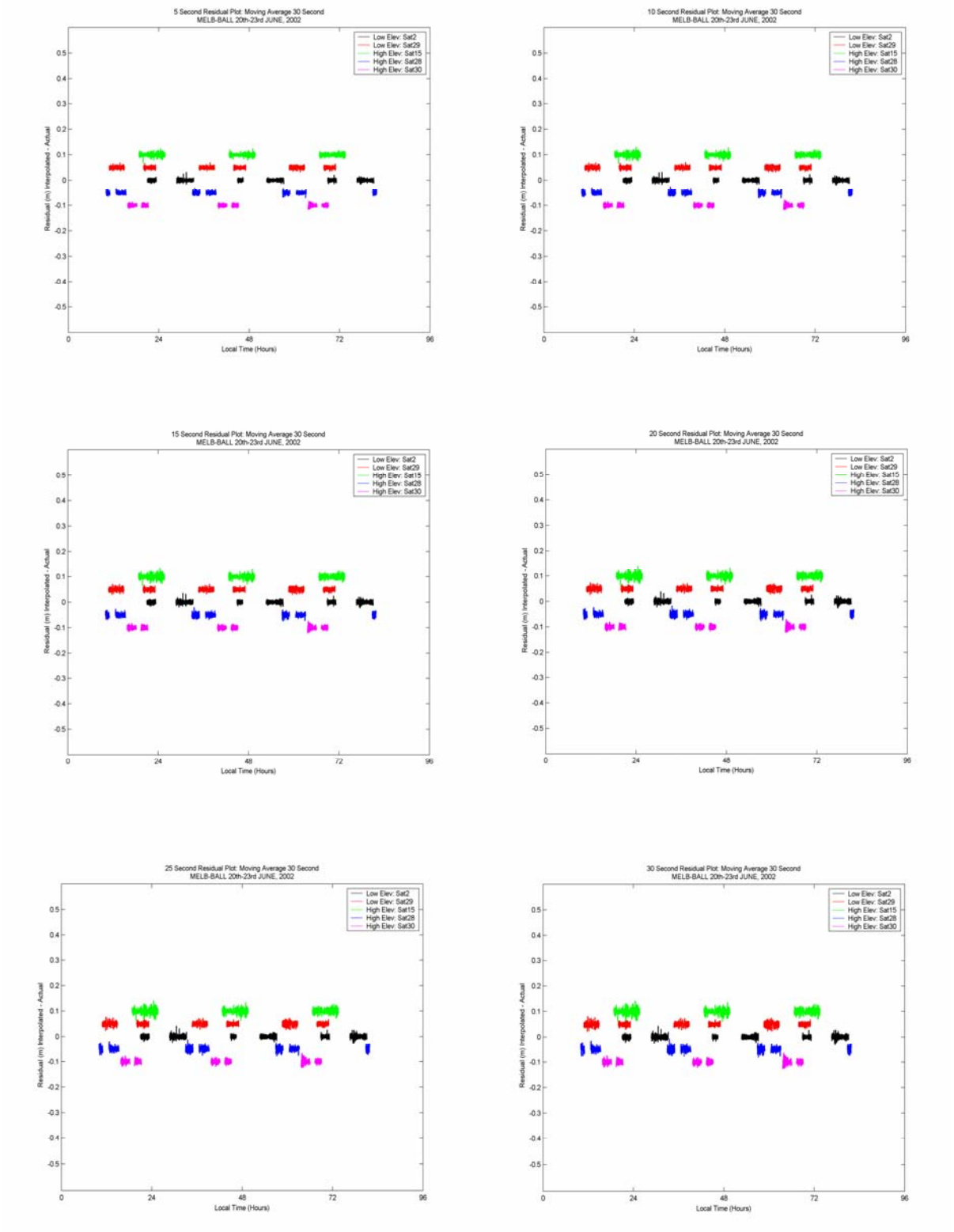

Moving average model: June, 20th – 23rd, 2002 Local time

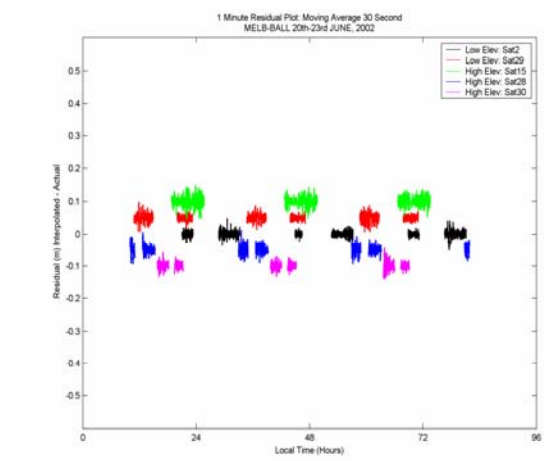

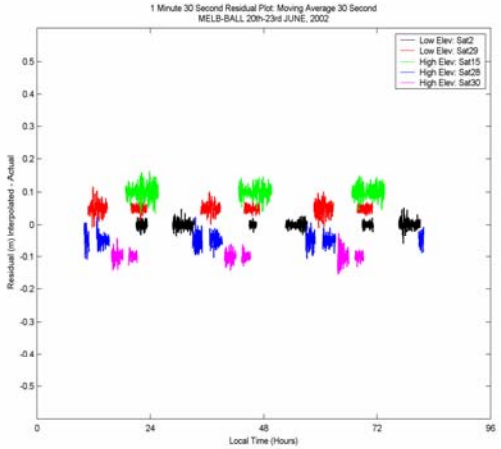

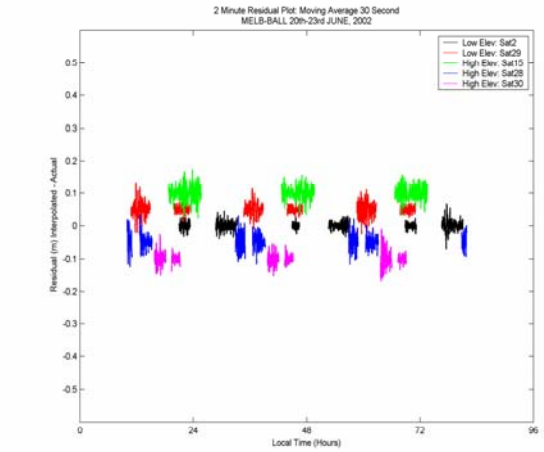

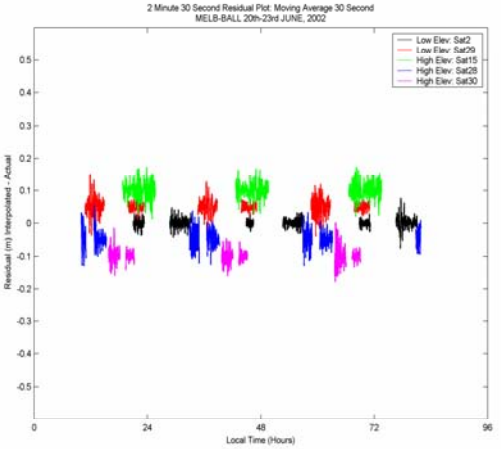

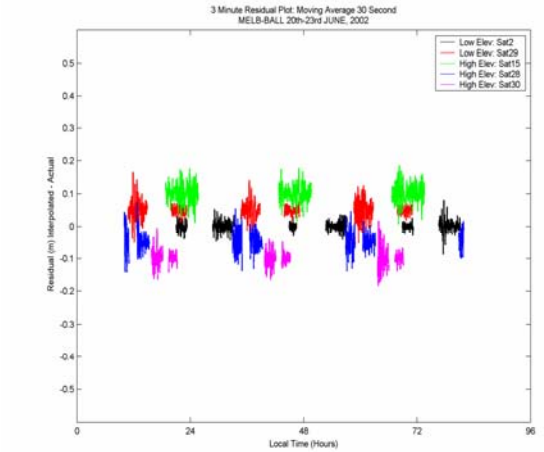

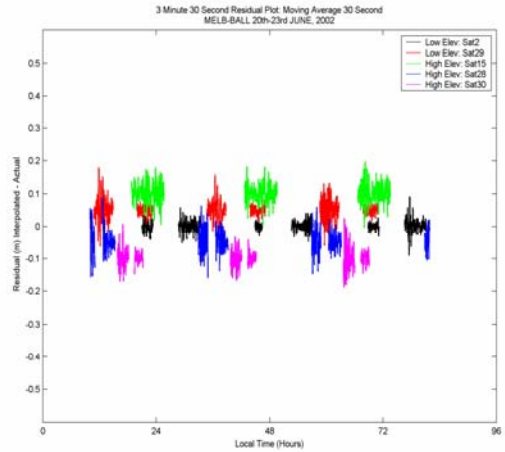

Moving average model: June, 20th – 23rd, 2002 Local time

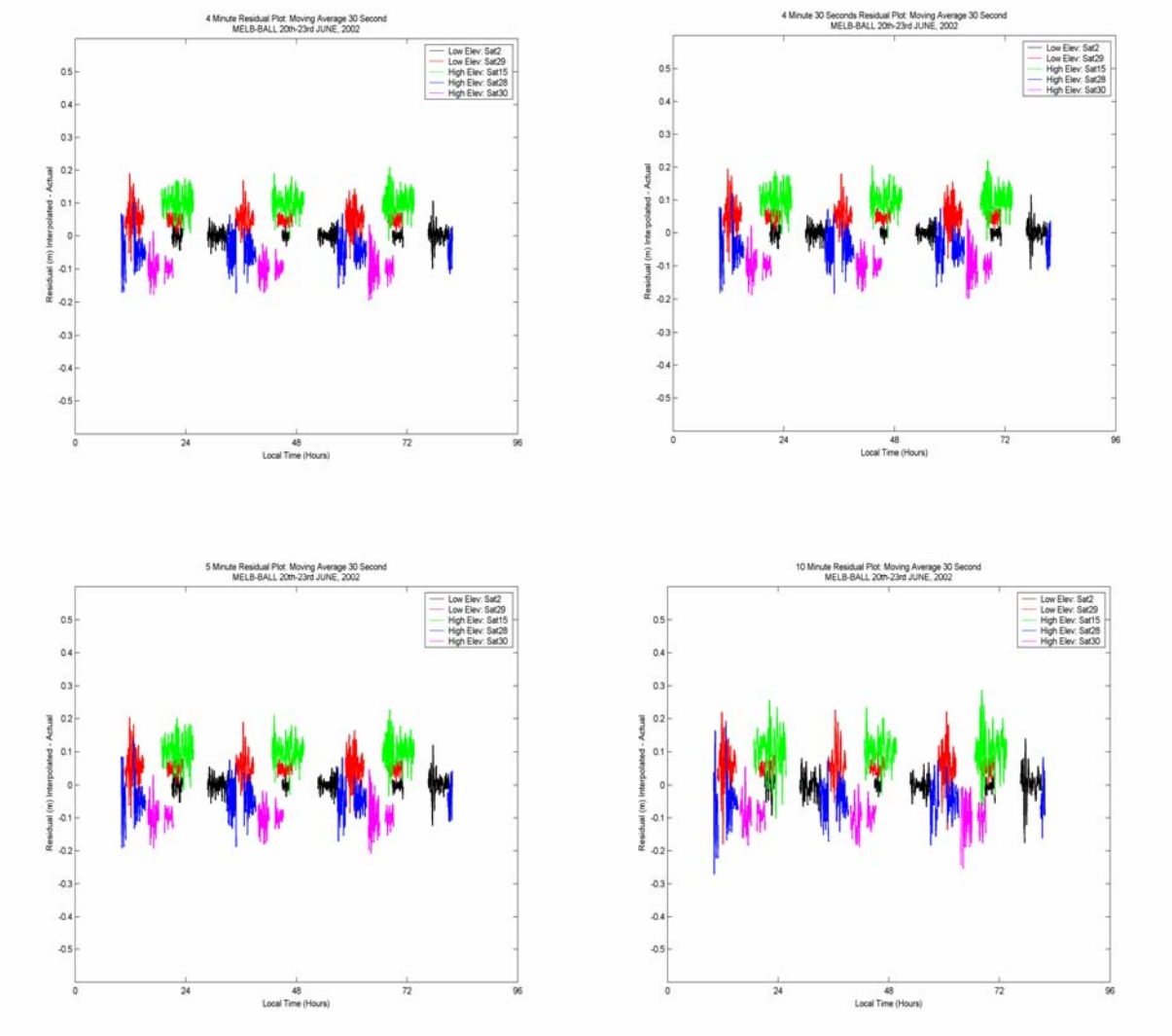

Appendix C: The residuals from the linear polynomial model

Linear polynomial model: September 22nd – 25th, 2001 Local time

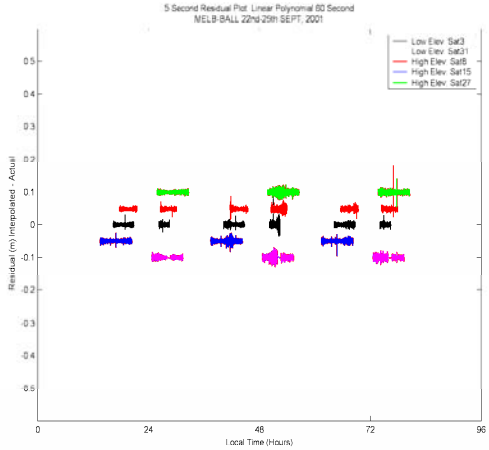

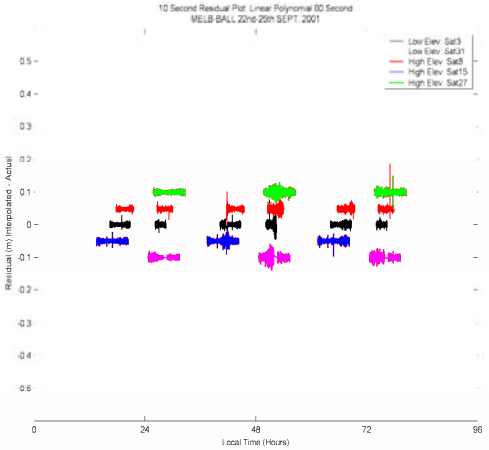

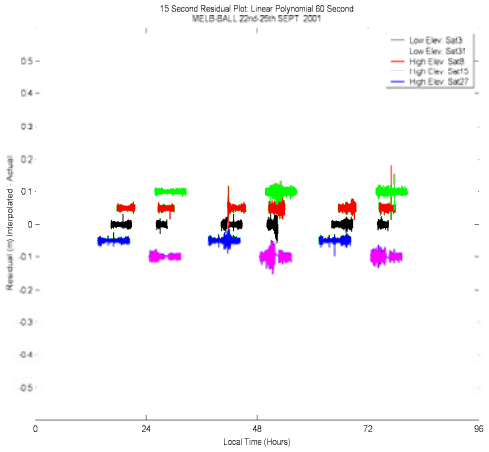

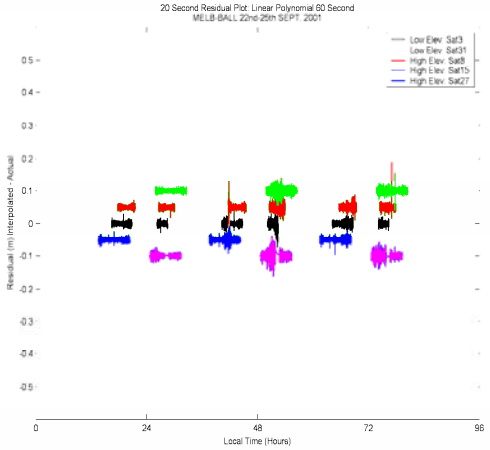

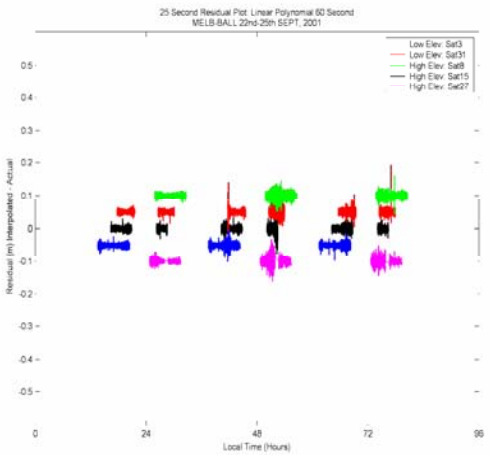

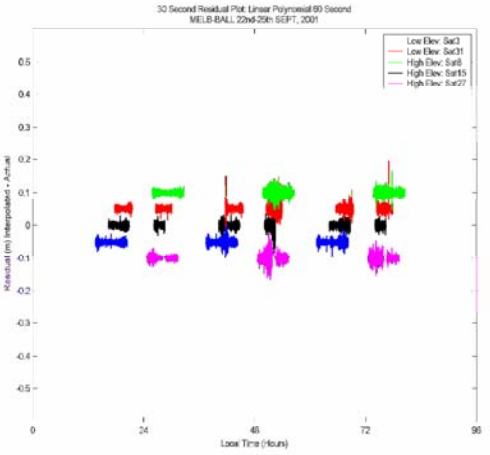

Linear polynomial model: September 22nd – 25th, 2001 Local time

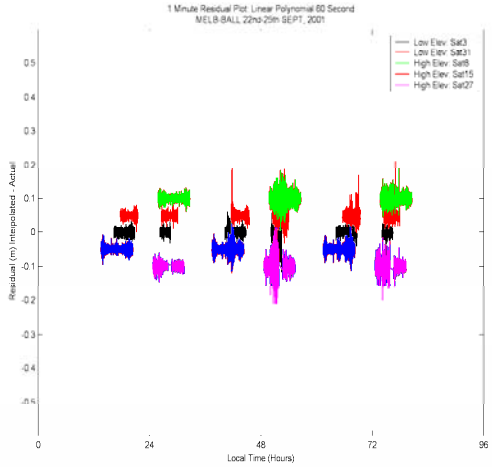

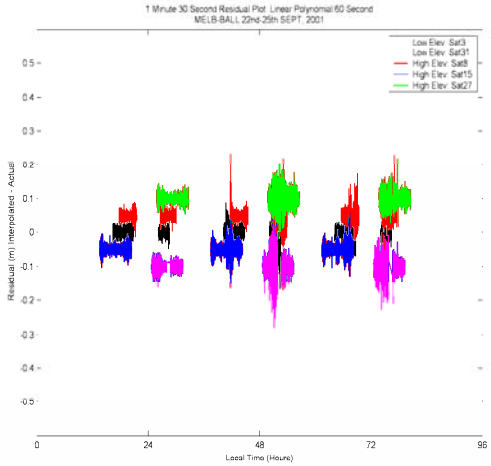

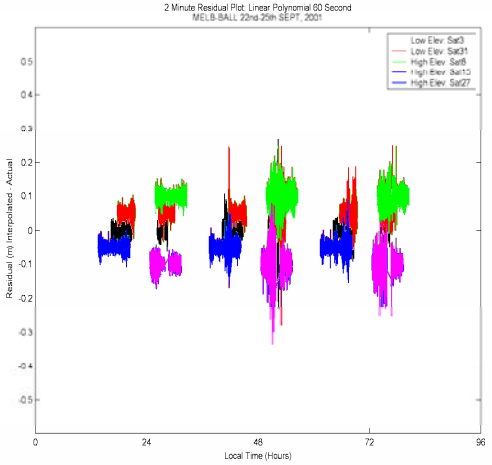

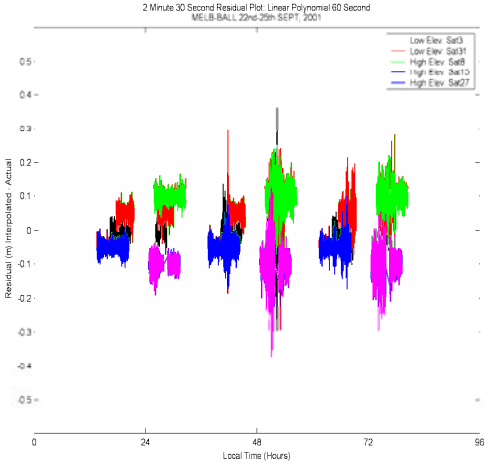

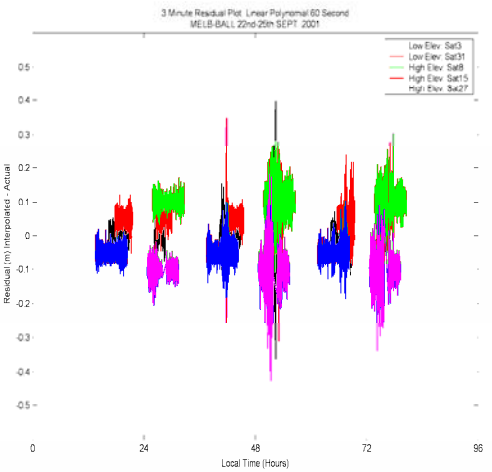

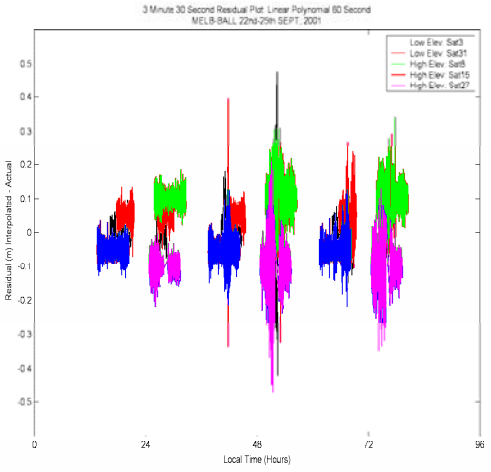

Linear polynomial model: September 22nd – 25th, 2001 Local time

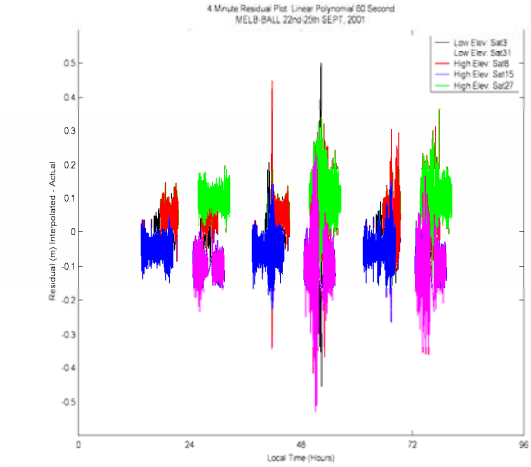

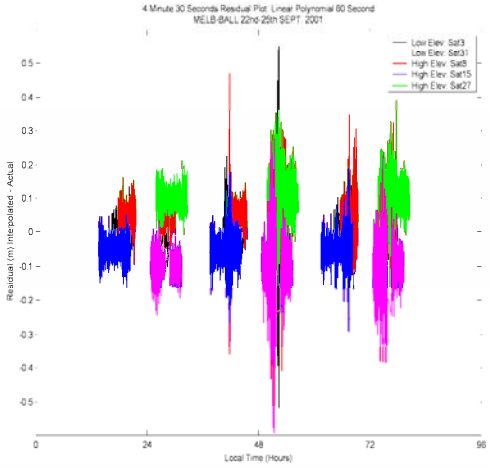

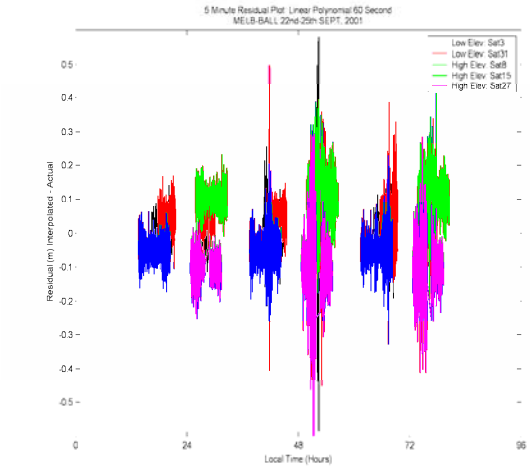

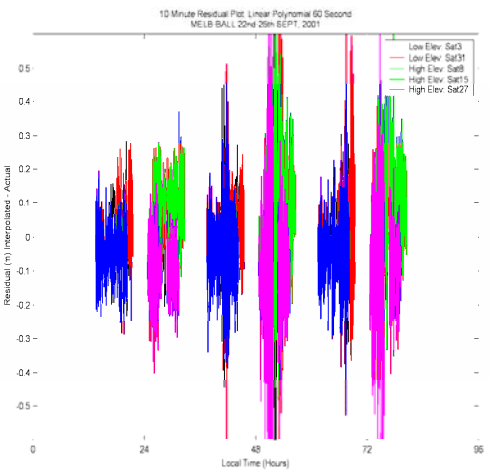

Linear polynomial model: December 20th – 23rd, 2001 Local time

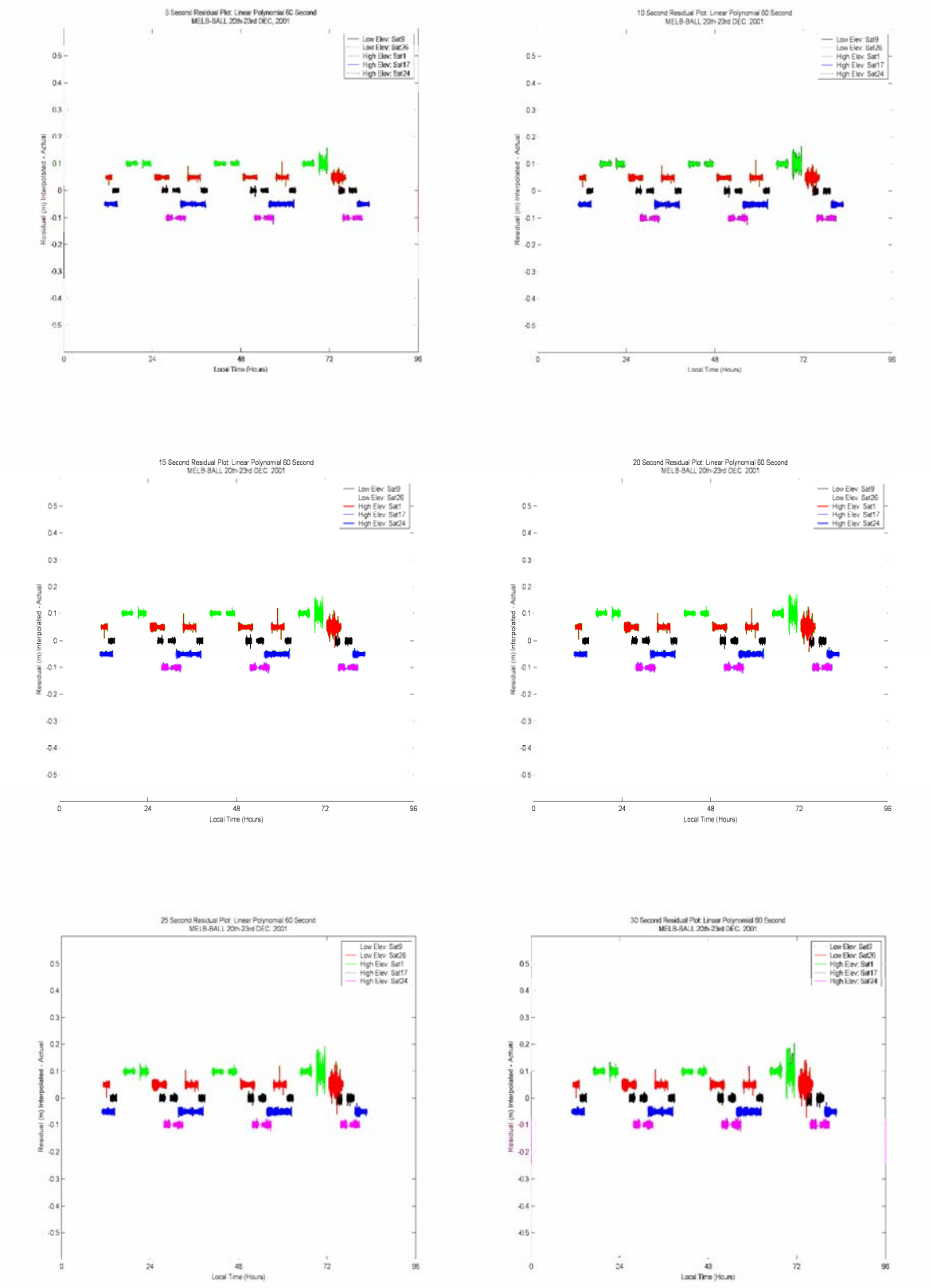

Linear polynomial model: December 20th – 23rd, 2001 Local time

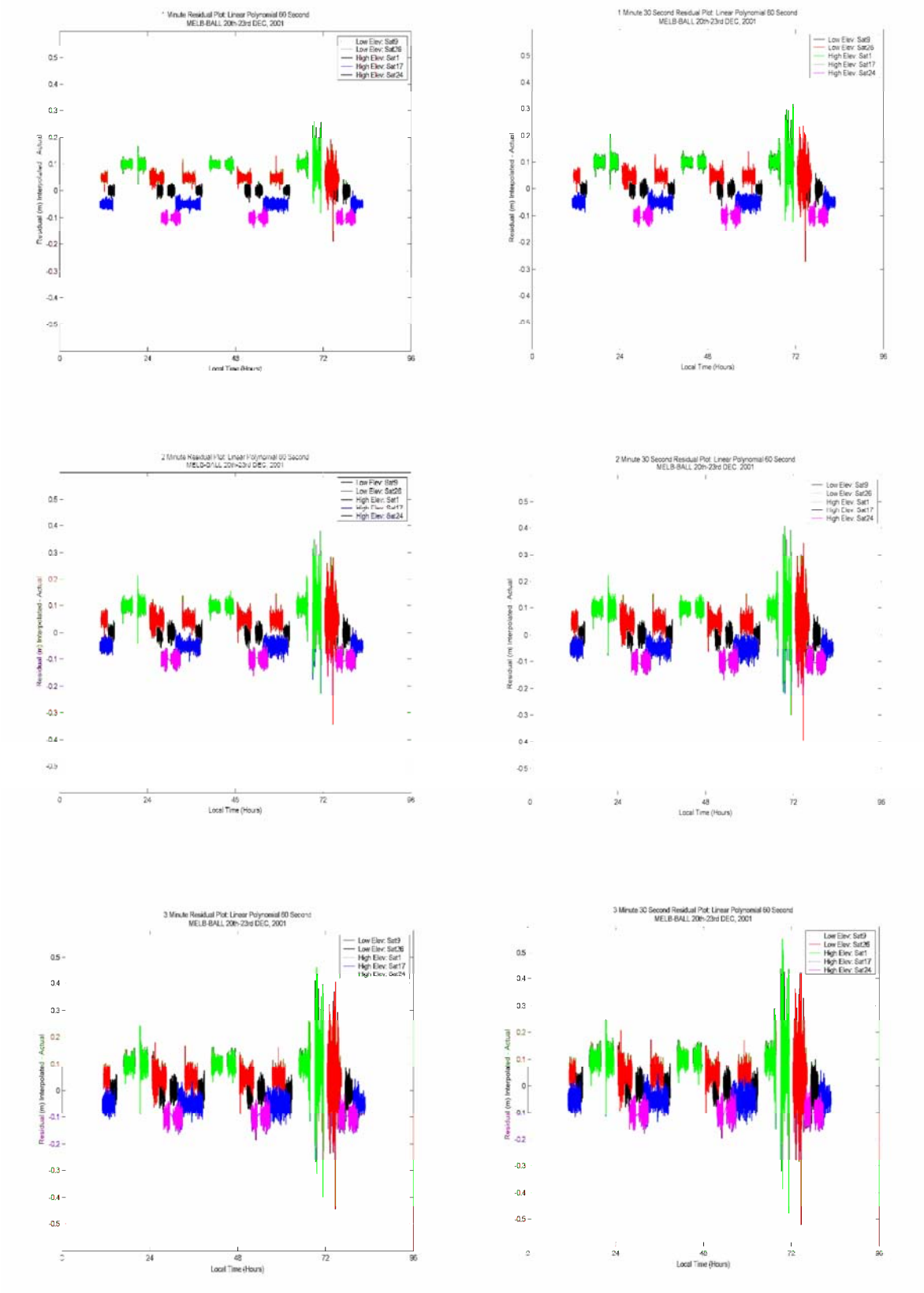

Linear polynomial model: December 20th – 23rd, 2001 Local time

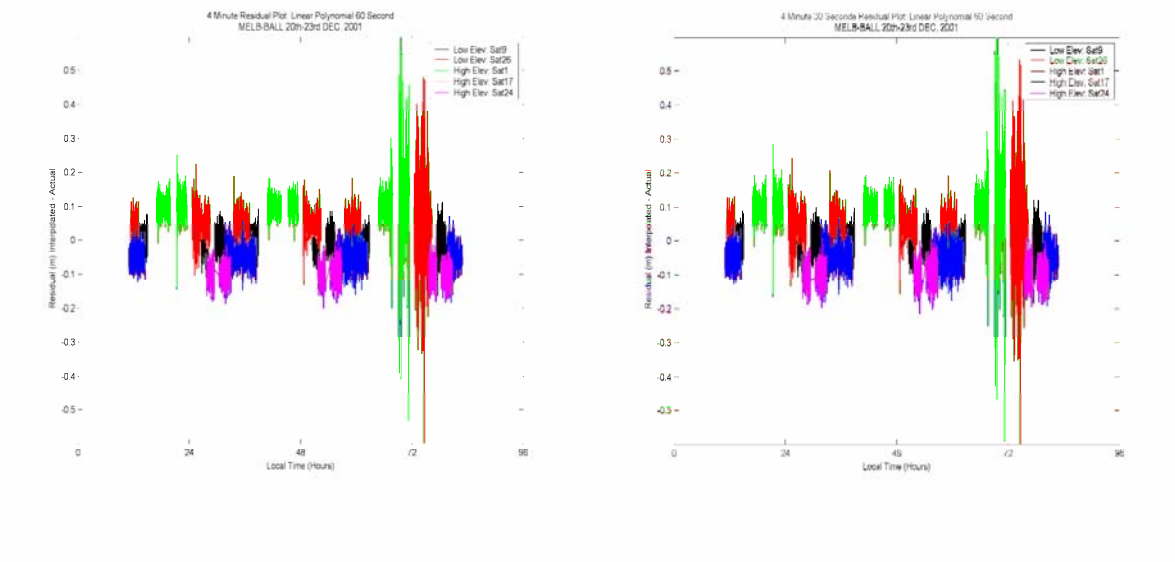

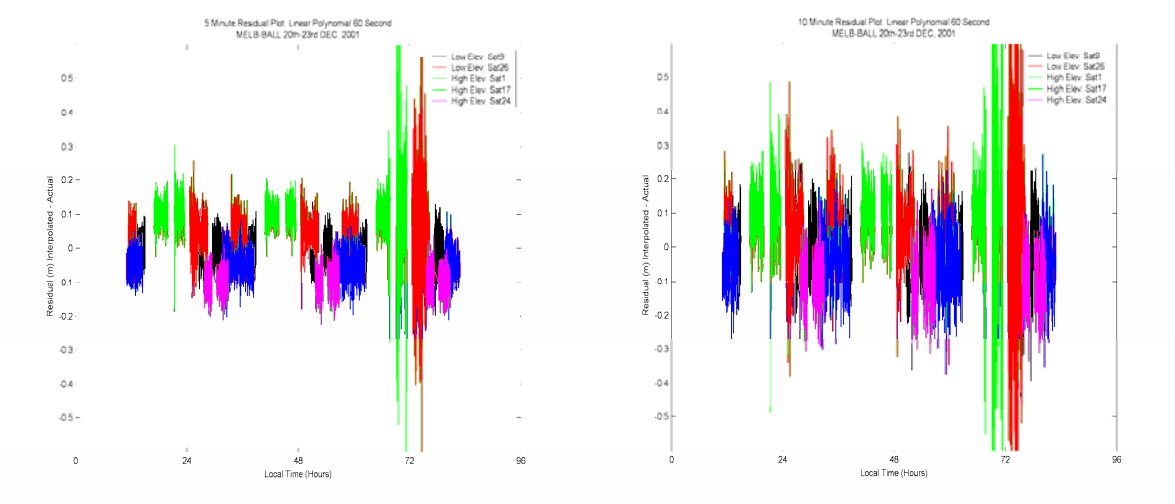

Linear polynomial model: March 19th – 22nd, 2002 Local time

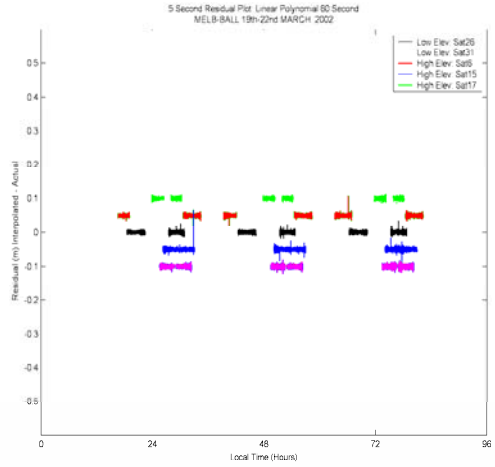

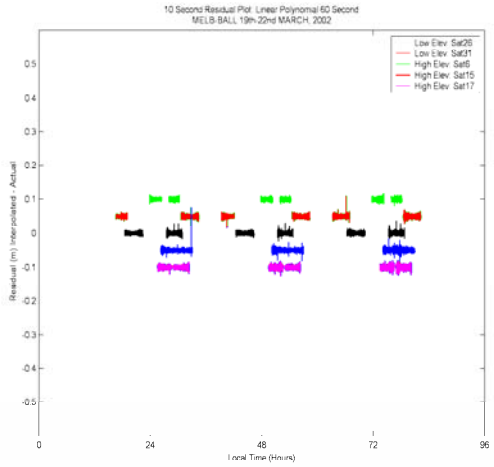

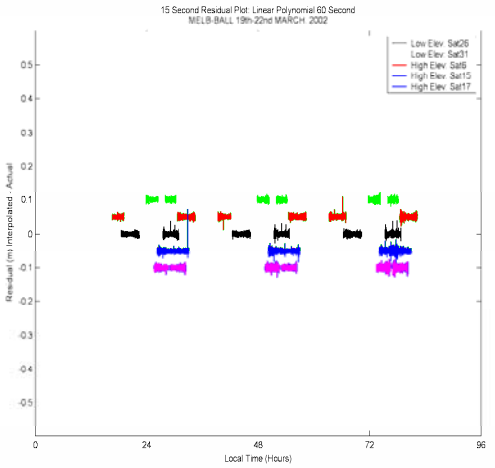

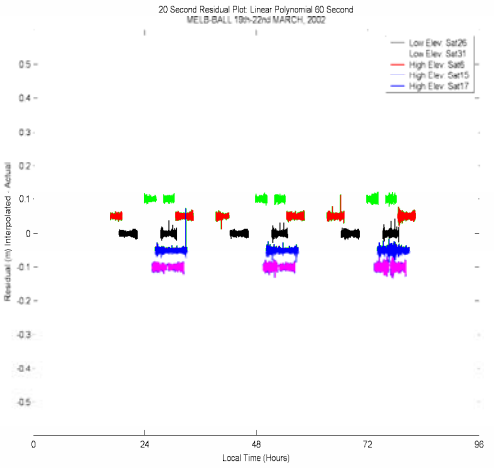

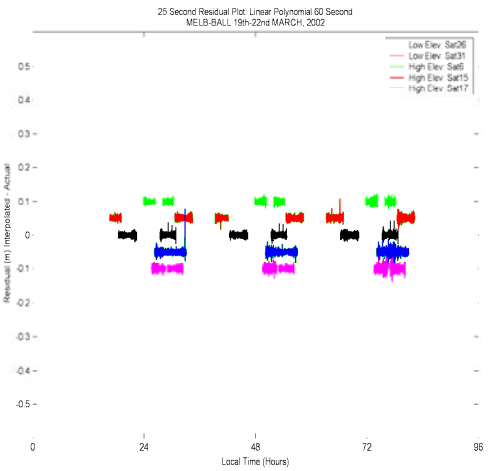

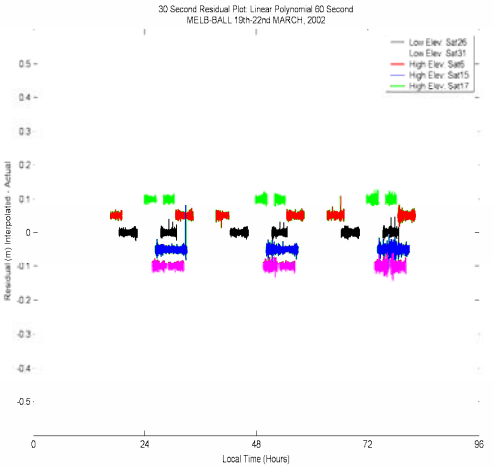

Linear polynomial model: March 19th – 22nd, 2002 Local time

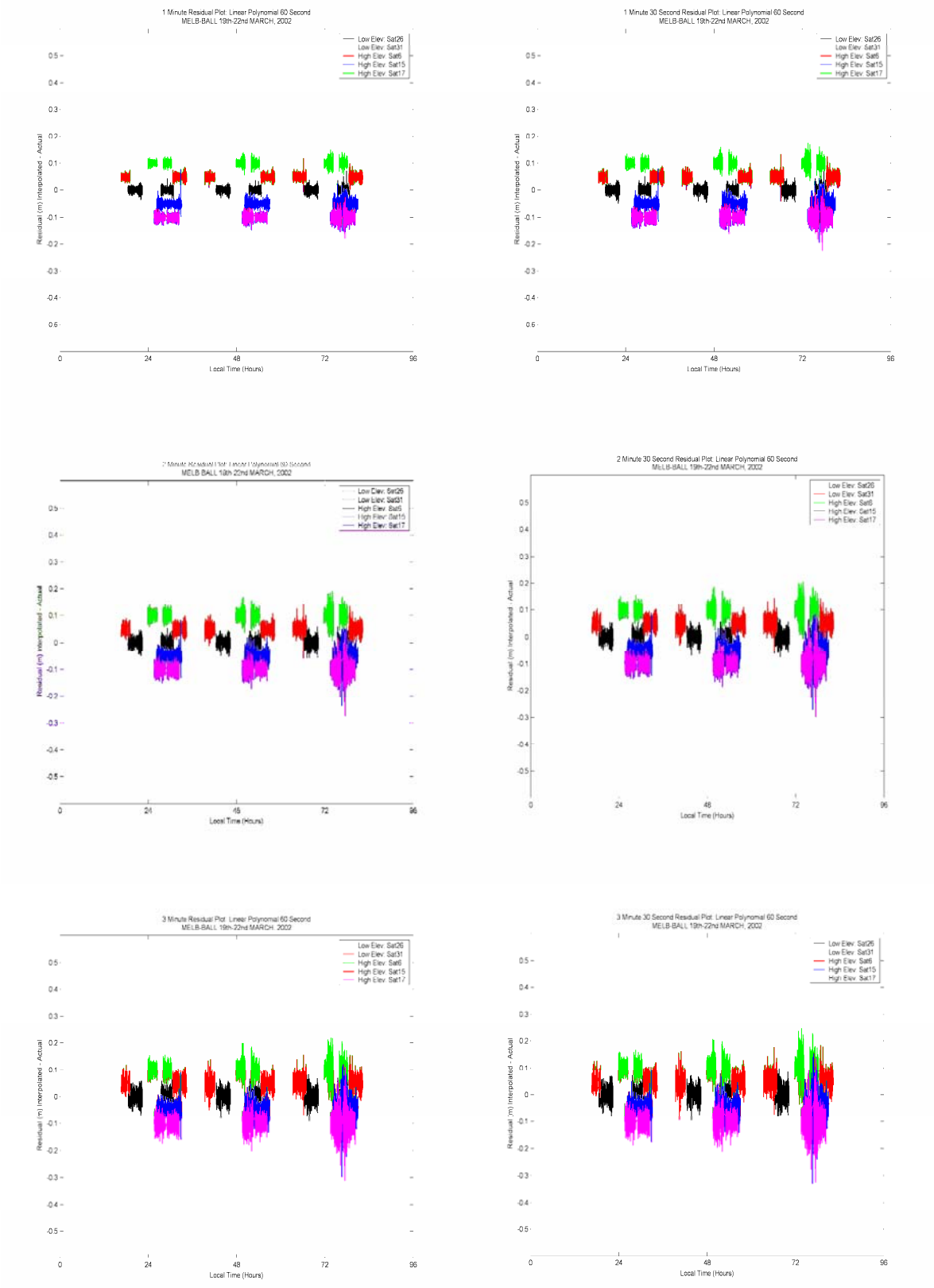

Linear polynomial model: March 19th – 22nd, 2002 Local time

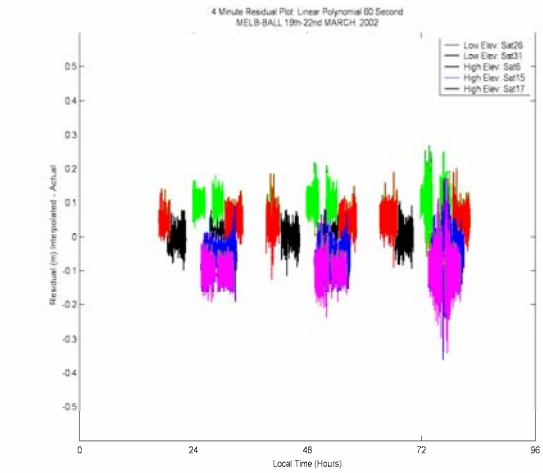

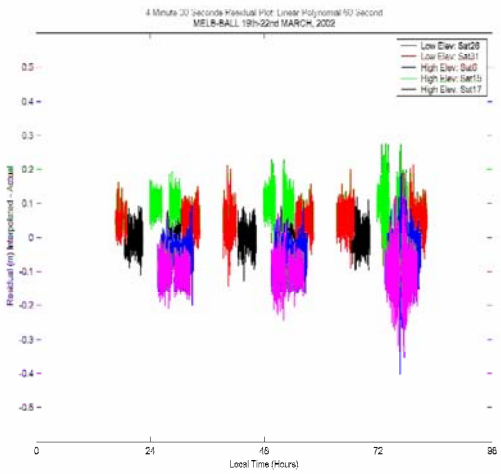

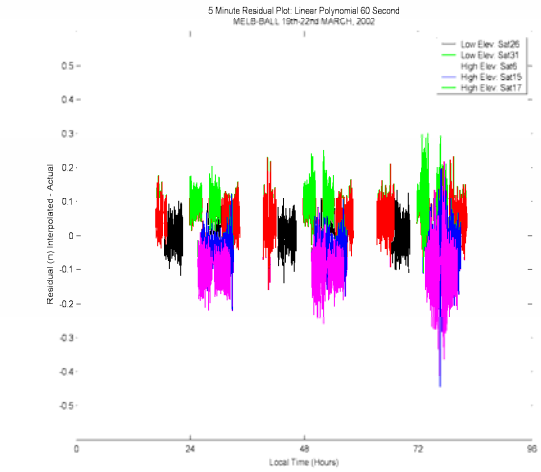

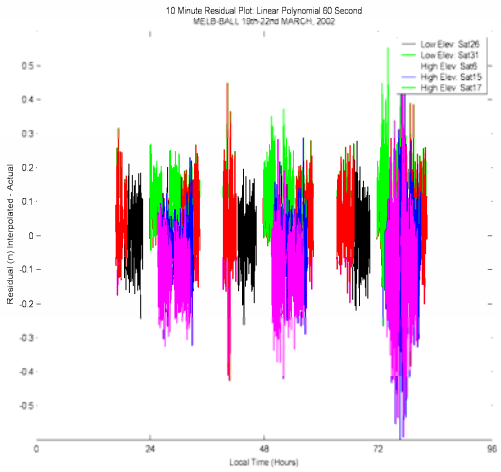

Linear polynomial model: June, 20th – 23rd, 2002 Local time

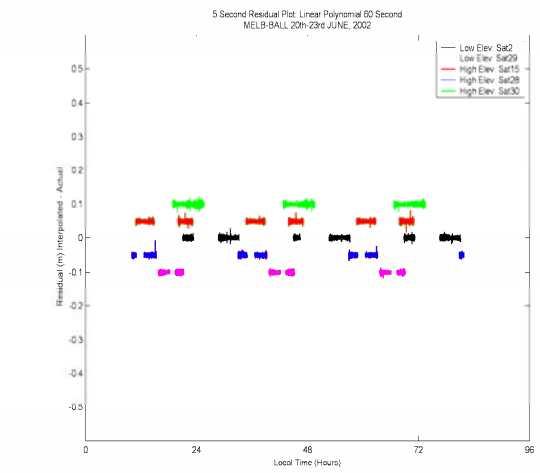

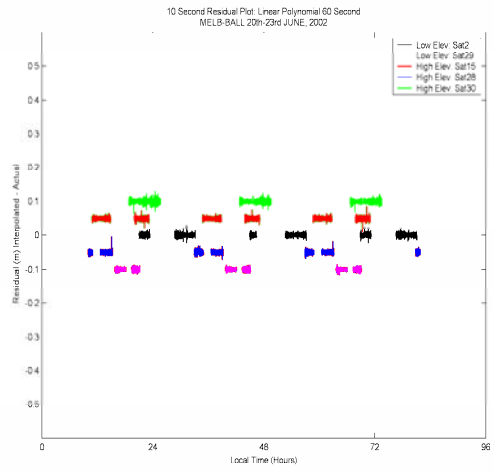

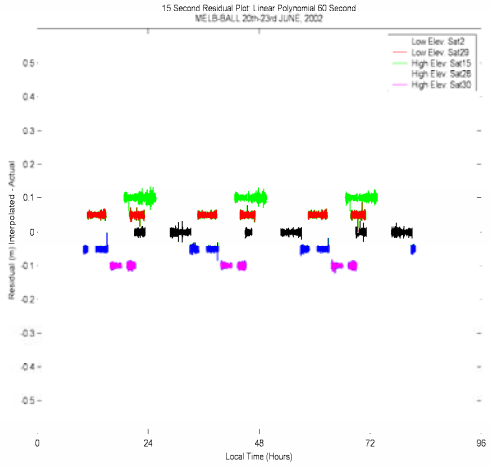

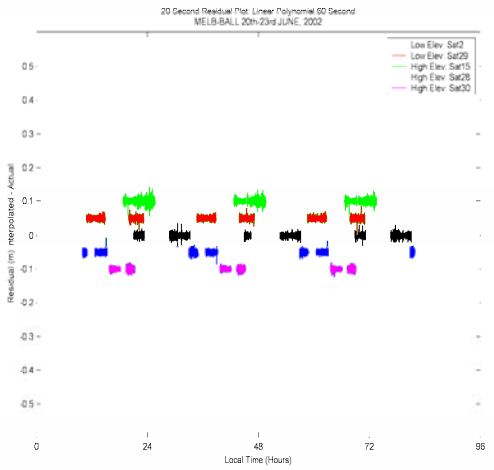

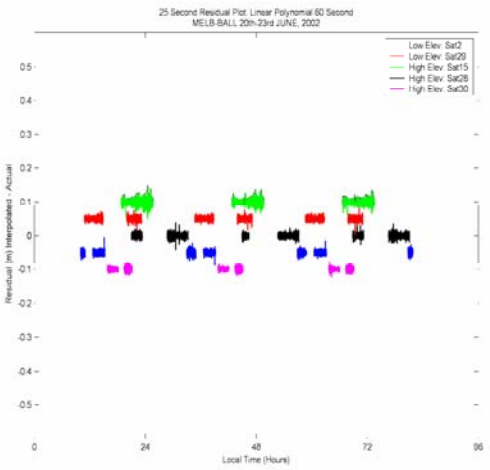

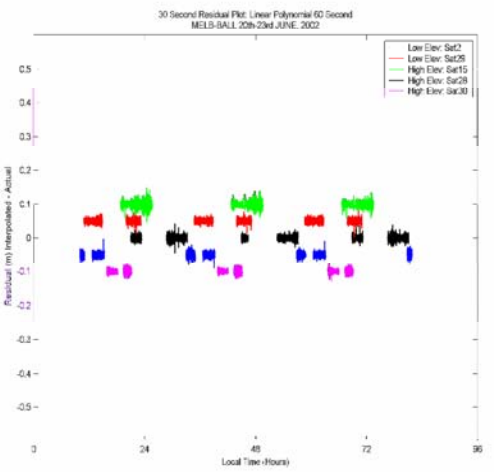

Linear polynomial model: June, 20th – 23rd, 2002 Local time

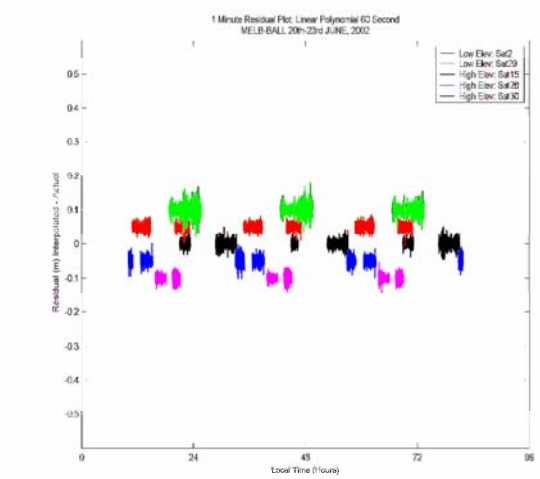

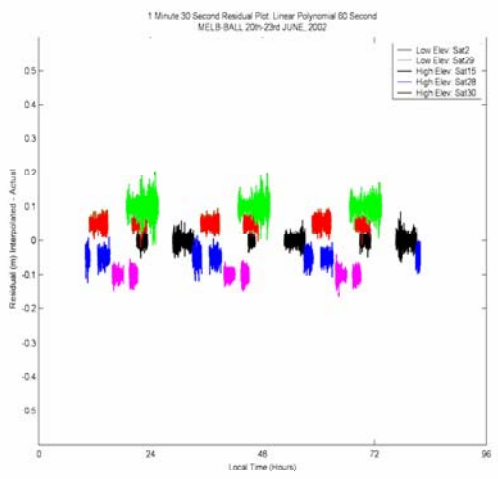

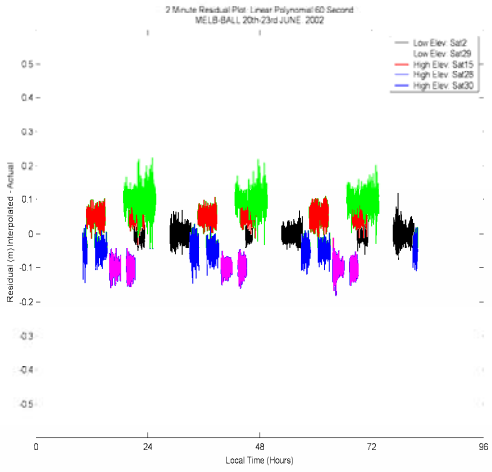

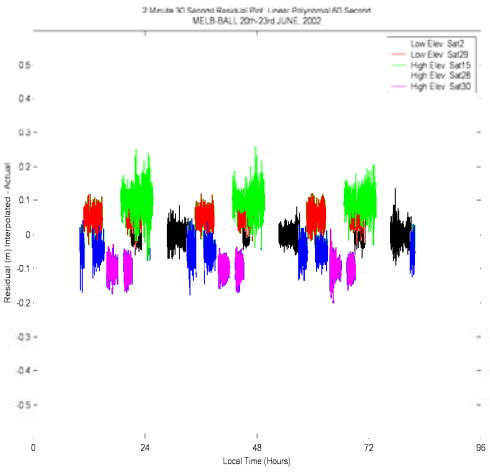

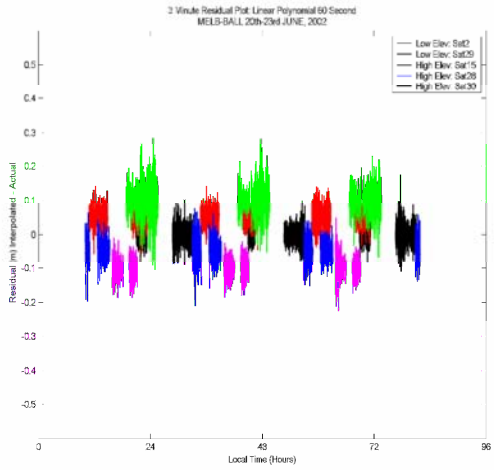

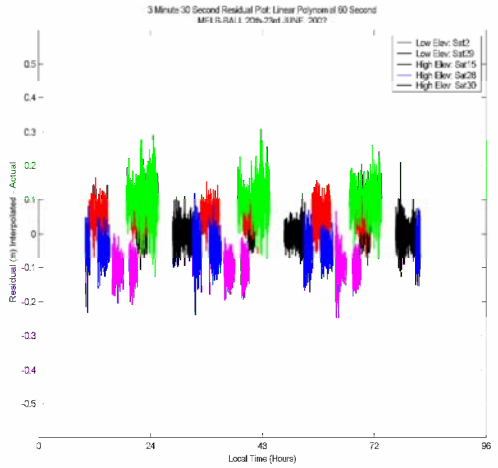

Linear polynomial model: June, 20th – 23rd, 2002 Local time

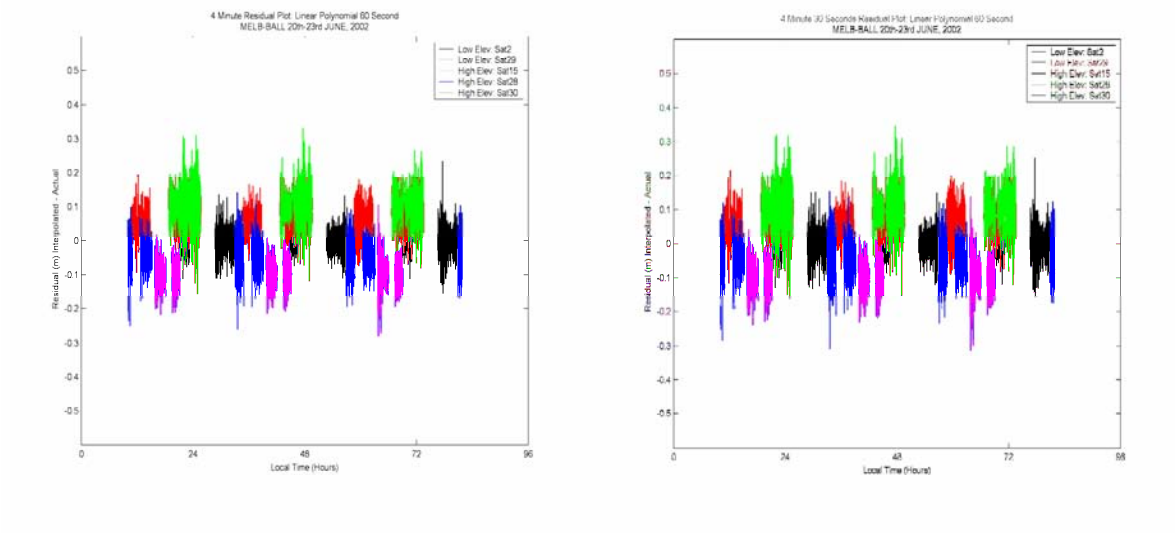

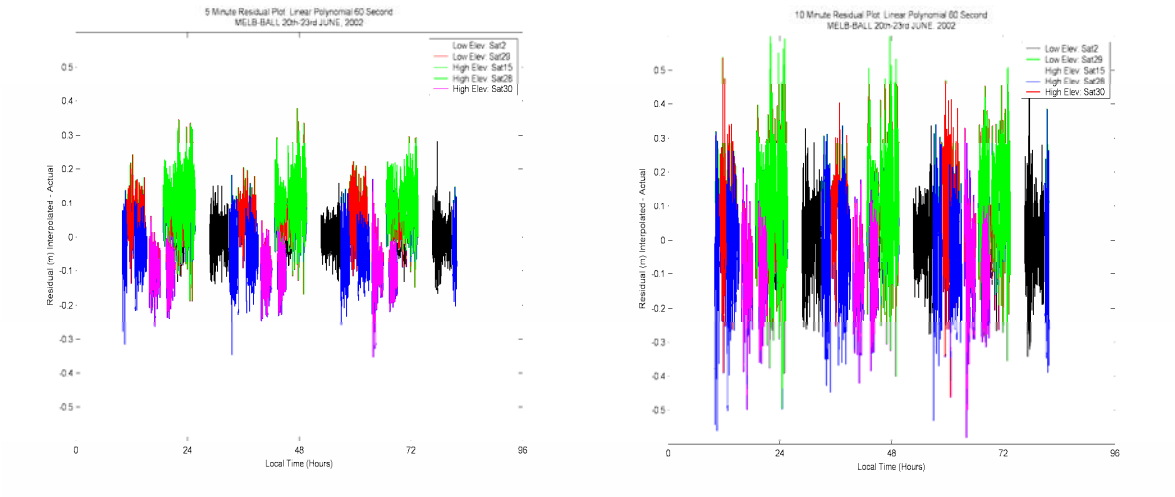

Appendix D: SPSS Version 14: ARIMA statistical readout

Melbourne – Ballarat Baseline: March 20th, 2001: 12.43-13.98 Local Time

ARIMA

```
[DataSet0]
```

Model Description[a]

Model Name	MOD_1
Dependent Series	VAR00001
Transformation	None
Constant	Not included
AR	1, 2, 3
Non-Seasonal Differencing	0
MA	None

Applying the model specifications from MOD_1

a. Since there is no seasonal component in the model, the seasonality of the data will be ignored.

ARIMA

Iteration Termination Criteria

Maximum Parameter Change Less Than	.001
Maximum Marquardt Constant Greater Than	1E+009
Sum of Squares Percentage Change Less Than	.001%
Number of Iterations Equal to	10

Case Processing Summary

Series Length		1114
Number of Cases Skipped Due to Missing Values	At the Beginning of the Series	0
	At the End of the Series	0
Number of Cases with Missing Values within the Series		0[a]
Number of Forecasted Cases		0
Number of New Cases Added to the Current Working File		0

a. Melard's Algorithm will be used for estimation.

Requested Initial Configuration[a]

Non-Seasonal Lags	AR1	AUTO
	AR2	AUTO
	AR3	AUTO

a. CONSTANT does not appear in the model.

Iteration History

	Non-Seasonal Lags			Adjusted Sum of Squares	Marquardt Constant
	AR1	AR2	AR3		
0	.760	.121	.111	.011	.001
1	.631	.180	.187	.011	.001
2	.605	.194	.199	.011	.000
3	.603	.195	.200	.011[a]	.000

Melard's algorithm was used for estimation.

a. The estimation terminated at this iteration, because the sum of squares decreased by less than .001%.

Residual Diagnostics

Number of Residuals	1114
Number of Parameters	3
Residual df	1111
Adjusted Residual Sum of Squares	.011
Residual Sum of Squares	.011
Residual Variance	.000
Model Std. Error	.003
Log-Likelihood	4849.210
Akaike's Information Criterion (AIC)	-9692.421
Schwarz's Bayesian Criterion (BIC)	-9677.374

Parameter Estimates

		Estimates	Std Error	t	Approx Sig
Non-Seasonal Lags	AR1	.603	.029	20.574	.000
	AR2	.195	.034	5.753	.000
	AR3	.200	.029	6.816	.000

Melard's algorithm was used for estimation.

Correlation Matrix

		Non-Seasonal Lags		
		AR1	AR2	AR3
Non-Seasonal Lags	AR1	1.000	-.578	-.329
	AR2	-.578	1.000	-.579
	AR3	-.329	-.579	1.000

Melard's algorithm was used for estimation.

Covariance Matrix

		Non-Seasonal Lags		
		AR1	AR2	AR3
Non-Seasonal Lags	AR1	.001	-.001	.000
	AR2	-.001	.001	-.001
	AR3	.000	-.001	.001

Melard's algorithm was used for estimation.